

RETURNING MATERIALS:
Place in book drop to remove this checkout from your record. FINES will be charged if book is returned after the date stamped below.

Synthesis, Characterization and Magnetic Properties of Crystalline Electrides and Alkalides

Ву

Ahmed Saad Ellaboudy

A DISSERTATION

Submitted to
Michigan State University
in partial fulfillment of the requirements
for the degree of

DOCTOR OF PHILOSOPHY

Department of Chemistry

1984

ABSTRACT

SYNTHESIS, CHARACTERIZATION AND MAGNETIC PROPERTIES OF CRYSTALLINE ELECTRIDES AND ALKALIDES

Ву

Ahmed Saad Ellaboudy

Two new crystalline alkalides, Rb⁺18C6.Na⁻ and Rb⁺18C6.Rb⁻ and the first crystalline electrides, Cs⁺(18C6)₂.e⁻, Cs⁺C222.e⁻ and Rb⁺18C6.e⁻ were synthesized, analyzed and characterized by optical, electrical and magnetic techniques.

Rb⁺18C6.Na⁻, Rb⁺18C6.e⁻ and Cs⁺(18C6)₂.e⁻ behave as semiconductors with apparent band gaps of 0.9, 0.4 and 0.9 eV respectively.

 23 Na-MASS-NMR spectra of MNaL $_n$ (M=K,Rb,Cs; L=18C6,C222; n=1,2) show only the Na $^-$ peak at ~61 ppm proving that they are all sodides. Na $^+$ C222.Na $^-$ shows the Na $^-$ peak and that of Na $^+$ C222. Field dependence and proton decoupling showed that Na $^+$ C222 is quadrupole shifted and broadened ($\frac{e^2qQ}{h}$ =1.2 MHz; η =0.1) while Na $^-$ is broadened by dipolar coupling to protons.

 133 Cs-MASS-NMR of the compounds Cs⁺(18C6) $_2$ N⁻ (N=I,SCN, Na,K,Rb) shows the Cs⁺ peak at ~-58 ppm, essentially independent of anion. Cs18C6 is the ceside, Cs⁺(18C6) $_2$.Cs⁻ since it shows peaks at -61 and -228 ppm. The electride

 $\text{Cs}^+(18\text{C6})_2.\text{e}^-$ shows only one peak (+81 ppm at ~-20°C) that shifted upfield with increasing temperature indicating a contact electron density of 2.39×10^{21} electrons·cm⁻³. CsC222 shows peaks at +138 and +238 ppm attributed to "exclusive" and "inclusive" Cs⁺ complexes respectively.

87Rb-MASS-NMR could not detect complexed Rb⁺ but Cs⁺(18C6)₂.Rb⁻ yielded an Rb⁻ peak at -187 ppm and KRb18C6 gave a weak doublet (-185 and -194 ppm).

Sodide salts generally showed a single EPR line at g=2.0023, often superimposed on two or three other lines. This was attributed to electron trapping at anionic vacancies. Rb⁺18C6.Na⁻ showed a narrow line at g=2.0023 and hyperfine lines (g=1.9974) due to electron coupling to the cation with $A_{\rm iso}=58.8$ and 196.6 G for $^{85}{\rm Rb}$ and $^{87}{\rm Rb}$ respectively (16% atomic character). CsC222 shows a very weak inhomogenously broadened axial symmetry powder pattern with $g_{\perp}=2.0020$ and $g_{\parallel}=1.9771$. Rb⁺18C6.e⁻ has a temperature independent Lorentzian EPR line at g=2.0017 with $\Delta H_{\rm p-p}=4.7$ G. Cs⁺(18C6) $_2$.e⁻ gave an asymmetric line $(g=2.0023, \Delta H_{\rm p-p}=0.5$ G, both independent of temperature from 3 to 250 K). The $\frac{A}{B}$ ratio increased with increasing temperature indicating substantial microwave conductivity and an apparent band gap of 0.1 eV.

 $Cs^+(18C6)_2.e^-$ magnetic susceptibilities very nearly obeyed the Curie-Weiss Law, $\chi_M^e = fC/(T-\theta)$ with f = 0.74, $\theta = -1.4$ K, while $Rb^+18C6.e^-$ and $Cs^+C222.e^-$ had only about 1% unpaired spins.

بسِّ الْكُنْ الْجُرِّ الْجُرْبِ

In the name of God the most merciful and the most beneficent.

To my wife, Fadia

ACKNOWLEDGMENTS

The author wishes to express his sincere gratitude to Professor James L. Dye for his guidance, encouragement and whole-hearted support throughout this study. I would like to thank those with whom I worked most closely, Drs. Long Dinh Le, Dheeb Issa, Bradley Van Eck; my colleagues in the solid state group, Odette Fussá, Mary Tinkham, Rui Huang, Zheng Li, Francoise Tientega and especially Margie Faber and Steve Dawes for their aid, discussions and moral support. Thanks are also extended to the enzyme group, Zexia Barnes and Iraj Behbahani.

Special thanks go to Dr. Pat Smith in the Analytical Laboratory of Dow Chemical Company and Professor Eric Oldfield's group in the Chemistry Department of the University of Illinois for their help in the magic angle NMR work.

Financial support is gratefully acknowledge from the Chemistry Department, Michigan State University through a teaching assistantship, National Science Foundation (Grant DMR 79-21979) for a research assistantship, the Dow Chemical Company for a summer 1983 fellowship and the SOHIO Company for a 1983-84 fellowship.

Thanks go to the glassblowers: Keki Mistry,

Manfred Langer and Scott Bankroff for their excellent

and timely service; for without their help this work

would have been impossible. Thanks also go to

Ms. Margy Lynch for doing an excellent job in typing

this Dissertation.

Thanks to my beloved University, Alexandria University in Egypt, the clerical staff in the Embassy of Arab Republic of Egypt—Cultural and Educational Bureau in Washington, D.C., especially to Mr. Hany El-Malty, and all my friends in the Egyptian Club in East Lansing, especially Mr. Mohsen Shabana for making me feel at home with their friendship and brotherhood.

Special thanks go to my family and my wife's family for their unending encouragement, understanding and moral support. Above all, a special "thank you" goes to my wife, Fadia, whose understanding and extremely long patience was vital to the completion of this degree. To her I dedicate this thesis.

TABLE OF CONTENTS

	P	AGE
LIST OF	TABLES	'iii
LIST OF	FIGURES	.ix
CHAPTER	I INTRODUCTION	.1
A.	Alkali Metal-Ammonia Solutions	.1
В.	Alkali Metal-Amines, Ethers and Other Solvents	5
c.	Metal-Ammonia Compounds	10
D.	Alkali Metal Anione (MT)	15
E.		16
F.	Macrocyclic and Macrobicyclic Diamine-	.10
Γ.	Polyethers	22
G.	Polyethers	26
н.	Objectives of the Present Work	20
п.	objectives of the Flesent work	32
СНУБИТЬ	II EXPERIMENTAL	31
A.		
***	1. Alkali metals	
	2. Complexants	35
	3. Solvents	37
В.		38
ζ.	General Synthesis Procedure	38
D.	Analysis	41
٥.	Analysis	42
	2. pH titration	44
	3. Flame emission	45
	4. Quantitative ¹ H NMR	. 45
Ε.	Sample Handling and Instrumental Techniques	. 46
	1. Optical absorption spectra	
	2. Pressed powder conductivity	48
	3. Solid state NMR	
	4. EPR spectra	
	5. Magnetic susceptibility	
F.	Model Salts	

	P	AGE
CHAPTER	III SYNTHESIS AND CHARACTERIZATION	53
A.	Introduction	53
в.	Introduction	54
	1. Method 1	54
	2. Method 2	55
	3. Method 3	56
c.	Results and Discussion	58
	1. Synthesis	.58
	2. Analysis	62
	3. Optical spectra	.68
	a. RbNal8C6 and RbNaC222	.69
	b. Rb18C6 and Rb218C6	69
	c. Cs18C6 and Cs $(18C6)_2$	73
	d. CsC222	74
	4. D.C. pressed powder conductivity	77
	5. Differential scanning calorometric (DSC)	
	studies	.85
CHAPTER	IV SOLID STATE NMR	91
Α.	Introduction	
В.	Magic Angle Sample Spinning (MASS)-NMR	93
	1. Direct magnetic dipolar interactions	94
	2. Chemical shift interactions	.97
	 Chemical shift interactions Electrical quadrupolar interactions 	100
c.	Results and Discussion.	109
•	Results and Discussion	109
	a. Identification of the species	109
	b. Frequency dependence and proton	
	decoupling	117
	2. 133Cs-MASS-NMR	124
	a. Species identification and frequency	124
	dependence	124
	dependence	120
	c. Electron doping in the ceside	130
	compound	1/12
	3. 87 Rb-MASS-NMR	1/10
	4. The chemical shifts of alkali metal	140
	anions	7 - 4
		154
CHAPTER	V MAGNETIC PROPERTIES OF ALKALIDES AND	
		, , ,
Α.	ELECTRIDES	15/
A.	1 Introduction	15/
	 Introduction	15/
	a. Trapped electrons in sodides	170
	a. Trapped efections in Sources	
	"F-center alkalides"	170
	b. Electrons in electrides	183
	i. EPR of singlet-ground state	
	electrides	183
	ii. EPR of doublet-ground state	
	electrides	186

		PAGE
В.	Magnetic Susceptibility	.198 .202 .202 .204
CHAPTER	VI CONCLUSIONS AND SUGGESTIONS FOR	
	FUTURE WORK	.212
A.	Conclusions	
в.		
BIBLIOG	RAPHY	218

LIST OF TABLES

TABLE	PAGE
I	Synthesis and Description of Crystalline Electrides and Alkalides 59
II	Results of the Analysis
III	DSC Results for Alkalides and an Electride 89
IV	Results of ²³ Na-MASS-NMR at 52.94 MHz 112
V	Proton-Decoupled and Frequency Dependence of the Chemical Shift and Linewidth of ²³ Na NMR
VI	133 _{Cs-NMR} Results
VII	87 Rb MASS-NMR Results
VIII	Chemical Shifts of Alkali Metal Anions 155
IX	Resonance Field of Some Hyperfine Lines 180
X	Parameters of the Curie-Weiss Equation for Cs ⁺ (18C6) ₂ .Cs ⁻

LIST OF FIGURES

FIGURE	PAG	Έ
1	Classification of EPR spectra (~296 K) of fluid metal solutions on the basis of the product $\langle \tau_M \rangle$ A_{iso} : THF = tetrahydrofuran, EA = ethylamine, 1,2PDA = 1,2-propanediamine, EDA = ethylenediamine, AM = ammonia [41]	.1
2	Packing of Na ⁺ C222 and Na ⁻ (solid circles) in the crystalline sodide Na ⁺ C222.Na ⁻ [30] 2	8
3	Apparatus for distribution of alkali metals under vacuum	6
4	Apparatus for the synthesis of crystalline electrides and alkalides	9
5	Apparatus for the optical spectra of thin films (5a) and hydrogen evolution (5b) 4	3
6	Optical spectra of films of RbNal8C6 () and RbNaC222 (····)	0
7	Optical spectra of films, made from methylamine solutions of Rb18C6 () and Rb218C6 () thin film, (····) thick film	'1
8	Optical spectra of films of the compounds Cs18C6 (—·—·—) and Cs(18C6) ₂ (———). Data for the compound Cs18C6 are taken from reference 98	5
9	Optical spectra of film of compound CsC222 7	6
10	Ohm's Law plot of polycrystalline powder of Rb+18C6.Na	1
11	Ohm's Law plot of polycrystalline powder of Rb+18C6.e	12
12	Ohm's Law plot of polycrystalline powder of Cs ⁺ (18C6) ₂ .e ⁻	3
13	A plot of log conductivity vs. reciprocal temperature of the compound Cs ⁺ (18C6) ₂ .Cs ⁻ (open circles) and Cs ⁺ (18C6) ₂ .e ⁻ (solid circles)	34

FIGURE	PAGE
14	A plot of log resistivity vs. reciprocal temperature for polycrystalline Rb+18C6.Na86
15	A plot of log resistivity vs. reciprocal temperature for polycrystalline Rb+18C6.e
16	DSC for a polycrystalline sample of Cs ⁺ (18C6) ₂ .Na ⁻ 88
17	DSC for polycrystalline samples of Rb+18C6.Na (
18	A diagram illustrating the motion of a typical inter-nuclear vector, r_{ij} , when a solid is rotated with angular velocity ω_r about an axis inclined at angle β to H_0 96
19	(a) NMR powder pattern of axially symmetric crystals; (b) ²³ Na-MASS-NMR spectrum of an equimolar mixture of NaCl and NaNO ₃ 106
20	Static (dotted line) and spinning (solid line) ²³ Na-NMR spectra of Na ⁺ 18C6.SCN at 132.35 MHz
21	Static and spinning ²³ Na-NMR spectra of Na+C222.Na at 52.94 MHz
22	23Na-MASS-NMR spectrum of one sample of K+18C6.Na at 132.35 MHz
23	²³ Na-MASS-NMR spectra of Na ⁺ C222.Na ⁻ at three different frequencies
24	Observed and simulated ²³ Na-NMR signal of Na ⁺ C222 in Na ⁺ C222.Na at different
25	frequencies
26	frequencies
27	23Na and 133Cs-MASS-NMR spectra of the compound Cs ⁺ (18C6) ₂ .Na ⁻
28	Static (top) and spinning (bottom) 133Cs-MASS-NMR spectra of the compound Cs ⁺ (18C6) ₂ .e ⁻ at 65.61 MHz
29	133Cs-MASS-NMR spectra of the two crystalline compounds Cs ⁺ C222.SCN ⁻ .H ₂ O (top) and Cs ⁺ C222.e ⁻ (bottom) at 42.24 MHz

FIGURE		F	PAGE
30	133Cs-MASS-NMR spectra at 65.61 MHz of the compound Cs+C222.e at different spinning frequencies: A: 1.8, B: 2.6, C: 3.8 and D: 4.0 KHz		137
31	133Cs-MASS-NMR spectrum of one sample of Cs+(18C6) ₂ .Cs- (method 2) at 65.61 MHz		144
32	133Cs-MASS-NMR spectrum of one sample of Cs+(18C6) ₂ .Cs (method 3) at 42.24 MHz		145
33	133Cs-MASS-NMR spectrum of one sample of Cs+(18C6) ₂ Cs-(method 3) at 65.61 MHz		146
34	133Cs (at 65.61 MHz) and 87Rb (at 163.6 MHz) MASS-NMR spectra of the compound Cs ⁺ (18C6) ₂ .Rb ⁻		152
35	87Rb-MASS-NMR spectrum of the compound K+18C6.Rb- at 163.6 MHz		153
36	Magnetic energy levels for I = 3/2 and S = 1/2. The solid lines are energy levels computed from Eq. (V.10); dotted lines are the corresponding first-order energy levels (Eq. (V.7)) [133]	• •	161
37	Variation of EPR signal amplitude with microwave power (P_O) for a homogeneously broadened line (solid curve) and an inhomogeneously broadened line (dotted curve))	165
38	Typical first derivative lineshape of the electron spin resonance absorption in thick metals		169
39	EPR spectra of polycrystalline sample of Na ⁺ C222.Na ⁻ at different microwave power levels		172
40	EPR spectrum of a polycrystalline sample of Cs ⁺ (18C6) ₂ .Na ⁻		174
41	Variation of the relative intensity of the central line of the EPR spectrum of Cs ⁺ (18C6) ₂ .Na with the square root of the microwave power level		175
42	EPR spectra of a polycrystalline sample of Cs ⁺ (18C6) ₂ .Na at different temperatures		177
43	EPR spectrum of a polycrystalline sample of Rb ⁺ 18C6.Na at 2.8 K		178
44	Variation of the relative intensity of the central line of the EPR spectrum of Rb+18C6.Na- with the microwave power		
	lovol		170

FIGURE	PAGE
45	EPR spectrum of a polycrystalline sample of Rb+18C6.e at 123 K
46	Variation of the relative intensity of the EPR line of Rb ⁺ 18C6.e ⁻ with the square root of the microwave power level
47	EPR spectrum of a polycrystalline sample of Cs ⁺ C222.e ⁻ at 2.8 K
48	Variation of the relative intensity of the EPR line of Cs ⁺ C222.e with the square root of the microwave power level
49	EPR spectrum of a polycrystalline sample of Cs ⁺ (18C6) ₂ .e ⁻ at 174 K (sample in 2 mm tube)
50	Variation of the linewidth (ΔH _{p-p}) of the EPR line of Cs ⁺ (18C6) ₂ .e with temperature
51	Variation of A/B ratio of the EPR line of Cs ⁺ (18C6) ₂ .e with temperature (sample in 3 mm tube)
52	a/ δ vs. A/B for spherical metal particles 193
53	Plot of the relative A.C. resistivity (solid line) at X-band microwave frequency and D.C. resistivity (dashed line) vs.
5 4	temperature
54	A plot of log relative microwave resitivity with 1/T
55	A plot of $1/\chi_{M}^{e}$ vs. T for a polycrystalline sample of Cs ⁺ (18C6) ₂ .e ⁻
56	A plot of χ_{M}^{e} vs. T for a polycrystalline sample of Cs ⁺ (T8C6) ₂ .Cs (method 3)
57	A plot of $\chi_{M_+}^e$ vs. T for a polycrystalline sample of Rb (18C6).e
58	A plot of χ_{M}^{S} vs. T for a polycrystalline sample of Cs+ $\overline{C2}22.e^{-}$

CHAPTER I

INTRODUCTION

The discovery of two new classes of ionic solids, named electrides and alkalides, came as a result of the use of macrocyclic polyethers to enhance the solubilities of alkali metals in amine and ether solutions. The similarity between these two new types of ionic solids and metal-ammonia compounds is striking. The behavior of the two classes of macrocyclic polyethers and their complex compounds with simple alkali metal salts provides a good model for the nature of the complex cation. Trapped electrons in solids (F-centers) and frozen solution (glasses) may well provide examples of a "dilute electride". Accordingly, all of these subjects provide background for the present work and will be reviewed here.

A. Alkali Metal-Ammonia Solutions

It has been over a century since Weyl in 1864 [1] discovered that sodium and potassium metals form blue-colored solutions in liquid ammonia when dilute and bronze-colored solutions when concentrated. Seven years later, Seely [2] recovered sodium and potassium from ammonia

solutions by solvent evaporation. He concluded that alkali metals do not react with liquid ammonia and that these solutions are similar to those of ordinary salts in water. Since that time, metal-ammonia solutions have attracted the attention of both chemists and physicists. This controversial field has already resulted in six conferences named "Colloque Weyl" [3-8] which have provided a great deal of information about the nature of these systems. However, the detailed nature of the species present is still the subject of much speculation and controversy.

In general, liquid ammonia dissolves alkali, alkaline earth (except Be), and Yb and Eu metals. The alkali metal solutions have been studied more extensively than those of other metals and will be the subject of this section.

The solubilities of alkali metals in liquid ammonia vary from 16 MPM (mole percent metal) for Na, K and Rb to 20 MPM for Li to 65 MPM for Cs and do not vary greatly with temperature. The properties of alkali metal-ammonia solutions vary from electrolytic for dilute and moderate concentrations to metallic for concentrated solutions. In the range of 3 to 9 MPM alkali metal-ammonia solutions exhibit a nonmetal to metal transition and, except for cesium solutions, cooling the homogeneous solution gives rise to liquid-liquid phase separation. A low-density bronze metallic phase floats on top of the more dense, less concentrated, dark blue phase. Only the optical and

magnetic properties of alkali metal-ammonia solutions will be reviewed here, since in principle much information can be extracted from the knowledge of these two properties.

For very dilute solutions (<10⁻³ MPM), the optical absorption spectrum of alkali metal-ammonia solutions consists of a distinct band in the infrared which drops to low absorbance on the low energy side. The position of maximum absorption, λ_{max} , is independent of the metal [9]. Based upon pulse radiolysis studies [10], this band is assigned to the solvated electron. It is universally accepted that only solvated electrons and solvated cations are present in very dilute solutions (<10⁻³ MPM). In the concentration range 10^{-3} to 10^{-1} MPM there is an observable red shift of the band position with solution composition. This was interpreted in terms of the presence of a second diamagnetic absorber and the results were confirmed by the change of the peak linewidth with temperature and pressure. For concentrated solutions only reflectance spectra were obtained and showed a plasma type absorption due to the conduction electrons [11].

O'Reilly [12,13] measured the Knight shifts [14] of $^7\mathrm{Li}$, $^{23}\mathrm{Na}$, $^{87}\mathrm{Rb}$, $^{133}\mathrm{Cs}$ and $^{14}\mathrm{N}$ nuclei in alkali metal-ammonia solutions at 298 K in the concentration range 0.1 to 1.0 mole·liter⁻¹. Although there are some discrepancies between his results and those obtained by McConnell and Hollm [15], and Acrivos and Pitzer [16], the general behavior is clear. The Knight shift results

indicated very small electron spin density at the metal nucleus (1% of the free-atom value) and a relatively large spin density at the nitrogen nuclei. The $^{14}{
m N}$ Knight shift appeared to be independent of the metal cation and increased with increasing metal concentration, while those of the alkali metal cations were independent of metal concentration and varied by a factor of 100 on going from Li to Cs. In contrast, the proton Knight shift [17] showed a "negative" electron spin density. The calculated average total spin density at the nitrogen nuclei was found to be a constant on the order of 6.44×10^{24} cm⁻³ and was independent of metal concentration [18]. The static [19-22] and microwave (EPR) [23-25] spin only susceptibility showed similar results. At high dilution ($\sim 6 \times 10^{-3}$ M) the free spin concentration was equal to the metal concentration and the susceptibility was independent of the metal cation up to 0.1 M. Increasing the metal concentration to 1.0 M gave an increase in the electronic susceptibility which was less than expected indicating that a spin-pairing process occurs in this region. Above 1.0 M the susceptibility increased, showing a metallic kind of behavior and indicating progressive electron delocalization. The EPR spectra of dilute alkali metal-ammonia solutions showed extremely narrow symmetrical lines of the order of a few millgauss in width [26,27]. The electron spin relaxation mechanism which gives rise to extremely narrow EPR lines is the modulated hyperfine interaction of the solvated electron with the nitrogen atoms

of the solvation shell. Also the relaxation times $(T_1 = T_2)$ are essentially independent of metal concentration at dilute to moderate concentrations. Although no resolved hyperfine splitting could be observed, the measured alkali metal Knight shifts reflected the cation-electron interaction which was washed out by the very short electron-nuclear correlation time (τ_M) . Increasing the metal concentration to the region of the non-metal to metal transition resulted in the appearance of highly asymmetrical EPR lines with A/B (ratio of the low-field amplitude to high-field amplitude of the first derivative EPR line) greater than 1, characteristic of metallic samples with thicknesses comparable to or greater than the skin depth. This is now known as the "Dysonian" lineshape [28].

In summary, one might speculate about the species present in alkali metal-ammonia solution as follows: in very dilute solutions alkali metals dissociate to solvated cations and the paramagnetic solvated electron. An increase in concentration leads to electron-cation interaction through the formation of "loose" aggregated complexes of the solvated electron such as $M_s^+ \cdot e_s^-$ (paramagnetic) and the triple ion $e_s^- \cdot M_s^+ \cdot e_s^-$ (diamagnetic). The very short electron correlation time τ_M gives the cation a bystander role in these solutions.

B. Alkali Metal-Amines, Ethers and Other Solvents

In low dielectric constant amines, ethers and amides, alkali metals dissolve to a lesser extent than they do in

ammonia. The dramatic decrease in the dielectric constant relative to ammonia solutions is of cardinal importance in determining the change in cation and electron solvation and hence electron-cation interactions. Then, the association of the solvated electron and solvated cation can no longer be described as weakly interacting ion-pair species and one can safely make the general comment that the majority of aggregate species are more "tightly bound" than in ammonia solutions. Therefore, metal-dependent properties are expected for these solutions rather than the "null results" of metal-ammonia solutions.

Optical absorption studies [29] of alkali metals in amine and ether solutions showed metal-dependent absorption spectra. In addition to the solvated electron band there is at least one more peak at higher energy which depends upon the metal cation. Based on pulse radiolysis studies [10] of alkali metal cation solutions in amine and ether solvents, the correlation of the band positions with the ns →np transitions in gaseous alkali atoms [30] and the similarity to charge transfer to solvent (CTTS) bands, the metal dependent bands were attributed to alkali metal anions [30]. Solutions of alkali metals (except Li and Na) in ethylenediamine (EDA) [29] showed bands of both the alkali metal anion and the solvated electron with absorbance ratios that increased with increasing metal concentration Li-EDA showed only the solvated electron band while Na-EDA showed only the Na band. The presence of one or two peaks

in the optical absorption spectrum may be understood in terms of the dissociation reaction

$$M^{-} \rightleftharpoons M_{s}^{+} + 2e_{s}^{-} \tag{I.1}$$

EPR spectra of alkali metal-amine solutions showed different behavior upon changing solvent polarity. Lithiummethylamine solutions are well characterized in terms of "ammonia-like" aggregate species [31,32]. A narrow EPR singlet, which is similar to those of dilute metal-ammonia solutions, is observed but in contrast to metal-ammonia solutions, a recent spin echo study [33] showed that the electron relaxation times are not equal. This suggested that the relaxation mechanism for dilute ammonia solutions (motional-modulation of the electron-nitrogen hyperfine interaction) cannot alone account for the inequality. Upon changing the solvent to ethylamine, lithium solutions showed resolved EPR signals due to coupling to the nitrogen nuclei. Sodium and potassium solutions in methylamine [34] showed no resolved hyperfine coupling but rather broad lines having g-values close to that of the free electron. On the other hand, rubidium and cesium solutions in methylamine and potassium, rubidium and cesium in ethylamine and n-propylamine [35] showed a resolved hyperfine pattern due to coupling to the metal nuclei, in addition to a central line of the solvated electron. A recent NMR study [36]

of methylamine solutions of sodium through cesium showed no evidence of an NMR signal.

Solutions of alkali metals in ethers received comparatively little attention compared with amine solutions.

Catterall [37] studied the EPR spectrum of saturated potassium solutions in tetrahydrofuran (THF). The spectrum consisted of two quartets and a central singlet due to coupling with the two naturally occurring isotopes of potassium and the isolated solvated electron respectively.

A very recent investigation of alkali metal amide solutions by NMR [36] showed a sharp (8-15 Hz) signal in the case of sodium solutions; thus far no signals have been reported from other alkali metals. The sodium signal was attributed to the Na anion based on the chemical shift results and no Na signal was observed.

Solutions of alkali metals in hexamethylphosphoramide (HMPA) are very interesting and worth mentioning. Although the high dielectric constant of HMPA (29.6 at 298 K) insured that only a single EPR line was found [38], similar to those in metal-ammonia solutions, the presence of a metal-dependent absorption band in the visible region [39] established a strong link with amine and ether solutions. The ²³Na NMR spectrum of Na-HMPA solution showed a single peak corresponding to Na and again no Na peak could be detected [40]. Attempts to observe other alkali metal anions have been unsuccessful in alkali metal-HMPA solutions [36]. When alkali metal-HMPA solutions were quenched

to liquid nitrogen temperature, glassy blue solids were formed. EPR studies [41] of these quenched solutions showed different behavior from that of the unfrozen solutions. The existence of several discrete localized excess electron states similar to those in amines and ethers was observed.

In summary, the results discussed above are understandable in terms of the quantitative picture first proposed by Dye [35] and used by Catterall [41]. In alkali metal solutions a simple ion-pairing theory predicts the equilibrium

$$M_s^+ + e_s^- \rightleftharpoons M_s^+ \cdot e_s^- (M_s)$$
 (I.2)

Two important factors govern the lifetime of the monomeric species $M_S^+ \cdot e_S^-$. They are the electron-nuclear correlation time, τ_M , which is a function of the electron relaxation rate and the dielectric constant of the solution and the hyperfine splitting (hfs) constant A, which is a function of the electron spin density at the nucleus. These two factors dictate whether or not a resolved metal hyperfine coupling is observed in EPR. In solvents of high dielectric constant (NH $_3$,HMPA), the average lifetime of M_S is short compared to the inverse of the hfs constant, i.e. $\tau_M^+ A << 1$. Therefore, a time average signal from e_S^- and M_S occurs and only a single absorption line is observed. In the low dielectric constant media such as amines and ethers, $\tau_M^+ A >> 1$ and signals from both

paramagnetic centers are observed. In addition, the presence of electronic paramagnetism will give rise to an extremely efficient electron-nuclear relaxation mechanism, hence the nuclear spin relaxation will be so rapid in amine and ether solvents that the NMR lines are broadened beyond detection. Figure 1 shows the classification of EPR results in alkali metal solutions on the basis of the product of $\tau_{\text{M}} \cdot A$ [41].

C. Metal-Ammonia Compounds

The phase diagrams of metal-ammonia systems [1] have a very remarkable feature, that is, the presence of a deep eutectic which reflects the appearance of crystalline compounds upon freezing saturated solutions of Li, Ca, Ba, Sr, Eu and Yb. These compounds have the composition Li(NH₃)₄ and M(NH₃)₆, where M = Ca, Ba, Sr, Eu and Yb [42]. The metallic nature of these compounds arises from the loss of one, in case of Li(NH₃)₄, and two, in case of M(NH₃)₆, electrons to the conduction band [43]. The ammonia molecules act as space-filling diluents to increase the metal-metal separation relative to that of the pure metal. Therefore, these compounds have large ionic radii and hence low electron density. Thus, they were classified as low-electron density metals or "expanded metals".

The alkaline earth hexaammines, $M(NH_3)_6$, are characterized by highly unusual structures [44]. They crystallize in a body-centered cubic (bcc) structure with the hexaammine

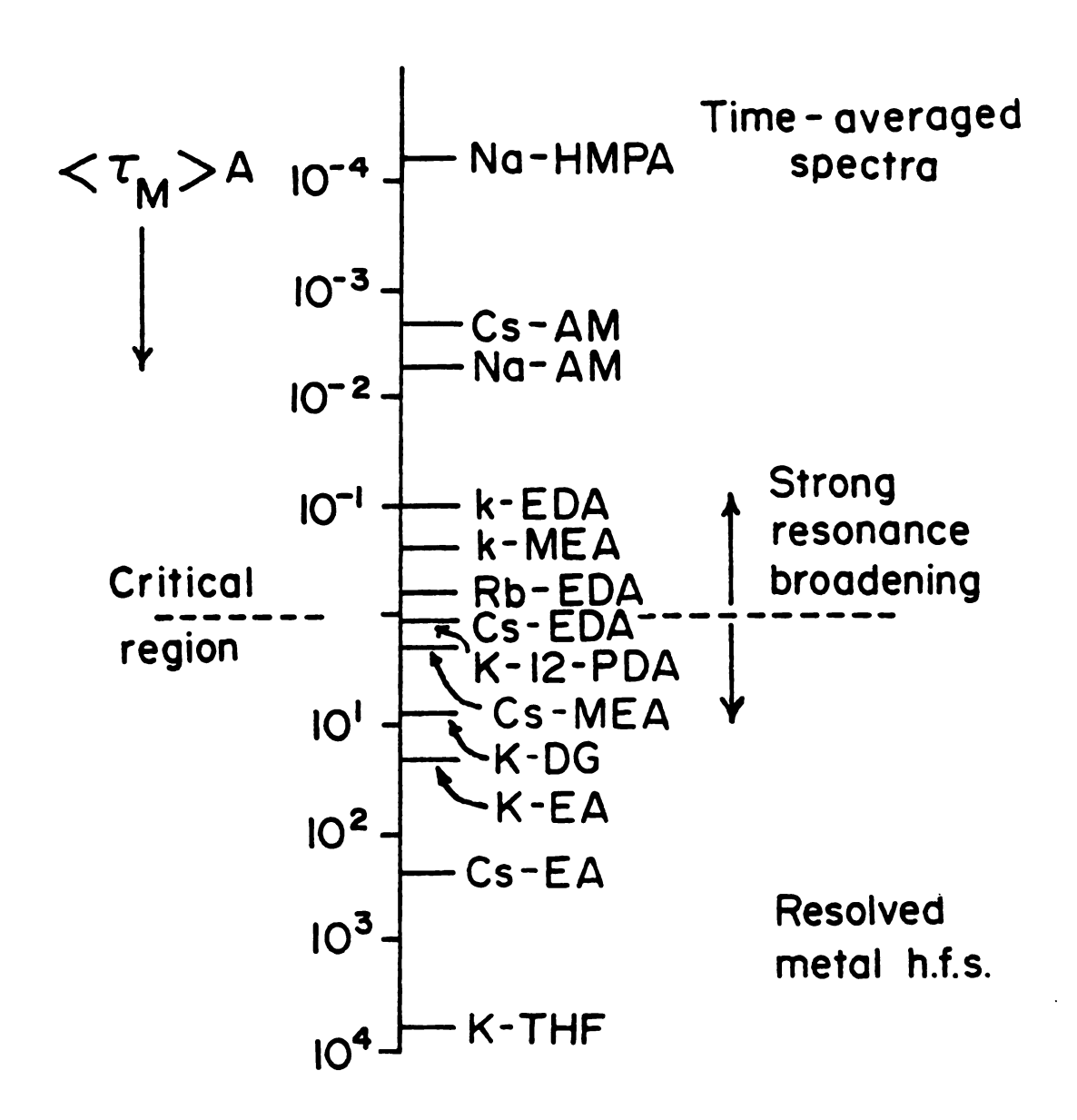


Figure 1: Classification of EPR spectra (~296 K) of fluid metal solutions on the basis of the product $\langle \tau_M \rangle_{A_{1SO}}$: THF = tetrahydrofuran, EA = ethylamine, 1,2PDA = 1,2-propanediamine, EDA = ethylenediamine, AM = ammonia [41].

complex located at each lattice site. The metal center is octahedrally coordinated to six nitrogen atoms of the six ammonia molecules. Sr(NH3)6 and Ba(NH3)6 undergo phase transitions near 40 K to rhombohedral and trigonal structures respectively, while $Ca(NH_3)_6$ showed no structural change down to 4 K. Powder neutron diffraction studies [45] highlight the unique structural aspects of these compounds. The fully deuterated calcium compound, Ca(ND3)6 showed highly distorted, nearly planar ammonia geometry in which there are two inequivalent sets of deuterons. One of the three N-D distances is ~0.1 Å shorter than the normal distance in pure ND_3 (1.00 Å). The other two N-D distances are extremely long (~1.4 Å). Also, the "pseudo-trigonal" axis of the ND3 molecule is not coincident with the metal-nitrogen bond but rather deflected by ~13°. Proton NMR studies of hexaammines [43] showed two linewidth narrowings in the range of 20-150 K. The unusual weak narrowing in the proton linewidths of $Ca(NH_3)_6$ in the range of 60-80 K and 70-100 K in the case of $Ba(NH_3)_6$ was observed previously for pure solid ammonia and was attributed to the transition from quantum tunnelling to thermally activated rotation of ammonia molecules [45]. Another strongnarrowing transition was observed for Ca(NH3)6 in the temperature range 100-130 K and, for $Ba(NH_3)_6$, above 140 K. This transition was interpreted in terms of rapid diffusion of thermally activated ammonia molecules. EPR studies of hexaammines [46,47] showed that a Dysonian line shape was

observed for Ca(NH3)6 and Sr(NH3)6, similar to concentrated alkali metal ammonia solutions, thus indicating metallic behavior. Although Ca(NH3)6 retained its line shape as the temperature was lowered, Sr(NH3)6 showed a transformation to a Lorentzian line shape as the temperature decreased to 8.5 K. This reflects electron localization in the $Sr(NH_3)_6$ compound where lowering the temperature tends to freeze out the conduction electrons and creates a small concentration of localized moments. One the other hand, the Ba(NH3)6 compound showed no EPR signal. Magnetic susceptibility measurements of hexaammines [48] showed strong temperature dependent susceptibilities. susceptibility of $Ca(NH_3)_6$ went through a maximum at about 10 K, a broad minimum at about 120 K and increased rapidly above 120 K. In all the temperature ranges the compound showed more paramagnetism than expected on the basis of the free electron model. In contast, $Sr(NH_3)_6$ and $Ba(NH_3)_6$ were essentially diamagnetic showing rapid reduction in the susceptibility as the temperature was lowered.

The compound Lithium tetraammine, $\text{Li}\left(\text{NH}_3\right)_4$ crystallizes from saturated lithium-ammonia solution. It exists in at least two crystalline forms. The low temperature structure was first thought to be hexagonal. However, neutron diffraction studies of $\text{Li}\left(\text{ND}_3\right)_4$ [49] showed that the compound has a body-centered cubic structure with $\underline{a}=14.80$ Å below 30 K, increasing to 15.03 Å at 85 K. The results were the same for the compound $\text{Li}\left(\text{NH}_3\right)_4$ except for the presence of an additional

phase above 82 K that was not observed for Li(ND3)4. This phase is cubic with a = 9.55 Å. However, Sienko and Stacy [50] re-examined the structure of $Li(NH_3)_4$ and suggested that the phase which forms between 82 and 25 K is also cubic with a = 14.93 Å while below 25 K a superstructure with period 2a is formed. Magnetic susceptibility studies [51] of $Li(NH_3)_A$ supported the presence of three solid phases. The susceptibility at high temperature (above 82 K) showed a temperature independent paramagnetism, characteristic of a metallic Between 82 and 25 K, the susceptibility was system. lower than that of the phase forming above 82 K but increased with decreasing temperature as expected for Curie-Weiss type of paramagnetism, indicating electron localization. The maximum susceptibility was achieved at about 25 K and then decreased with the formation of another phase below 25 K indicating an antiferromagnetic interaction. The $Li(ND_3)_4$ compound showed similar behavior except that the transition at 82 K was absent.

Clearly, metal ammonia compounds are very interesting systems which provide rich information about the nature of the non-metal to metal transition. An understanding of the compounds might help to understand and solve the "dilemma" of metal-ammonia solutions, and hence more studies are required.

D. Alkali Metal Anions (M⁻)

Our knowledge of the chemistry of alkali metals tells us that they are exceptionally good electron donors and form the +1 oxidation state with an inert gas configuration. However, the existence of the -1 oxidation state in the gas phase was known for over 35 years [52]. Golden et al. [53] were the first to propose that M is a major species in alkali metal-ammonia solutions. However, there was no evidence for its existence, probably because of the fact that ammonia is "too good" a solvent so that it greatly enhances the dissociation of M to the solvated cation and solvated electrons. In contrast, the presence of the metaldependent band in the optical spectra of alkali metal-amine and ether solutions established the existence of M in these solutions. However, the complete proof was provided when Dye et al. [54,55] reported the fingerprint NMR spectra of Na, Rb and Cs in solutions in amines and tetrahydrofuran. The ²³Na NMR spectra of sodium solutions containing the added complexing agent cryptand 222 showed the presence of two sodium peaks. The chemical shifts of both peaks were remarkably solvent independent which was in contrast to that of the solvated sodium cation. The chemical shift of the low field (high frequency-less shielded) peak was the same as for sodium in Na⁺C222.I⁻. The other peak had a nearly identical chemical shift to that of the gaseous sodium anion and an extremely narrow linewidth (<3 Hz in THF), which

attested to the highly spherical and well shielded nature of the species. These two peaks were assigned to the sodium complex cation and the sodium anion. The absence of any solvent-induced paramagnetic shift in the case of the Na peak indicated that the 2p orbital was well shielded from the interaction with the solvent by the completely filled 3s orbital. The Rb and Cs spectra in these three component systems were similar to that of Na. Recently, it has been shown [56] that Na can be formed in the presence of a reducible group such as carbonyl in sodium-diethylacetamide solution. The isolation of the crystalline compound Na C222.Na by Dye et al. [57,58] provided the final proof of the existence of the alkali metal anion as a stable, long lived anion in the gas, fluid and solid phases.

E. Trapped Electrons in Solids

The phenomenon of "excess" electrons or "electron trapping" in solids is known to occur in both ordered (F-centers) and disordered (aqueous and organic glasses) systems.

In crystalline materials [59] such as alkali halides and hydrides "excess" electrons can be brought into the system by irradiation of the crystal with high energy photons or particles, by electrolysis at high temperature, or by heating the salt in an alkali metal atmosphere. The electrons are trapped at anion vacancies; hence, a low

concentration of trapped electrons is expected. It was found that only 0.1% of the radiation-produced electrons are trapped in crystalline alkali halides. Optical spectra of F-centers [60] in alkali halide crystals showed broad bell shaped absorption bands. The positions of the bands were dependent on temperature, pressure and alkali halide used. Ivey [61] correlated the transition energy of the trapped electron in F-centers in salts with the NaCl structure to the interionic distance a by means of a simple emperical equation known as the Möllow-Ivey relation:

$$v_{\rm m} = 17.6 \ \underline{a}^{-1.84}$$
 (I.3)

• . •

where $\nu_{\rm m}$ is the frequency of the absorption maximum in eV. Equation (I.3) predicts a shift to higher energy (lower wavelength) with decreasing interionic distance. Indeed, the values of $\nu_{\rm m}$ vary from 250 nm for LiF (smallest <u>a</u>) to 785 nm for CsI (largest <u>a</u>). The EPR of F-centers [59] showed two kinds of spectral lines mainly due to electron interaction with the nearby nuclei. The first type, which applies to most of the alkali halide F-centers, consists of a single, broad, Gaussian shaped line without any further structure. The linewidth varies from 47 to several hundred Gauss. The second type showed a resolved hfs with a discernible number of components on the order of 10 to 100. The g-values are slightly decreased from that of the free

electron indicating a weak interaction of the electron with its surroundings and hence very small spin-orbit coupling to the lattice. The important feature of the EPR spectra was that they are independent of temperature, method of preparation and the concentration of the centers. However, further irradiation of F-centers leads to the formation of aggregate centers for which the EPR spectra were different. For example, irradiation of F-centers in KCl crystals with light in the F-band gave an EPR line which was narrower and less strongly saturated than the undisturbed F-centers. ENDOR studies of F-centers [62,63] gives a great deal of information about the electron nuclear interaction through the dependence of the spectral patterns upon the crystal orientation and the further quadrupole splitting of the Therefore, the hfs constants to nuclei in the first and higher order coordination shells, the elements and axes of the anistropic hfs and the quadrupolar interaction tensor could be determined.

In contrast to the F-center, where the electrons are trapped in pre-existing traps, aqueous and organic glasses provide very rich media for trapping high concentrations of electrons at low temperatures [64]. The discovery of electron trapping in water as a transient optical spectrum in the visible by pulse radiolysis [65] opened the door to a new field of study of electron trapping in polar and non-polar matrix glasses. In a similar manner to F-centers, electrons can be trapped in aqueous and organic glasses by exposing

the latter to high energy ionizing radiation at low temperatures [66]. The change in the optical and magnetic resonance properties with time suggests that the process of electron trapping in matrix glasses can occur in two stages [67]. The first stage involves the localization of the "presolvated" electron which depends upon the relative energies of the conduction electron level of the medium (V_o) and the total ground state energy of the localized electron relative to vacuum (E_+) . Kevan [68] suggested that the criterion of electron localization in glassy matrices is that $E_+ < V_0$. The second stage in electron trapping is the solvation of the electrons, in which rearrangements of the surrounding solvent molecules take place by the induced electron polarization. To study a two step mechanism of electron trapping requires very delicate techniques on the pico- and nanosecond time scales as well as liquid nitrogen and helium temperatures. Kinetic changes associated with the conversion of the pre-solvated to the solvated electron have been studied by pulse radiolysis and photoionization in glasses [64]. It was found that, regardless of the nature of the medium, the pre-solvated electron absorbs light in the infrared with λ_{max} about 1500 nm, while the solvated electron absorbs further in the blue with λ_{max} ranging from near the infrared to the visible. In contrast to the situation in liquids, disordered glasses show that the decay of the pre-solvated electron band is faster than the growth of the solvated electron band and the process

is not first order as in liquid [68]. The optical absorption results were interpreted in terms of the two mechanisms known as the molecular reorientation and trap-redistribution mechanisms [69]. In the first mechanism the electrons are trapped initially in shallow traps and by means of the strong electric field produced by the electrons, the molecular dipoles reoriented themselves to form deeper traps. In the second interpretation, it was postulated that both shallow and deep traps already exist in glassy matrices. Initially the electrons are trapped in shallow traps and by thermal excitation the electrons are excited out of the shallow traps and preferentially redistributed into the deeper ones. EPR spectra of trapped electrons in glassy matrices [69] consist of a single Gaussian line with nearly the free electron g-value. The EPR line is usually superimposed on the radical spectrum associated with the matrix molecules. The observed Gaussian line is consistent with inhomogenous broadening due to unresolved hfs of the protons. This is verified by the change in the linewidth of EPR line upon isotopic substitution of the protons by deuterons. In amine glasses, the EPR linewidth depends upon the type of amine used. It was found that the linewidths range from 24 to 25 Gauss for primary amines, 6 to 14 Gauss for secondary amines and 3 to 4 Gauss for tertiary amines. similarity of the linewidth between tertiary amines and hydrocarbons suggests that the nearest neighbor atoms to the trapped electrons in tertiary amine glasses were the

alkyl group while the significant line broadening in primary and secondary amines indicates interactions with the nitrogen nucleus. Kevan and co-workers [70,71] studied the solvation process of pre-solvated electrons in polar and nonpolar matrix glasses by using the ENDOR technique at the proton They found that the matrix proton ENDOR linefrequency. widths were smaller when irradiation was carried out at 77 K instead of 4 K. The linewidth analysis showed that the increase in the average electron-proton distance upon warming the sample from 4 K to 77 K is mainly due to the solvation process. However, most of the information about the structure of the solvated electron in glasses came from the analysis of electron spin echo modulation [72,73]. Two pulse and three pulse electron spin echoes were applied to the solvated electron in CH₃CH₂OD, CH₃CD₂OH and CD₃CH₂OH. The orientation of the solvent molecules around the electron was determined by selective deuteration without simultaneously generating proton modulation. results showed that there were four ethanol molecules in the first solution shell around the electron with electrondeuteron distances of 3.8, 3.3 and 2.2 Å for CD_3 , CD_2 and OD respectively. For 10 M aqueous NaOH glasses, only water molecules were found in the first solvation shell and the electron was octahedrally coordinated to six water molecules with the water OH bond directed towards the electrons.

F. Macrocyclic and Macrobicyclic Diamine-Polyethers

The period 1967-1969 brought the discovery of two new classes of multidintate polyether ligands which opened the door to a new field of study in the coordination chemistry of alkali and alkaline earth metal compounds. These two classes of ligands are macrocyclic polyethers known as "crown ethers" and macrobicyclic diamine polyethers known as "cryptands".

Pedersen [74] synthesized 33 cyclic polyethers which contained 9 to 90 atoms including 3 to 20 oxygen atoms in the ring. The lower members of this class, which contain 4 to 10 oxygen atoms, formed stable complexes with the cations of alkali and alkaline metal salts. The complexation with metal cations was verified by the changes in the infrared and ultraviolet spectra of the ligands, by the increasing solubility of the metal salts in organic solvents, and, in many cases, by the isolation of crystalline solids. The discovery of crown ethers was followed by the synthesis of macrocyclic diamine polyethers by Lehn et al. [75]. This class of ligands contains three polyether strands which are joined by two bridgehead nitrogens. The IUPAC names of the compounds in these two ligand classes are quite lengthy so that trival names were proposed for them. For crown ethers, the following nomenclature procedure was suggested: (a) the number and kind of hydrocarbon ring, (b) the total number of atoms in the ring, (c) the class name, crown and

(d) the number of oxygen atoms in the ring. For example the ligand 2,3,11,12-dibenzo-1,4,7,10,13,16-hexaoxa-cyclooctadeca-2,11 diene is referred to simply as dibenzo-18crown-6. For macrobicyclic diamines, the nomenclature starts with (a) the class name, cryptand or c, (b) the number of oxygen atoms in each of the three polyether strands, and (c) the kind of hydrocarbon ring. example, the compound 4,7,13,16,21,24-hexaoxa-1,10diazabicyclo(8,8,8)hexacosane is simply cryptand 222 or C222. The structures of the two ligand classes are different. Crown ethers are two dimensional systems with distorted D_{nd} symmetry. The 18-crown-6 molecule has a lower symmetry than D_{3d} with the three nonequivalent -O-CH2-CH2-O-units. In contrast to crown ethers, cryptands are three dimensional ligands and their conformations depend on whether the nitrogen lone pair is directed towards the cavity (endo) or outside the cavity (exo) [76]. Three comformations are known for cryptands. These are exo-exo, exo-endo and endo-endo. Both crown ethers and cryptands form stable complexes with alkali and alkaline earth metal cations in polar and nonpolar media [77-79]. The strong cation complexation versus cation solvation determines whether stable complexes will be formed or not. Pedersen [74] and Izatt [80] showed that the cation radius and the cavity size of the crown are the most important governing factors that determine the complex stability. The "best" stable complex forms when the cavity

and cation sizes match. For example, the selectivity of 18-crown-6 for the K⁺ cation was demonstrated by the formation of a complex 10 to 100 times more stable than the corresponding Rb⁺ and Cs⁺ complexes.

Crystalline compounds of alkali and alkaline earth salts that contain the crown ethers or cryptands were isolated [81]. For cryptand systems, only the 1:1 complexes were formed regardless of the cation valency. Weiss et al. [82] isolated crystalline compounds with the formulae LiC211.I, NaC222.I, KC222.I, RbC222.SCN.H2O and CsC22.SCN.H2O. Their structures were determined by X-ray diffraction studies, which showed that the metal cation is completely enclosed in the cryptand cavity. This reflected the great flexibility of the cryptand and its ability to adapt, to some extent, its molecular cavity to the cation size. The compounds LiC2ll.I and KC222.I have tetragonal and hexagonal structures respectively, while RbC222.SCN.H2O and CsC222.SCN.H2O have monoclinic structures. NaC222.I apparently has a hexagonal structure but the results of X-ray diffraction analysis showed that the hexagonal structure was a twin component that contained two molecular species in a trigonal unit cell. In contrast to cryptand systems, 1:1 and 1:2 complexes of alkali metal salts with crown ethers were isolated. Crystalline compounds of the formula $M \cdot 18$ -crown-6.SCN, where M = K, Rb, Cs were isolated and analyzed [83-85]. X-ray diffraction studies showed

that they have monoclinic structures with approximately Dad symmetry [86]. In these compounds, the three-O-CH₂-CH₂-Omoieties of the ligand are equivalent; all the torsion angles about C-C bonds are close to 65° and those about the C-O bonds are close to 180°. The six oxygen atoms of the 18-crown-6 alternated about 0.2 Å above and below their mean plane and also the oxygen-cation distances were unequal. For K.18-crown-6.SCN the K⁺ cation is sitting exactly at the center while in the cases of Rb and Cs complexes the cations are displaced from the mean plane by 1.19 Å for Rb and 1.44 Å for Cs. The out-of-plane cations (Rb and Cs are directed towards each other and are bridged by the two thiocyanate ions. The crystalline compound Na.18-crown-6.SCN was formed only in the hydrated form [87]. The structure is monoclinic but the 18-crown-6 conformation is remarkably distorted because the Na cation is too small to fit the cavity. Five of the six oxygen atoms are nearly coplanar, while the remaining oxygen is drawn out of the mean plane of the other five oxygen atoms by 1.95 Å to give a somewhat irregular pentagonal pyramidal coordination of the Na tion. A water molecule is coordinated to the opposite apex of the bipyramid. An important difference between cryptand and crown ether compounds is the distance between the metal cation and the anion. In cryptates the cationanion distances are larger than those in crown ether complexes. This indicates that the open axial position in

the crown ether systems allows much more cation-anion interaction than in cryptand compounds.

Recently, another new class of polyethers was synthesized, which is known as "Lariat" ethers [88-91]. The "Lariat" ether contains a flexible donor group side arm which can be attached either to a carbon atom of the ring (carbon-pivot) or to a nitrogen atom that replaces one of the ether oxygens (nitrogen-pivot). In general, "Lariat" ethers greatly enhance the cation binding to the crown ring through dynamic additional interaction of the flexible side arm with the macro-ring cation. It was found that nitrogen-pivot "Lariat" ethers are much more effective in cation binding enhancement than were the cation-pivot ethers and both form stronger complexes than the simple macrocyclic systems.

G. Alkalides and Electrides

After the discovery of crown ethers and cryptands,

Dye and co-workers used them to expand the concentration

range of alkali metals in amine and ether solutions. The

results of Dye et al. [55,57] confirmed the great selectivi
ty of crown ethers and cryptands towards alkali metal

cations and the formation of genuine alkali metal anions

in solutions. Their work led to an important question at

that time. For this three component system, especially

at high concentration, what was the nature of the solid

in equilibrium with the solution? Before answering

this question, two important experimental facts should be considered: (1) when a 0.2 M sodium solution in ethylamine containing the added complexing agent cryptand 222 with mole ratio R = 2 (R = moles of metal/moles of complexant) was cooled, a crystalline golden compound of stoichiometry Na₂C222 spontaneously appeared [92]; (2) very reactive paramagnetic blue powders were formed upon solvent evaporation from solutions of alkali metals and C222 with R = 1 [93]. Characterization of the golden crystals and the blue powders led to the classification of these compounds as alkalides and electrides respectively. They can be defined as compounds in which the alkali metal cation (M⁺) is encapsulated in the cage of the polyether (L) and the negative ion is either the alkali metal anion (N^-) [alkalide, $M^+L_n \cdot N^-$] or the trapped electron (e_t^-) [electride, M⁺L₁.e⁻].

The parent alkalide compound, $Na^+C222.Na^-$, was stable for a long period of time in vacuum or in inert atmosphere below 0°C. However, it was sensitive to air, decomposed by water to yield H_2 gas and thermally melted at 83°C to produce sodium metal and C222 [93]. Figure 2 shows the ion-packing in crystalline $Na^+C222.Na^-$. It can be described as closest-packed sodium cryptate cations with the sodium anion occupying the octahedral holes. The unit cell is hexagonal with $\underline{a} = 8.83$ Å and $\underline{c} = 29.26$ Å. The sodium anions form parallel planes perpendicular to the three-fold axis. The sodium cation inside the cryptand

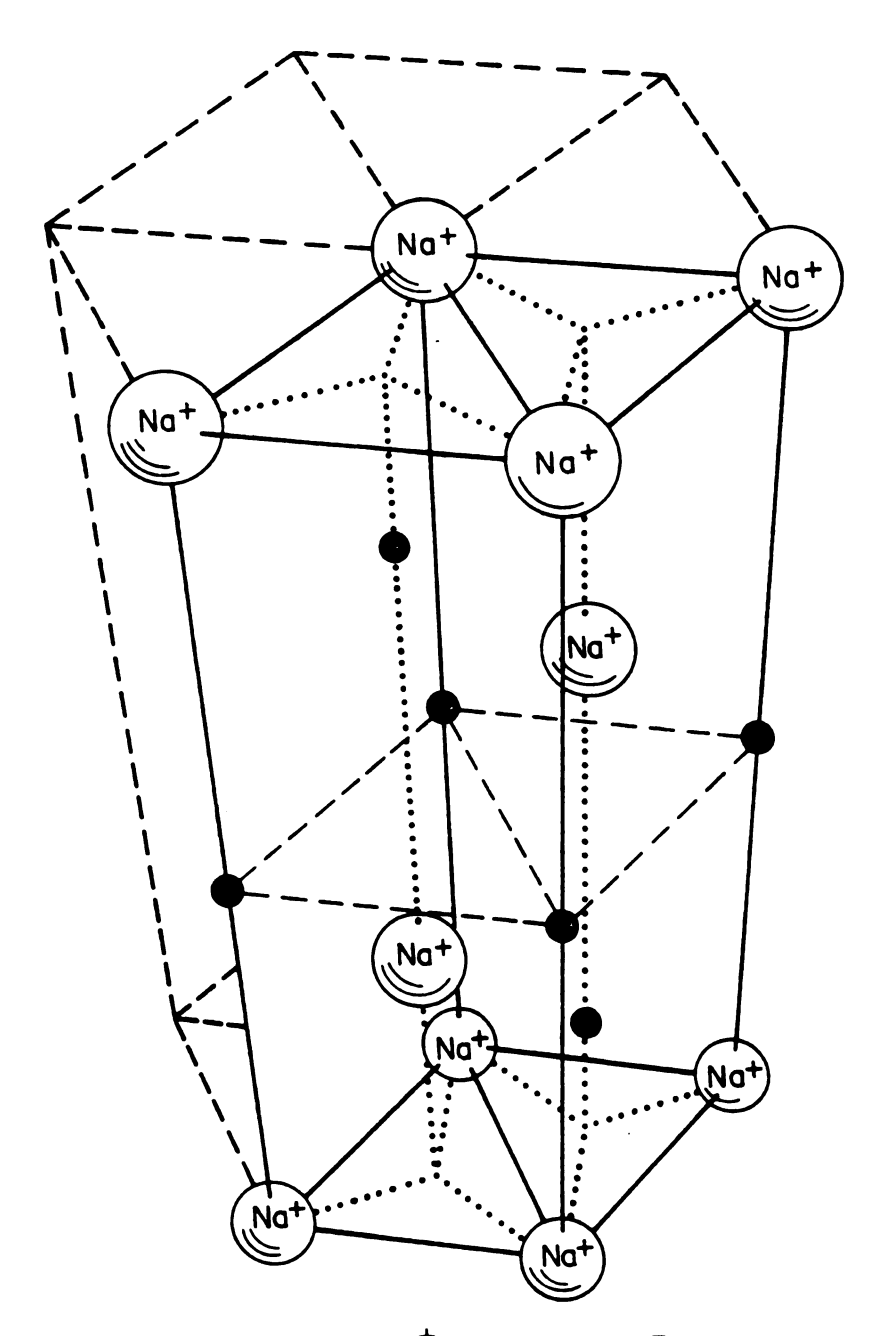


Figure 2: Packing of Na⁺C222 and Na⁻ (solid circles) in the crystalline solid Na⁺C222.Na⁻ [30].

has a closest distance 7.06 Å to the sodium anion. Although Na⁺C222.Na⁻ crystals have a metallic appearance, magnetic and electrical measurements [57] have shown that they are diamagnetic and semiconducting with a 2.5 eV band gap.

Dye et al. [94] explored the synthesis of other crystalline alkalides by using cryptands and crown ethers. The analysis of some of the crystals was in good agreement with the proposed stoichiometry. On the other hand, some crystals showed poor agreement with the proposed stoichiometry due to co-precipitation of metal or contamination with decomposition product. The optical spectra of solvent free thin films of homonuclear alkalides M⁺L.M⁻, where L is C222, showed the characteristic peaks for Na⁻, K⁻, Rb⁻ and Cs⁻ with the absorption maxima occurring at wavelengths very close to those of M⁻ in ethylenediamine [95].

At the beginning of the present research, no crystalline electrides had been synthesized and only powdered electrides prepared by solvent evaporation had been studied. Three electride systems had been studied by optical spectroscopy, magnetic susceptibility and EPR measurements. These systems are Li-C211 [96], K-C222 [97] and Cs-18C6 [98].

The properties of the Li-C2ll system depend upon the mole ratio R. Optical spectra of dry films of Li-C2ll with R < 1.15 showed low absorption in the infrared region below 4,000 cm⁻¹, peaks at 5,000 and 7,000 cm⁻¹ and a shoulder on the high energy side at ~12,000 cm⁻¹. These

results indicate that the electrons were trapped at different nonequivalent sites. On the other hand, a "plasma" type of absorption spectrum, characteristic of conduction electrons, was observed for films with R=2.

EPR results confirmed those of the optical spectra. Samples which showed multiple absorptions in the optical spectra also showed multiple EPR signals below 30 K, while those with "plasma" spectra showed highly asymmetrical (Dysonian) line shapes. In all cases the g-values were near or at the free electron g-value, which suggests a weak interaction between the electrons and the complexed cation. The linewidths of the EPR lines were narrow with ΔH_{n-n} only about 0.5-0.6 Gauss at about 60 K, but the linewidth increased gradually with decreasing temperature to 1.5 Gauss at 3 K. The change of the EPR line intensity with temperature suggests that a spin pairing process is taking place at low temperatures. The magnetic susceptibility of the Li-C2ll system [99] showed a substantial spin-pairing in the temperature range of 20 to 70 K depending upon the mole ratio R. At high temperatures the electronic susceptibility obeyed the Curie-Weiss law and it reached a maximum, then decreased towards zero at liquid helium temperatures. The results suggest that a nonmetal to metal transition may occur in the Li-C2ll system between R = 1.15 and 2.

The optical spectra of dry films of K-C222 with R = 1 showed time-dependent spectra. Initially two peaks at

11,000 and 6,500 cm⁻¹ were observed and attributed to K⁻ and the trapped electron (e_t) respectively. With time, the trapped electron peak grew at the expense of the K⁻ peak which finally decayed to a shoulder. The final spectra of the "annealed" film showed a "plasma"-type spectrum. When R was equal to 2, only the K⁻ peak was observed. EPR spectra showed an asymmetrical line with a g-value equal to 2.0023 and the linewidth varied from 0.4-0.6 Gauss at 4 K to 0.1-0.4 Gauss at 181 K. It was found that only ~0.024% of the total spin contributes to the EPR signal, indicating that most of the electrons are paired.

The Cs-18C6 system showed a variation from localized to delocalized electron states upon changing the mole ratio R. Optical spectra of dry films with R equal to 0.5 and 1 show the trapped electron peak at 6,500 cm⁻¹ while one with R=1.5 shows a major peak at 10,500 and a minor one at 8,000 cm⁻¹. The former peak was attributed to Cs⁻ while the latter was due to trapped electrons. Films made with R=2 give "plasma"-type spectra. Magnetic susceptibility and EPR studies of Cs-18C6 systems show two kinds of behavior which confirm the results of the optical studies. For R=0.5 and 1, weak asymmetrical EPR lines and very small paramagnetism were observed which could be fitted to electron-trapping in two noninteracting Curie-Weiss sites. In contrast, powders with R=2 show only a small temperature-independent paramagnetism and very

broad EPR linewidths with ΔH_{p-p} equal to 30 Gauss at low temperatures reducing to 6 Gauss above 140 K.

The preparation of powdered electrides by solvent evaporation suffers from a number of disadvantages, such as contamination of the powder with non-volatile decomposition products, non-uniformity of the powder because of excess metal or complexant, and the precipitation of non-equilibrium forms whose properties change with time. It is difficult therefore to form a quantitative picture of these systems. However, one can qualitatively conclude that electrides exhibit properties that depend upon the electron density of the system. These properties range from electron localization and spin pairing to electron delocalization and near-metallic behavior.

H. Objectives of the Present Work

In solid state chemistry research, a major goal is the search for new compounds, followed by their characterizations. However, electrides and alkalides with their unusual anion formation are very interesting compounds with diverse properties. Their nature and structure can be characterized by analytical and spectroscopic techniques. Specifically, magnetic resonance studies (EPR and NMR) with their great ability to determine intrinsic "local" character permit the study of the microscopic environment of specific constituents of these ionic salts. The

objectives of the present work can be summarized as follows:

- (1) Attempts to prepare and characterize crystalline alkalides from elemental alkali metals with 18-crown-6 as a complexing agent.
- (2) The search for a single crystal electride had been a distinct goal for a long time in our laboratory. Accordingly, attempts were made to prepare and characterize crystalline electrides by using cesium and rubidium metals with the complexing agents 18-crown-6 and cryptand 222. The syntheses of crystalline alkalides and electrides will be discussed in Chapter III.
- (3) The distinction between species in the case of heteronuclear alkalides such as M^+L_n . N^- or N^+L_n . M^- , and differentiating between different chemical formulae for a given stoichiometry were two problems in our laboratory. Therefore, the use of the magic angle sample spinning (MASS) NMR technique as a powerful tool to identify and distinguish species in crystalline alkalide and electride compounds will be very useful. The MASS-NMR results will be discussed in Chapter IV.
- (4) Electron-electron and electron-cation interactions in alkalides and electrides can be studied by EPR and magnetic susceptibility techniques. The results will be shown in Chapter V.
- (5) Conclusions drawn out of the present work and suggestions for future work will be discussed in Chapter VI.

CHAPTER II

EXPERIMENTAL

A. Materials

1. Alkali metals

Lithium metal was an Alfa Ventron product with 99.9% metallic purity. It was received as ribbon under argon and treated in an argon-filled inert atmosphere box (drybox) [100]. The lithium ribbon was cut into small pieces with clean Cu-Be knives and weighed on a model RTL Cahn electrobalance inside the dry-box. The small lithium metal pieces were then loaded into thin walled glass tubes of 15 cm length and 0.5 cm 0.D. which were sealed to Kontes Teflon high vacuum valves. After removal from the dry-box, the tubes were connected to the vacuum line and vacuum seal-offs were made at a pressure of ca. 10⁻⁵ torr. Only shiny, silver-colored pieces were used in electride and alkalide syntheses.

Sodium, potassium and rubidium metals were Alfa

Ventron products and cesium was a gift from the Dow Chemical

Company. The metals were supplied in glass ampoules with

breakseals under an argon atmosphere. They were always

transferred under vacuum and were distributed into small diameter tubes with the help of the apparatus shown in Figure 3. The metal ampoules were sealed to the apparatus and the entire system was connected to the vacuum line. At a pressure of ca. 10⁻⁵ torr the breakseal was broken by a clean, glass-covered iron rod. The metal was then heated under vacuum and allowed to run into the three reservoirs. Vacuum seal offs were made at the constrictions and the metals were then heated and distributed into small tubes whose inside diameters had been previously measured.

2. Complexants

When the complexing agents, cryptands and crown ethers were received, they were kept in a freezer at ~-10°C prior to purification and in an evacuated desiccator in the dark at room temperature after purification.

18-Crown-6 (18C6 or IUPAC: 1,4,7,10,13,16-hexaoxa-cyclooctadecane) was purchased from PCR, Inc. or from Parish Chemical Co. and was recrystallized from purified acetonitrile before sublimation. Cryptand 222 (C222 or IUPAC: 4,7,13,16,21,24-hexaoxa-1,10-diazabicyclo[8.8.8]-hexacosane) was vacuum sublimed without recrystallization. 18C6 and C222 were sublimed under vacuum at 60° and 110°C respectively by using a vacuum sublimer (ACE Glass Inc.) which allowed sublimation of ~5 grams at one time.

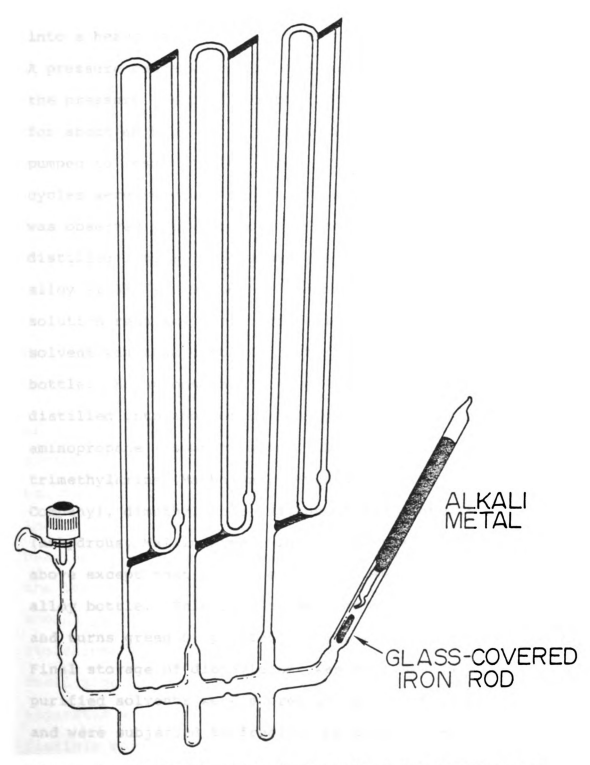


Figure 3: Apparatus for distribution of alkali metal under vacuum.

3. Solvents

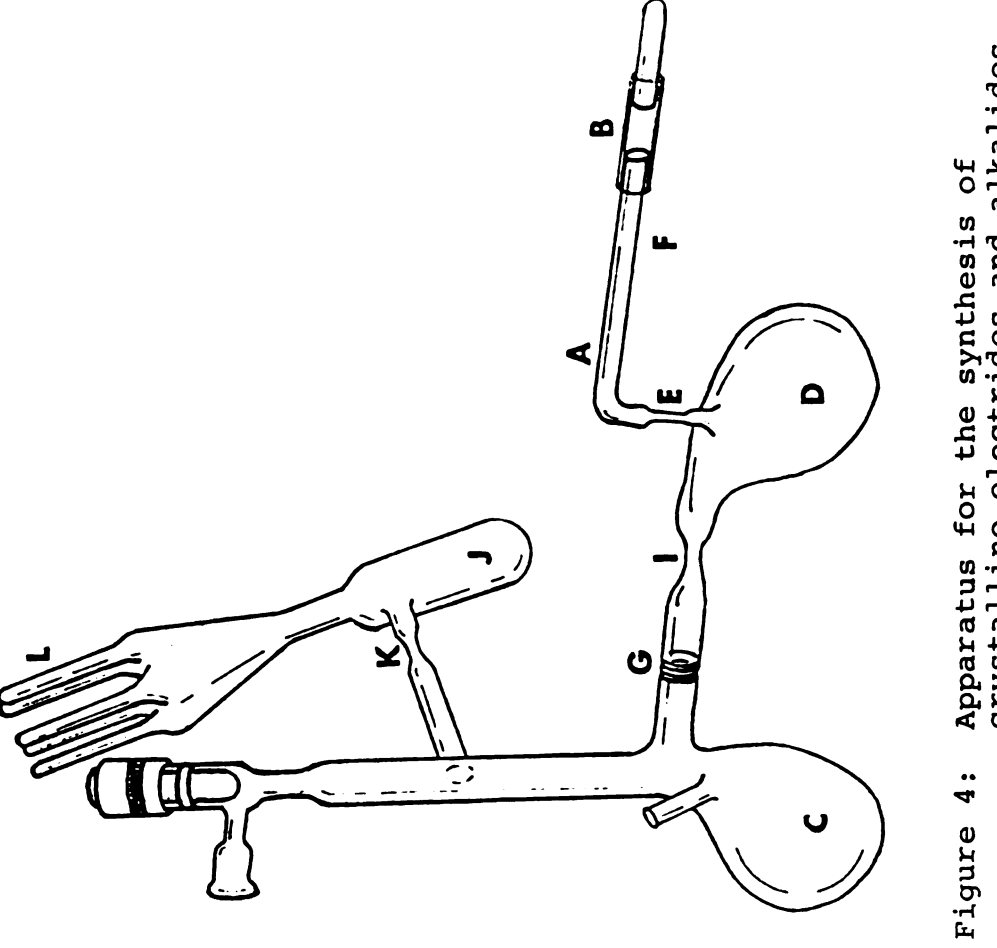
Methylamine (Matheson) (~750 mL.) was first loaded into a heavy-walled bottle over calcium hydride (4-5 gms). A pressure gauge was connected to the bottle to monitor the pressure inside the bottle. The solvent was stirred for about an hour, then frozen with liquid nitrogen and pumped to less than 10^{-5} torr. The stir-freeze-pump cycles were repeated several times until no gas evolution was observed while stirring. The solvent was then distilled into a pre-evacuated bottle that contained Na-K alloy (1:3) (~40 mmoles) and stored overnight. If the solution retained its characteristic blue color the solvent was then distilled into the heavy-walled storage bottle. Solutions that did not show the blue color were distilled into another Na-K alloy and left overnight. 2aminopropane (isopropylamine) (Estman Organic Chemical), trimethylamine (Matheson), n-pentane (J.T. Baker Chemical Company), dimethylether (Matheson) and diethylether (anhydrous, Mallinckrodt, Inc.) were treated as described above except that benzophenone had been added to the Na-K alloy bottle. This reagent acts as a moisture indicator and turns green or purple when the solutions are dry. Final storage of diethylether was over Na-K alloy. All purified solvents were stored in vacuum storage bottles and were subjected to freeze-pump-thaw cycles occasionally before use.

B. Glassware Cleaning

The glassware was first treated with an HF cleaner which contained 28 M HF, acid detergent, HNO₃ and deionized water with 5, 2, 33 and 60 V/V percentage respectively. Following the HF cleaner, the glassware was rinsed immediately, at least five times, with deionized water after which it was partially filled with freshly prepared aqua regia (3 HCl: 1 HNO₃) and left overnight. The glassware was then rinsed several times with deionized water followed by seven rinses with conductance water. Finally, it was dried at ~200°C for several hours.

C. General Synthesis Procedure

The apparatus used in the synthesis of crystalline electrides and alkalides is shown in Figure 4. A measured amount of metal(s) sealed in a calibrated tube(s) which had been scribed with a glass-cutting knife, was introduced into the side-arm A, which was connected to a flexible heat shrinkable Teflon tubing at B. The other end of the Teflon tube was capped with a sealed tube. A weighed amount of the complexant that corresponded to the desired stoichiometry was introduced into the vessel C through a small side-arm that was then sealed off. The entire apparatus was connected to the vacuum line through a flexible metal tube (Cajon Company) and evacuated to ca.



Apparatus for the synthesis of crystalline electrides and alkalides.

the Teflon tube and broken under dynamic vacuum. The broken metal tube(s) was then moved to the constriction E and a vacuum seal-off was made at F. The metal(s) was distilled into chamber D and the metal side-arm A was sealed off at E.

Since lithium metal cannot be distilled, the apparatus was slightly modified to include another side-arm attached to the chamber D. The side-arm had a coarse frit to separate lithium metal from the other metal in chamber D. At a pressure of less than 10-5 torr., an amount of solvent (reaction solvent) [(~10 mls/mmole complexant)] was distilled into the chamber C to dissolve the complexant. The apparatus was removed from the vacuum line and immersed in a dry ice-isopropanol bath at ~-40°C. complexant solution was transferred through a coarse frit G into the metal-containing compartment D. After metal dissolution, a partial evaporation of the reaction solvent was followed by the distillation into D of another solvent(s) (crystallization solvent(s)). The solution was filtered through the frit G into C and cooled to dry ice (-78°C) or acetone-liquid nitrogen (~-92°C) temperatures to precipitate the crystals. When the precipitate had settled, the supernatant liquid was poured into D, frozen with liquid nitrogen and removed by making a vacuum sealoff at I. A washing solvent was then distilled into C and the slurry of liquid and the crystals was poured into the side-arm J. The supernatant liquid was repeatedly poured

into C and distilled back to J to wash the crystals free of excess complexant. Finally, the solution at C was frozen with liquid nitrogen, the crystals were pumped to ~10⁻⁵ torr and a seal-off was made at K. The dry crystals were poured into the sample tubes L that were immersed in liquid nitrogen so that flame-seal-offs could be made. The sample tubes were kept in a freezer at -78°C until needed.

D. Analysis

Because of the tendency of crystalline electrides and alkalides to decompose thermally, elemental analysis was not practical. Instead, a "home-built" analytical scheme was constructed based upon the decomposition reaction of the crystalline compounds with water in a closed vacuum system [100]. The decomposition reactions of electrides and alkalides can be written as follows:

$$M^{+}L_{n}.N^{-} + 2H_{2}O \longrightarrow M^{+} + N^{+} + nL + 2OH^{-} + H_{2}^{+} \longrightarrow$$
 (II.1) alkalide

$$M^{+}L_{n}.e^{-} + H_{2}O \longrightarrow M^{+} + nL + OH^{-} + \frac{1}{2}H_{2}^{+} \longrightarrow$$
 (II.2) electride

The amount of hydrogen evolved, pH titration of the solution, flame emission to detect the metal content

and quantitative proton NMR combine to give the stoichiometry of the compound. The experimental techniques used with this analytical scheme will be discussed below.

1. H₂ evolution

A scribed sample tube was first cleaned by acetone and weighed quickly enough, at room temperature, to prevent sample thermal decomposition. In a glove bag that had been purged several times with dry nitrogen gas, the sample tube was carefully broken and dropped into a preevacuated H2 evolution apparatus. The apparatus used is shown in Figure 5b. It has a large surface area to allow the crystals to spread out. The apparatus was removed while cold from the glove bag and connected to the vacuum line of the hydrogen collection apparatus [100]. The entire system was evacuated to $\sim 10^{-5}$ torr and conductance water, which had been degassed three times through freeze-pump-thaw cycles, was condensed onto the sample at low temperatures. The sample was then allowed to react with water very slowly while it was cold to prevent any thermal decomposition. The hydrogen evolved was pumped manually by a Toepler pump through two liquid nitrogen traps and collected in a known volume pipet. The cycles with a mercury leveling bulb were repeated a number of times until two consecutive readings of the mercury height were the same. The atmospheric pressure

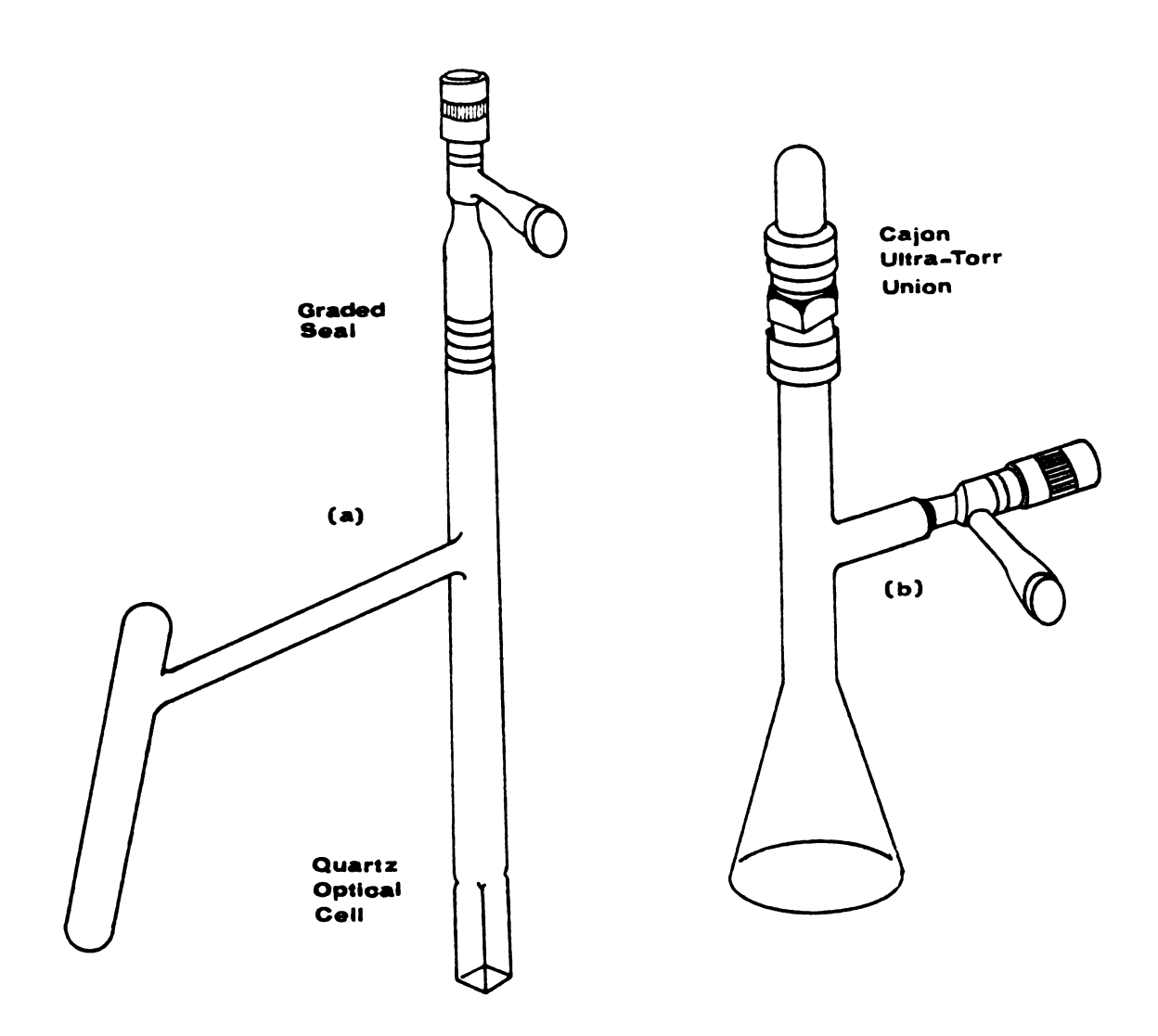


Figure 5: Apparatuses for the optical spectra of thin films (5a) and hydrogen evolution (5b).

and temperature at the pipet were measured and the number of moles of hydrogen was calculated using the ideal gas laws.

2. pH Titration

During hydrogen gas collection water was condensed into the liquid nitrogen traps which left a white-dry residue in the analysis vessel. Under an inert atmosphere, the apparatus was opened and a known volume of standardized HCl solution was added in excess. The solution was then transferred into another container and divided into three portions for pH titration, flame emission and H NMR. A known volume of the first portion was titrated with a standarized NaOH solution by using a pH electrode (Corning, catalog number 476050) and a digital pH meter (Orion Research model 701A) which had been calibrated with buffer solutions. The titration buret, which contained NaOH solution, had a glass sheath which allowed a continuous flow of dry nitrogen gas to prevent CO₂ absorption by the base. The number of gram equivalents of NaOH at the end point is equivalent to that of unreacted HCl from which the number of moles of base in the residue could be evaluated. The broken sample tube was cleaned, dried and weighed so that the mass of the sample could be determined.

3. Flame emission

A known volume of the second portion of solution was diluted to a predetermined volume in order to adjust the concentration on the basis of the expected concentration (ppm) of the metal ion(s) in the sample. A series of standard solutions of the appropriate metal(s) were prepared by dilution of 1000 ppm standard solutions (Aldrich Chemical Company, Inc.). The emission intensity for the alkali metal atoms was read from a digital averager that was connected to the flame emission instrument (Jarrel Ash). The instrument was adjusted for maximum emission at the wavelength of the corresponding element. The emission from conductance water was measured between every reading to give the background or noise level. A calibration curve was constructed by plotting the emission values for the standard solutions against the concentration in ppm. The amount of the metal(s) in the sample could then be determined from its emission value and the calibration curve.

4. Quantitative ¹H NMR:

The number of moles of the complexant was determined by quantitative proton NMR. Samples for NMR measurements were treated in two different ways. First, the third portion of the acidic solution was neutralized with NaOH and allowed to evaporate to dryness in a partially

evacuated desiccator with "Drierite" as a drying agent. The white residue was pumped to insure complete dryness and dissolved in D20. Second, a new weighed sample tube was used and the sample was allowed to react with D20. This method was also used to determine the solvent content, if any, in the crystals. For both samples, a known weight of sodium acetate was added as an internal standard to give approximately a 1:1 mole ratio between the complexant and sodium acetate protons.

H NMR spectra were recorded on a Bruker 250 MHz Fourier transform NMR instrument. In the case of 18C6, the solution gave two NMR peaks corresponding to the CH2-protons of the crown ether and to CH3-protons of the acetate. The areas under the peaks were determined by fitting the line to a Lorentzian line shape with a line fitting program provided by Bruker that gives the linewidth at the half height and the peak amplitude [101]. In the case of cryptand 222, which has multiple peaks for the cryptand protons for which the line fitting routine cannot be used, the areas were determined by the integration procedure.

E. Sample Handling and Instrumental Techniques

Due to the sample sensitivity to temperature, moisture and oxygen all sample handling was carried out in an inert atmosphere glove-bag at low temperatures.

1. Optical absorption spectra

The apparatus used in the optical absorption studies is shown in Figure 5a. It was made of fused silica glass to avoid sodium contamination from Pyrex and consisted of a quartz optical cell, a side-arm reservoir and Kontes high vacuum valve. The clean apparatus was first evacuated to insure complete dryness and brought into a glove-bag that had been flushed several times with dry nitrogen gas. The sample tube was broken in the glovebag while it was cold and a few crystals were dropped into the bottom of the optical cell. The apparatus was removed from the glove-bag and connected to the vacuum line while the optical cell was immersed in a dry ice-isopropanol bath at ~-40°C. After attaining a pressure of less than 10^{-5} torr , methylamine or dimethylether was distilled into the optical cell. The apparatus was removed from the vacuum line and the crytals were shaken until completely dissolved. A portion of the solution was transferred into the side-arm reservoir and the solution in the optical cell was diluted by distilling some solvent into the cell from the reservoir. A thin solvent-free film was made by rapidly shaking the solution in the optical cell at ~-40°C while the bulk frozen solution in the reservoir was kept at liquid nitrogen temperatures. flash solvent evaporation caused film formation by the splashing of the solution onto the cell walls. Because of the nature of this method the film prepared was often not

uniform and it was necessary sometimes to repeat the process to get a film of the proper thickness.

The optical spectra were recorded on a double beam spectrophotometer (Beckman DK-2) which was modified to permit temperature control of the sample compartment. The temperature of the sample compartment was measured with a copper-constantan thermocouple placed near the cell and connected to a digital temperature readout (Doric model DS-350). The spectra were recorded from 2500 nm (4,000 cm⁻¹) to 400 nm (25,000 cm⁻¹) and normalized to unit amplitude after subtracting the base line. The base line was obtained by determining the spectrum of an empty cell.

2. Pressed powder conductivity

Conductivity measurements of electrides and alkalides were made by using the apparatus designed and described by Michael R. Yemen [102]. A glove-bag around the apparatus was purged several times with dry nitrogen. The sample tube was broken inside the glove-bag and the crystals were loaded between two stainless steel electrodes into a heavy walled 2 mm I.D. fused silica tube. The sample was compressed by means of a steel spring whose force constant had been measured. Ohm's law behavior was first checked by measuring the current at various voltages, then the current through the sample was measured at constant voltage as a function of temperature.

3. Solid state NMR

High resolution alkali metal NMR spectra for crystalline electrides and alkalides were obtained by using the magic angle sample spinning (MASS) technique. measurements were done in the analytical laboratory of Dow Chemical Company (Midland, Michigan) and in the National Science Foundation Regional NMR Center (University of Illinois, School of Chemistry). At Dow, a Bruker CXP high power pulse spectrometer was used. It is equipped with an Aspect 2000 computer system. Oxford Instruments superconducting magnets of 4.6975 Tesla (200 MHz) and 8.4558 Tesla (360 MHz) field strength were used to obtain the spectra. At the University of Illinois, spectra were recorded on a "home-built" Fourier transform NMR spectrometer [103] with a 11.7440 Tesla (500 MHz), 3.5-inch bore solenoid (Oxford) and a Nicolet 1280/293B data system with a control Data Corporation disk. In both measurements a standard multinuclear Andrew-Beam MASS-NMR probe was used. The spinners were made of either Delrin or do polymethylmethacrylate and were spun at the "magic angle" with a spinning rate of 2-4 KHz. The "magic angle" was set using ⁷⁹Br in a sample of KBr. The spinning gas was cooled by passing it through a coil immersed in an acetone-dry ice bath. This gave a sample temperature between -12 and -16°C. The spinners were loosely filled with the crystals in an inert atmosphere glove-bag.

chemical shifts were measured with respect to the infinitely diluted aqueous alkali metal cations. Upfield (diamagnetic) shifts were negative.

4. EPR spectra

Samples for EPR measurements were loaded in 2-4 mm O.D. "spectrosil" fused silica glass tubes connected to Kontes high vacuum valves. The sample tubes were broken in an inert atmosphere glove-bag and a few crystals were loaded into the spinner while they were cold. The tubes were evacuated to less than 10^{-5} torr and a vacuum seal-off was made while the sample was immersed in liquid nitrogen. X-band EPR spectra were recorded on a Bruker model 200 EPR spectrometer. Above 100 K a Varian model 4341 variable temperature controller was used and the temperature at the sample was calibrated with a copper-Constantan thermocouple and a Doric model DS-350 digital readout system. Temperatures below 100 K were provided by a continuous flow-helium system (Oxford Instruments Model ESR9) and measured with a thermocouple (Au +0.03% Fe/ chromel) placed just below the sample. EPR modulation frequencies of 12.5 and 100 KHz were used with amplitudes low enough to avoid distortion of the lineshapes. Power studies were made to insure the absence of saturation effects. The q-values were evaluated by measuring the magnetic field at the microwave frequency. An NMR Gauss meter (Model ER035M) with 1 mG resolution was used to

measure the magnetic field while the microwave frequency was measured to ±0.01 MHz with a frequency counter (Hewlett-Packard Model 5245L). The accuracy of this system was checked with a diphenylpicrylhydrazyl (DPPH) sample.

5. Magnetic susceptiblity

. . •

Magnetic susceptibilities were measured with an S.H.E. computer-controlled variable temperature superconducting quantum interference device (SOUID) spectrometer capable of measurements at temperatures between 1.7 and 400 K. The crystalline samples were loaded in an inert atmosphere glove-bag into small cylindrical containers (inside dimensions 8.5 mm by 6.5 mm diameter) made of either an aluminum silicon alloy or Delrin. Prior to loading the sample, a thread 15-20 cm long was attached to the bucket through four holes. The sample filled bucket was removed from the glove-bag and transferred under liquid nitrogen to another glove-bag placed around the SQUID's airlock. The bucket was loaded into the airlock by attaching the thread to the hook of the driving tape. The airlock was evacuated and pressurized with helium three times, then the sample was loaded into the SQUID. The sample was centered between the two measuring coils by examining the analog voltage from the SQUID output. At every temperature, the SQUID was allowed to take ten readings and an average value was printed out. Readings of 10% difference

at the same temperature were rejected and the measurements were repeated. The computer printout, P, is the total magnetic moment in e.m.u. divided by the field in Gauss and by the total scale factor (which is the scale of the SQUID control multiplied by the scale of the sample measurement control). To correct for the diamagnetism of the sample and the bucket, the sample was ejected from the SQUID and allowed to decompose at room temperature in the airlock. The electronic contribution to the susceptibility was calculated from the equation

$$\chi_{M}^{e} = \frac{P(\text{sample+bucket}) - P(\text{decomposed sample+bucket})}{\text{number of moles in the sample}}$$
 (II.3)

F. Model Salts

Conventional salts in which the alkali metal cations are complexed by crown ethers or cryptands were prepared by procedures similar to those of Pedersen [74,77] and Weiss [76]. The salts, together with the stoichiometric amounts of complexant (mole ratio 1:1 or 1:2), were dissolved in either hot methanol or 1-propanol, the solutions were filtered, concentrated by evaporation and allowed to cool until crystals formed. Conventional salts without complexants were reagent grade and were used without further purification.

CHAPTER III

SYNTHESIS AND CHARACTERIZATION

A. Introduction

The most difficult problem encountered in the synthesis of crystalline alkalides and powdered electrides was solution decomposition. In general, alkali metal solutions in amine and ether solvents are thermodynamically unstable with respect to solvent reduction. This results in the disappearance of the characteristic blue color of the solution even in the presence of macrocyclic-polyether complexing agent. The decomposition reaction in an amine solvent can be described as,

$$e_s^- + RNH_2 \longrightarrow RNH^- + \frac{1}{2}H_2^+$$
 (III.1)

The nature of the decomposition reaction in an ethereal solvent is unknown. Kinetically stable metal-complexant solutions can be prepared if the solvent, metal, complexant and glassware are appropriately treated to remove all easily reducible impurities. Also, the rate of such a decomposition reaction can be greatly reduced to a negligible value by lowering the temperature.

In general, three procedures can be followed to synthesize solid electrides and alkalides [30]. These are solvent evaporation, direct vapor deposition and crystallization from solution. Only the last procedure was studied in the present work. Three methods of crystallization were used and will be discussed here. The classification of these three methods is based upon the kind of solvents used and/or the added stabilizing agent.

B. Methods of Synthesis from Solution

1. Method 1:

Prior to the present work, crystalline alkalides were prepared [94] by either using ammonia as a reaction solvent, with its great ability to dissolve the alkali metals and the complexant or methylamine to dissolve the complexant and then the metals with agitation at reduced temperatures. In some cases, the metal and complexant were dissolved simultaneously. The crystallization solvent(s) was 2-aminopropane and diethylether or n-pentane. This method has been slightly modified as follows: ammonia was eliminated as a reaction solvent to avoid the formation of bronze-colored metallic drops which form during solvent evaporation and which are hard to dissolve and often resulted in metal precipitation.

Instead, methylamine was used, since the solubility of 18-crown-6 in it is high enough to give a clear solution

before pouring onto the metal film. In the case of cryptands 222 and 211, simultaneous dissolution of metal(s) and complexant was achieved by moving the solution back and forth between the metal and complexant compartments. The crystallization solvent always included some methylamine, i.e. the reaction solvent was never distilled to dryness or near dryness. Finally, the washing solvent was diethylether since crown ethers and cryptands have high solubilities in it. This method was found to be very useful for the preparation of crystalline alkalides but not for electrides since rapid decomposition occurred upon adding 2-aminopropane.

2. Method 2:

Dheeb Issa [98] attempted to prepare the crystalline compound, Csl8C6Li, which might have been analogous to the crystalline sodide Cs⁺18C6.Na⁻, by dissolving equimolar amounts of Cs, Li and 18-crown-6 in methylamine. He found that the solution was much more stable than one containing only cesium and dark blue crystals were formed upon adding a mixture of 2-aminopropane and diethylether to a concentrated solution at reduced temperatures (~-78°C). Surprisingly, the crystals contained very little lithium as indicated from the analysis [104] which showed a 1:1 stoichiometry of Cs to 18-crown-6. This method was generalized to involve adding lithium metal in small amounts as a stabilizing

agent when using methylamine as a reaction solvent, a mixture of methylamine, 2-aminopropane and diethylether as a crystallization solvent and diethylether as a washing solvent.

Solutions of lithium metal in amine and ether solvents contain only the solvated lithium cation and the solvated electron since there is no evidence for the formation of lithide ion (Li) in these solutions. Also, the cationelectron interaction is very weak as indicated from optical absorption and EPR studies [31,32]. Since the lithium cation size is too small to fit the 18-crown-6 or cryptand 222 cavity, complexation of lithium by 18-crown-6 or cryptand 222 is unlikely to occur. Also, Dye et al. [30] by using a modified Born-Haber cycle, estimated that the lithide compounds, M⁺L_n.Li⁻ are thermodynamically unfavorable compared to the corresponding electride M^TL_n.e and lithium metal. This was confirmed by the absence of lithium in all of the systems studied. simple explanation for solution stabilization in the presence of dissolved lithium metal is that lithium is acting as a scavenger to inhibit autocatalytic decomposition processes, probably by reaction with free radicals or anion radicals which take part in a chain decomposition reaction. Perhaps lithium reacts with R° to form lithium alkyl [30] which is less reactive than lithium metal.

3. Method 3:

. . .

Professor J.L. Dye [30], during his sabbatical year (1983-84) at A.T.T. Bell Laboratories, examined the use of non β -hydrogen solvents, such as dimethylether and trimethylamine, for the synthesis of alkalides and electrides. He found that such solvents greatly stabilized solutions of alkali metals with complexants and that much more stable crystalline alkalides could be prepared relative to those prepared by methods 1 or 2. Accordingly, this method has been tested and generalized to be the "best" method to date for the preparation of crystalline electrides and alkalides from solution. In this method, dimethylether is used as a reaction solvent while a mixture of dimethylether and trimethylamine is used as the crystallization solvent and trimethylamine as a washing solvent. metal-complexant solutions in dimethylether were found to be stable for days at temperatues as high as 0 to -10°C and for more than six months at -78°C. Some of the crystals formed were found to be much more stable than those prepared by methods 1 or 2. However, the rigorous purification procedures for metal, complexants and solvents are still required since the electride and alkalide salts are intrinsically unstable even in the absence of solvent.

C. Results and Discussion

1. Synthesis

Table I describes the synthesis of crystalline electrides and alkalides by the three methods mentioned before. For completeness, the last column is added to give the final assignments since some crystals precipitated from solutions of different stoichiometry tend to be the same. Each of the crystals described here has a metallic appearance and the fact that some of the crystals (e.g. Rb⁺18C6.Na⁻) showed different colors when precipitated from different solutions can probably be explained in terms of different illumination conditions and/or different degrees of roughness of the crystal surfaces.

Three categories of the crystals have been synthesized during the course of study of the present work. First, five new crystalline compounds were synthesized for the first time. These are RbNal8C6, Rb₂l8C6, Rbl8C6, Cs(18C6)₂ and CsC222. Second, the attempted syntheses of six compounds were unsuccessful either because they don't exist or because of the precipitation of another more thermodynamically stable compound from the solution. These systems are Na₂l8C6, NaC222, Rb(18C6)₂, Cs₂l8C6, Cs₂C222 and CsNaC222. Third, crystalline compounds that had been previously synthesized and characterized in our laboratories, were prepared for further investigation.

Synthesis and Description of Crystalline Electrides and Alkalides. Table I:

1	1	
Reaction Stoichiometry	Crystal Description	Final Assignments
RbNa18C6	Bronze-colored needles—stable at room temperatures for several hours—melt to give blue liquid when decompose upon heating.	Rb 18C6.Na
cs_2c22	Dark bronze-colored needles—stable up to -20°C.	Cs ⁺ C222.e ⁻
CsNaC222	Golden crystals—stable at room temperature for days.	Na ⁺ C222.Na ⁻
LiNaC211	Silver-blue flat crystals-stable at room temperature for about an hour.	Li +C211.Na-
Na_218C6	Grey and white mixture.	Na metal + 18C6
NaLiC222	Golden hexagonal crystals—stable at room temperature for days.	Na ⁺ C222.Na ⁻
CsLiC222	Dark red, needle shaped crystals—stable up to -20°C —decompose violently at room temperature.	cs ⁺ c222.e ⁻
${ m cs}_2$ LiC222	Dark red, needle shaped crystals +drops of Cs metal.	cs [†] c222.e ⁻
Table I Continues	.83.	

Table I Continued.

Reaction Stoichiometry	Crystal Description	Final Assignments
CsLi18C6	Dark blue to violet flat crystals-stable at room temperature for about one-half hour.	cs ⁺ (18C6) ₂ cs ⁻
CsLi (18C6) ₂	Black rod-shaped crystals—stable at room temperature for several hours.	cs ⁺ (18C6) ₂ .e ⁻
${\tt Cs_2Lil8C6}$	Dark blue to violet flat crystals + Cs metal.	$\mathrm{cs}^+(18\mathrm{C6})_2\mathrm{cs}^-$
RbLi18C6	Bronze-colored needles—stable at room temperature for about an hour.	Rb18C6
RbLi (18C6) ₂	Bronze-colored needles +white crystals that partially dissolve in the washing solvent.	Rb18C6
CsNa18C6	Dark copper-colored flat crystals—stable at room temperatures for days.	Cs ⁺ (18C6) ₂ .Na ⁻
$CsNa(18C6)_2$	Dark copper-colored flat crystals—stable at room temperature for days.	Cs ⁺ (18C6) ₂ .Na ⁻
KNa18C6	Dark red crystals—stable at room temperature for several hours.	K ⁺ 18C6.Na ⁻
RbNaC222	Copper-colored flat crystals—stable at room tempera- ture for several hours.	Rb + C222.Na

Table I Continues.

Table I Continued.

Reaction Stoichiometry	Crystal Description	Final Assignments
KNaC222	Greenish bronze-colored needles-stable at room temperature for several hours.	K ⁺ C222.Na ⁻
CsC222	Dark red needle-shaped crystalsstable up to ~10°Cdecompose violently at room temperature.	cs ⁺ c222.e ⁻
Cs18C6	Mixture of red and black crystals—stable at room temperature for several hours.	Cs ⁺ (18C6) ₂ Cs ⁻ + Cs ⁺ (18C6) ₂ .e ⁻
Cs(18C6) ₂	Black rod-shaped crystals—stable at room tempera- ture for several hours.	cs ⁺ (18C6) ₂ .e ⁻
Rb18C6	Blue needle-shaped crystals—stable at room temperature for about one-half hour.	Rb18C6
Rb (18C6) ₂	Blue needle-shaped crystals +white powder.	Rb18C6 +18C6
Rb ₂ 18C6	Greenish copper-colored crystals-stable at room temperature for three days.	Rb 18C6.Rb

These compounds are KNa18C6, CsNa18C6, KNaC222, RbNaC222, LiNaC211, Rb₂C222 [94] and Cs18C6 [104].

In general, method 3 proved to be the "best" method for synthesizing crystalline electride and alkalide salts from solution. This method has many advantages over the other two methods that can be summarized as follows: 1) The high solubilities of 18-crown-6 and cryptand 222 in dimethylether make solution preparation easy; 2) The insolubilities of alkali metals in dimethylether ensure that the only way that solubility can be achieved is through complexation; it avoids the presence of excess uncomplexed metal cations in solutions; 3) The solutions have excellent stability which allows us to use somewhat elevated temperatures (~0° to +10°C) when dissolving the metals; 4) The high vapor pressure of dimethylether allows it to be condensed into or removed from the solution very easily; and 5) The low dielectric constant of trimethylamine tends to increase the yield of crystals.

2. Analysis

The results of the analysis of the five new crystalline compounds and the crystals of the system CsNal8C6 are listed in Table II). It is clear that for the five new compounds the stoichiometries of the crystals are the same as the solution stoichiometry except for crystals prepared in the presence of lithium metal, in which case, the crystals were almost free of lithium.

It is worthwhile mentioning the reasons for the synthesis of some of the new compounds and the unsuccessful attempts to synthesize the six other compounds since this may shed some light on problems faced in the past. dark blue crystals of stoichiometry Cs18C6 [104] could be either of the two compounds, the electride Cs +18C6.e -, or the alkalide Cs (18C6) 2Cs . If this substance is the electride, i.e., if the Cs⁺ cation tends to form a 1:1 complex with 18-crown-6, then perhaps the corresponding Ceside Cs 18C6.Cs, analogous to Cs 18C6.Na, should exist. On the other hand, if it is an alkalide, i.e., if the Cs⁺ cation tends to form a 1:2 complex with 18-crown-6, then the corresponding electride Cs⁺(18C6)₂.e⁻ should exist. Indeed, black shiny crystals were precipitated from a 2-aminopropane-diethylether solution with the solution stoichiometry of Cs(18C6), in the presence of dissolved lithium metal. Also the same crystals could be obtained from dimethylether-trimethylamine solutions in the absence of any lithium. However, solutions of stoichiometry Cs₂18C6 in the presence of lithium metal yield only dark blue crystals and cesium metal when precipitated. The results indicated that the Cs⁺ cation is more likely to form 1:2 complex compounds with 18-crown-6 when precipitated out of solution. is true, then the compound Cs18C6 should be a ceside Cs⁺(18C6)₂.Cs⁻ rather than the electride Cs⁺18C6.e⁻ as initially assigned. This conclusion can be confirmed by

Table II: Results of the Analysis.

Reactant's Stoichiometry	Sample Size	H ₂	Ю	Flame Emission	nission	Comples	Complexant by:	orva tal
ML, N	moles • 10	Collection	Titration	Σ	Z	H NMR	Titration	Stoichiometry
Rb18C6Na	1.326 (0)	1.886 (+3.3)	3.508 (-3.9)	1.884 (+3.2)	1.918 (+5.0)	1.831 (+0.3)	Ì	RbNa18C6
Rb ₂ 18C6	2.427 (0)	2.342 (-3.5)	4.722 (-2.7)	4.342 (-10.5)	1	2.049 (-15.6)	1	Rb_2 18C6
Rb ₂ 18C6	3.279 (0)	3.251 (-0.9)	6.220 (-5.2)	6.581 (-0.4)	1	3.198 (-2.5)	1	Rb_2 18C6
Rb18C6	3.235 (0)	1.513 (6.5)	3.255 (+0.6)	3.181 (1.7)	1	3.092 (-4.4)	1	Rb18C6
Cs (18C6) ₂ Li	2.575 (0)	1.093 (-15.1)	2.482 (-3.6)	2.462 (-4.4)	0.04 (+1.6)		l	cs(18C6) ₂
Cs(18C6) ₂ Li	2.275 (0)	1.073 (-5.7)		1	1	2.027 (-10.9)	I	cs(18C6) ₂
Cs(18C6) ₂	2.172 (0)	1.039 (-4.3)	2.119 (-2.4)	2.116 (-2.6)		4. 188 (-3.6)	1	cs(18C6) ₂
CsC222Li	2.663 (0)	1.337 (+0.4)	2.724 (+2.3)	2.892 (+8.6)	<0.04 <(+1.6)	l	2.352 (-11.7)	CsC222
CsC222Li	2.023 (0)	1.005 (-0.6)	1	1		2.155 (+6.5)	1	
Cs18C6Na	2.770	1		1		3.971 (+43.3)	1	Cs (18C6) ₂ Na
	1.888 ^b (0)					3.971 (+5.1)		
Notes to Table II on followi	10 II on for	Jowing Dage	٥					

Notes to Table II on following page.

Notes to Table II.

^aBased upon reactions II.1 and 2. Values given are the number of moles $\times 10^4$ while number of parentheses represent percent derviation from the presumed stoichiometry. $^b\mathrm{Calculation}$ based upon the compound stoichiometry Cs(18C6) $_2\mathrm{Na.}$ some other results which have been obtained in our laboratory. The compounds $Cs^+(18C6)_2.K^-$ [105] and $Cs^+(18C6)_2Rb^-$ [106] were precipitated from amine and ether solutions. In summary, solutions of cesium metal and other alkali metals precipitated the compounds $Cs^+(18C6)_2.e^-$, $Cs^+(18C6)_2.K^-$, $Cs^+(18C6)_2.Rb^-$ and $Cs^+(18C6)_2.Cs^-$. The compound which is not consistent with this result is CsNal8C6. Accordingly the analysis of this compound was repeated and it was found that the 18C6 content is more consistent with the stoichiometry $Cs(18C6)_2.Na$ rather than Cs18C6Na.

For the rubidium compounds, the same kind of procedure was followed after crystals of stoichiometry Rb18C6 had been synthesized but the results were quite different. Three trials to prepare Rb(18C6), resulted only in the precipitation of white crystals of 18C6 together with shiny, bronze-colored needles of Rb18C6. On the other hand, solutions of reactant stoichiometry Rb₂18C yield greenish-coppery crystals which have the same stoichiometry as the solution. Adding to this, crystals of stoichiometry RbNal8C6 are more likely to be a sodide than a rubidide, since solutions of stochiometry Na₂18C6 yield crystals only in the presence of solvent, but form a white-gray powder, probably of sodium metal and 18-crown-6, when the solvent is removed. This indicates that compounds which have the Na cation complexed with 18-crown-6 cannot be formed in the absence of solvent. These results suggest that, in

contrast to the Cs⁺ cation, the Rb⁺ cation forms 1:1 complexes with 18-crown-6, when precipitated from amine and ether solutions. Although the 1:1 rubidium and cesium thiocyanate complexes with 18-crown-6 have similar crystal structures [86], the 1:1 complex for rubidium and the 1:2 complex for cesium appear to be the most thermodynamically stable forms regardless of the solution stoichiometry.

Dye et al. [94] reported the formation of two crystalline compounds from 2-aminopropane solutions with reactant stoichiometries Cs₂C222 and CsNaC222 when they used ammonia as the reaction solvent. The analysis of these two systems was poor, which made it difficult to assign the compound stoichiometries. It was of great interest to compare the properties of these two compounds to the new compound of stoichiometry CsC222. Out of 6 attempts to reproduce the synthesis of Cs₂C222 by the previous method only one was successful in yielding crystals. However, when lithium metal was used to stabilize the solution (method 2) the same kinds of crystals were easily prepared but they were mixed with the cesium metal. When a solution of stoichiometry CsNaC222 (method 1) was allowed to cool, golden colored crystals of Na⁺C222.Na⁻ were formed. On the other hand, when crystals of stoichiometry CsC222 were dissolved in dimethylether and were allowed to react with a sodium film followed by adding trimethylamine and then cooling

and Na⁺C222.Na⁻) were formed as indicated from solid state ²³Na and ¹³³Cs NMR. These results suggest that the packing of the complex cation Cs⁺C222 does not leave holes large enough to be occupied by alkali metal anions or else the compound Cs⁺C222.e⁻ is thermodynamically more stable than the corresponding alkalide Cs⁺C222.M⁻. It should be mentioned at this point that the formula Cs⁺(C222)₂.Cs⁻ for crystals with stoichiometry CsC222 is rejected since it is known that only 1:1 complexes are formed between alkali metals and cryptand 222 [82]. Accordingly, the stoichiometry CsC222 implies that the compound should be an electride Cs⁺C222.e⁻.

3. Optical Spectra

The optical absorption spectra of thin, solvent-free films have been obtained by dissolving the crystals in methylamine or dimethylether followed by fast solvent evaporation into a side-arm that was kept in liquid nitrogen to avoid any solvent effects on the spectra.

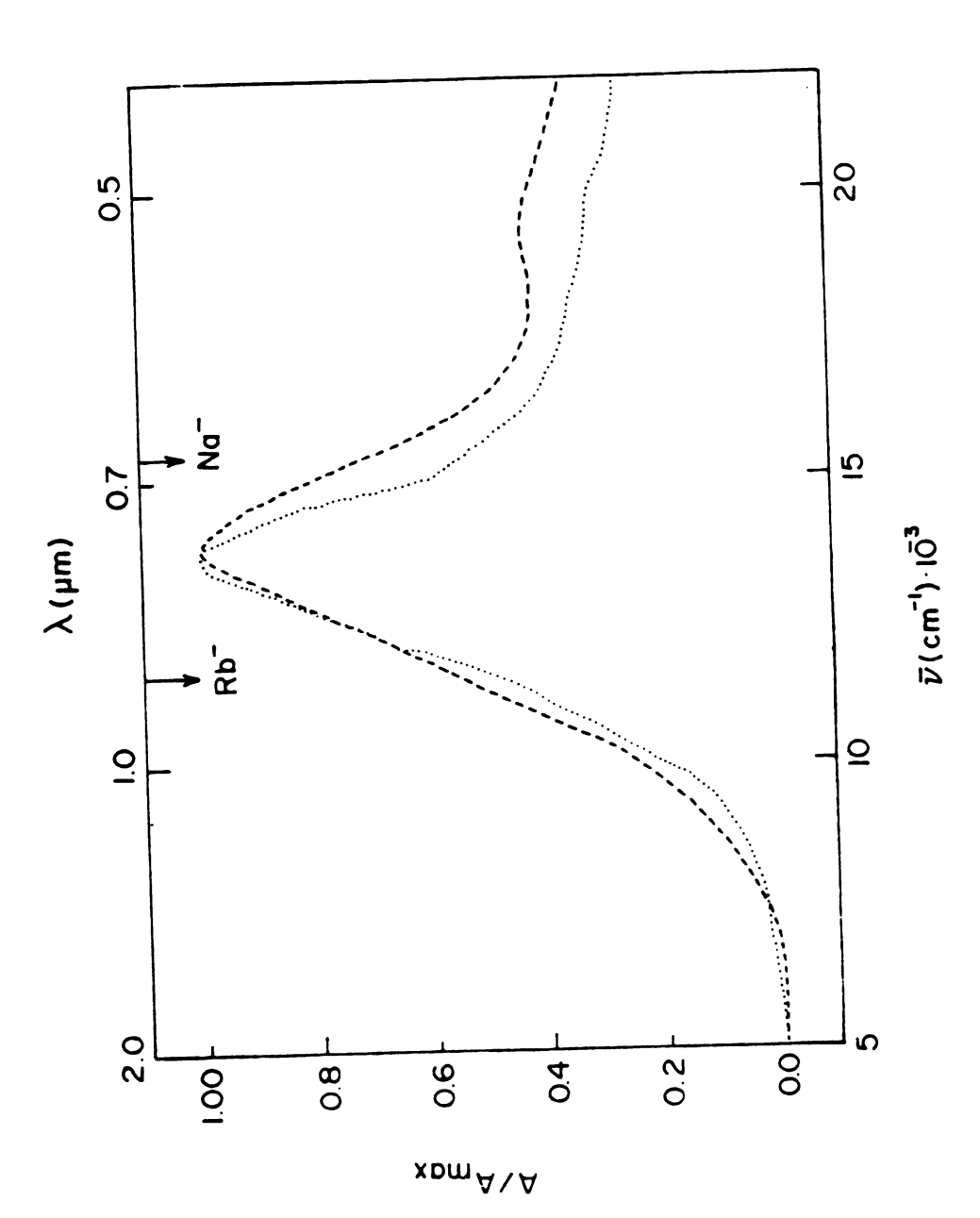
Because of the nature of the film preparation the spectra were often artificially broadened. The optical spectra of films made from crystalline compounds of stoichiometries RbNal8C6, RbNaC222, Rb18C6, Rb₂18C6, Cs(18C6)₂ and CsC222 will be discussed below.

a. RbNa18C6 and RbNaC222

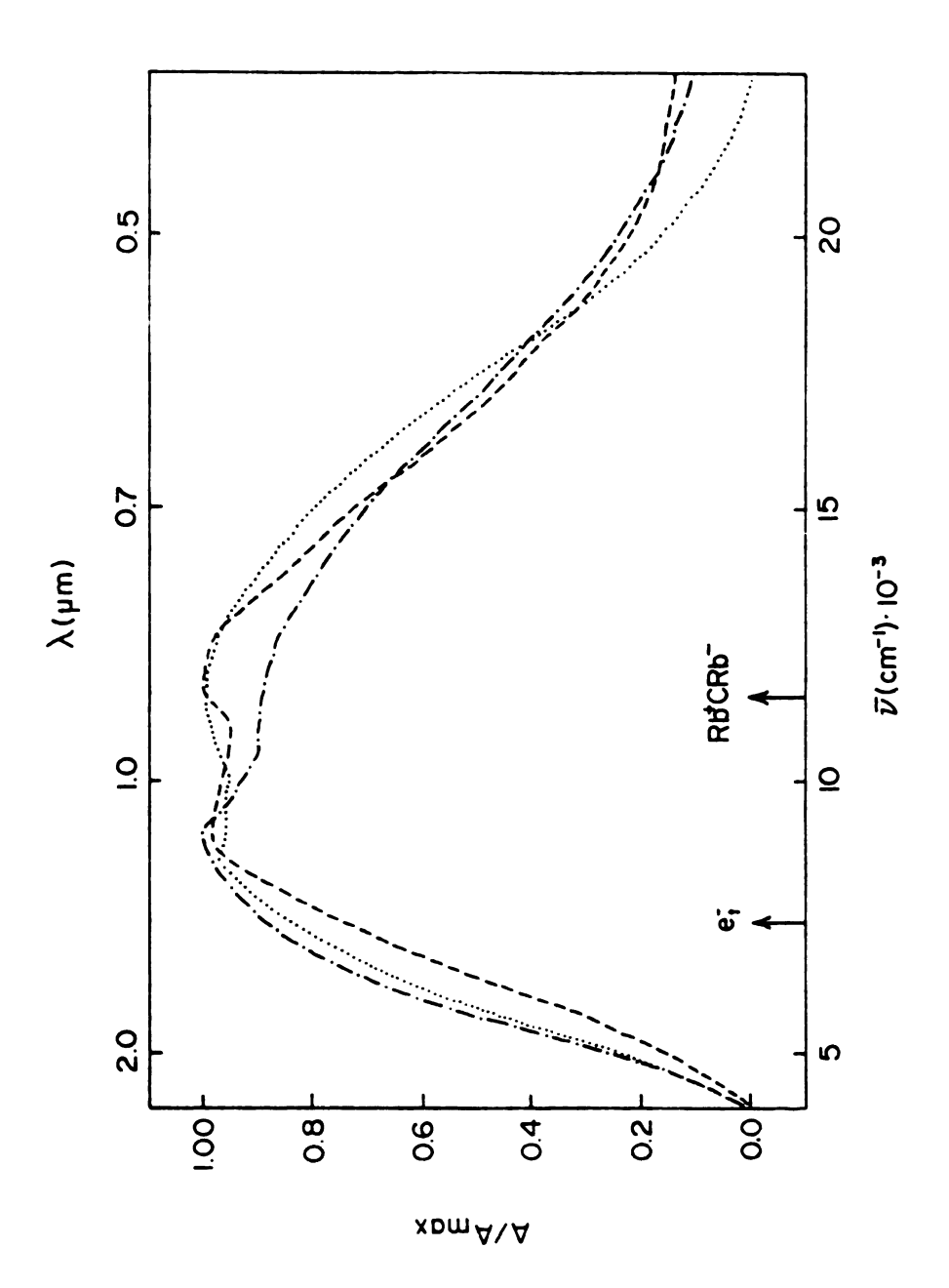
The optical absorption spectra of films made by evaporating methylamine from solutions of the two compounds are shown in Figure 6. Both compounds show essentially the same spectrum with an absorption maximum at 13,800 cm⁻¹ and a pronounced shoulder on the high energy side, at 19,500 cm⁻¹ for RbNa18C6 and 19,900 cm⁻¹ for RbNaC222. These features are similar to those observed with films produced from solutions of Na⁺C222.Na⁻ except that in the latter case the band position is at 15,400 cm⁻¹. If the major band is due to Na then Rb 18C6 and Rb C222 cause a red shift of 1600 cm⁻¹ from the position of the Na band in Na⁺C222.Na⁻. If, on the other hand, the absorptions are due to Rb, then a blue shift of 2200 cm 1 from the absorption of Rb in Rb C222.Rb has occurred. Because of this uncertainty, the optical spectra do not permit us to determine whether these two compounds are sodides, rubidides or mixed systems.

b. Rb18C6 and Rb218C6

Figure 7 shows the optical absorption spectra of films of the two crystalline compounds of stoichiometries Rb18C6 and Rb₂18C6. Films of Rb18C6 made from methylamine solutions showed two peaks at 11,600 and 8,900 cm⁻¹, presumably due to Rb and trapped electrons (e_t) respectively. Films of Rb₂18C6 showed different behavior depending upon the solvent used to make the film and the



Optical spectra of films of RbNa18C6 (----) and RbNaC222 (....). Figure 6:



Optical spectra of films made from methylamine solutions of Rb18C6 (----) and Rb218C6 (----) thin film, (....) thick film. Figure 7:

concentration of the solution from which films were made. Films made by dissolving the crystals in dimethylether showed a spectrum with two peaks at 11,050 and 6,900 cm⁻¹, corresponding to Rb and e respectively. However, when methylamine was used instead of dimethylether, metal precipitation occurred and the spectrum showed a peak at 9,000 and a shoulder at 11,600 cm⁻¹. When the initial film was redissolved, and the solution concentrated by solvent evaporation, the spectrum of the resulting film had a peak at 11,600 and a shoulder at 8,500 cm⁻¹. Although it is difficult to assign the chemical formula of the two compounds based upon the optical spectra, some conclusions can be drawn. If we assume that a 1:1 complex forms between the Rb + cation and 18-crown-6, then the compound Rb18C6 should be an electride Rb 18C6.e . The formation of the Rb band in the optical spectra can be explained in one of two ways. First, complexation of Rb⁺ with 18-crown-6 in solution may not be strong enough to prevent decomplexation; i.e. the following equilibria may occur:

$$Rb^{+}18C6.e_{(s)}^{-}$$
 solution, $Rb^{+}18C6+e_{solv}^{-}$ (III.2)

$$Rb^{+}18C6 + 2e_{solv}^{-}$$
 $Rb^{-} + 18C6$ (III.3)

Second, a solid state reaction may occur in the film of the type

2Rb⁺18C6.e⁻ Rb⁺18C6.Rb⁻ + 18C6 (III.4)

which would mean that the rubidide, Rb⁺18C6.Rb⁻, is thermodynamically more stable than the electride, Rb⁺18C6.e⁻. However, metal precipitation from the methylamine solution of Rb₂18C suggests that in the presence of methylamine the electride Rb⁺18C6.e⁻ is thermodynamically favored over Rb⁺18C6.Rb⁻. In dimethylether solution no metal precipitation occurred and yet the spectrum still shows bands of both Rb⁻ and e_t⁻. In general, the results do not provide clear-cut information about the species in the crystals.

c. Cs18C6 and Cs(18C6) 2-

The crystalline compound of stoichiometry Cs18C6 was synthesized by Dheeb Issa [104]. The optical spectra of thin solvent-free films of this compound exhibit time-dependence. Initially the spectra show the absorption band attributed to both Cs and to trapped electrons (et), however, with time the absorption due to Cs decreases and that due to et increases. This suggests that the electride is the thermodynamically stable form. Accordingly this compound was assigned to be the electride, Cs 18C6.e although the sandwich ceside, Cs (18C6) Cs, could not be ruled out. The stoichiometry Cs(18C6) immediately suggested that this compound is the electride Cs (18C6) e. The optical spectrum of a thin film obtained by dissolving the crystals in methylamine

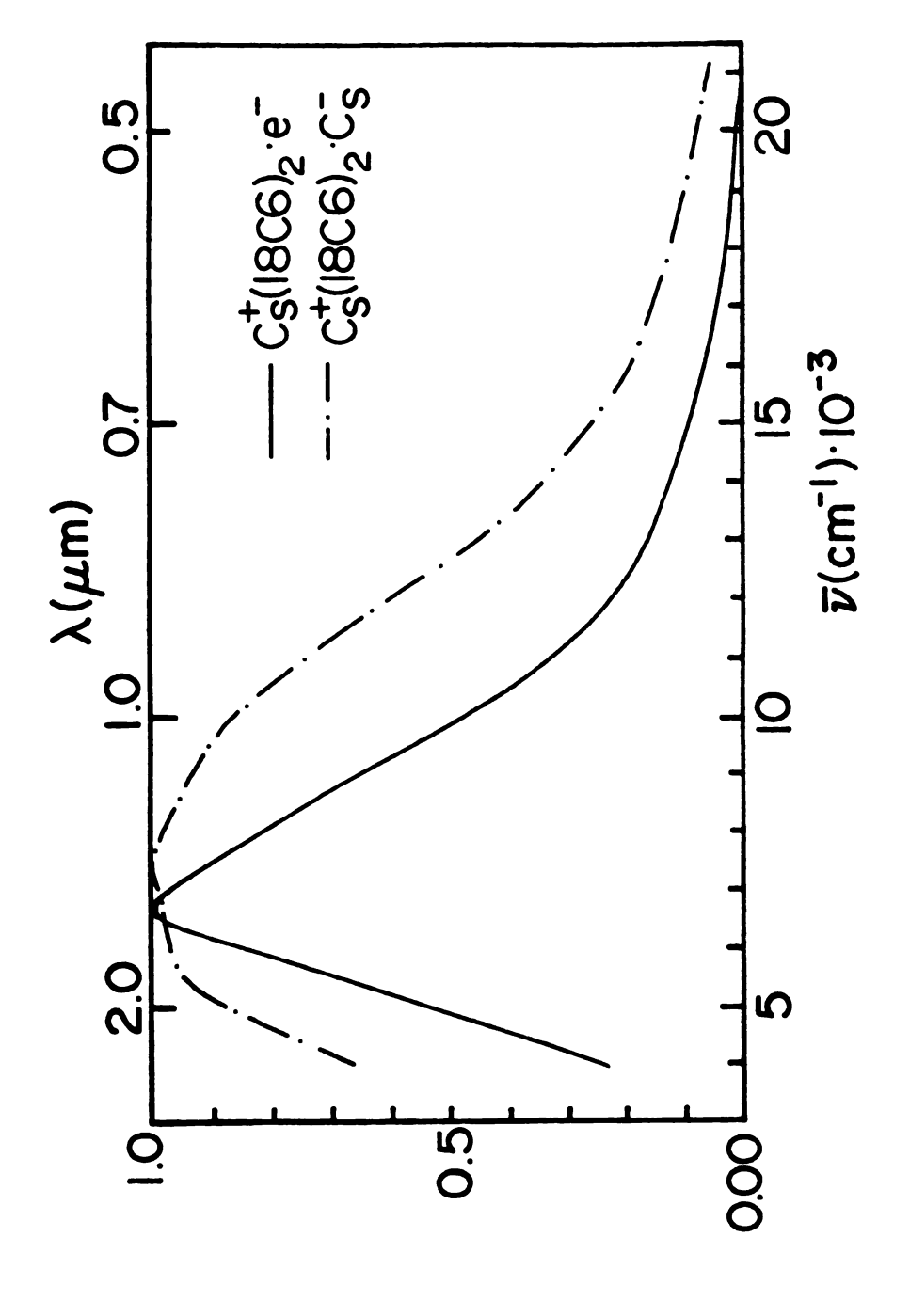
shows only a single narrow peak at 6,700 cm⁻¹, independent of time, as expected for an electride. Figure 8 shows a comparison of the optical spectra of the two compounds. These results suggest that either the two compounds are electrides, Cs⁺18C6.e⁻ and Cs⁺(18C6)₂.e⁻ or that the former is a ceside, Cs⁺(18C6)₂.Cs⁻. The latter assignment was later confirmed so that the change in the optical spectrum of a film of Cs18C6 with time can best be explained in terms of the solid state reaction in the film

$$Cs^{+}(18C6)_{2}.Cs^{-} \longrightarrow Cs^{+}(18C6)_{2}.e^{-} + Cs_{(s)}$$
 (III.5)

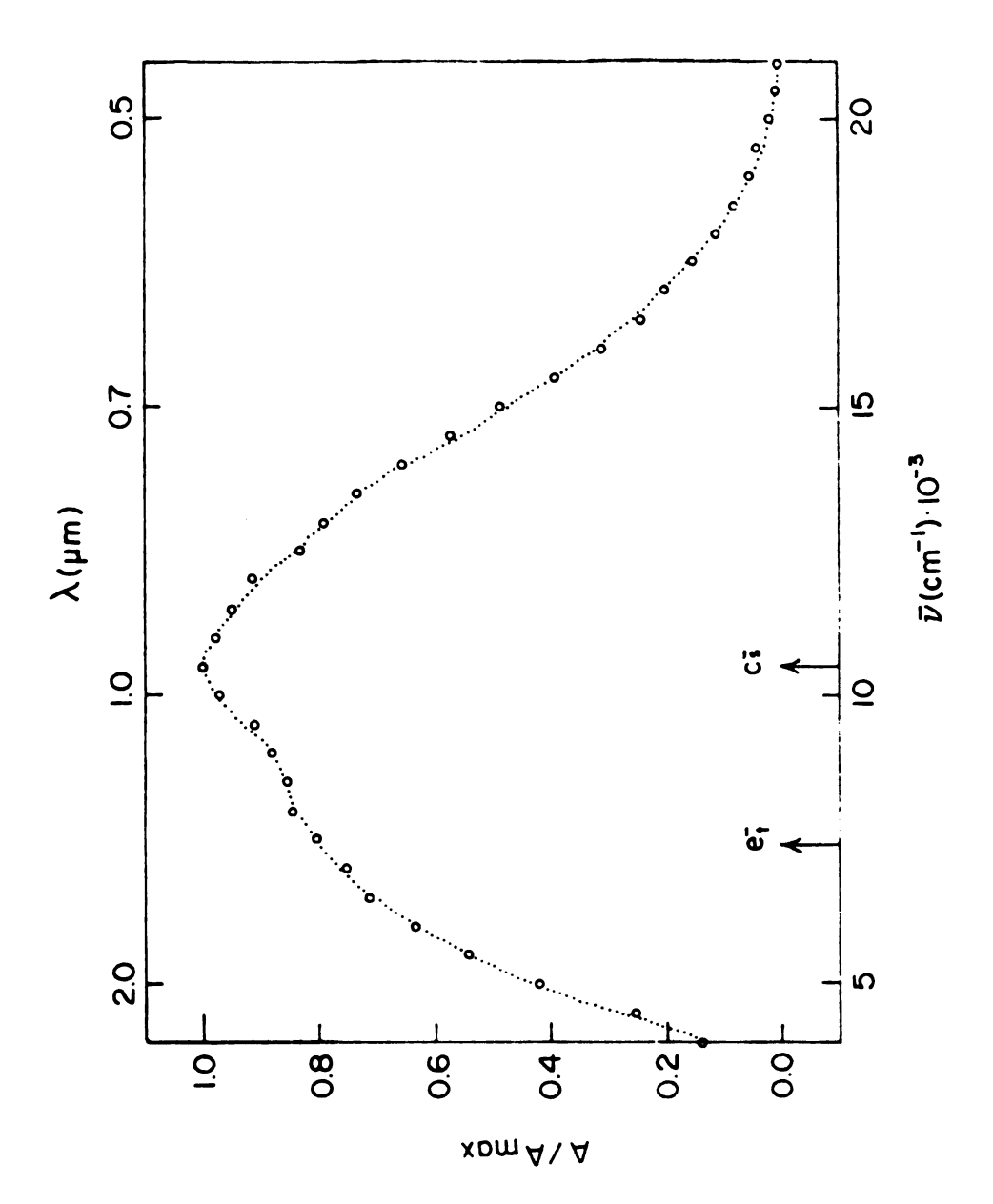
i.e. the electride is thermodynamically favored over the ceside.

d. CsC222

Figure 9 shows the optical absorption spectrum of the compound CsC222. Although the stoichiometry of the compound implies that it is the electride Cs⁺C222.e⁻, the spectrum shows a band at 10,500 cm⁻¹ which could be due to Cs⁻ and a shoulder at ≈8,000 cm⁻¹ attributed to the trapped electron. The formation of Cs⁻ could occur in solution through the decomplexation of the compound. That this could happen was confirmed by the formation of Na⁺C222.Na⁻ when the compound, CsC222, was allowed to react with sodium metal after dissolving it in



Optical spectra of films of the compounds Cs18C6 (--.-) and Cs(18C6)₂ (----). Data for the compound Cs18C6 are taken from reference 98. Figure 8:



Optical spectra of film of the compound CsC222. Figure 9:

dimethylether. The formation of the Na⁺C222 cation, as indicated from ²³Na solid state NMR, requires the release of the cryptand 222 from the original compound. Also solutions of cesium salts and cryptand 222 in non-polar solvents contain two kinds of Cs⁺C222 complexes as indicated by the ¹³³Cs NMR [107] measurements. These two cation complexes are the inclusive complex, in which the cesium cation is situated in the center of the cryptand cavity, and the exclusive complex, in which the cation is partially enclosed in the cavity of the ligand but is still partially solvated. If this is the case in methylamine solutions of CsC222, then the exclusive complex could provide an easy way for the formation of the Cs anion during fast evaporation of the solvent. any event, no definite conclusion can be reached about this system and more discussion will be deferred to the next chapter.

4. D.C. pressed powder conductivity

For an intrinsic semiconductor, at a given temperature, there is a non-vanishing probability that some electrons will be thermally excited across the band gap, E_g . Accordingly, the number of holes in the valence bands and the number of electrons in the conduction band will be equal. The conductivity is then given by

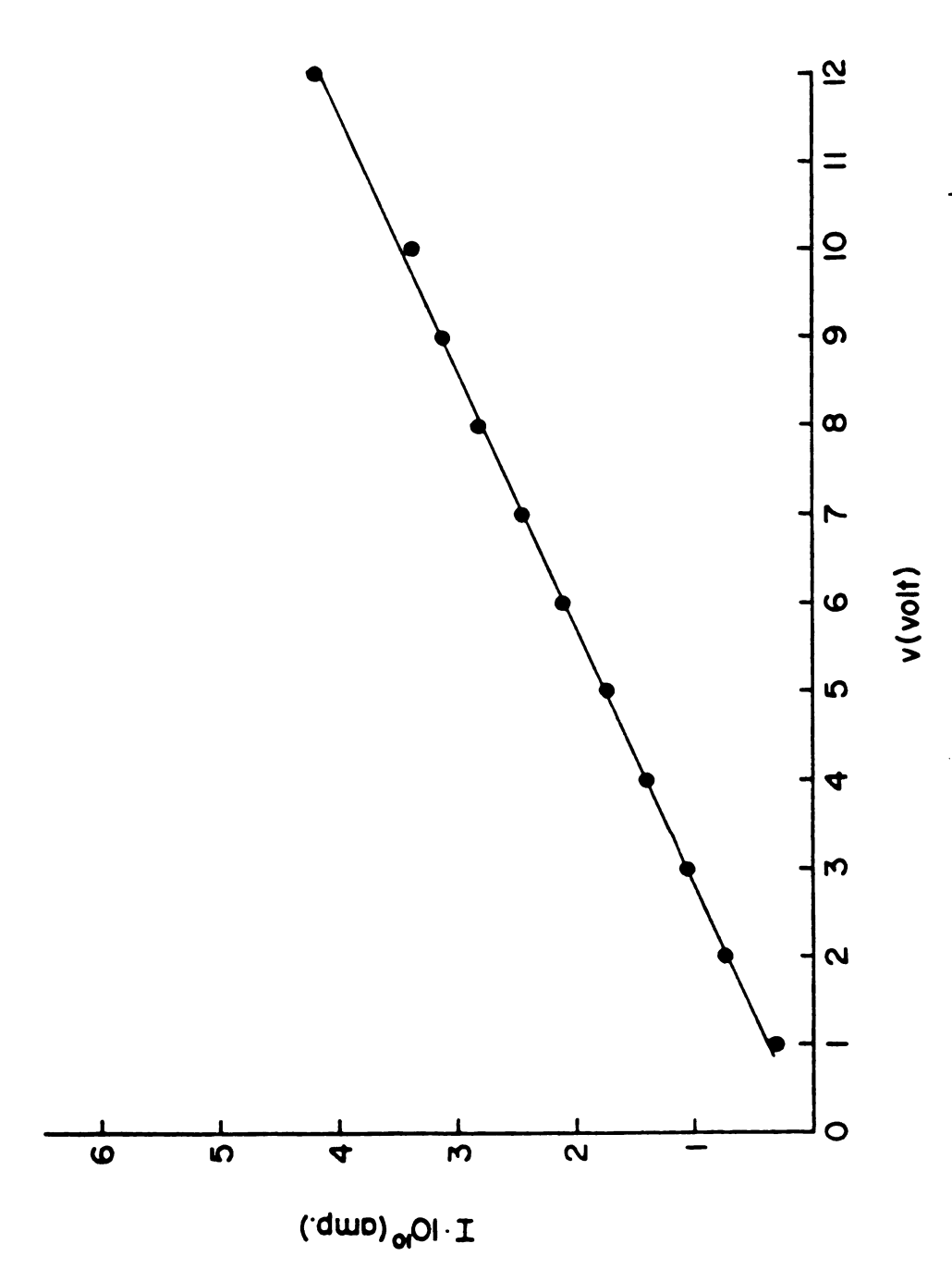
where $\sigma_{_{\!\infty}}$ is the limiting specific conductance at infinite temperature. However, intrinsic semiconductivity exists only in extremely pure substances and more commonly the resistance is characteristic of an extrinsic semiconductor or "doped" semiconductor. Two types of extrinsic semiconductors are known depending upon the position of the impurity energy level relative to those of the conduction and valence bands. In the P-type semiconductor the impurity energy level (E_a) lies close to the valence band (E_{v}) . If this level is empty then electrons can be excited from the valence band to the acceptor impurity level. An example of the P-type semiconductor is boron doped germanium which has an apparent band gap of 0.0104 eV [108] corresponding to the difference between the acceptor and valence band levels $(E_a - E_v)$. A value of 0.67 eV is reported for pure germanium corresponding to the difference in energy between conduction and valence bands $(E_C - E_V)$ [108]. On the other hand, if a filled or partially filled impurity level lies close to the conduction band, then electrons can be donated to the conduction band; this is called N-type semiconductivity. An example of an N-type semiconductor is the F-center in alkali metal halide crystals where electrons occupy anion site vacancies due to crystal defects [109]. apparent band gap in this case, will correspond to the energy difference between the conduction and donor energy level $(E_C - E_d)$.

In general, conductivity in semiconductors arises from electron-hole formation in the conduction and valence bands (or in impurity bands). The behavior of both intrinsic and extrinsic semiconductors with temperature is exactly the same since, in principle, conductivity originates from electron-hole formation where the electrons are thermally excited to the conduction band from the valence band (intrinsic) or donor impurity band (N-type-extrinsic) or to the acceptor impurity band from the nearby valence band (P-type-extrinsic). notable difference is the limiting conductance at infinite temperature. For an intrinsic semiconductor, one expects to have equal populations of electrons in the valence and conduction bands at infinite temperature leading to a metallic conductivity value. On the other hand, an extrinsic semiconductor should yield a much smaller value for the limiting specific conductance at infinite temperature simply because the number of states available to donate or accept electrons is not enough to yield a metallic value and the conductivity due to impurities should approach a limiting value at high temperatures that is smaller than that of a metal.

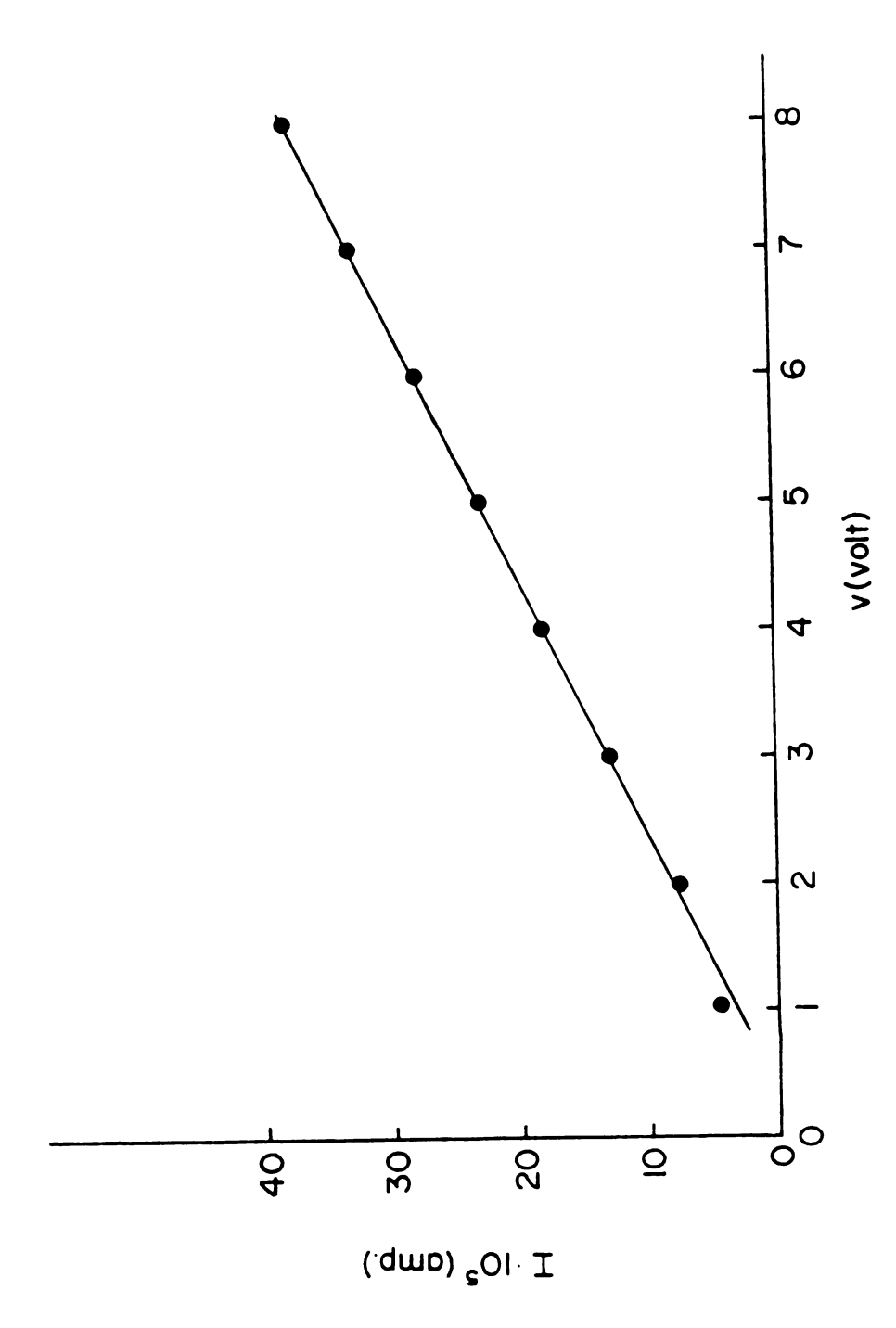
Although the parent sodide compound, Na⁺C222.Na⁻ has a bright golden metallic appearance, the D.C. powder conductivity measurements showed that it is a semiconductor as indicated from the linar relationship of ln R versus 1/T. The slope of the line gave an apparent band-gap of

2.4 eV [102]. Extrapolation of the straight line to infinite temperature gave an intercept which corresponds to metallic conductivity ($\sigma > 10^6$ ohm⁻¹ cm⁻¹). The results show that Na⁺C222.Na⁻ is an intrinsic semiconductor. On the other hand, the compound Cs⁺(18C6)₂.Na⁻ shows an apparent band-gap ranging from ~ 0.6 to ~ 1.5 eV with σ_{∞} in the range of 10^{-2} to 10 ohm⁻¹ cm⁻¹ [98], indicating that the compound might be an extrinsic semiconductor.

In the present research, D.C. pressed powder conductivity determinations were made on three crystalline compounds, RbNa18C6, Rb18C6 and Cs(18C6)2. This was first done by checking Ohm's Law (Figures 10-12) by reading the current (I) versus the voltage (V) at a given temperature. Then the current was measured at a constant voltage (~5 Volt) as a function of temperature and the resistivity (ρ) or the conductivity ($\sigma = 1/\rho$) was calculated for each sample. Figure 13 shows the plot of $\ln \sigma$ versus 1/Tfor the compound Cs(18C6)₂. The data for the compound Cs18C6 [98] have been included for comparison. Both compounds gave straight lines with slopes that correspond to apparent band-gaps of 0.9 and 0.8 eV for Cs(18C6), and Cs18C6 respectively. However, the values for the limiting specific conductance at infinite temperature were about 10^2 and 1 ohm⁻¹ cm⁻¹ for Cs(18C6)₂ and Cs18C6 respectively. This may indicate that $Cs(18C6)_2$ is an intrinsic semiconductor while Cs18C6 is an extrinsic



Ohm's Law plot of polycrystalline powder of Rb 18C6.Na . Figure 10:



Ohm's Law plot of polycrystalline powder of Rb 18C6.e. Figure 11:

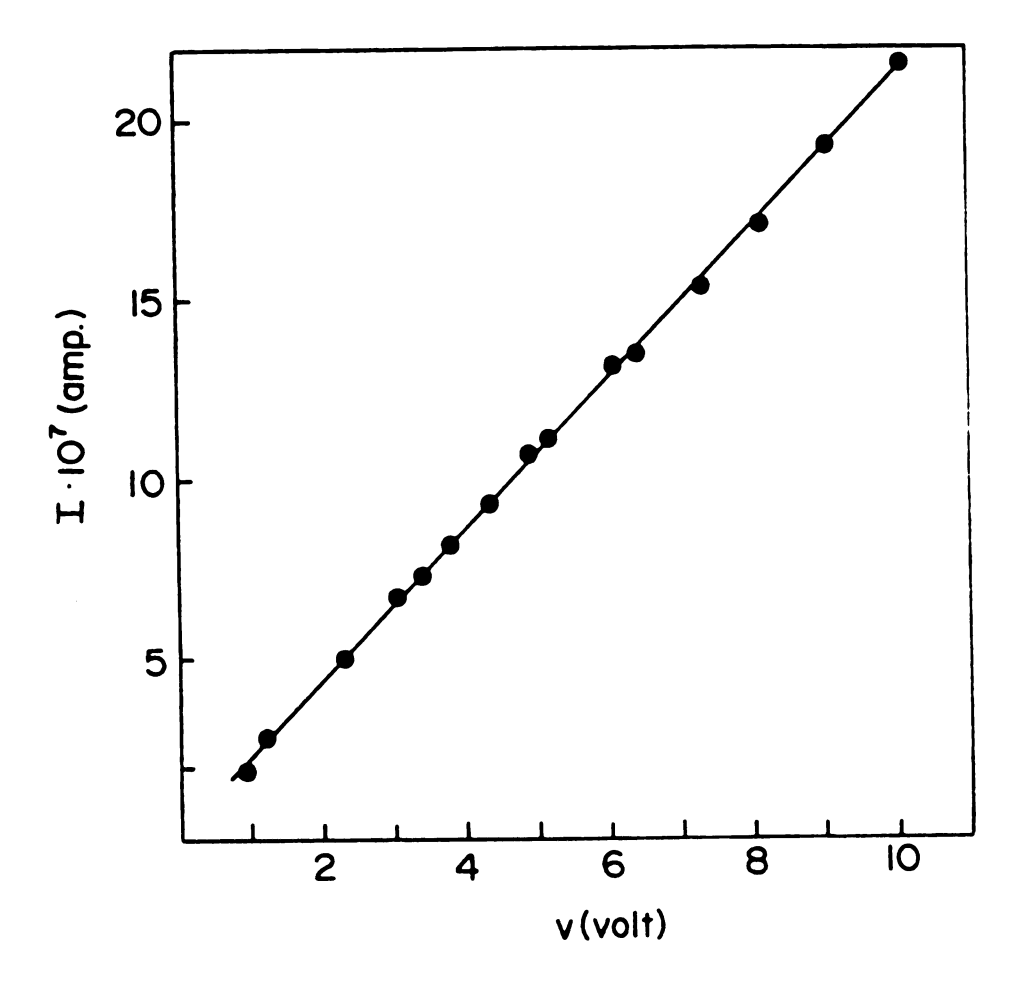


Figure 12: Ohm's Law plot of polycrystalline powder of Cs+(18C6)₂.e⁻.

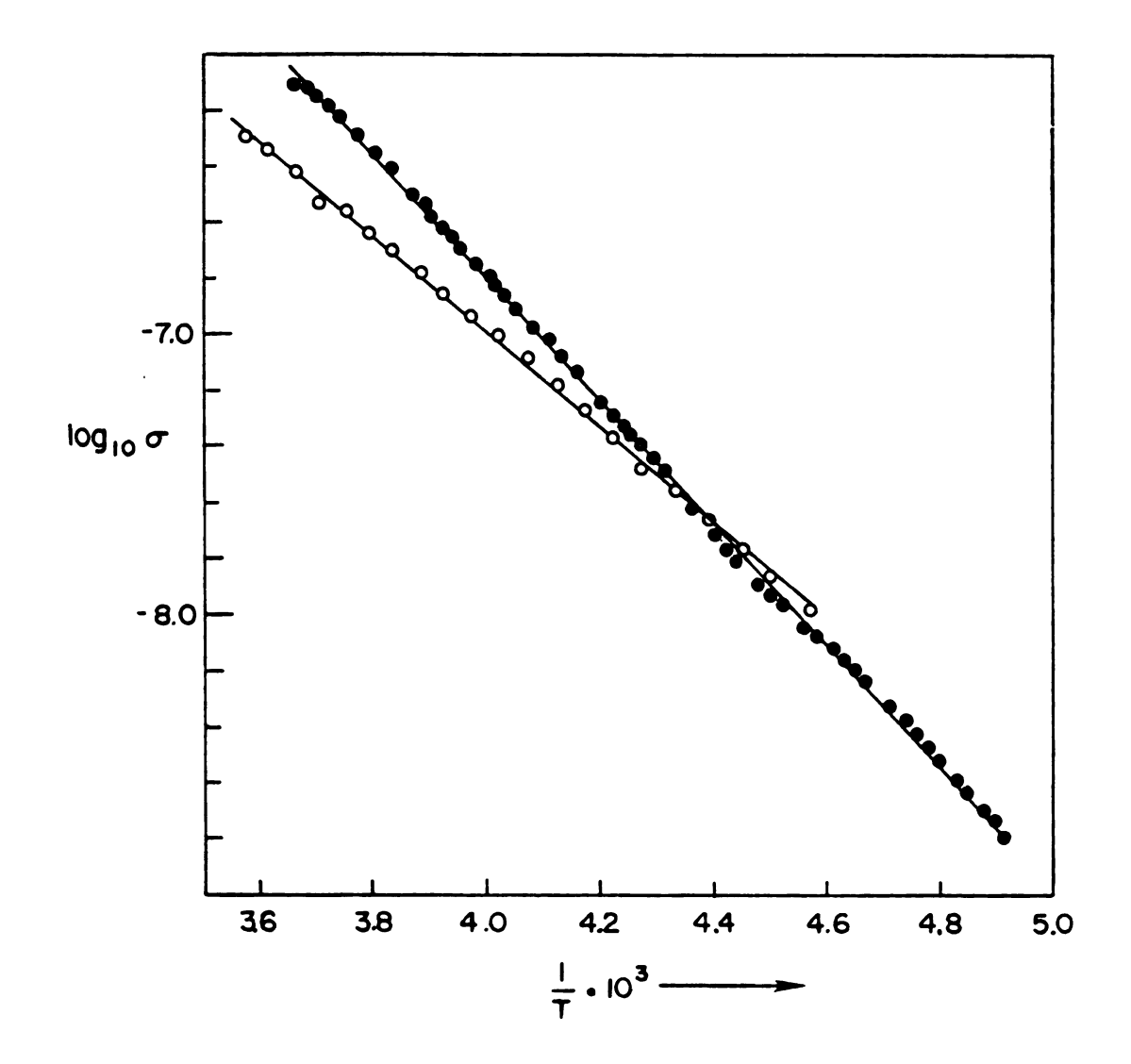


Figure 13: Plot of log conductivity vs. reciprocal temperature of the compound Cs⁺(18C6)₂.Cs⁻ (open circles) and Cs⁺(18C6)₂.e⁻ (solid circles).

semiconductor. Although the value of 0.8 eV for the band-gap of the compound Cs18C6 is proably too small for a pure ceside, the value for σ_{∞} indicates that the compound is most likely to be a doped ceside.

Figures 14 and 15 show the plots of $\ln \rho$ versus 1/Tfor the two compounds RbNa18C6 and Rb18C6. It has been found that the samples show higher conductance at a given temperature when the temperature is first increased and then decreased, but that the slopes of the lines are almost the same. A similar behavior had been found to be observed for samples of KNa18C6 and CsNa18C6 except that the samples showed more resistance when the temperature was first increased and then decreased [98]. These two types of behavior can be explained in terms of changes in the resistance with sample packing in the quartz cell of the apparatus or the presence of decomposition products which affect the resistance but not the band-gap. calculated band-gaps for the two compounds RbNa18C6 and Rb18C6 were 0.9 and 0.4 eV respectively indicating that they are probably extrinsic semiconductors.

5. Differential Scanning Calorometric (DSC) studies:

The melting and decomposition temperatures of some of the alkalides and the electride Cs(18C6)₂ were measured by Professor J.L. Dye during his stay at the A.T.T. Bell Laboratories. The results are summarized in Table 3. A typical DSC trace is shown in Figure 16 for

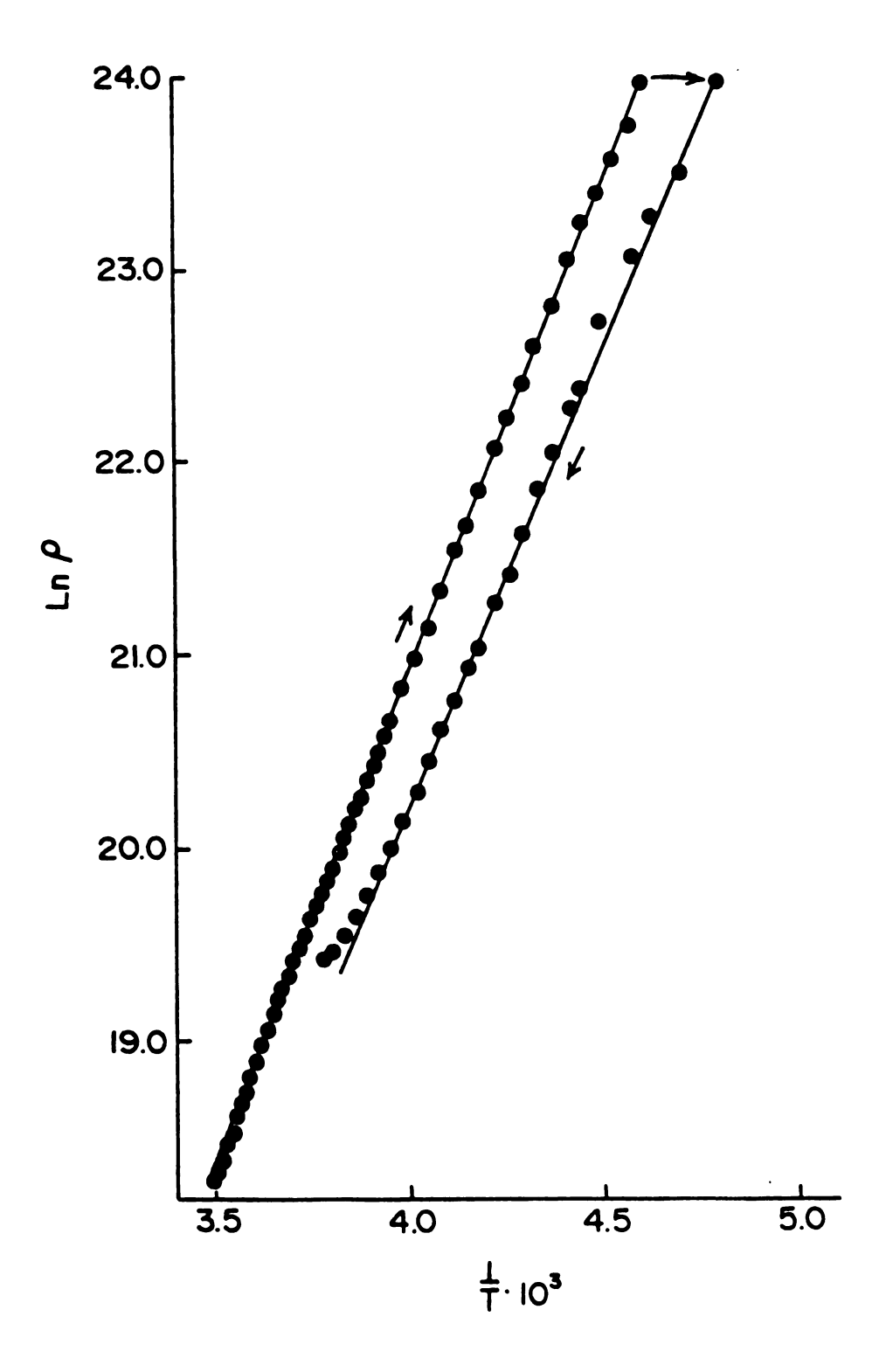


Figure 14: Plot of log resistivity vs. reciprocal temperature for polycrystalline Rb 18C6.Na .

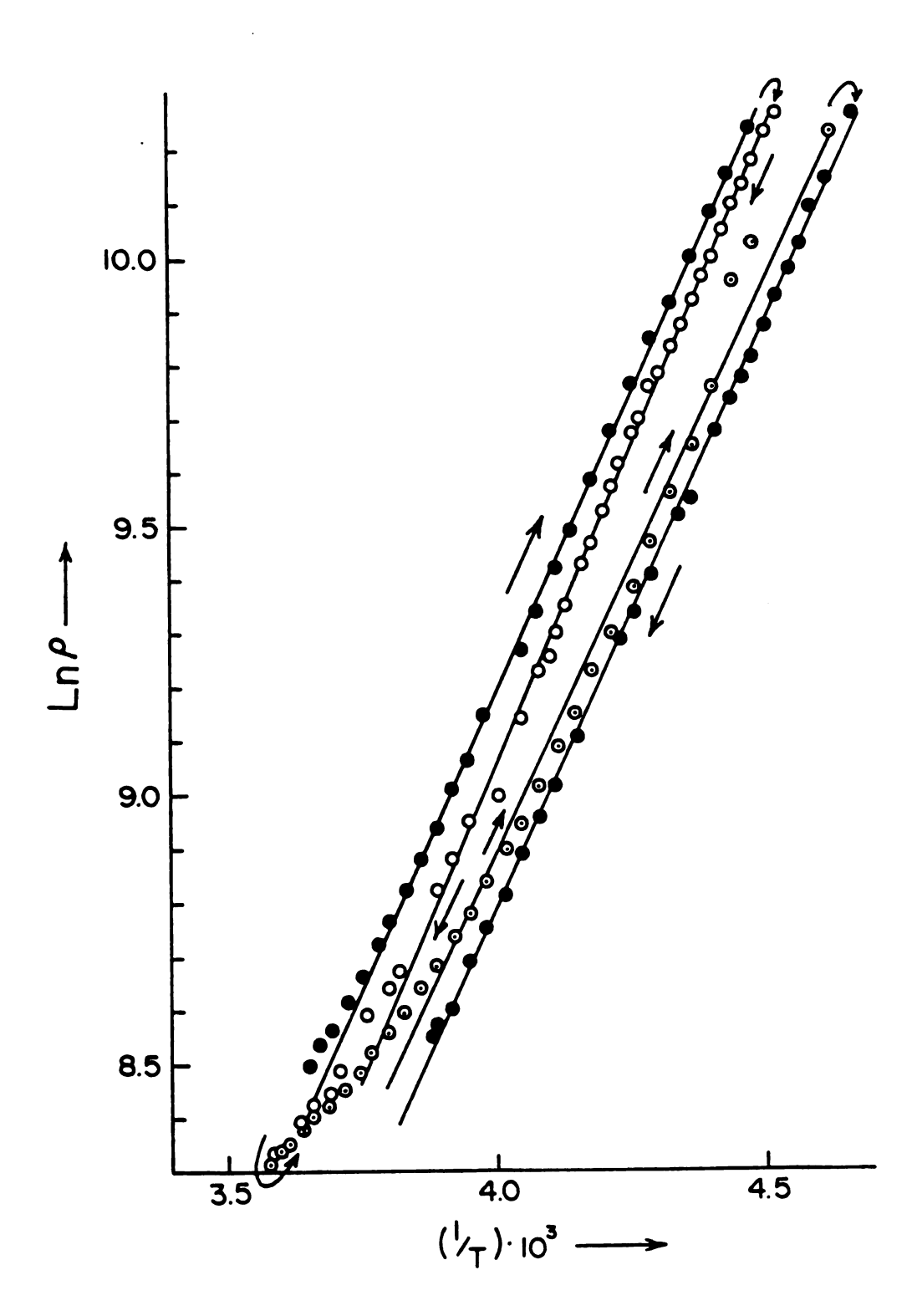
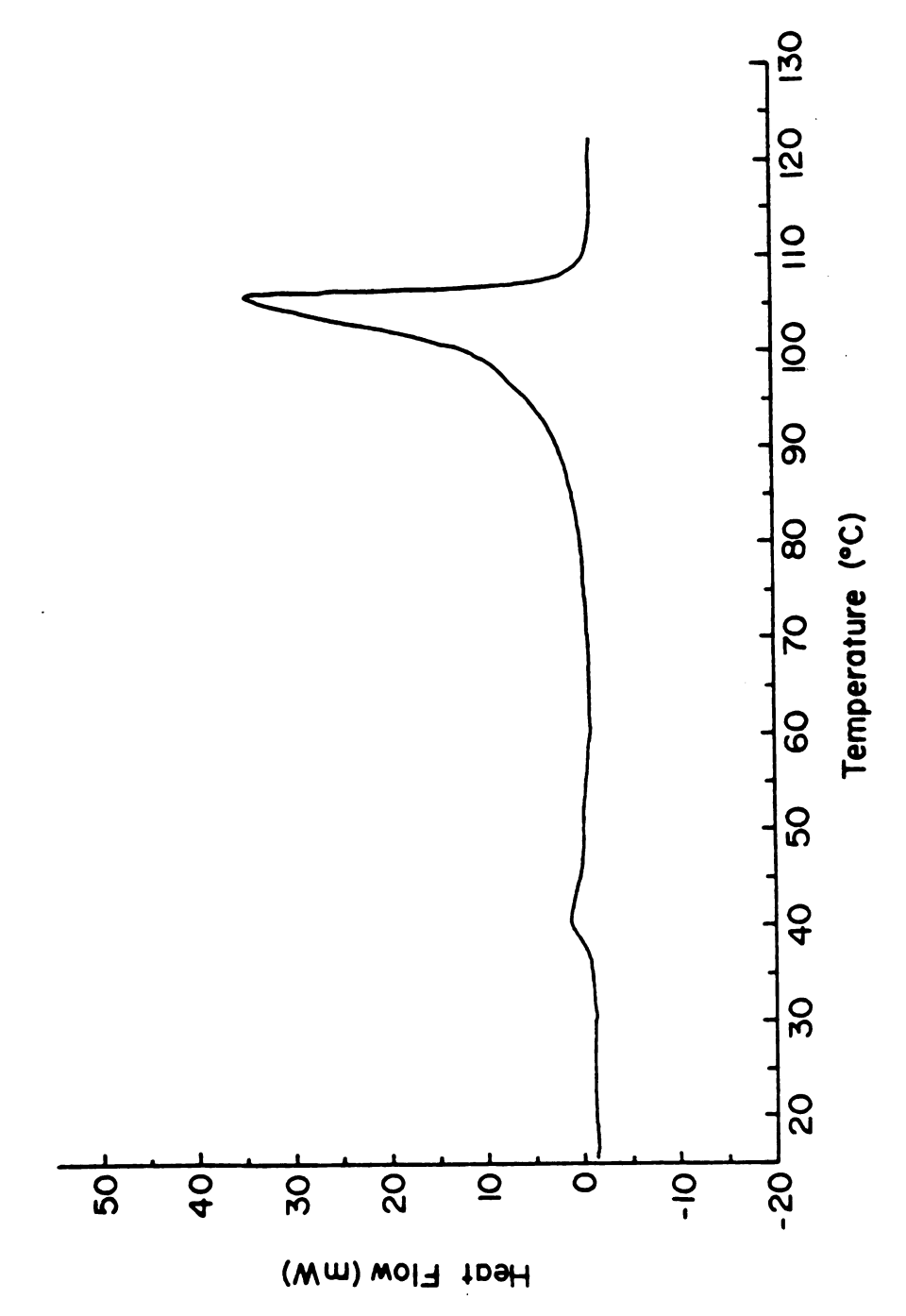


Figure 15: Plot of log resistivity vs. reciprocal temperature for polycrystalline Rb⁺18C6.e⁻.



DSC for a polycrystalline sample of Cs (18C6) 2.Na . Figure 16:

the compound Cs(18C6)₂Na. The compound starts to melt at about 38.5°C (endothermic process) and the temperature for maximum decomposition, which corresponds to the position of the large exothermic peak, is 107°C. Figure 17 shows the DSC trace for the two compounds Rb18C6Na and Cs(18C6)₂. These compounds showed behavior similar to that of Cs(18C6)₂Na but other processes apparently occur during decomposition.

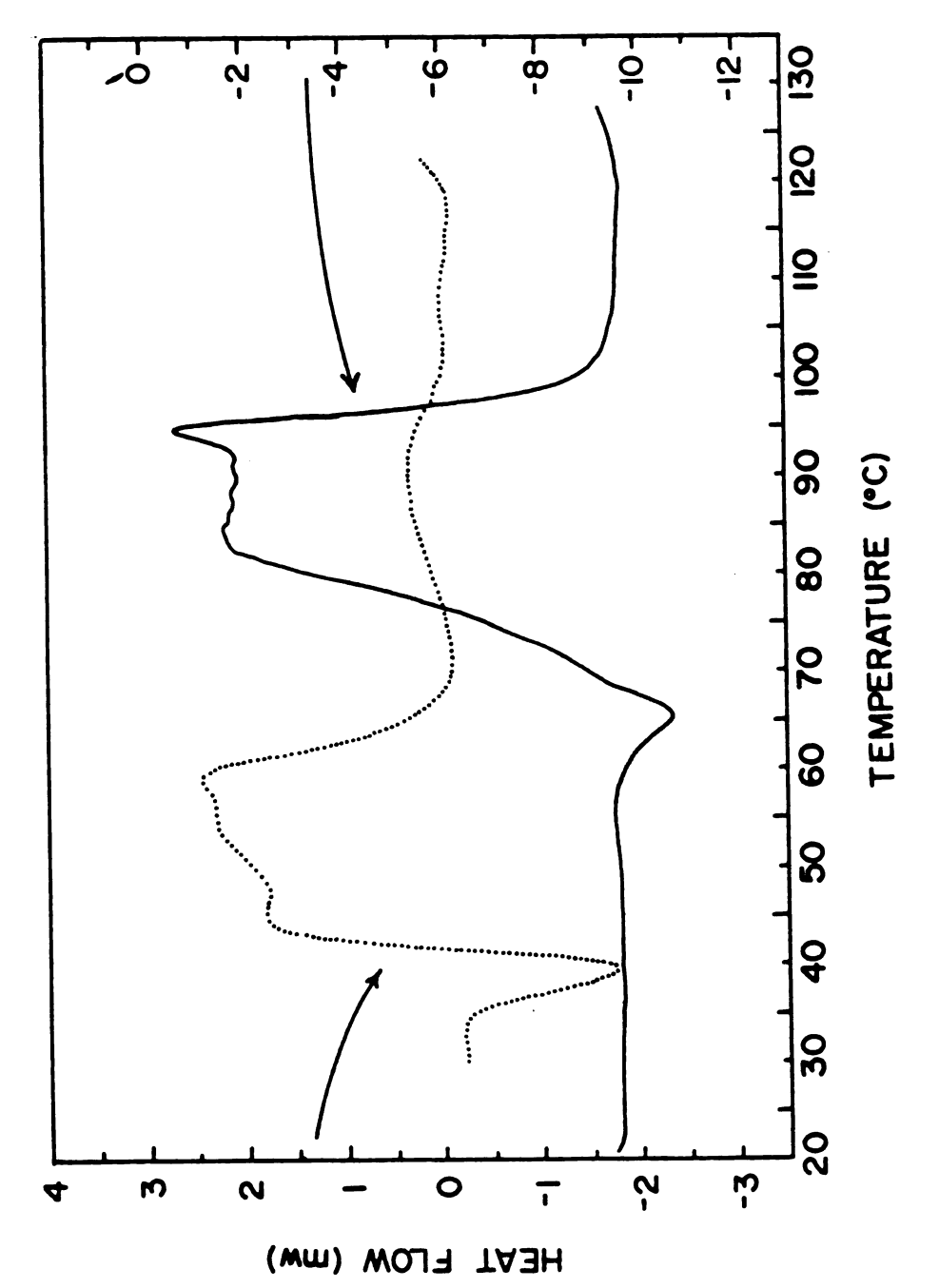
Table III: DSC Results for Alkalides and an Electride

Compound	Melting Point (°C)	Decomposition Temp. (°C)
RbNaC222	~50 ^a	63
CsNa(18C6) ₂	38.5 ^b	107
RbNal8C6	~66	92
Cs18C6	60 ^{b,c}	95
Cs(18C6) ₂	36	~60

^aInflection during decomposition.

Endothermic signal superimposed on exothermic peak.

^cSmall endothermic signal at ~36-38°C.



DSC for polycrystalline samples of Rb 18C6.Na (-cs (18C6) 2.e (....). Figure 17:

CHAPTER IV

SOLID STATE NMR

A. Introduction

The results obtained in Chapter III show that two main problems remain concerning the assignments of species present in crystalline salts of electrides and alkalides. First, the analysis gives only the stoichiometries and cannot differentiate between two different species that have the same stoichiometry. An example is the compound of stoichiometry Rb18C6. The analysis cannot differentiate between the electride Rb⁺18C6.e⁻ and the rubidide Rb⁺(18C6)₂.Rb⁻. However, in some cases, e.g. Cs(18C6)₂ and Rb₂18C6, the analysis tells us immediately that the first must be an electride, Cs⁺(18C6)₂.e⁻, while the second is a rubidide Rb⁺18C6.Rb⁻.

Second, a problem lies in the measurements of the optical spectra of films. The crystals are first dissolved in a given solvent; the solvent is then rapidly evaporated to produce the film. Therefore, the absorbance of the film might reflect the species present in solution which may or may not be the same as in the crystals. Therefore

decomplexation, equilibria between species with different molecular formulae and dissociation of alkali metal anions into cations and solvated electrons as well as solid state reactions in the film should be considered in interpretating the optical spectra. Our assignment of the optical bands is based on the results obtained from studies of alkali metal anions in alkali metalethylenediamine solutions [29] and in films produced by solvent evaporation from solutions of stoichiometry M2C222 [95]. Such band assignments will only be valid if we assume that the nature of the absorber is independent of the environment. In fact, this is not strictly true since it was found that the band position of alkali metal anions in solution and in films as well as that of the trapped electron are sensitive to the solvent or crystalline environment. For example, the compound RbNa18C6, which is likely to be a sodide, shows an absorption band that lies between those corresponding to Na and Rb in the two compounds Na C222.Na and Rb⁺C222.Rb⁻. Films produced from solutions of stoichiometry LiC211 [96] showed several different absorption bands that must correspond to different sites for the trapped electrons since no metal anions are formed. The band positions of some of these trapped electrons lie in the range of the absorption maxima of Rb and Cs in both solutions and films. Consequently, the unequivocal assignment of the species present in

these salts from optical spectra alone is not possible and another technique is needed to determine the nature of the species present in electride and alkalide compounds.

B. Magic Angle Sample Spinning (MASS)-NMR

Nuclear magnetic resonance spectroscopy is a powerful way to probe the microscopic environment of a particular constituent in a given sample. It is wellknown that NMR spectral lines of solutions are much narrower than those of solids. This very substantial difference in behavior arises from the static anisotropic interactions to which the nuclei are subjected in the solid state. A good example to illustrate this is the H-NMR linewidth of water and ice. The resonance line of ice is a million times broader than that of liquid water. Line broadenings in solids result from magnetic dipolar, chemical shift, electron-coupled nuclear spin (J-coupling) and quadrupolar interactions. In fluids, the rapid random thermal motion averages most of the anistropic interactions (except second-order quadrupolar contributions) and effectively removes them from the spectrum. Building upon this simple idea, in a rapidly rotating solid, if the speed of rotation is high enough and the angle of rotation is properly chosen, only the isotropic interactions should contribute to the spectrum. is the basic principle of the MASS-technique, first developed by Andrew [110,111] and Lowe [112] in 1959.

Three kinds of interactions are of great interest to the present work and will be discussed in detail. These are the magnetic dipolar, chemical shift anisotropy and electron-quadrupolar interactions.

1. Direct magnetic dipolar interactions:

The origin of the magnetic dipolar interaction arises from the modification of the magnetic environment of a nucleus by the field due to the magnetic moments of neighboring nuclei. The magnitude of such a field can vary between $\pm 2\mu/r^3$, where μ is the nuclear magnetic moment and r is the distance between the two nuclei [113]. Accordingly, nuclei of the same kind will experience various fields depending on their position and orientation in the solid, and magnetic resonance will occur over a range of frequencies so that the spectral line will be broadened.

The truncated dipolar interaction Hamiltonian, for all nuclear pairs i,j is given by [114]

$$\mathcal{H}_{D} = \sum_{i < j} A_{ij} (3 \cos^{2} \Theta_{ij} - 1)$$
 (IV.1)

where A_{ij} is given by

$$A_{ij} = \frac{1}{2} \gamma_{i} \gamma_{j} h^{2} r_{ij}^{-3} (I_{i}.I_{j}^{-3} I_{iz}^{I} I_{jz})$$
 (IV.2)

in which γ is the nuclear gyromagnetic ratio, r_{ij} is the internuclear distance, θ_{ij} is the angle between r_{ij} and the Zeeman field H_0 , and I and I_z are the spin angular momentum operator and its z-component respectively. In fluids, this interaction Hamiltonian averages to zero due to the rapid tumbling motion, and the fact that the isotropic average value of $\cos^2\theta$ is $\frac{1}{3}$. Hence the effect of the dipolar interaction is eliminated from the spectra. If the solid specimen is rapidly rotated with an angular velocity ω_r around an axis inclined at an angle β to the direction of the magnetic field, the angle θ_{ij} can be expressed in terms of other angles of the system as shown in Figure 18. This gives

$$\cos \theta_{ij} = \cos \alpha_{ij} \cos \beta + \sin \beta \cos (\omega_r t + \phi_{oij})$$
 (IV.3)

There are two ways to deal with Equations (IV.1) and (IV.3). In the first method, the substitution of Equation (IV.1) into (IV.3) results in a time dependent Hamiltonian $\mathcal{H}_{D}(t)$ which is given by

$$\mathcal{H}_{D}(t) = \sum_{i < j} A_{ij} \left[\frac{1}{2} (3 \cos^{2} \beta - 1) (3 \cos^{2} \alpha_{ij} - 1) + \frac{3}{2} \sin 2\beta \right]$$

$$\cdot \sin 2\alpha_{ij} \cos (\omega_{r} t + \phi_{oij}) + \frac{3}{2} \sin^{2} \beta \sin^{2} \alpha_{ij}$$

$$\cdot \cos 2(\omega_{r} t + \phi_{oij}) \right] \qquad (IV.4)$$

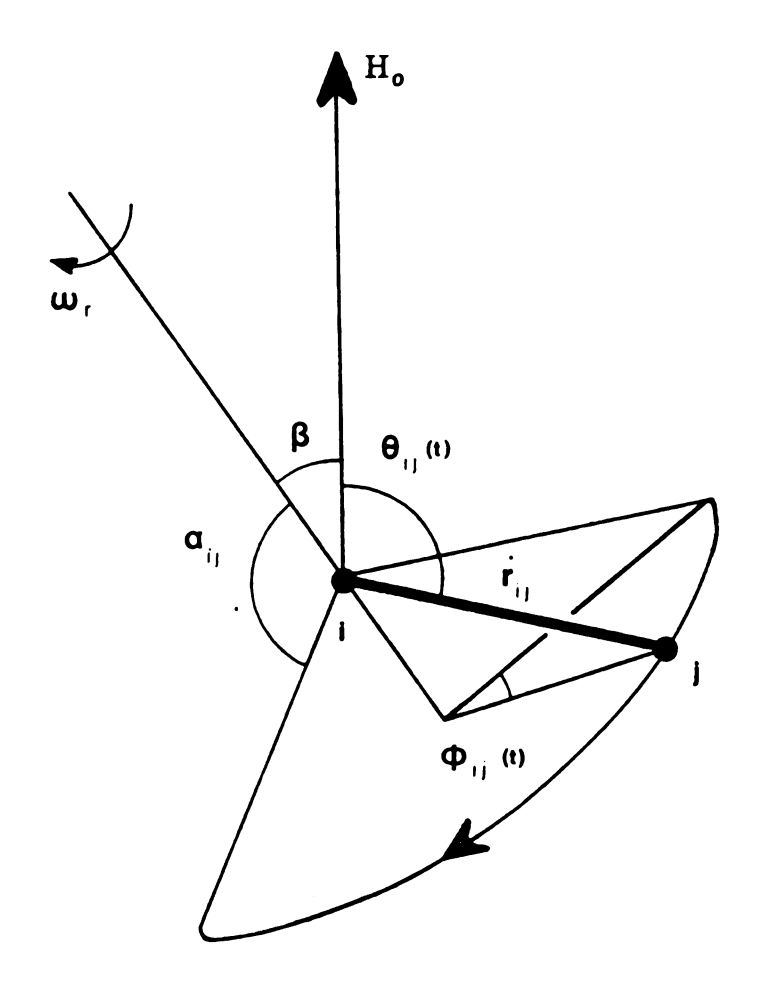


Figure 18: Diagram illustrating the motion of a typical internuclear vector, r_{ij} , when a solid is rotated with angular velocity ω_r about an axis inclined at angle β to H_O .

The first term in Equation (IV.4) is a constant and can give a reduced dipolar interaction and narrower spectrum by an appropriate choice of the angle β . By comparing Equation (IV.1) and the first term of Equation (IV.4) we can see that the line will be reduced in width by a factor of $\frac{1}{2}(3\cos^2\beta-1)$. If β is the "magic angle" $\cos^{-1}\sqrt{1/3}$, then a maximum reduction in width will be achieved. The second and third terms in Equation (IV.4) are periodic in time with frequencies ω_{r} and $2\omega_{\text{r}}$ and have mean values of zero. It has been shown [115,116] that these two items give rise to "rotational echoes" in the time domain which lead to "spinning sidebands" in the frequency domain on either side of the central resonance spectrum. The time-average Hamiltonian $\mathcal{H}_{\mathbb{D}}(\mathsf{t})$ at the "magic angle" will thus go to zero as in the case of fluids.

The second approach for dealing with both Equations (IV.1) and (IV.3) is the same, in principle, as the first one and will be discussed in the next section.

2. Chemical shift interactions:

Atoms in a magnetic field H_0 acquire a diamagnetic moment by virtue of the induced orbital motion of their electrons. These electrons produce a secondary magnetic field which will act on all of the nuclei present. The magnitude of this field will be proportional to the applied magnetic field H_0 . Thus, the local magnetic

field at the position of the nucleus will be given by [113]

$$H_{local} = H_0(1-\sigma) \tag{IV.5}$$

where σ is a dimensionless constant, independent of the field but dependent on the chemical environment, that is called the "screening constant". In a solid, because of the anisotropy of the chemical environment around a given nucleus, the NMR line will represent resonances of different chemically distinct environments of nuclei of a given type. This results in line broadening of the NMR spectrum. The chemical shift interaction of the nuclei in a non-metal can be represented by the Hamiltonian [116]

$$\mathcal{H}_{S} = \hbar \sum_{i} \gamma_{i} \sigma_{izz} I_{iz} H_{0}$$
 (IV.6)

Let us represent the principal values of σ by σ_p (p=1,2,3...,) and the direction cosines of its principal axes with respect to H_0 by λ_{ip} . Then

$$\sigma_{izz} = \lambda_{i1}^2 \sigma_{i1} + \lambda_{i2}^2 \sigma_{i2} + \lambda_{i3}^2 \sigma_{i3}$$
 (IV.7)

Again, in liquids the isotropic average value of λ^2 is $\frac{1}{3}$ so that

$$\sigma_{izz} = \frac{1}{3} \operatorname{tr} \sigma_{i} = \sigma_{i}$$
 (IV.8)

where σ_i is the scalar chemical shift encountered in the high resolution NMR spectrum in a fluid medium. In the MASS experiment, if χ_{ip} is the angle between the principal axis of σ_i and the rotation axis, then

$$λ_{ip}(t) = \cos \beta \cos \chi_{ip} + \sin \beta \sin \chi_{ip} \cos (ω_r t + ψ_{ip})$$
 (IV.9)

where ψ_{ip} is the azimuthal angle of the pth principal axis of σ_i . Now, to deal with Equations (IV.6) and (IV.9), let us consider the time average of $\lambda_{ip}^2(t)$ which can be given by

$$\frac{\lambda_{ip}^{2}(t)}{\lambda_{ip}^{2}(t)} = \cos^{2}\beta \cos^{2}\chi_{ip} + \frac{1}{2}\sin^{2}\beta \sin^{2}\chi_{ip}$$

$$= \frac{1}{6}(3\cos^{2}\beta - 1)(3\cos^{2}\chi_{ip} - 1) + \frac{1}{3}$$
(IV.10)

Substituting Equation (IV.10) into (IV.7) we get

$$\overline{\sigma_{izz}} = \frac{1}{2} \sin^2 \beta tr \sigma_i + \frac{1}{2} (3 \cos^2 \beta - 1) \sum_{p \neq p} \sigma_{ip} \cos^2 \chi_{ip}$$
 (IV.11)

At the "magic angle" β is equal to $54^{\circ}47'$, so that

$$\overline{\sigma_{izz}} = \frac{1}{3} \operatorname{tr} \sigma_{i} = \sigma_{i}$$
 (IV.12)

which is the same as for a liquid and the time average Hamiltonian $\overline{\mathcal{H}_S(t)}$ [replacing Equation (IV.12) into (IV.6)] will be the same as the Hamiltonian for liquids. However the time-dependent Hamiltonian will include periodic terms in ω_r and $2\omega_r$ which again give rise to the "spinning sidebands" at multiples of $\omega_r/2\pi$. It should be mentioned that when the chemical shift is expressed in Hertz (Hz) it becomes directly proportional to the applied field. It follows that chemical shift effects will be best observed at as high a field strength as possible, when they make the maximum contribution to the spectrum.

3. Electric quadrupolar interactions:

Nuclei with spin I > $\frac{1}{2}$ possess an electric quadrupole moment that can be attributed to a non-spherically symmetric nuclear charge distribution. The electric-nuclear quadrupole interactions in nuclear magnetic resonance can be divided roughly into two regions according to the magnitude of these interactions relative to Zeeman interactions. The first is called the "high field" case in which the nuclear electric quadrupole interaction energy is assumed to be small as compared to the interaction energy of the nuclear magnetic moment with the external magnetic field. In this case, the quadrupolar effects manifest themselves only as more or less significant perturbations of the purely magnetic interactions. The perturbation can split the resonance

line into several components whose number depends upon the nuclear spin. When the electrostatic field gradient at the nuclear position can be calculated the separation in frequency between these components yields the nuclear quadrupole moment. Accordingly, the quadrupolar interactions can result in a fine structure of the resonance line, because of overlapping lines, and may lead instead to a broadening or apparent loss of intensity of the resonance line. Furthermore, these interactions often reduce significantly the relaxation time necessary for the spin system to attain thermal equilibrium.

The second region is known as the "low field" case or the pure quadrupolar resonance. In such a case the quadrupole interaction can be so large that it becomes responsible for almost the entire dependence of the energy of a nucleus on its spin orientation. Only the first case will be considered here and will be discussed below.

The Hamiltonian for the interaction between the nuclear quadrupole moment and the electric field gradient is given by [114]

$$\mathcal{H}_{Q} = \sum_{i} \frac{eQ_{i}}{6I_{i}(2I_{i}-1)} (I_{i} \cdot V_{i} \cdot I_{i})$$
 (IV.13)

in which eQ_i is the nuclear electric quadrupole moment of nucleus i and V_i is the electric field gradient tensor

at its site. For simplicity a single crystal will be considered and we will assume that the electric field gradient has cylindrical symmetry so that the asymmetry parameter $\eta = (V_{XX} - V_{YY})/V_{ZZ}$ vanishes [114], where V_{XX} , V_{YY} and V_{ZZ} are the principal axes values of the electric field gradient tensors. The Hamiltonian can then be rewritten as

$$\mathcal{H}_{Q} = \frac{e^{2}qQ}{4I(2I-1)} \begin{bmatrix} \frac{1}{2}(3\cos^{2}\theta-1)(3I_{z}^{2}-I(I+1)) \\ +\frac{3}{2}\sin\theta\cos\theta[I_{z}(I_{+}+I_{-})+(I_{+}+I_{-})I_{z}] \\ +\frac{3}{4}\sin^{2}\theta(I_{+}^{2}+I_{-}^{2}) \end{bmatrix}$$
(IV.14)

where Θ is the angle between the principal axis of the electric field gradient tensor and the laboratory axis, and eq = V_{ZZ} . The quadrupolar Hamiltonian can be treated as a perturbation of the Zeeman Hamiltonian, \mathcal{H}_Z , and the calculation is extended to include the second-order terms, so that

$$E_{m} = E_{m}^{(0)} + E_{m}^{(1)} + E_{m}^{(2)}$$
 (IV.15)

and the frequencies that correspond to the spin transition $m \leftarrow -- m-1$ will be given by

$$v_{m} = \frac{E_{m-1} - E_{m}}{h} = v_{T} + v_{m}^{(1)} + v_{m}^{(2)}$$
 (IV.16)

where ν_L is the Larmor frequency of the nucleus and $\nu_m^{\,(1)}$ is the first-order splitting of the energy levels and is given by

$$v_{\rm m}^{(1)} = v_{\rm O} (m - \frac{1}{2}) \left[\frac{1}{2} (3 \cos^2 \Theta - 1) \right]$$
 (IV.17)

where $\boldsymbol{\nu}_{O}$ is the nuclear-quadrupole frequency and is given by

$$v_{O} = \frac{3e^{2}qQ}{h2I(2I-1)}$$
 (IV.18)

and e^2Q/h is the electric quadrupole coupling constant of the nucleus. The second-order frequency shift, $v_m^{(2)}$, is given by [117]

$$v_{m}^{(2)} = \left(\frac{v_{Q}^{2}}{12v_{L}}\right) |f_{1}^{H}|^{2} [24m(m-1) - 4a + 9] - \frac{1}{2} |f_{2}^{H}|^{2}$$

$$\times [12m(m-1) - 4a + 6] \qquad (IV.19)$$

where a = I(I+1), $|f_1^H| = \sqrt{3/2} \sin \theta \cos \theta$ and $|f_2^H| = 1/2\sqrt{3/2} \sin^2 \theta$.

For quadrupolar nuclei of half-integer spin, such as alkali metals (except ^6Li), the frequency of the central transition $-\frac{1}{2}$ is not shifted in first-order by the quadrupole interaction because the first-order shift $\nu_m^{(1)}$ vanishes for $m=\frac{1}{2}$ as indicated by Equation (IV.17). The frequencies of the other transitions will be shifted and satellite lines will appear on each side of the central

line. The second-order frequency shift of the central transition $(-\frac{1}{2}\longleftrightarrow\frac{1}{2})$ can be obtained by replacing m in Equation (IV.9) by $\frac{1}{2}$ and is given by

$$v_{\frac{1}{2}}^{(2)} = \frac{-v_{\frac{Q}{2}}^{2}}{16v_{\frac{1}{2}}} (a - \frac{3}{4}) (1 - \cos^{2}\theta) (9 \cos^{2}\theta - 1)$$
 (IV.20)

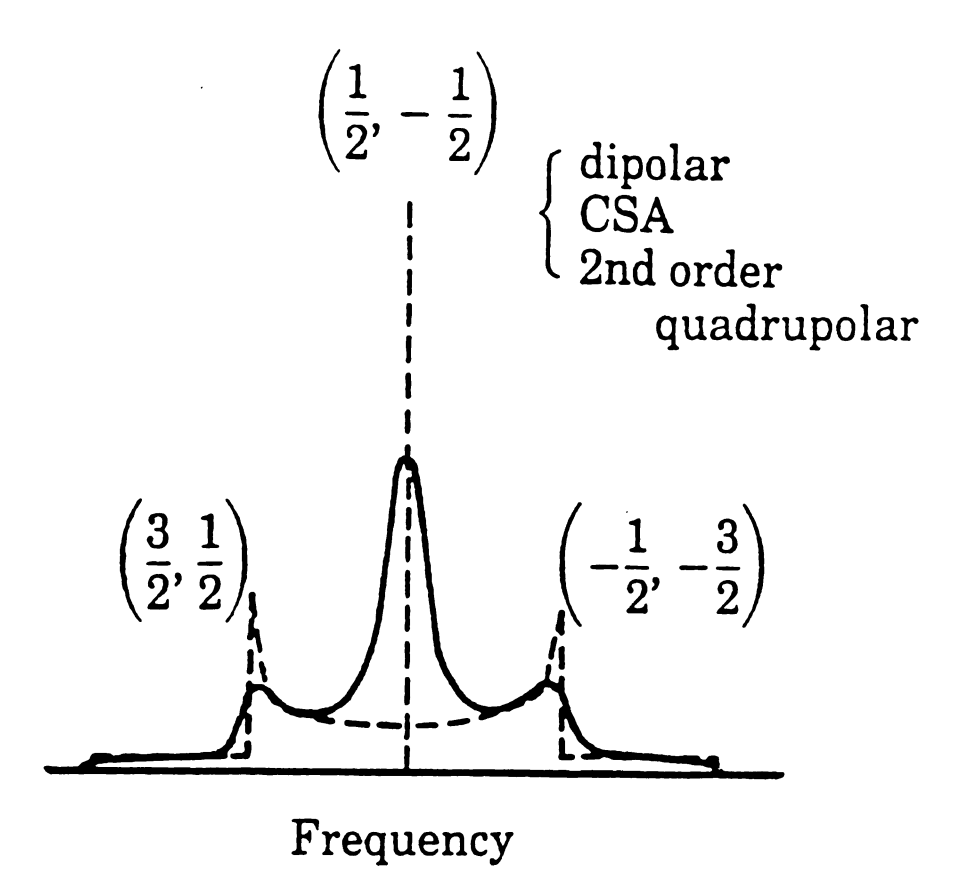
Figure 19a shows the NMR powder pattern of a nucleus of spin I = $\frac{3}{2}$ and the effect of first- and second-order quadrupolar interactions on the three transitions [118]. Frequently, the satellites are spread out over such a large frequency range that their wings become unobservable and it is well accepted that only the central transition is observable for the half-integer spin nuclei in non-cubic solids. This has been demonstrated by E. Oldfield et al. [118] who showed that the 23 Na-MASS-NMR spectrum of a mixture of equimolar amounts of NaCl (e^2 qQ/h $_{\sim}$ 0) and NaNO $_3$ (e^2 qQ/h $_{\sim}$ 0.3 MHz) (Figure 19b) consists of two 23 Na lines of different intensities. The two lines correspond to the three spin transitions in 23 Na in NaCl and only the central spin transition ($\frac{1}{2}\longleftrightarrow -\frac{1}{2}$ in NaNO $_3$.

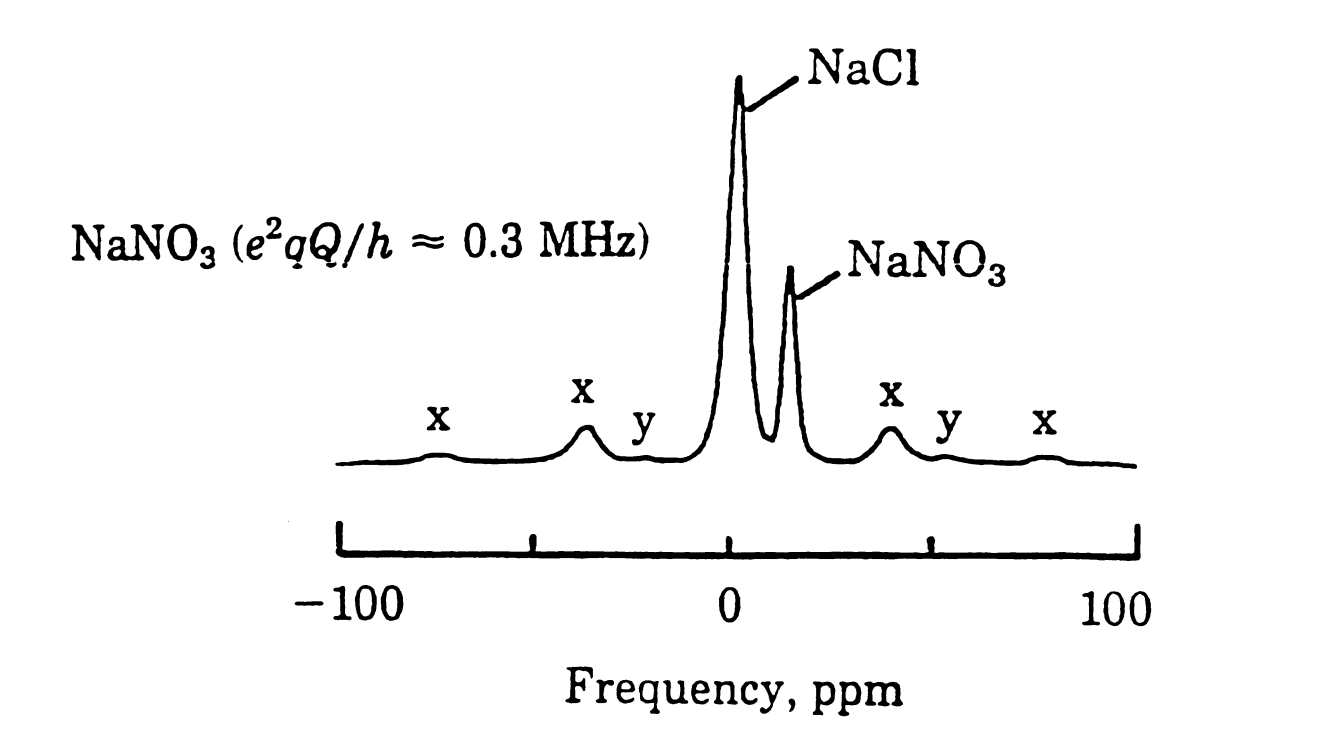
The effect of high-speed sample-rotation on the quadrupolar interaction in solids has been theoretically studied by Cunningham and Day [119]. They found that when the sample is rotating with an angular velocity $\omega_{\bf r}$ around an axis included at an angle β to the magnetic field, the first-order time-averaged diagonal terms of

Figure 19a(Top):

Spin I = 3/2 NMR powder pattern of an axially symmetric crystal showing the effect of first-order quadrupolar interaction (broken line) and second-order quadrupolar, dipolar, chemical shift (CSA) interactions (solid line) [114].

Figure 19b(Bottom): 23Na-MASS-NMR spectrum of equimolar mixture of NaCl and NaNO3. Resonance lines labeled x and y represent the spinning side bands [118].





the quadrupolar Hamiltonian are given by

$$\overline{\mathcal{H}}_{Q}(t) = \frac{e^{2}Qq}{16I(2I-1)} (3I_{z}^{2}-I^{2}) (1+\eta) (1-3\cos^{2}\beta) (1-3\cos^{2}\theta)$$
(IV.21)

Clearly, at the magic angle $(\cos^{-1}\sqrt{1/3})$ the first-order quadrupolar broadening can be eliminated provided that there is a sufficiently high rotation speed compared to the lifetime of a spin state, so that a given nucleus has ample time to "see" all orientations. Although the first-order quadrupolar interaction vanishes for the central transition of half-integer spin nuclei, the second-order effect is not averaged to zero by the magic angle experiment. This led to a general belief that the spectra of quadrupolar nuclei would be intractable. Contrary to that belief, it has been shown [120] that relatively high resolution spectra may be obtained from quadrupolar systems with half-integer spin by using the MASS-technique.

Equation (IV.20) predicts a residual linebroadening of \approx (e²qQ/h)² ν_L which is of the order of \approx 60 KHz for a quadrupolar coupling constant of 1 MHz and a Larmor frequency of 15 MHz. However, the detailed expression for the static second-order effect [(Equation (IV.20)] suggests that operation at high field (high ν_L) and preferably large I can make the experimental spectra tractable. In addition, when the numerical factors in

the full expression of $v_{\frac{1}{2}}^{(2)}$ are taken into account, there is a dramatic decrease in the residual linewidths [118] $(v_{\frac{1}{2}}^{(2)} \approx 10 \text{ ppm})$ upon fast spinning of the sample.

In summary, fast specimen rotation about an axis oriented at the angle β introduces the factor $\frac{1}{2}(3\cos^2\beta-1)$ into the time-average Hamiltonians which represent magnetic dipolar, chemical shift and first-order quadrupolar interactions. In fact, Andrew [115, 116] showed that the same factor also appears in the time-average Hamiltonian representing the indirect-electron-coupled spin-spin interaction. At the "magic angle" $54.74\,^\circ$ the anisotropic parts of these interactions are eliminated from the center of the spectrum and appear as spinning sidebands at each side of the spectrum at multiples of $\omega_{\rm r}/2\pi$ i.e. increasing the rate of rotation will move the sidebands further out. The intensities of these sidebands fall rapidly with increasing $\omega_{\rm r}$ as $\omega_{\rm r}^{-2n}$ for the nth sideband.

Finally, it is worth mentioning some of the limitations and factors that affect the resolution in the MASS technique. Although a relatively narrow NMR-line can be obtained from the MASS experiment, this is achieved at the expense of the information contained in the interactions described before. Three important factors greatly affect the resolution in the MASS experiment. These factors are, imperfect adjustments of the magic angle, angular instability and insufficiently

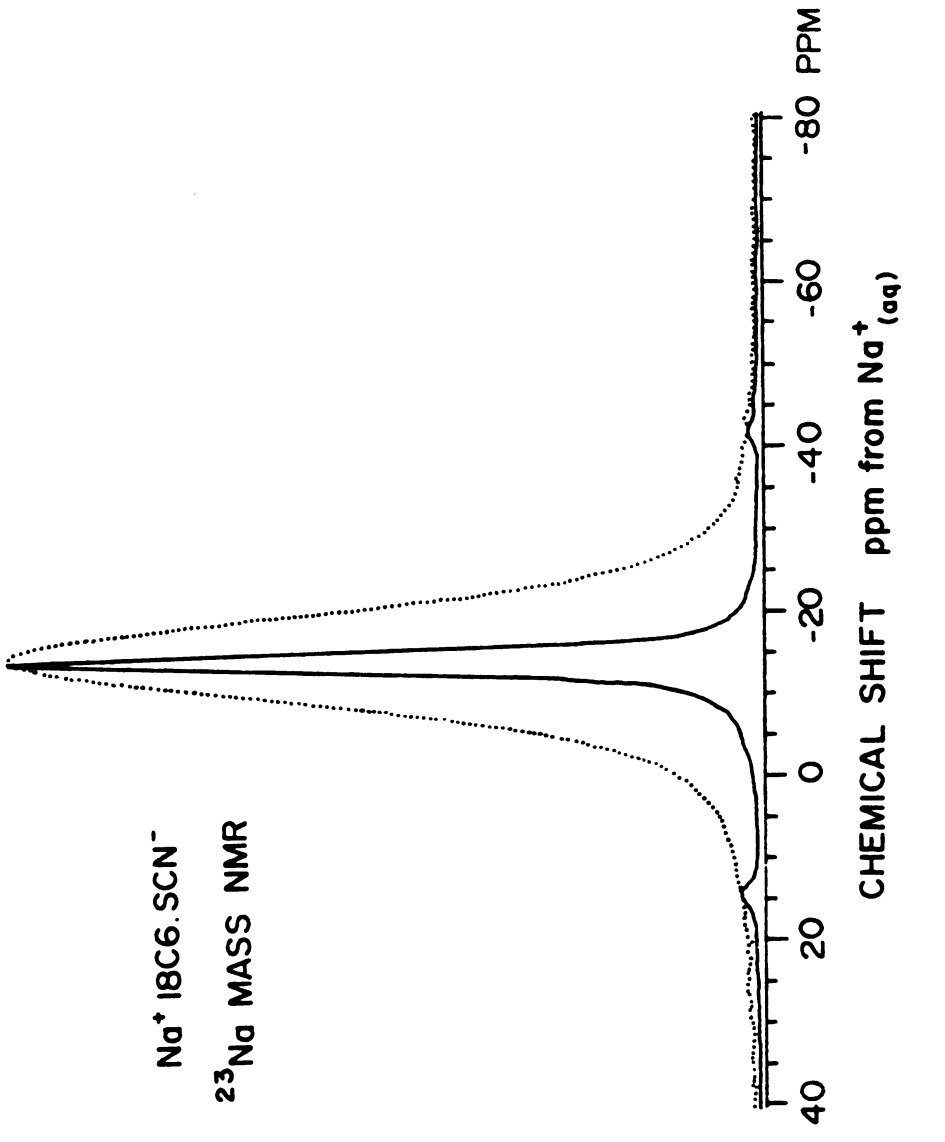
fast spinning. If the angle β deviates from the "magic" value by a small angle ε , 0.1° , the residual linewidth will be $\sqrt{2\varepsilon}$ of the original width [116]. Accordingly, the spinner axis must remain in adjustment and must not wander, wobble, or precess significantly from its correct orientation. In the MASS-experiment all of the interactions described above can be removed from the spectrum only if the spinning speed is high enough to average these interactions. For example, for the magnetic dipolar interaction, the spinning frequency should be equal to (or greater than) YH where H is the field produced by the other magnetic nuclei at the position of the nuclei in question. Accordingly, proton-MASS-NMR is totally intractable unless the protons in the system are very dilute or are largely separated from each other.

C. Results and Discussion

1. ²³Na-MASS-NMR:

a. Identification of the species

The sodium nucleus ²³Na, which has 100 percent abundance and spin 3/2, has an electric quadrupole moment on the order of 0.14 × 10⁻²⁴ cm² [121]. Consequently, the quadrupolar broadening in sodium salts may vary from 0 to 30 KHz [120]. Figure 20 shows a comparison between the MASS and static NMR spectra of Na⁺18C6.SCN⁻ measured



Static (dotted line) and spinning (solid line) ²³Na-NMR spectra of Na⁺18C6.SCN⁻ at 132.35 MHz. Figure 20:

at 132.35 MHz (500 MHz proton frequency). The linewidth of the Na⁺ signal was reduced by a factor of 4 upon spinning the sample at the "magic angle" ($\beta = \cos^{-1} \sqrt{1/3}$) with a spinning frequency of 3.7 KHz.

Table IV gives the chemical shifts (referred to Na (ag) at infinite dilution) and the linewidths of some conventional salts both with and without complexing agents and for a number of crystalline sodides. listed chemical shifts are not corrected for secondorder quadrupolar shifts of the resonance. The last column in Table IV contains the position of the optical absorption band of thin films prepared from methylamine solutions. The only homonuclear compound studied was Na C222.Na and its static and spinning spectra are shown in Figure 21. The MASS-spectrum contains two ²³Na signals that correspond to the sodium-cryptate cation and the sodium anion (Na). For heteronuclear sodides only a single 23Na peak was observed. The chemical shifts of these single peaks are in the range of -53 to -63 ppm which is quite different from the value obtained for the Na⁺ cation in model salts (~20 ppm). The corresponding chemical shift of the gaseous sodium atom is -61 ppm [124] while the calculated chemical shift for the gaseous sodium anion is -64 ppm [125]. Clearly, all of these alkalides are sodides and the concentration of Na+, either free or complexed is too low to give a detectable NMR signal. Dye et al. [55] reported an average value

Table IV: Results of ²³Na-MASS-NMR at 52.94 MHz

Compound	δ (ppm) ^a	Δν _ι (Hz)	Optical peak (cm ⁻¹)
Na (aq)	0	25	
NaCl	+ 8	140	
NaBr	+ 6	200	
NaI	- 3	160	
Na [†] 18C6.SCN [¯]	-22	700	
Na ⁺ C222.SCN ⁻	-21	1120	
Na ⁺ C222.I ⁻	-21	1300	
Na ⁺ C222.Na	-24	1200	
Na ⁺ C222. <u>Na</u> ⁻	-61	290	15,400 ^b
K ⁺ C222.Na ⁻	-61	400	15,100°
Rb ⁺ C222.Na ⁻	-61	360	13,800
LiC211.Na	-63	850	
K ⁺ 18C6.Na	- 56	120	14,000 ^đ
Rb ⁺ 18C6.Na ⁻	-60	90	13,800
Cs ⁺ (18C6) ₂ .Na ⁻	-62	75	14,600 ^d
K ⁺ (12C4) ₂ .Na ⁻	-61	51	13,100 ^e

^aChemical shifts of separate samples were generally reproducible to ±1 ppm.

^bReference 95.

^CReference 122.

dReference 98.

eReference 123.

fAqueous, infinite dilution.

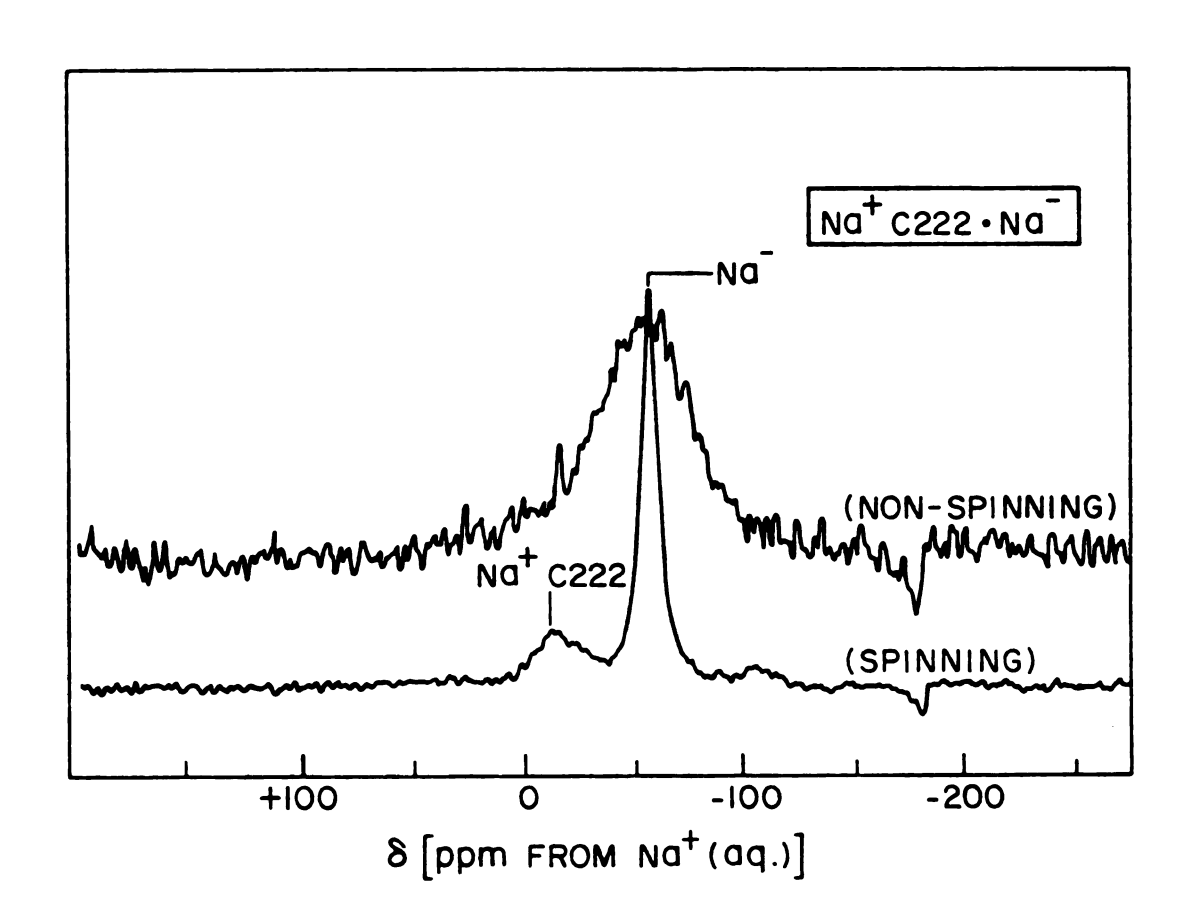


Figure 21: Static and spinning ²³Na-NMR spectra of Na+C222.Na- at 52.94 MHz.

of -62 ppm for the chemical shift of Na in different solvents, nearly independent of the solvent. Out of the eight sodides studied, six have anionic chemical shifts that range from -61 to -63 ppm and the other two, K[†]18C6.Na and Rb[†]18C6.Na, have chemical shifts of -58 and -60 ppm respectively. These two alkalides also have a substantial concentration of trapped electrons in the crystals as indicated by EPR spectroscopy (see next chapter). The interaction of such trapped electrons with Na might cause this paramagnetic (downfield) shift. However MASS-NMR spectra of some samples of Rb 18C6.Na and K⁺18C6.Na showed two Na peaks. For example, Rb18C6Na (at 52.94 MHz) showed two peaks at -62 and -53 ppm with linewidths of 40 and 530 Hz respectively while K18C6Na (at 132.35 MHz) showed two peaks at -60 and -57 ppm with linewidths of 180 and 223 Hz respectively. This behavior is not reproducible from one sample to another but was only observed for one sample of each while most of the samples studied showed only one Na peak. Figure 22 shows the MASS-NMR spectrum of K⁺18C6.Na⁻ at 132.35 MHz.

In general, the results obtained here, together with those from solution [55] suggest that the chemical shift of Na in the solid state as well as in solution, is remarkably insensitive to the nature of the sodide or the solvent. Also, the absence of any significant paramagnetic shift relative to the gaseous sodium anion

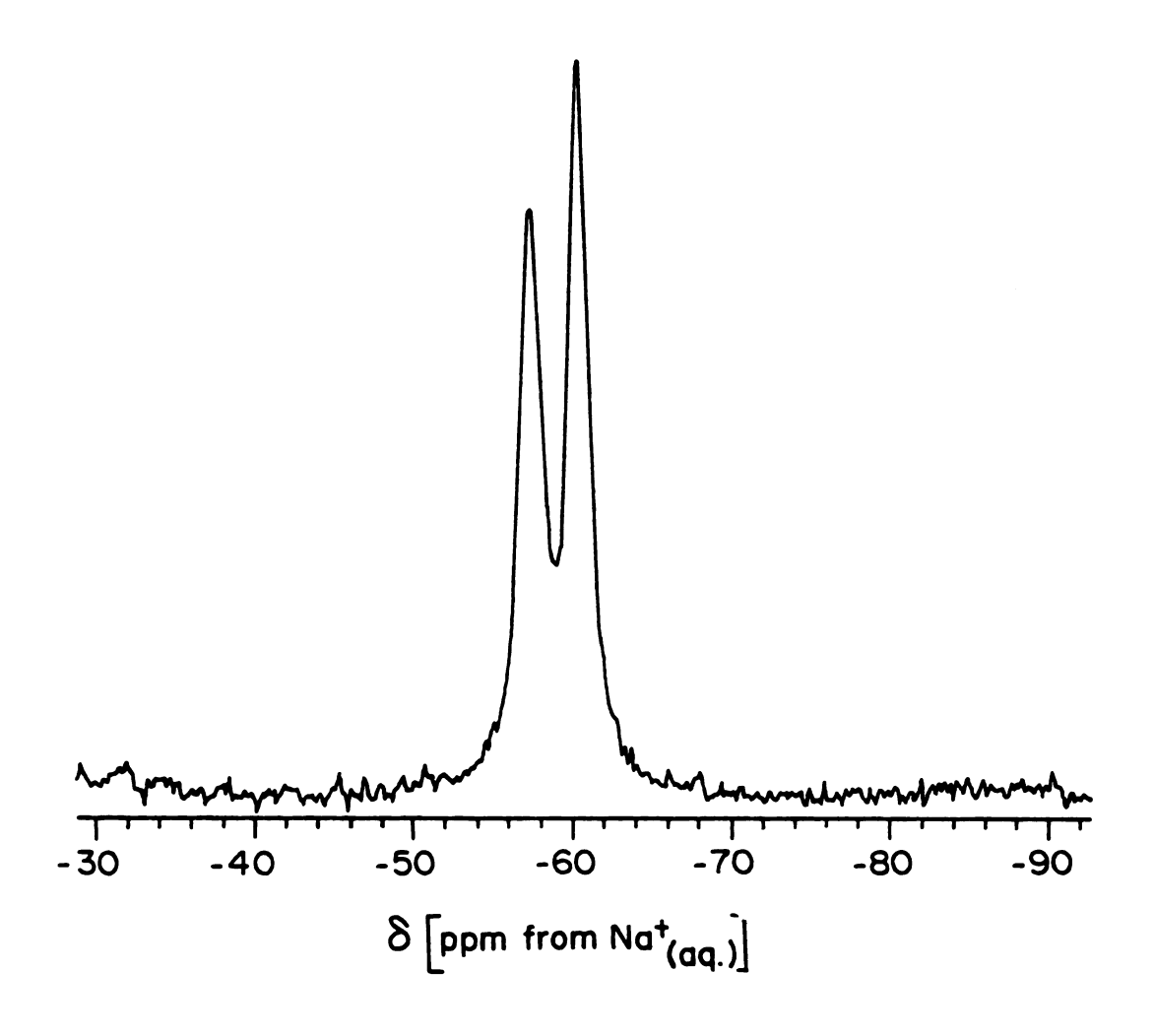


Figure 22: 23 Na-MASS-NMR spectrum of one sample of K⁺18C6.Na⁻ at 132.35 MHz.

suggests that the sodium anion exists in solid or solution as a "gas-like" anion with its 2p-orbital well shielded from the environment by the completely filled 3s-orbital. On the other hand, the position of the optical absorption bands are very sensitive to the environment. This is not unexpected since large solvent-dependent shifts have also been observed for the position of the optical absorption band of Na in solution [126]. This suggests that the excited state of Na (3s 3p) is very sensitive to the nature of the complex cation in the solid and the solvent in solution.

The variation of the linewidths among different compounds is rather interesting. The substantially narrower peaks for the Na in the crown ether salts compared to the cryptate case suggests greater interaction in the cryptate sodides and/or enhanced relaxation via interaction with the nitrogen atoms of the cryptand. narrow lines of the crown ether sodides suggest a rather symmetric environment and isolation from the neighboring cations. Similar line narrowing is observed in the model salts but in this case for the Na⁺-complex cation. Na⁺-18-crown-6 NMR line is narrower than that of the Na⁺-cryptate. This suggests a greater asymmetry of the electric field gradients at the Na⁺-cryptate. These electric field gradients are determined largely by the complexant environment and not by the nature of the anion.

b. Frequency dependence and proton decoupling

The results obtained for the linewidth of both the Na complex cation and Na suggest that there are significant interactions between the sodium nucleus and its environment. In general, the MASS-NMR line contains the residual magnetic dipolar, chemical shift interactions and the second-order quadrupolar effect which is not averaged to zero in the MASS-experiment. The residual chemical shift anisotropy is dependent on the magnetic field since the total spectral breadth is directly proportional to the applied field. The second-order quadrupolar frequency shift is inversely proportional to the Larmor frequency, i.e. to the applied magnetic field, and the spectrum gets narrower and the resonance position is shifted downfield upon increasing the magnetic field [see Equation (IV.20)]. In sodides formed with crown ethers and cryptands any magnetic dipolar interactions must arise mainly from the interactions of the sodium nucleus with the complexant protons and the nitrogen atoms of the cryptands. Sodium-homonuclear magnetic coupling is probably weak because of the large separation between the nuclei and the shielding of the Na by the complexant. Interaction with other magnetic nuclei such as 13 C and 17 O is negligible because their spins are very dilute. Table V summarizes the chemical shifts and linewidths of the sodide salts studied at three Larmor frequencies, 52.94, 95.29 and 132.35 MHz which correspond

Proton-Decoupled and Frequency Dependence of the Chemical Shift and Linewidth of $^{23}{
m Na}$ NAR Table V:

			_											
		MHz	Δν _λ , Hz	310	514	610	250	84	I	223	109	i	1	82
		132.35 MHz	δ, ppm	-13	-10	6-	-61	-61	ł	-57	-61	i	I	-61
	upled	MHz	Δν _k , Hz	I	I	720	190	210	270	185	20	75	64	48
	H-coupled	95.29	o, ppm	1	i	-11	-61	-61	-61	-57	-60	-62	-61	-61
		MHz	Δν, Hz	700	1300	1200	290	170	225	120	06	75	06	51
		52.94	%, ppm	-22	-21	-24	-61	-61	-63	-56	09-	-63	-61	-61
	peldno	MHz	Δν ₃₂ , Hz	610	680	860	30	30	09	78	40	70	45	33
of "Na NMR	¹ H-decoupled	52.94 MHz	δ, ppm	-22	-20	-20	-61	-62	-63	-58	09-	-63	-61	-61
of	Compound			Na 18C6.SCN	Na ⁺ C222.I	Na C222.Na	Na + C222. Na	K ⁺ C222.Na ⁻	Rb + C222.Na	K 18C6.Na	Rb 18C6.Na	cs ⁺ (18C6) ₂ .Na ⁻	K ⁺ (15C5) ₂ .Na	K ⁺ (12C4) ₂ .Na ⁻

to 200, 360 and 500 MHz proton frequencies. The effect of proton decoupling at 52.94 MHz is also included in the table. The Na⁺ signal in Na⁺C222.Na⁻ and the model salts seems to be only partly broadened by the proton-Na- dipolar interactions since the linewidths are still of the order of several hundred Hertz. The most interesting point is the quadrupolar powder pattern observed for the Na⁺ peak of Na⁺C222.Na⁻ and Na⁺C222.I⁻ but not for Na⁺18C6.SCN⁻. This indicates that quadrupolar interaction is the main source of line-broadening in the Na⁺ cryptate signal.

As expected for a quadrupolar system, the Na+cryptate chemical shift moves downfield and approaches its isotropic value, -9 ppm, at high magnetic field. This chemical shift value is in agreement with the value obtained for Na⁺-cryptate in solution with various solvents (-9 \pm 1 ppm) [55]. Figure 23 shows the MASS-NMR spectra of the compound Na⁺C222.Na⁻ at three frequencies and at 52.94 MHz with proton decoupling. A computer lineshape simulation [127] for the Na⁺-cryptate signal with proton decoupling showed the same lineshape with an asymmetry parameter equal to 0.1 and a quadrupolar coupling constant of 1.2 MHz. These parameters were used to predict the lineshape and isotropic chemical shift at Larmor frequencies of 95.29 and 132.35 MHz. Figure 24 shows a comparison between the observed and simulated spectra.

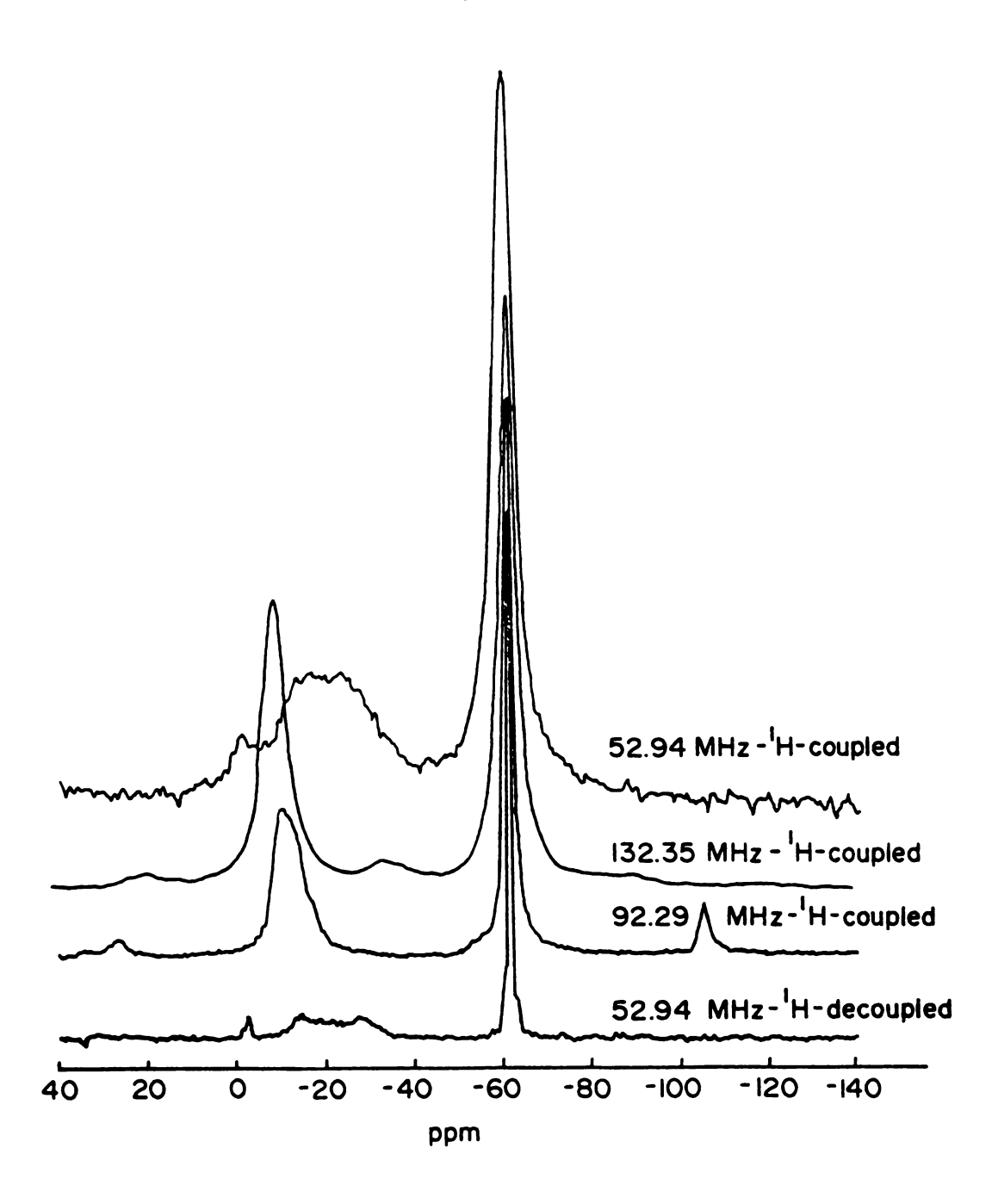


Figure 23: ²³Na-MASS-NMR spectra of Na⁺C222.Na⁻ at three different frequencies.

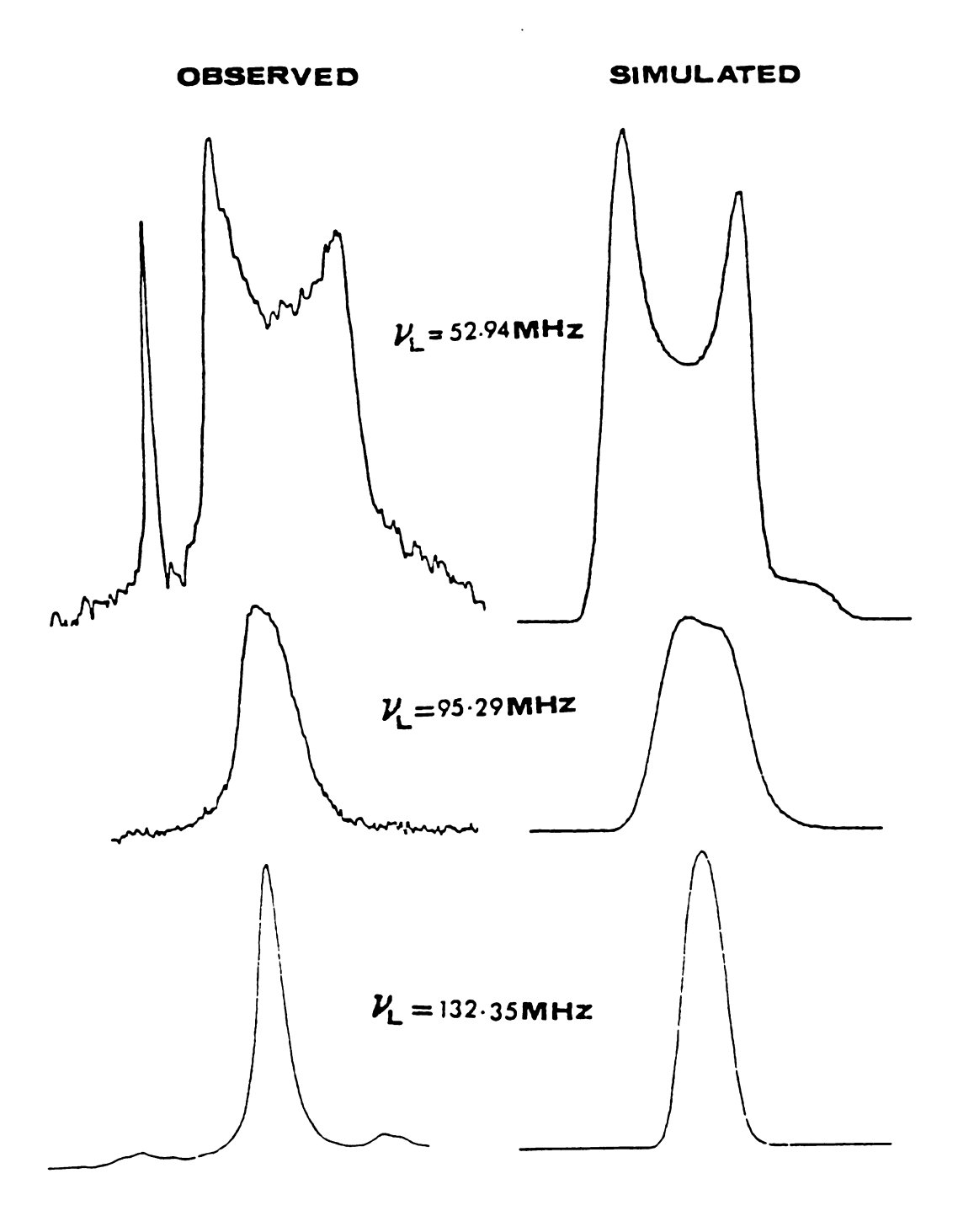


Figure 24: Observed and simulated Na-NMR signal of Na+C222 in Na+C222.Na at different frequencies.

The chemical shifts of the Na in all of the sodide salts remained constant when the field was increased indicating that the quadrupolar effect is minimal for this species. However, some of the Na lines showed a line broadening at higher fields which might be due to field inhomogeniety and/or residual chemical shift anistropy. On the other hand, the Na linewidths are greatly affected by proton decoupling. For example the Na signal in Na C222.Na is narrowed by a factor of 10 upon decoupling the protons. This indicates that the electric field at the Na is nearly symmetrical and implies near centrosymmetry of the Na anion.

In summary, line broadening is mainly due to quadrupolar interactions for the Na⁺-complex cation. This interaction dominates all other interactions present at low fields. At high magnetic fields the second-order quadrupolar effect is greatly reduced and the chemical shift approaches its isotropic value. The quadrupolar interactions are absent for Na⁻ because of its symmetry and magnetic dipolar coupling with the nearby protons of the complexant is the main source of line broadening. Figure 25 shows the MASS-²³Na NMR spectra of K⁺C222.Na⁻ at 52.94 MHz with and without proton decoupling and at 95.29 MHz.

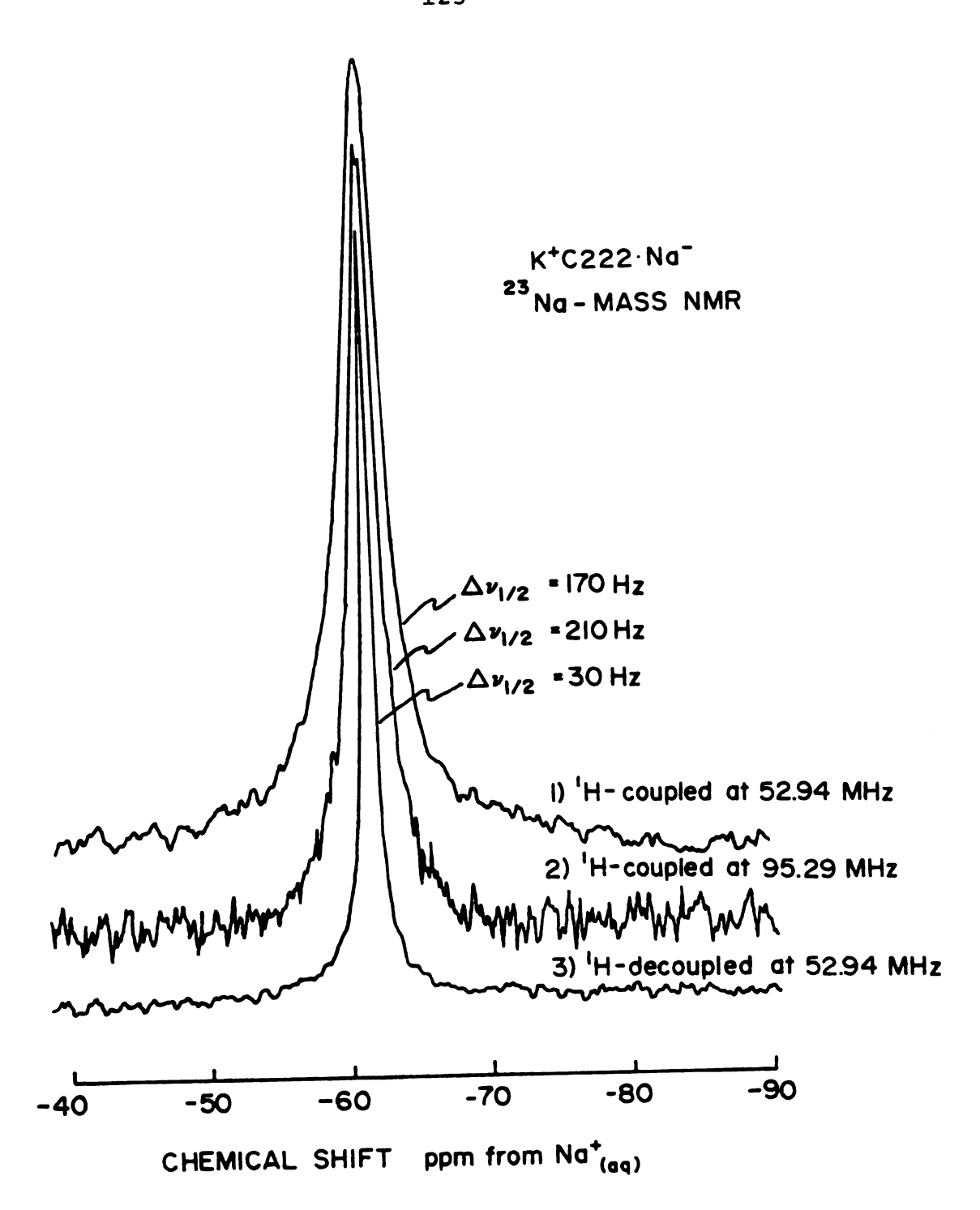


Figure 25: 23Na-MASS-NMR of K⁺C222.Na at different frequencies.

2. 133 Cs MASS-NMR

a. Species identification and frequency dependence

The cesium nucleus ¹³³Cs, which has 100 percent abundance and spin 7/2 has an unusually small electric quadrupole moment, -3 × 10⁻²⁷ cm² [121]. In general in solids the quadrupolar broadening in cesium salts is of the order of 10³ Hz and first-order theory suffices to describe it [115]. Accordingly, relatively narrow lines would be expected for cesium salts since, in principle, first-order frequency splitting is averaged to zero by spinning the sample at the magic angle [119].

Table VI summarizes the chemical shifts (referred to infinitely dilute $Cs^+_{(aq)}$) and the linewidths at 47.24 and 65.61 MHz (which correspond to 360 and 500 MHz proton frequencies) for cesium salts both with and without cation complexants and for a number of cesium-containing electrides and alkalides. Among the simple cesium salts only CsTPB shows no 133 Cs-NMR signal probably because it is too broad to be detectable. The model compounds of simple cesium salts with 18-crown-6 show narrower peaks compared to the corresponding salts without complexing agents, which indicates higher symmetry at the Cs⁺ cation upon complexation. The chemical shifts of 1:1 complex cations of Cs⁺ with 18-crown-6 depend on the anion and complexation of the Cs⁺ cation by 18-crown-6 causes upfield shifts relative to those of simple cesium salts.

Table VI: 133 Cs-MASS-NMR Results

	42.24	MHz	65.61 MHz	MHZ
	δ ^a , ppm	δ ^a , ppm Δυ _χ , Hz	6ª, ppm	Δν _k , Hz
0.7 M CsI (aq)	-23	30	-23	0.6
CSSCN	+190	190		1
CsC1	+232	125		1
CsBr	+264	1		1
CsI	+284	420	1	1
CSTPB			1	1
_cs_18c6.scn_	+73	100	1	
cs [†] 18C6.I	+171 ^b	280	+179	700
$\operatorname{Cs}^+(18C6)_2.\operatorname{SCN}^-$	-59	7.0	1	
$cs^{+}(18C6)_{2}I^{-}$	-59	47	- 59	80
$\mathrm{Cs}^+(\mathrm{18C6})_{\mathrm{2}}\mathrm{TPB}^-$	-43		-47	200
cs ⁺ c222.scn ⁻ c	+50, +275	210, 420		1
cs ⁺ c222.scn ^{- d}	+238		+238	133

Table VI Continues.

Table VI Continued.

	42.24 MHz	MHZ	65.61 MHz	MHz
	δ ^a , ppm	Δν _λ , Hz	νdd 'ρ	Δν _k , Hz
cs ⁺ c222.c1 ^{- d}	+167	860	İ	
cs [†] c222.1 ^{- d}	+232, +254	63, 135		
$cs^{+}(18C6)_{2}.e^{-}$	+81	135	68+	235
Cs ⁺ (18C6) ₂ .Na ⁻	-61	40	-62	160
$\mathrm{Cs}^+(18\mathrm{C6})_2.\mathrm{K}^-$	- 58	85	- 58	188
Cs ⁺ (18C6) ₂ .Rb ⁻	-57	115	-57	65
$\frac{\text{Cs}^+}{1806}$	-61	175	-49, -40	168, 300
$\operatorname{Cs}^+(18C6)_{2}.\underline{\operatorname{Cs}}^-$	-228	350	-230	435
CsC222.e_	+138, +238	320, 140	+134, +240	500, 350

 a Referred to infinitely dilute Cs $^{+}$ aq $^{-}$ Triplet peak.

^cSample prepared according to the directions of Weiss et al. [82].

 $^d\mathbf{Sample}$ prepared by solvent evaporation from a methanol solution.

This indicates less donation of electron density to the cesium ion in the complex than in simple salts. Salts that contain the 1:2 "sandwich" complex cation of Cs⁺ with 18-crown-6 show narrower peaks than those with the 1:1 complex. The chemical shift of the 1:2 complex is almost anion independent and the resonance position is shifted upfield relative to the 1:1 complex. This indicates that even more shielding from the counter-ion is achieved by adding a second ligand molecule to the 1:1 complex to form the "sandwich" complex. The results obtained here for solids are similar to those obtained by Dye and Popov [128,129] for solutions. They found that the 1:1 complex shows both solvent and anion dependent chemical shifts while the "sandwich" complex shows neither solvent nor anion dependency.

The NMR results for both solid and solution show that simple cesium salts can form both 1:1 and 1:2 complexes with 18-crown-6 in solution or in the crystalline state. The formation of 1:1 or 1:2 complexes in the solid state depends, however, on the method of preparation. For example, solutions of stoichiometries CsSCN.18C6 and CsSCN.(18C6)₂ formed the crystalline compounds Cs⁺18C6.SCN⁻ and Cs⁺(18C6)₂.SCN⁻, respectively, when the crystals were precipitated from 1-propanol solutions, but a mixture of 1:1 and 1:2 complexes were formed when a methanol solution of stoichiometry CsSCN.18C6 was evaporated to near dryness and allowed to cool to 0°C.

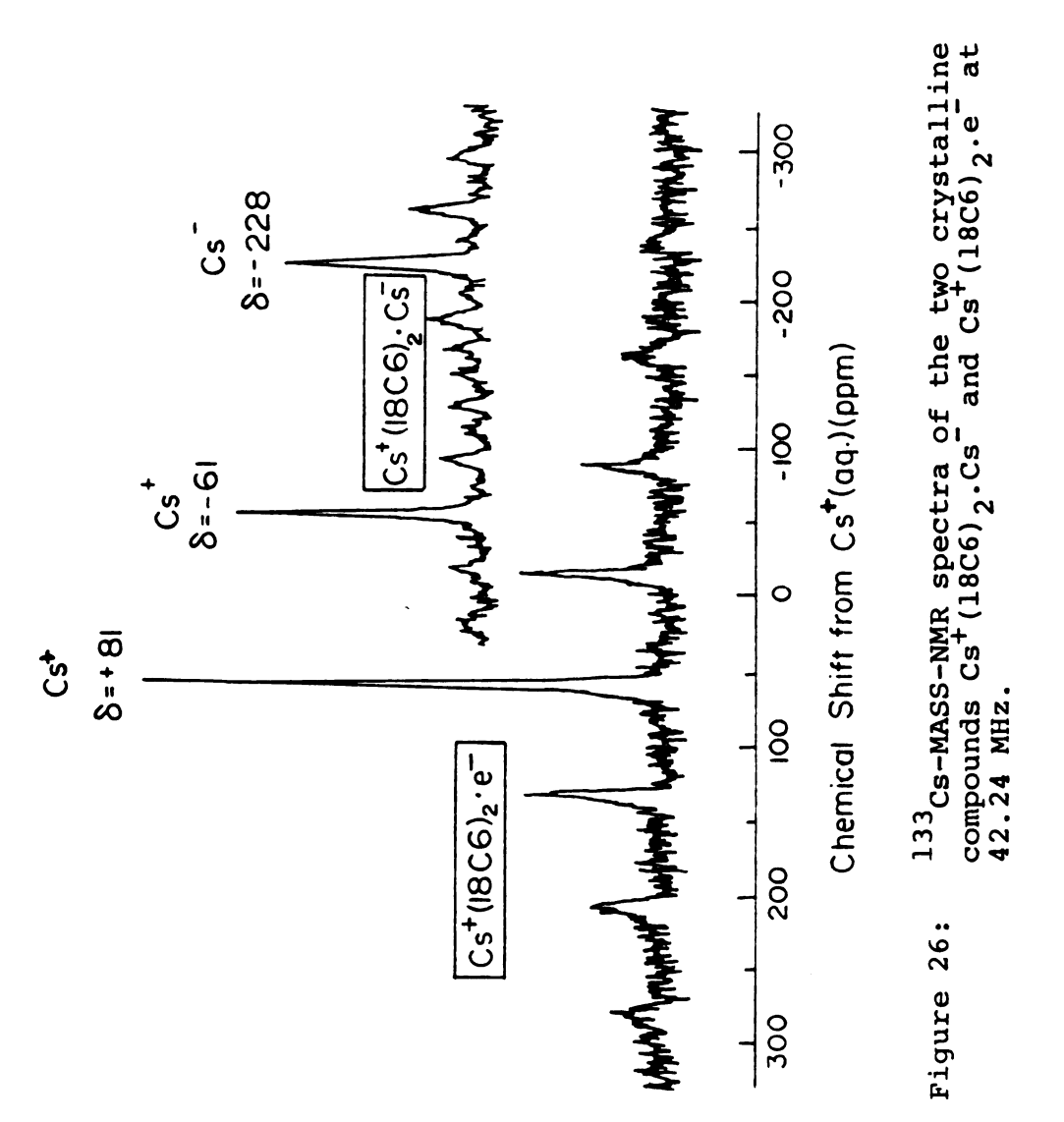
For cesium-containing electride and alkalide salts, 133 Cs-MASS-NMR provides an easy way to identify the species present in these compounds. Figure 26 shows a comparison between the ¹³³Cs-NMR spectra of the two compounds of stoichiometries Cs18C6 and Cs(18C6), measured at 47.24 MHz. The compound Cs18C6 shows two 133Cs-NMR lines at -61 and -228 ppm. The -61 ppm chemical shift value is in agreement with the chemical shift of the Cs tation in the "sandwich" complex Cs (18C6); the other peak is diamagnetically shifted to -228 ppm, which is close to the chemical shift value obtained for the Cs anion in THF solutions (-292 ppm) [55]. These results clearly show that the compound Cs18C6 is a ceside Cs⁺(18C6)₂.Cs⁻ and not an electride, Cs⁺18C6.e⁻ as initially presumed [104]. On the other hand the compound $Cs(18C6)_2$ shows only a single $^{133}Cs-NMR$ peak as expected for the electride Cs⁺(18C6)₂.e⁻. The resonance position of the electride peak is shifted about 140 ppm downfield (paramagnetic shift) from the expected position of the Cs cation in the "sandwich" Cs (18C6), complex. origin of this shift will be discussed later.

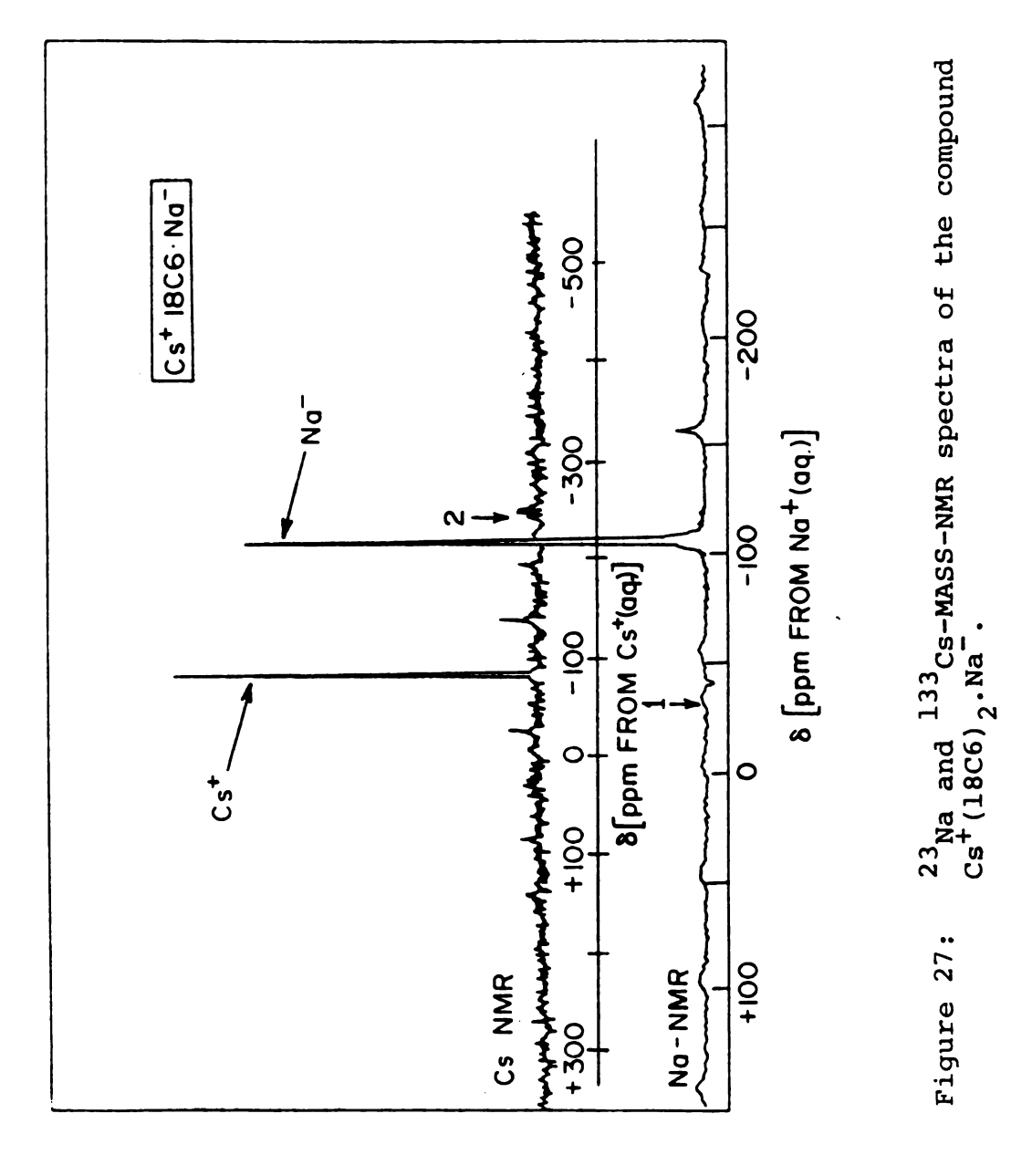
The other alkalide compounds, $CsNa(18C6)_2$, $CsK(18C6)_2$ and $CsRb(18C6)_2$ show only a single ^{133}Cs -NMR peak that corresponds to the Cs^+ cation in the $Cs^+(18C6)_2$ complex. This indicates that these compounds are $Cs^+(18C6)_2$.Na $^-$, $Cs^+(18C6)_2$.K $^-$ and $Cs^+(18C6)_2$.Rb $^-$ respectively. The results confirm that in contrast to model salts that

can form both 1:1 and 1:2 complexes of the Cs⁺ cation and 18-crown-6, only the 1:2 complex forms when alkalides or electrides are allowed to precipitate from amine and ether solutions, regardless of the solution stoichiometry. Figure 27 shows both ²³Na and ¹³³Cs-NMR spectra of the compound Cs⁺(18C6)₂.Na⁻ which was initially believed to be Cs⁺18C6.Na⁻ [94].

Increasing the magnetic field (i.e. increasing Larmor frequency) does not affect the resonance position, but the NMR lines at 65.61 MHz are broader than those at The line broadening is observed for the central transition $(-\frac{1}{2} \longleftrightarrow +\frac{1}{2})$ as well as for the total spectrum. The results indicate that quadrupolar interactions are minimal and that chemical shift anisotropy and magnetic dipole interactions are the main sources of line broadening in these compounds. This could be verified by examining the spinning spectrum with and without proton-decoupling and by studying the powder pattern of the static spectrum at different magnetic fields. The former was unavailable because of instrument limitations and the latter has not yet been done. However the static spectra of all cesium compounds which contain the "sandwich" $\operatorname{Cs}^+(18C6)_2$ complex show nearly the same powder pattern at 65.61 MHz.

Figure 28 shows the static and spinning spectra of the compound Cs⁺(18C6)₂.e⁻. The static spectrum shows the asymmetric profile characteristic of an axially symmetric chemical shift tensor similar to that observed





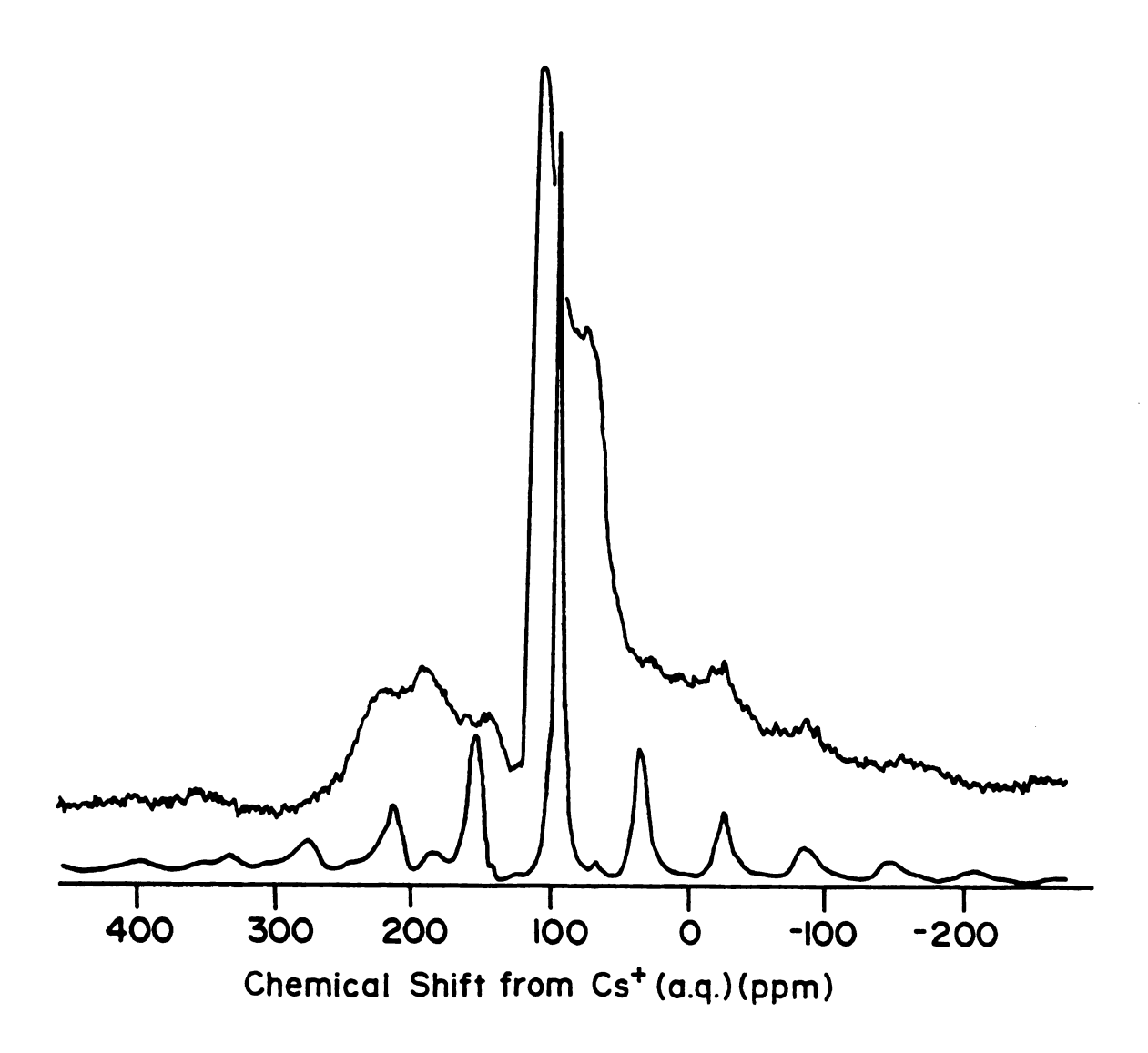


Figure 28: Static (top) and spinning (bottom) 133Cs-MASS-NMR spectra of the compound Cs⁺(18C6)₂.e⁻ at 65.61 MHz.

by Andrew et al. for 111Cd metal [130]. The isotropic chemical shift that is obtained by spinning the sample at the "magic" angle does not coincide with the peak position of the central transition of the static spectrum. This is expected since the anisotropic part of the chemical shift interactions is removed by spinning the sample at the magic angle leaving only the istropic part of it and appearing as spinning side bands. The structure that appears on both sides of the central transition $(-\frac{1}{2}\longleftrightarrow+\frac{1}{2})$ in the static spectrum must be due to other spin transitions of ¹³³Cs which collapse to a single line by spinning the sample at the magic angle. The fact that all cesium cations in the "sandwich" complex Cs (18C6), produce similar static NMR spectra indicates that local structure around Cs tations in these compounds is determined mainly by the complex cation and not by the anion.

The cesium-cryptate system shows rather interesting behavior. It is known that the Cs⁺ cation forms only 1:1 complexes with the cryptand 222. Dye and Popov [107] found that two types of complexed cations can be formed between Cs⁺ and C222 in solutions of simple cesium salts and C222 in non-polar solvents. These are the "inclusive" and "exclusive" complexes in which the Cs⁺ cation is totally inside the cavity ("inclusive") or partially complexed by the ligand ("exclusive"). However, X-ray diffraction studies of the compound Cs⁺C222. SCN⁻.H₂O [82]

show that there is only one cesium cation complex in this compound, the "inclusive" complex. The \$^{133}Cs-MASS-NMR spectrum of a polycrystalline sample of this compound, prepared according to the direction of Wiess et al. [82], showed, however, the presence of two \$^{133}Cs-NMR lines at +50 and +275 ppm, while samples prepared by dissolving equimolar amounts of CsSCN and C222 in methanol followed by solvent evaporation to dryness showed only one peak at +238 ppm. This demonstrates that cryptates with the Cs⁺ cation in either "inclusive" or "exclusive" sites (or both) can be formed depending upon the conditions used to prepare the compound.

The electride of stoichiometry CsC222 prepared by method 2 (see Chapter III) and the crystals formed from solutions of reactant stoichiometries Cs₂C222 (method 1), Cs₂C222Li (method 2) and CsC222 (method 3) all have two 133Cs-NMR lines at +138 and +238 ppm. The relative peak intensities vary from one preparation to another. However, the results indicate that regardless of the solution composition only one type of compound is formed with the stoichiometry CsC222. The peak positions and the variation of the peak intensity with the sample preparation method indicate that neither of these two peaks can be due to the Cs⁻ anion. The compound must, therefore, be an electride, Cs⁺C222.e⁻, with either two different sites for the Cs⁺ cation or two different kinds of crystals. Figure 29 shows a comparison between the

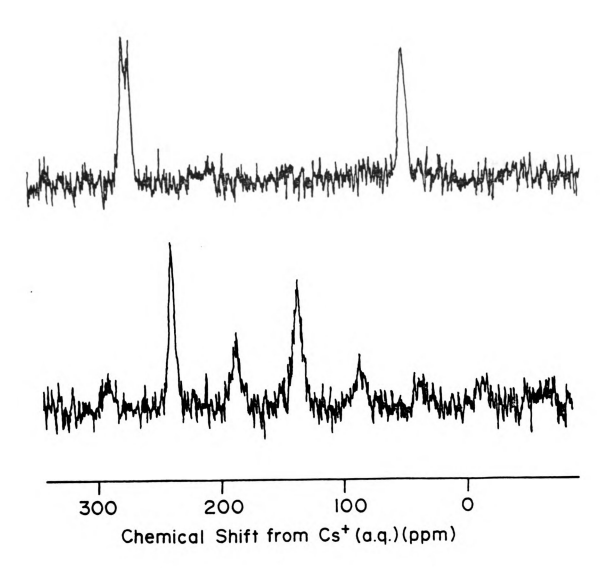


Figure 29: 133Cs-MASS-NMR spectra of the two crystalline compounds Cs⁺C222.SCN⁻.H₂O (top) and Cs⁺C222.e (bottom) at 42.24 MHz.

133Cs-MASS-NMR spectra of the two compounds Cs⁺C222.SCN⁻.

H₂O and Cs⁺C222.e⁻ measured at 47.24 MHz.

It is difficult, based upon the NMR results, to determine whether these two cesium sites are present in a single crystal (mixed crystal) or if the compound CsC222 consists of two crystalline forms (mixture of crystals). However, the +238 ppm peak in the CsC222 NMR spectrum is close to the +244 ppm limiting value obtained for a 1:1 mixture of CsSCN and C222 in methanol solution at low temperatures [107]. This resonance was attributed [107] to the "inclusive" complex between the Cs + cation and cryptand 222. The large paramagnetic shift occurs because the cryptand cavity has been deformed or stretched to permit inclusive complexation of the large Cs⁺ cation. This tightly fitting cesium ion inside the stretched cavity results in strong overlap of the lone-pair orbitals of the ligand and the outer p-orbital of the Cs+ cation, which causes large downfield (paramagnetic) shifts. The other peak at +138 ppm might be due to the "exclusive" complex, in which the Cs tation is partially enclosed in the cryptand cavity to give weaker overlap and less paramagnetic shift. The intensities of the two 133Cs-NMR peaks depend on the method of preparation of the compound CsC222. The crystals of CsC222 prepared by methods 1 and 2 show comparable intensities of the two signals while the compound prepared by method 3 shows mainly the signal of the "exclusive" complex. Figure 30

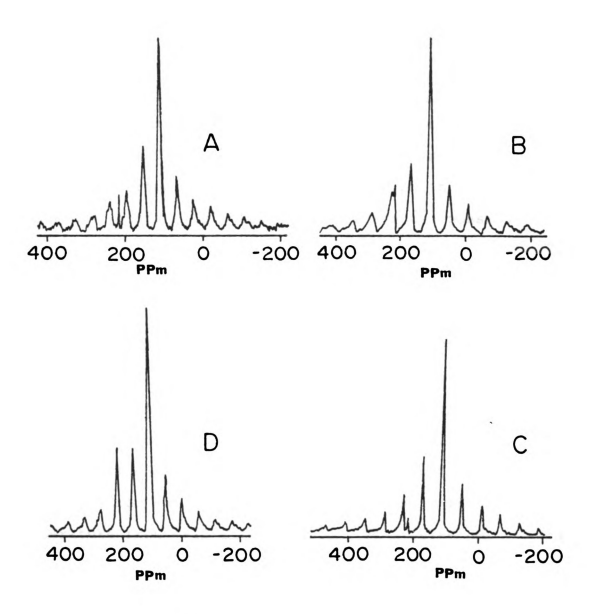


Figure 30: 133 Cs-MASS-NMR spectra at 65.61 MHz of the compound Cs^{*}C222.e⁻ at different spinning frequencies: A: 1.8, B: 2.6, C: 3.8 and D: 4.0 KHz.

shows the ¹³³Cs-MASS-NMR spectra at different spinning speeds of the compound Cs⁺C222.e⁻ prepared by method 3.

b. The chemical shift of Cs⁺(18C6)₂.e⁻

The resonance position of the Cs⁺ cation in the compound Cs (18C6) 2.e is shifted about 140 ppm downfield from the expected position for a Cs⁺ cation in the "sandwich" complex Cs⁺(18C6)₂. There are two possible sources of this shift. These are the structural and paramagnetic effects. The former presumes that the structures are different and should be temperature independent. If the shift is due to the paramagnetism of the sample, however, one expects a strong dependence of the shift on temperature that would approach the "normal" chemical shift value as the temperature goes to infinity. The chemical shift of the compound Cs + (18C6) 2.edecreased from +89 to +74 ppm upon increasing the temperature from ≈-20°C to ≈+15°C. This rules out structural difference between the electride and model compounds or alkalides, Cs⁺(18C6)₂.N⁻, where N⁻ is the alkali metal anion, as the origin of the 140 ppm shift. However, if we consider the +61 ppm obtained for the chemical shift of the Cs⁺ cation in the compounds $\mathrm{Cs}^+(18\mathrm{C6})_2.\mathrm{Cs}^-$ and $\mathrm{Cs}^+(18\mathrm{C6})_2.\mathrm{Na}^-$ as the "normal" chemical shift of the compound Cs + (18C6) 2.e at infinite temperature then the plot of δ vs. $\frac{1}{T}$ should yield a straight line if the 140 ppm shift is due to the paramagnetism of the

sample. Indeed, the plot of the chemical shift (δ) of the compound $\text{Cs}^+(18\text{C6})_2.e^-$ versus $\frac{1}{T}$ yield a straight line which is compatible with Curie-Law behavior of this compound.

For a system with unpaired spins the paramagnetic effect can occur through the presence of actual electron density in an S-state at the nucleus, the so-called "contact" or "Fermi" shift, or through space by dipolar effects which is called the "pseudo-contact" shift [121]. The "contact" shift, $\Delta v_{\rm C}$ in a paramagnetic substance of isotropic g-value is given by

$$\frac{\Delta v_{c}}{v} = \frac{\Delta H}{H} = \frac{\chi_{a}}{Ng_{e}\beta g_{N}\beta_{N}} = \frac{-8\pi}{3N} \chi_{\rho}(N)$$
 (IV.22)

where ΔH is the local magnetic field produced by the unpaired electron at the nucleus, χ is the spin-only susceptibility, a is the isotropic hyperfine splitting constant, N is Avogadro's number, g_e and g_N are the electron and nuclear g-factors, β and β_N are the electron and nuclear magnetons respectively and $\rho(N)$ is the electron density at the nucleus. The "pseudo-contact" shift occurs whenever there is an unpaired electron in a molecule. This dipolar effect, transmitted through space and felt by the nucleus, causes a paramagnetic shift. In solution with an isotropic g-value, this dipolar effect is averaged to zero by rapid rotation of the molecules in the field. In

solids and in solutions with anisotropic g-tensors, the magnitude of the dipolar contribution to the magnetic field at the nucleus of interest from the unpaired electron density will depend on the orientation of the molecule with respect to the field.

The "pseudo-contact" contribution to the shift, $\Delta\nu_{i}\,(\rho c)\,, \mbox{ at the nucleus is given by [121],}$

$$\frac{\Delta v_{i}(p)}{v} = \frac{1}{3N} \left[\chi_{z} - \frac{1}{2} (\chi_{x} + \chi_{y}) \right] \left(\frac{3 \cos^{2} \theta_{i} - 1}{r_{i}^{3}} \right)_{av}.$$

$$- \frac{1}{2N} (\chi_{x} - \chi_{y}) \left(\frac{\sin^{2} \theta_{i} \cos^{2} \phi_{i}}{r_{i}^{3}} \right)_{av}. \tag{IV.23}$$

where $\chi_{X'}$, $\chi_{Y'}$, χ_{Z} are the susceptibility components, and the angles θ and ϕ are the polar angles of the vector $\mathbf{r_i}$. The last equation should average to a very small value under the condition of fast spinning of the sample at the magic angle because of the term $3\cos^2\theta_{\mathbf{i}}$ -1. For an axially symmetric system, $\chi_{\mathbf{x}}$ is equal to $\chi_{\mathbf{y}}$ and the second term of Equation (IV.23) vanishes. Therefore, the "pseudo-contact" contribution to the shift should vanish for an axially symmetric system in the MASS experiment. It should be mentioned that both the contact and pseudo-contact shifts depend on the susceptibility of the sample. However, Garroway et al. [131] and Stoll et al. [132] reported that magic angle sample spinning should remove bulk susceptibility broadening in a powder of randomly shaped particles, provided that the

susceptibilities of the particles are small and isotropic. On the other hand, the effects of anisotropic susceptibilities are <u>not</u> removed by magic angle spinning because they are analogous to chemical shift screening by nearby currents [131], since both interactions are electron-nuclear dipolar in origin. However, the anisotropic magnetic susceptibility tensors should be averaged to $\frac{1}{3}$ of the trace by spinning the sample at the magic angle.

The linewidth of the central transition as well as the total spectral breadth in the MASS-NMR spectrum of the compound Cs (18C6) 2.e are comparable to those of the model salts and the alkalide compounds with the general formula Cs (18C6)2.X . This indicates that line broadening due to any anisotropic magnetic susceptibility of the sample has been removed by spinning the sample at the magic angle. Since the powder pattern of the static spectrum of the compound Cs⁺(18C6)₂.e⁻ shows the asymmetric profile characteristic of an axially symmetric system, the "pseudo-contact" term cannot contribute appreciably to the shift. Therefore, the 140 ppm shift in the resonance position of the compound Cs + (18C6) 2.e is mainly due to the contact shift. The presence of electron density at the nucleus requires, however, a hyperfine coupling which normally gives splitting in the EPR spectrum. In most of the cases it also is associated with an electronic q-shift. Neither hyperfine splitting nor a g-shift is observed in the EPR spectrum

of the compound Cs⁺(18C6)₂.e⁻. The absence of hyperfine splitting could, of course, result from fast spin exchange among the electron spins which would "wash out" the hyperfine pattern and result in a very narrow EPR line. In fact the linewidth of the EPR line of the compound Cs⁺(18C6)₂.e⁻ is very narrow (0.5 G) and it is temperature independent. The absence of an electronic g-shift associated with spin-orbit coupling could be cancelled because of symmetry. For example, the EPR lines of gaseous alkali metal atoms reflect the presence of a large contact density at the nucleus but there is not an appreciable g-shift [133].

c. Electron doping in the ceside compound:

The ¹³³Cs-MASS-NMR at 47.24 MHz of the "pure" ceside compound, Cs⁺(18C6)₂.Cs⁻ (Figure 26), which was prepared by method 2, shows two ¹³³Cs-NMR lines. One line, which corresponds to the Cs⁻ anion, is diamagnetically shifted to -228 ppm relative to infinitely dilute Cs⁺_(aq) and is broader than the line that corresponds to Cs⁺ in the Cs⁺(18C6)₂ complex. At 65.61 MHz another sample of the compound Cs⁺(18C6)₂.Cs⁻ had an NMR spectrum that contained three lines at chemical shifts of -210, -50 and -40 ppm. These correspond to the presence of one site for the Cs⁻ anion that gives a chemical shift of -210 ppm and two sites for the complex Cs⁺(18C6)₂

(at -50 and -40 ppm). Figure 31 shows the MASS-NMR spectrum of the compound $Cs^+(18C6)_2.Cs^-$ at 65.61 MHz.

The "pure" electride compound Cs (18C6)2.e shows a single ¹³³Cs-NMR peak whose resonance position depends on the temperature and is paramagnetically shifted by the presence of a large concentration of the unpaired spins. For the compound corresponding to reactant stoichiometry Cs18C6, prepared by method 3, the MASS-NMR spectrum at 47.24 MHz shows the presence of at least three peaks at +74, -52 and -242 ppm respectively (Figure 32). The peak at -242 ppm also has a shoulder at -210 ppm. At 65.61 MHz another sample (also prepared by method 3) had an NMR spectrum which contained five NMR lines at -228, -210, -52, -50 and +93 ppm (Figure 33). The three lines obtained for one sample at 47.24 MHz and five lines obtained from another preparation are consistent with the presence of a mixture of two compounds: Cs⁺(18C6)₂.e⁻ and Cs⁺(18C6)₂.Cs⁻. Only one line (at +74 and +93 ppm) can be attributed to the compound Cs (18C6) 2.e while either one or two lines are present for Cs⁺(18C6)₂ and for the Cs⁻ anion in the compound Cs + (18C6) 2.Cs -. Magnetic susceptibility measurements of this mixed system showed that the sample contained ≈17% unpaired spins. However, further MASS-NMR and magnetic susceptibility studies [134] showed that samples of this mixed system with different susceptibilities have essentially the same chemical shift values and the same number of NMR lines. In other words, the chemical

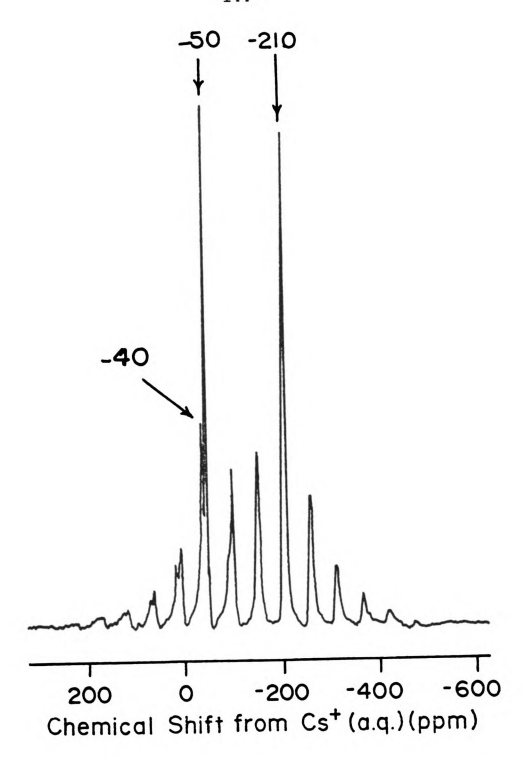
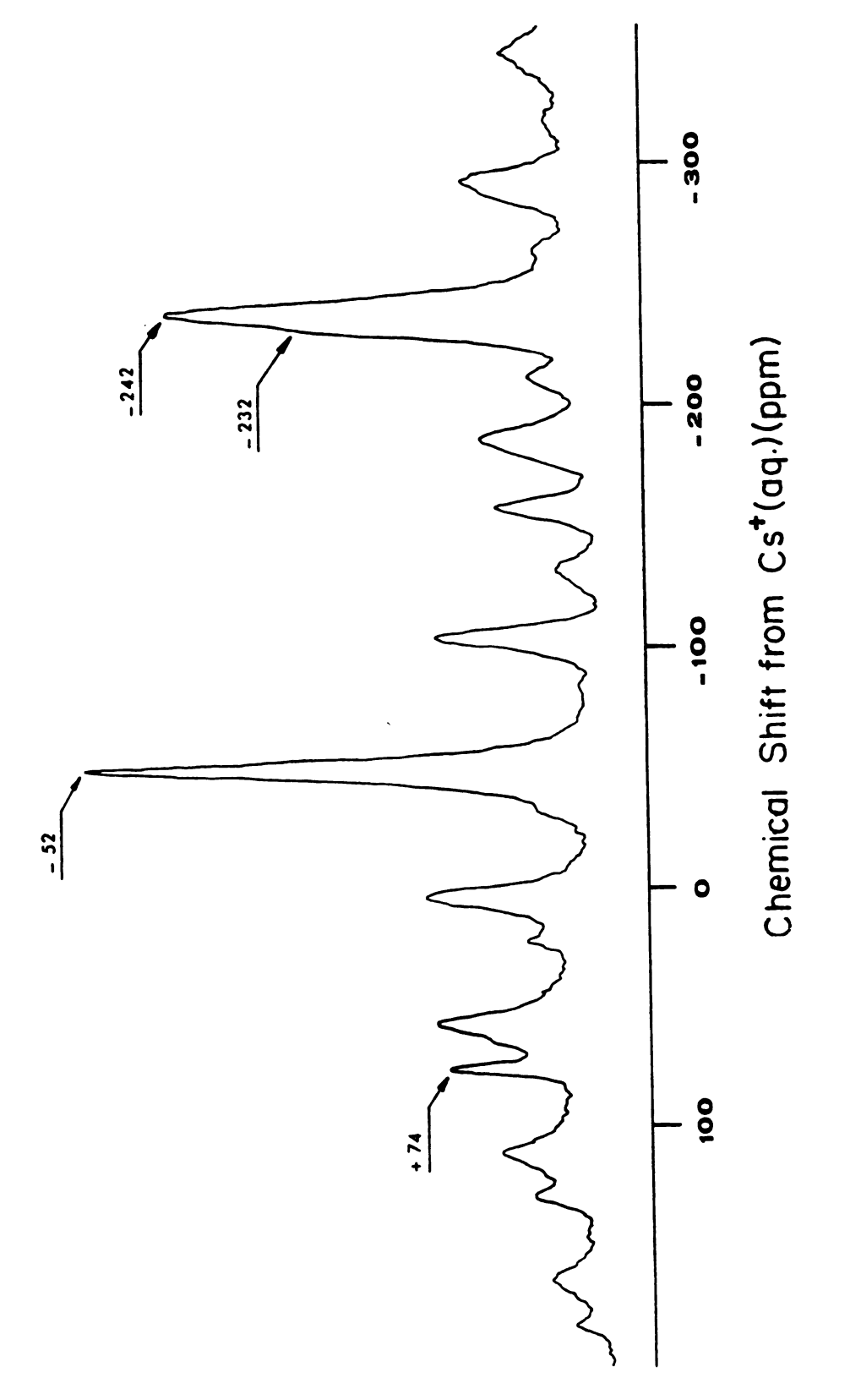


Figure 31: 133Cs-MASS-NMR spectrum of one sample of Cs+(18C6)₂.Cs (method 2) at 65.61 MHz.



 $^{133}\mathrm{Cs-MASS-NMR}$ spectrum of one sample of $\mathrm{Cs}^+(18\mathrm{C6})_2\mathrm{Cs}^-$ (method 3) at 42.24 MHz. Figure 32:

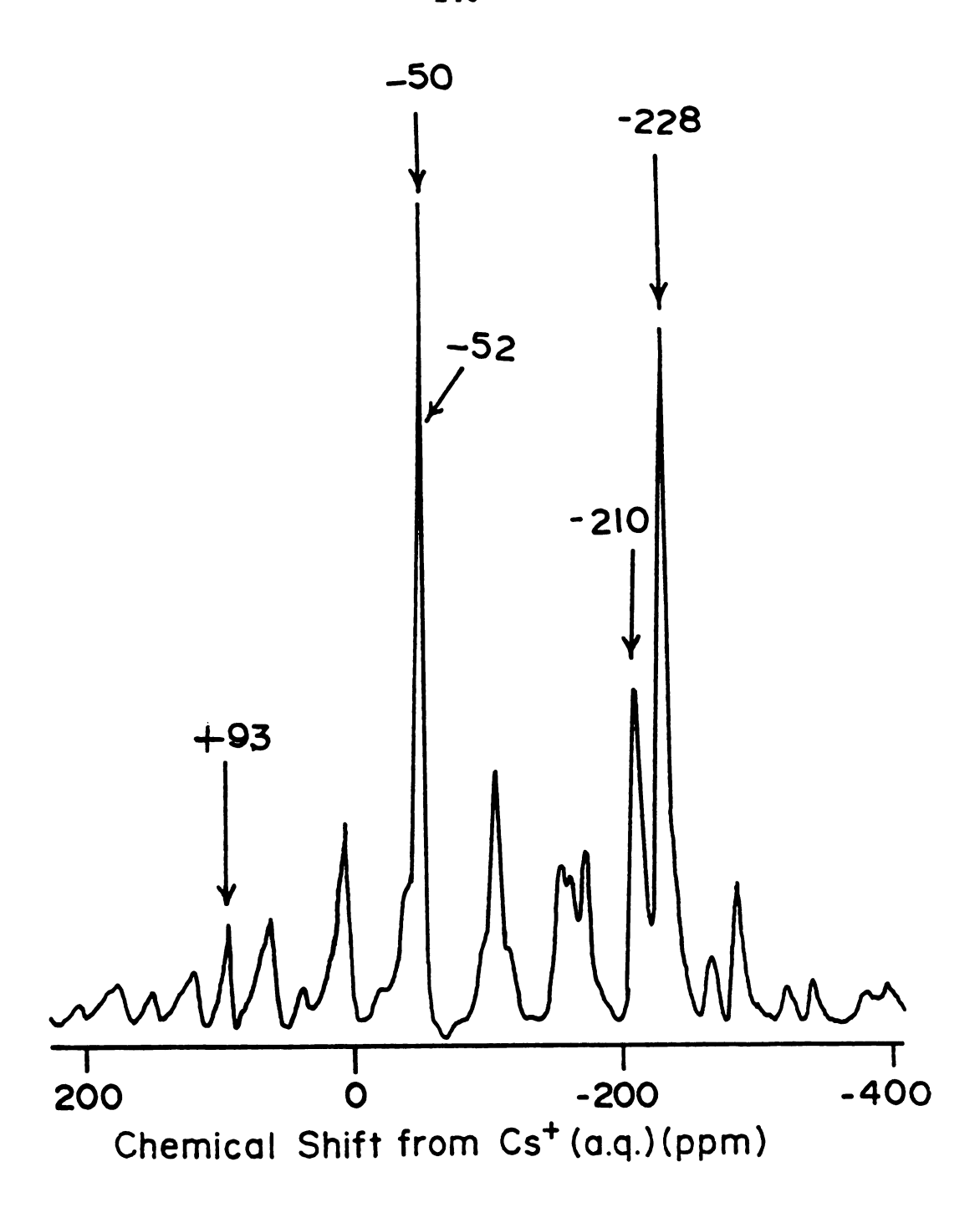


Figure 33: 133Cs-MASS-NMR spectrum on one sample of Cs⁺(18C6)₂Cs⁻ (method 3) at 65.61 MHz.

shifts are independent of the bulk susceptibility of the sample. This indicates that a mixture of the two compounds is present in the polycrystalline samples rather than mixed crystals of one type.

The results are complicated, however, by the chemical shift values obtained for the Cs line in the "pure" ceside and in the mixed system. Three values of the Cs chemical shift were observed in the samples studied. These values are -242, -228 and -210 ppm. It is difficult to tell which one of the three values represents the chemical shift of the "pure" Cs anion because some electron doping was observed for every sample by EPR and magnetic susceptibility measurements. The presence of three resonance lines for the Cs anion suggests different degrees of electron doping in the various preparations of the ceside compound. The presence of electron doping could also explain the presence of two sites for the complex cation Cs⁺ (18C6)₂. It would be a mistake, however, to consider the most diamagnetic shift, -242 ppm, as the chemical shift of the least doped ceside, because electron doping could cause either an upfield or a downfield shift if it operates via a spin polarization process.

In general, the electride can always be produced along with the ceside compound because of the method of preparation. Also, the ceside crystals could be doped by electrons to different extents depending on the

method of preparation. Until some structural information is available, the origin of the multiple lines for the $\mathrm{Cs}^+(18C6)_2$ and Cs^- will remain unclear.

3. 87 Rb-MASS-NMR

The rubidium nucleus has two isotopes, 85Rb with a natural abundance of 72.8% and spin 5/2, and ⁸⁷Rb with 27.2% natural abundance and 3/2 spin. The magnetic properties of these two isotopes are quite different. The 85 Rb nucleus has the largest electric quadrupolar moment among the alkali metal nuclei. A typical value of 0.31×10^{-24} cm² [121] has been reported for the electric quadrupolar moment of ⁸⁵Rb. Although ⁸⁷Rb has an electric moment of only 0.15×10^{-24} cm² [121], which is very close to that of the ²³Na nucleus, the natural linewidth of 87 Rb is much larger than that of 23 Na in solution. This difference in linewidth is due to the large Steinheimer antishielding factor [135] of the Rb⁺ cation compared to that of the Na tation. The Steinheimer antishielding factor, $1 + \gamma_m$, is a measure of the effective field gradient, V,, produced at an atomic nucleus as a result of polarization effects in the core electron distribution induced when the atom as a whole is exposed to an electric field gradient [135]. It is given by the equation

$$V_{22} = V_{22}^{O}(1+\gamma_{\infty})$$
 (IV.24)

in which V_{ZZ}^{O} is the field gradient caused by charge distributions outside of the atom. The Steinheimer antishielding factor for the Na $^+$ cation is 6.18 while that of the Rb $^+$ cation is 56.0 Accordingly, the 87 Rb NMR line should be nearly ten times broader than the 23 Na NMR line for equal asymmetries of the field at the nucleus.

Equation (IV.19) for the second-order quadrupolar broadening tells us that nuclei with higher spin and larger Larmor frequencies will give narrower NMR lines. However, the ratio of the product $\nu_{\rm L}.2I(2I-1)$ for the two Rb isotopes is almost unity. Therefore, there is no preference of one isotope over the other, as far as linewidths are concerned. The relative sensitivity at constant field for $^{87}{\rm Rb}$ is, however, 12 times larger than that for $^{85}{\rm Rb}$. Accordingly, all studies of rubidium NMR solutions have used the isotope $^{87}{\rm Rb}$ rather than $^{85}{\rm Rb}$.

Table VII summarizes the ⁸⁷Rb-MASS-NMR results for the chemical shifts (referred to as infinitely dilute Rb⁺_(aq)) and the linewidths obtained for simple rubidium salts and two alkalide compounds at 65.5 and 163.6 MHz (which corresponds to 200 and 500 MHz proton frequencies respectively). The RbCl salt shows a relatively narrow line compared to RbSCN. The latter shows the quadrupolar splitting characteristic of the NMR powder pattern for nuclei in which the quadrupolar interaction dominates the NMR line broadening. Among the model salts and all

Table VII: 87 Rb MASS-NMR Results

	65.50 MHz	MHZ	163.6 MHz	MHz
Compound	ψdd '9	Δν _k , Hz	ψdd '9	νγ, Hz
0.1 M RbCl (aq)	9.0-	1	9.0-	-
RbC1	+127	244	+127	1
Rbscn	1	1	-26	2100
Rb ⁺ 18C6.SCN	no signal	1	no signal	1
Rb 18C6.C1	no signal		no signal	I
Rb 18C6.Br	no signal	1	no signal	1
Rb 18C6.Na	no signal		no signal	1
Rb 18C6.Rb	no signal	1	no signal	1
K ⁺ 18C6.Rb ⁻		I	-185,-194	358, 555
$cs(18C6)_2Rb^-$	-193	700	-187	334
Rb ⁺ 18C6.e ⁻	no signal	1	no signal	
Rb ⁺ C222.e ⁻	no signal	1	1	1
Rb + C222.Rb -	no signal	1	1	1
Rb ⁺ C222.Na ⁻	no signal	1	l	

electride and alkalide compounds, only two alkalides show rubidium-NMR signals. These are Cs⁺(18C6)₂.Rb⁻ and K⁺18C6.Rb⁻. The former shows a single ⁸⁷Rb-NMR line at -193 ppm (at 65.50 MHz) while the latter shows two peaks at -185 and -194 ppm (at 163.6 MHz). The positions of these peaks are very close to the Rb signals obtained at -185 and -197 ppm for 0.1 M Rb C222.Rb solutions in ethylenediamine and tetrahydrofuran respectively [55]. Figure 34 shows the $^{133}\mathrm{Cs}$ and $^{87}\mathrm{Rb}$ MASS-NMR spectra of the compound Cs⁺(18C6)₂.Rb⁻ and Figure 35 shows the 87 Rb-MASS-NMR spectrum of the compound K18C6Rb at 163.6 MHz. It is clear from the two figures that for the same number of scans the ⁸⁷Rb NMR signals for the compound K18C6Rb are much weaker than the signal obtained for the compound Cs + (18C6) 2. Rb -. This indicates that the compound K18C6Rb may be a mixture of K+18C6.Rb and Rb+18C6.K, although other possible electride compounds such as K⁺18C6.e and Rb⁺18C6.e may be present also. The presence of two ⁸⁷Rb signals in the NMR spectrum of the compound K18C6Rb is not surprising since it has been seen before for some Na and Cs compounds. However, the absence of an Rb signal in the two compounds Rb 18C6.Rb and Rb⁺C222.Rb⁻ is surprising since a recent EXAFS study [106] has shown that the former is indeed a rubidide. This suggests that the presence of Rb with a large quadrupolar coupling constant somehow "washes out" the Rb signal or that the cation-anion interaction in these

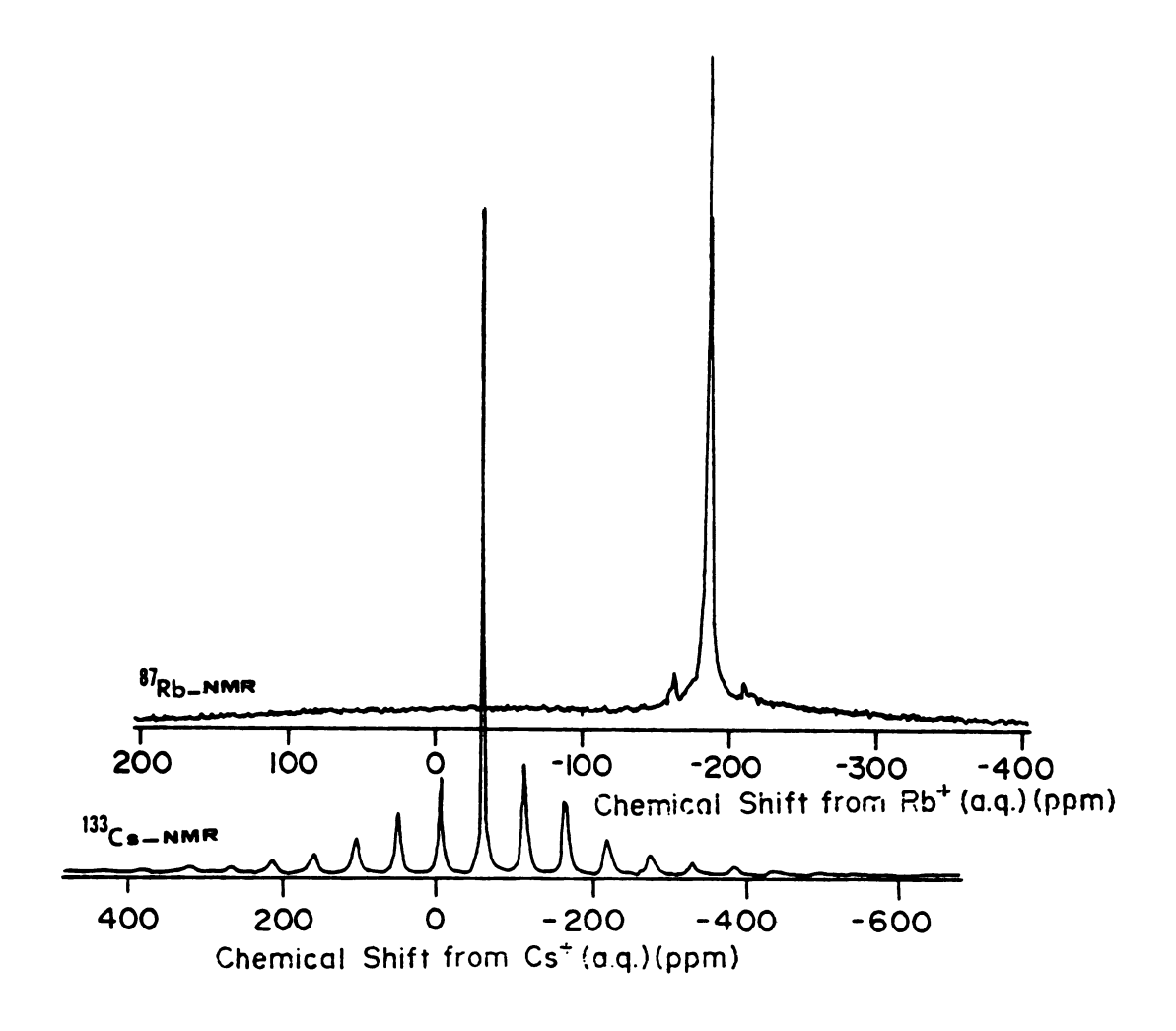


Figure 34: 133 Cs (at 65.61 MHz) and 87 Rb (at 163.6 MHz) MASS-NMR spectra of the compound Cs⁺(18C6)₂.Rb⁻.

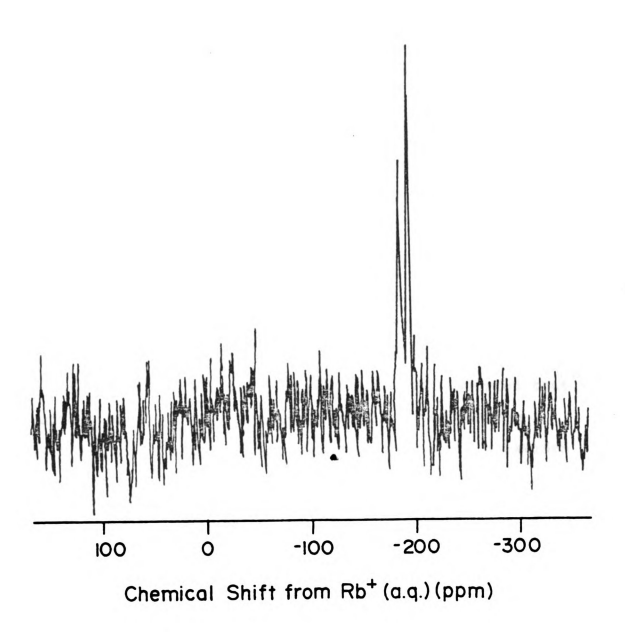


Figure 35: $$^{87}\rm{Rb\text{-}MASS\text{-}NMR}$ spectrum of the compound K*18C6.Rb $^-$ at 163.6 MHz.

compounds plays an important role since an NMR signal from Rb has recently been observed in the compound Rb (15C5)₂.Rb [136] (but no Rb signal was observed). This recent observation of the Rb in the compound Rb (15C5)₂.Rb also provides strong evidence that the compound of stoichiometry Rb18C6 is not the rubidide, Rb (18C6)₂.Rb, otherwise, a signal from Rb would be expected.

No signal could be detected from the Rb⁺ cation complexed by 18-crown-6 or cryptand 222. This is probably because the line broadening decreases the signal below the detection limit in these compounds is a result of quadrupolar interaction. Dye et al. [55] reported that a signal of 4,000 Hz linewidth could be detected from 0.4 M Rb⁺C222.I solution in methanol. Since the linewidth of Na⁺C222 in the solid is nearly 40 times broader than that in solution, we expect the linewidths of Rb⁺18C6 and Rb⁺C222 lines to be of the order 100 to 160 KHz which is beyond the limit of detection.

In summary, ⁸⁷Rb-MASS-NMR does not provide species identification in electride and alkalide compounds that contain the complexed Rb⁺ cation but, in some cases, the Rb⁻ peak can be seen very easily.

4. The chemical shifts of alkali metal anions

Except for Na the NMR peaks of alkali metal anions in solution [55] as well as in the solid state are

paramagnetically shifted from that of the gaseous alkali metal atom [124]. Although the comparison should really be made with respect to the gaseous alkali metal anion, there are no data available for the calculated chemical shifts of Rb and Cs. Table VIII summarizes the average chemical shifts of alkali metal anions in solution and in solids referred to the gaseous alkali metal atoms.

Table VIII: Chemical Shifts of Alkali Metal Anions

Alkali metal anion	Solution ^a	Solid
Na -	<u>~</u> −2	≈ 0
Rb -	<u>~</u> +20	≃ +21
Cs	<u>~</u> +52	≃ +117

^aData taken from reference 55.

Paramagnetic shifts usually indicate that there is an interaction between molecules or ions in the vicinity of the ion and the outer p-orbitals of the alkali metal species. A shift for M is somewhat unexpected since the alkali metal anion has the ns² configuration that should provide shielding of the outer (n-1)p-orbital. An explanation for the observed shift is as follows:

The chemical shift of the alkali metal anion increases with increasing atomic number. This suggests that, except for Na, the ground state of the alkali metal anion is not purely an s-state and that mixing of states to involve p- and d-states is possible. The interaction of the

np-orbital of the ground state with the environment will result in a paramagnetic shift that will depend on the degree of mixing.

CHAPTER V

MAGNETIC PROPERTIES OF ALKALIDES AND ELECTRIDES

A. Electron Paramagnetic Resonances (EPR)

1. Introduction

In the electron paramagnetic resonance experiment, the degeneracy of the spin (Zeeman) energy levels is removed because of the coupling of the external magnetic field, H, to the magnetic moments of the unpaired spins. Transitions between the Zeeman levels can be induced by radiation of the appropriate frequency, ν . For noninteracting (isolated) spins the spin Hamiltonian, $\mathcal{N}_{\rm S}$, is given by

$$\mathcal{H}_{S} = -g\beta \overline{H} \cdot \overline{S} \tag{V.1}$$

where \overline{S} is the electron spin operator and g is the electronic g-factor of the system. Since the electron has a spin of 1/2, this leads to the transition energy

$$\Delta E = hv = g\beta H \qquad (V.2)$$

which gives rise to a single EPR line that occurs at a magnetic field (resonance field) $H_{\rm O}$ equal to $h\nu/g\beta$. When the electrons interact with nearby nuclei, such that there is an actual electron density at the nucleus in an S-state because of this interaction, the total Hamiltonian of the system is given by [137]

$$\mathcal{H} = -g\beta \overline{H} \cdot \overline{S} + \Sigma g_{N} \beta_{N} \overline{H} \cdot \overline{I}_{j} + \Sigma A_{j} \overline{I}_{j} \cdot \overline{S}$$
 (V.3)

where \overline{I}_j and A_j are the spin operator and the hyperfine coupling constant for the jth nucleus respectively. The first two terms in Equation (V.3) represent the electronic and nuclear Zeeman interactions while the third term is the "Fermi" contact term which represents the nuclear-electron interaction. The magnitude of the isotropic hyperfine coupling constant in Gauss is given by

$$A_{iso}(G) = (8\pi/3) g_N \beta_N |\psi(0)|^2$$
 (V.4)

where $|\psi(0)|^2$ is the normalized time average probability that the electron and its associated magnetic moments are at the nucleus. A more accurate equation for the Hamiltonian [Equation (V.3)] should replace the scalar quantities A_{iso} and g by tensor quantities and should include an additional term which describes the quadrupolar interaction which will affect the electron-nuclear energy levels. Two cases can be considered to obtain the eigenvalues of the Hamiltonian described by Equation (V.3). First, in the high field limit where

the hyperfine coupling constant is only a small fraction of the applied magnetic field, i.e. $A_{iso} << H$, the spin Hamiltonian can be rewritten as

$$\mathcal{H} = g\beta \overline{H} \cdot \overline{S}_{z} + \Sigma g_{N} \beta_{N} \overline{H} \cdot \overline{I}_{zj} + \Sigma A_{iso} \overline{S}_{z} \cdot \overline{I}_{zj}$$
 (V.5)

and the energy eigenvalues can be given by first order perturbation theory as:

$$E(m_s, m_I) = g\beta H_o m_s - g_N \beta_N H_o m_I + g\beta A_{iso} m_I m_s$$
 (V.6)

where $g\beta H_{O}^{}m_{S}^{}$ and $g_{N}^{}\beta_{N}^{}H_{O}^{}m_{I}^{}$ are the electronic and nuclear Zeeman energies respectively, and $m_{I}^{}$ and $m_{S}^{}$ are the allowed nuclear and spin quantum numbers associated with I and S respectively. The selection rule for the allowed spin transition is that $\Delta m_{S}^{}=\pm 1$ and $\Delta m_{I}^{}=0$. Accordingly, the transition energy, ΔE , will be given by

$$\Delta E = g\beta H_0 + m_I g\beta A_{iso}$$
 (V.7)

where, $m_I = -I, -I+1, \dots, I-1, +I$. This results in 2I+1 hyperfine lines with spacing between adjacent lines of $A_{iso}(G)$.

Second, in the case of $A_{iso} >> H$ (low field case) and $A_{iso} \leq H$ (intermediate field case), the electron and nuclear moments are tightly coupled to give a resultant total spin angular momentum $F(\overline{F} = \overline{S} + \overline{I})$ in which its

z-projection, m_F , is given by: $m_F = m_S + m_I$. Breit and Rabi [138] gave the eigenvalues of the Hamiltonian in Equation (V.3) in the low and intermediate case as:

$$E(F, m_F) = -\frac{\Delta W}{2(2I+1)} + g_N \beta_N H_O m_F \pm \frac{\Delta W}{2} \left[1 + \frac{4m_F}{2I+1} + x^2 \right]^{\frac{1}{2}}$$
 (V.8)

where ΔW is the zero-field splitting and is given by

$$\Delta W = E_{I+S}(H=0) - E_{I-S}(H=0)$$

$$= \frac{A_{iso}g\beta(2I+1)}{2}$$
(V.9)

and $x = H_0 (g\beta + g_N \beta_N)/\Delta W$. The positive sign in Equation (V.8) goes with F = I + S and the negative sign goes with F = I - S. Figure 36 shows the energy level diagram (taken from reference [133]) for the system with $I = \frac{3}{2}$ and $S = \frac{1}{2}$ in the high and low field cases. The selection rule for absorption is $\Delta m_F = I$, so that the transition energy is given by

$$\Delta E = g_N \beta_N H_O + \frac{\Delta W}{2} \left[\left[1 + \frac{4m_F^P x}{2I+1} + x^2 \right]^{\frac{1}{2}} + \left[1 + \frac{4m_F^L x}{2I+1} + x^2 \right]^{\frac{1}{2}} \right]$$
 (V.10)

where m_F^P and m_F^L refer to the upper and lower states respectively.

There are two important EPR parameters that determine the resonance position and in some cases the shape of the EPR line. These are the electronic g-factor and the

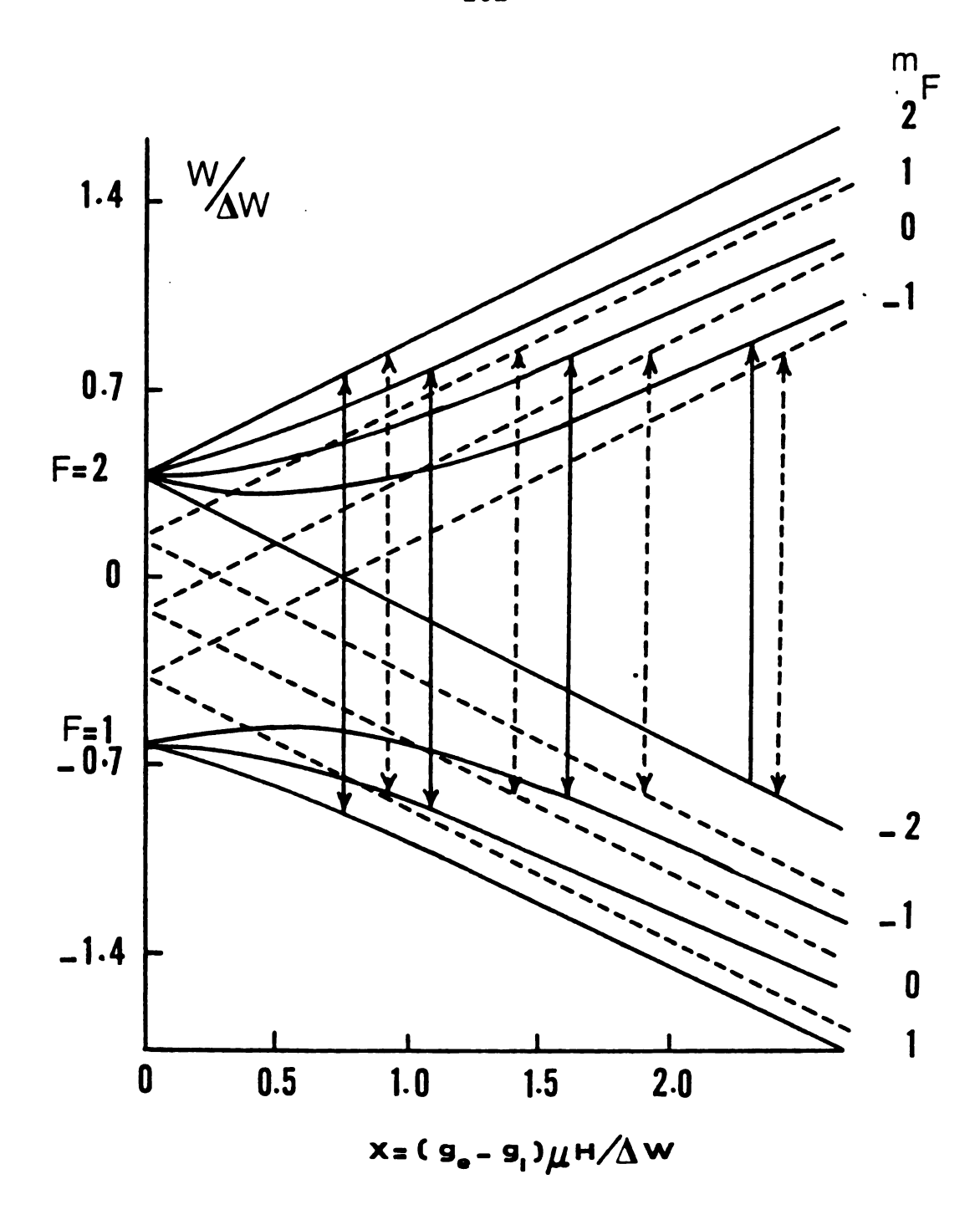


Figure 36: Magnetic energy levels for I = 3/2 and S = 1/2. The solid lines are energy levels computed from Eq. (V.10); the dotted lines are the corresponding first order energy levels (Eq. (V.7)) [133].

hyperfine splitting constant, A. The electronic g-factor describes the interaction of the electron with its environment and is given by,

$$g = \frac{3}{2} + \frac{S(S+1) - L(L+1)}{2J(J+1)}$$
 (V.11)

where S, L and J are the spin, orbital and total angular momentum quantum number respectively. Therefore, the g-factor is a measure of the mixing of spin and orbital angular momentum for the electron giving the EPR signal. For a system where the orbital angular momentum has no contribution to the total moment, i.e. spin only angular momentum, S is equal to J, therefore g is equal to 2. A more accurate value for the free electron g-value, g_{e} , is 2.0023193 [139]. Deviation from the free electron g-value is usually interpreted in terms of spin-orbit coupling because of the interaction of the electron with its environment. In dilute solution of low viscosity the g-factor is a scalar but in a single crystal or powder the g-factor depends on the orientation of molecules with respect to the field and then the q-factor is a tensor. In general, anisotropy in the g-factor arises from coupling of the spin angular momentum with the orbital angular momentum. The spin angular momentum is oriented with the field, but the orbital angular momentum, which is associated with the electrons moving in molecular orbitals, is locked to the molecular wavefunction.

Anisotropy in the hyperfine coupling constant, A, arises from the dipolar interaction between the electron and nuclear moments which depends on the electron-nucleus separation and the orientation of the electron-nucleus vector with respect to the magnetic field. Anisotropy in the hyperfine interaction results in line broadening of the hyperfine components and hence $\mathbf{m}_{\mathbf{I}}$ dependence of the hyperfine lines.

Line broadening in EPR arises mainly from the interaction of the unpaired electrons with the thermal vibrations of the lattice (spin-lattice relaxation). In addition, there are sources of line broadening that can be divided into two main groups. These are inhomogenous and homogenous broadening. In the first case, the unpaired electrons in the sample are subjected to slightly different effective magnetic fields. The observed line is then a superposition of a large number of individual components, each slightly shifted from the others. the solid state, the anisotropic interactions in a randomly oriented system result from the anisotropic g and A and give rise to inhomogeneity. In addition to these sources of line broadening, the presence of unresolved hyperfine interaction because of a large number of hyperfine components or because of weak electron-nuclear coupling will result in inhomogeneous broadening. The lineshape for an inhomogeneously broadened EPR line is Gaussian.

Homogeneous broadening arises from magnetic dipole interactions between the unpaired spins which depend on the relative orientations of the dipoles with respect to the magnetic field as well as the separation between the interacting dipoles. Another source of homogeneous broadening is electron-spin exchange which is viewed as a bimolecular reaction in which two unpaired electrons exchange their spin states. If the electron spin exchange occurs at a rate comparable to or faster than the hyperfine frequency then a time averaged broad signal will be observed. For systems in which the electrons exchange their spins very rapidly, (normally systems of high spin concentration), the time averaged hyperfine field as well as the field produced because of magnetic dipole interactions are averaged to zero and a sharp, narrow EPR line is observed. This case of electron spin-exchange is called "exchange narrowing" and is observed for pure solid free radicals [139]. The lineshape of a homogeneously broadened EPR line is Lorenzian. One characteristic difference between inhomogeneously and homogeneously broadened EPR lines is the saturation behavior of the EPR line as a function of the microwave power, Po, which is shown in Figure 37. For a homogeneously broadened line, the EPR signal amplitude increases with increasing P until it reaches a maximum and then decreases. On the other hand, the inhomogeneously broadened line's

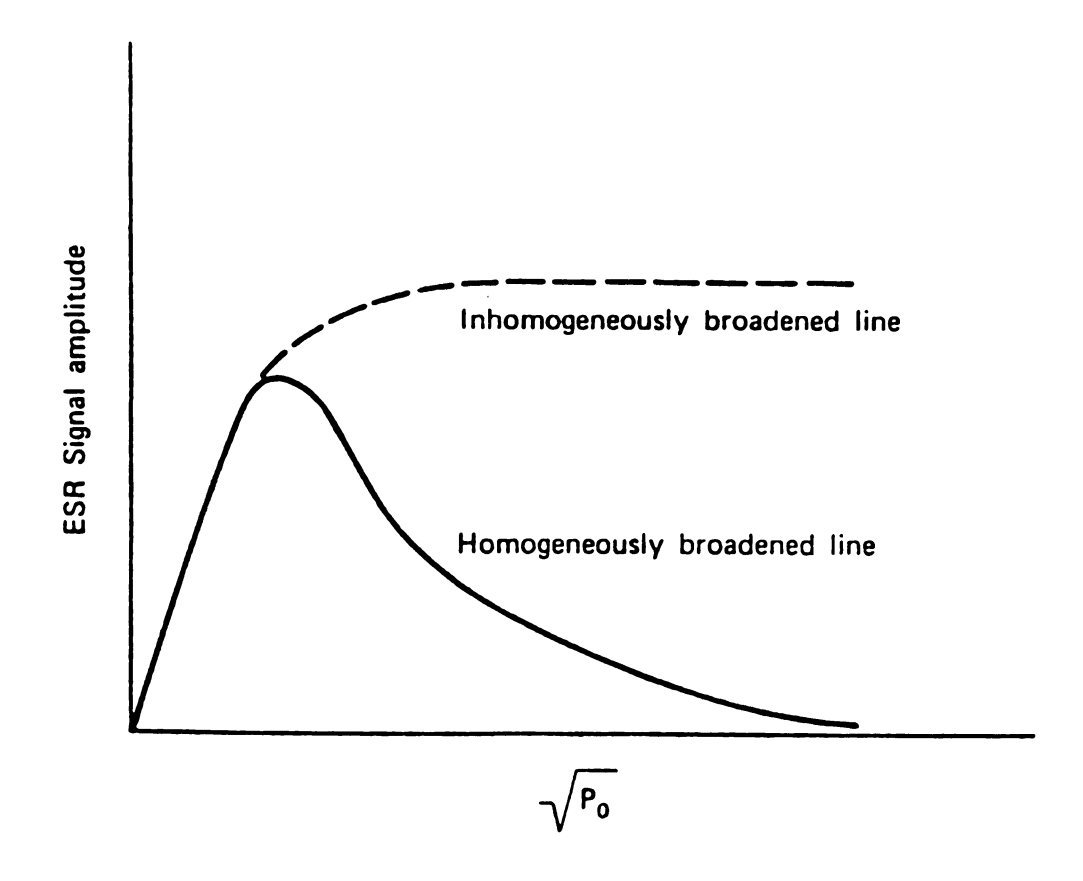


Figure 37: Variation of EPR signal amplitude with microwave power (P_0) for a homogeneously broadened line (solid curve) and an inhomogeneously broadened line (dotted curve).

amplitude first increases with increasing P_{0} and then levels off.

One final point is worthy of mention concerning the factors that affect lineshapes and the positions of EPR lines. This is the interaction of the electron with a nucleus that has a large quadrupolar moment $(I \ge 1)$. This has the effect of broadening the EPR lines as well as affecting the separation between the hyperfine lines in two ways: (1) a displacement of the energy level, and hence the resonance field, by a constant amount and (2) a change in the separation of the energy levels that causes the spacing between adjacent EPR lines to be greater at the ends of the spectrum than in the middle. However, in some cases, the quadrupolar interaction also causes the appearance of additional lines that are normally forbidden by the selection rule $\Delta m_T = 0$ [121].

The paramagnetic resonance observed in metals is called conduction electron spin resonance (CESR) and was first observed by Griswald, Kip and Kittel [140]. Dyson [141] and Kip [142] treated the problem of CESR theoretically by using a highly idealized model of electrons in the metal. The electrons are assumed to diffuse as free particles, and the electron magnetic moments are treated as free particle moments. The lineshape of the CESR signal is highly unsymmetrical and is determined by the skin depth, δ , the diffusion time, T_D , which is the time it takes an electron to diffuse

through the skin depth, the electron spin relaxation time, T_1 , the spin-lattice relaxation time, T_2 , (for metals $T_1 = T_2$) and T_T , which is the time it takes an electron to traverse the sample. Two main cases were considered in the lineshape calculation. These are the "classical skin effect" and "anomalous skin effect". In the first case, the skin depth, δ , is large compared with the electron mean free path, Λ . In this case, the "classical" skin depth, δ , is given by [141],

$$\delta = \left(\frac{c^2}{2\pi\sigma\omega}\right)^{\frac{1}{2}} \tag{V.12}$$

where σ is the microwave conductivity of the metal at frequency ω and c is the speed of light. If δ is not large compared to Λ we have the "anomalous skin effect" and the penetration of the microwaves is controlled by Λ .

Dyson [141] treated the case for which $T_T >> T_D$ and $T_T >> T_2$ which can be applied to a thick plate metal sample whose thickness is large compared to the skin depth. In this case the EPR is highly unsymmetrical with 2.7 < A/B < 20. The absorption, P, is expressed by

$$P = -\frac{\omega H_1^2 R^2 \omega_0^T 2^{S\delta}}{8} \frac{R^4 (x^2 - 1) + 1 - 2R^2 x}{\left[(R^2 x - 1)^2 + R^4 \right]^2}$$

$$\times \left[\frac{2\xi}{R (x^2 + 1)^{\frac{1}{2}}} + R^2 (x^2 + 1) - 3 \right]$$

$$+ \frac{2R^2 (1 - R^2 x)}{\left[(R^2 x - 1)^2 + R^4 \right]^2} \left[\frac{2\eta}{R (x^2 + 1)^{\frac{1}{2}}} + R^2 (x - 1) - 3 \right]$$
(V.13)

in which S is the surface area of the sample and,

$$R = (T_D/T_2)^{\frac{1}{2}}$$

$$x = (\omega - \omega_0) T_2 \equiv \gamma T_2 (H_0 - H)$$

$$\xi = (\text{sign of } x)[(1+x^2)^{\frac{1}{2}}-1]^{\frac{1}{2}}$$

$$\eta = [(1+x^2)^{\frac{1}{2}}+1]^{\frac{1}{2}}$$

The lineshape given by Equation (V.13) is asymmetric and commonly known as Dysonian lineshape (Figure 38).

Webb [143] extended Dyson's derivation to spherical metal particles of radius a, in the classical skin effect where the skin depth is not much larger than the particle size. The absorption is expressed by

$$P = \kappa [C^* + (3F_0 | 2u^2)C^* - (3F_0^* | 2u^{*2})C]$$
 (V.14)

where,

$$\kappa = \sqrt{2} \omega \omega_{O} \chi \tau H_{1}^{2} \left(\frac{4}{3} \pi a^{3} \right)$$

$$C = F_0^2 G_0^2 - \frac{7}{2} F_2^2 G_2$$

$$F_0 = 1-u\cot u$$
, $u = \left(\frac{a}{\delta}\right)\left(1+i\right)$

$$F_2 = (2|\sqrt{5})[3+F_0(1-9/u^2)]$$

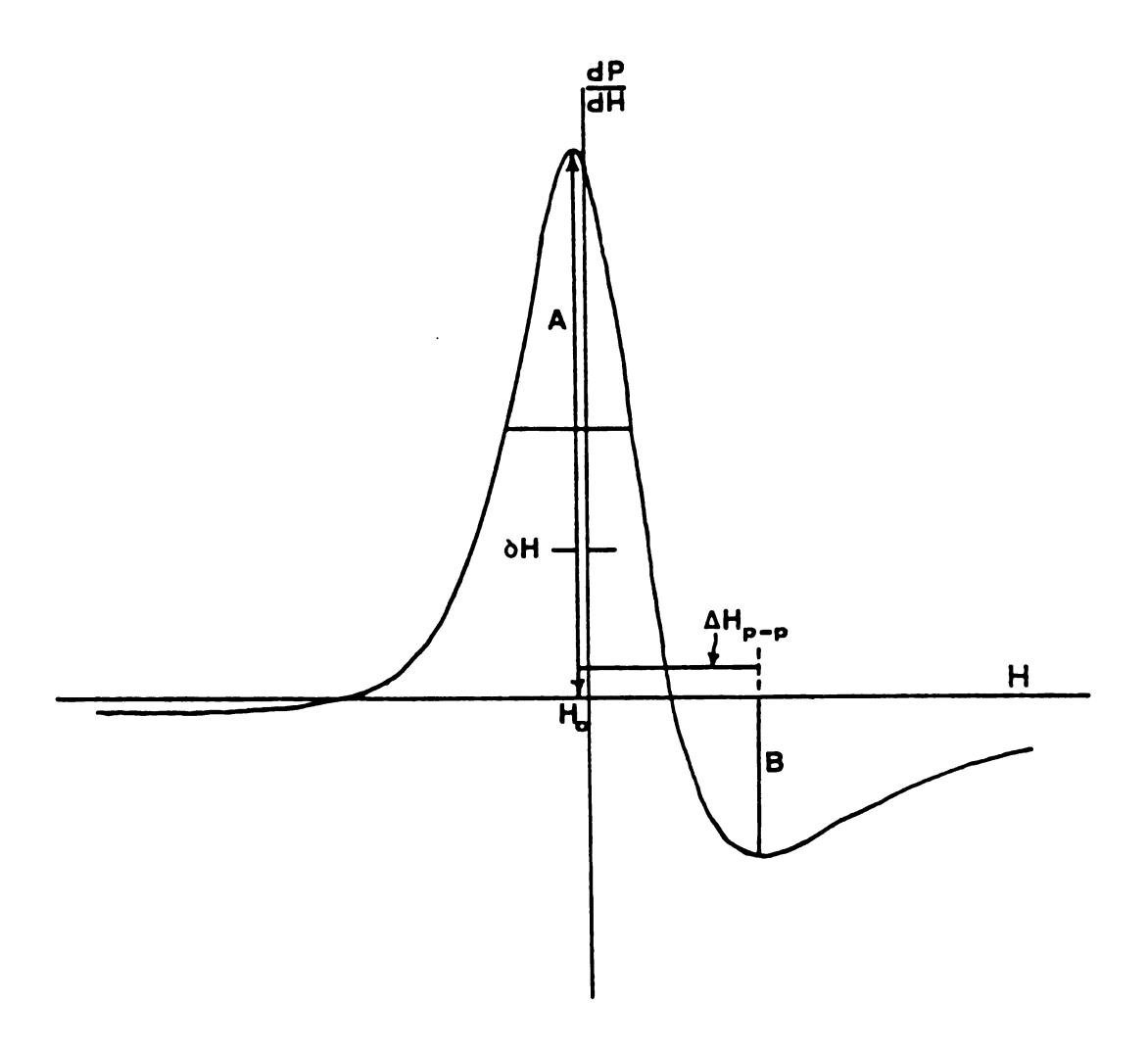


Figure 38: Typical first derivative lineshape of the electron spin resonance absorption in thick metals.

$$G_0 = \sum_{n} [(u^2 - R_{0n}^2)^2 (R_{0n}^2 - \omega^2) (1 - \sigma | R_{2n}^2)]^{-1}$$

$$\omega^2 = i(\omega - \omega_0) \tau - \tau | T_1$$

$$\tau = 2(a^2/\delta^2)T_D$$

$$T_D = 3\delta^2 | 2v\Lambda$$

where ν is the velocity of the electrons. R_{on} and R_{2n} are determined from the relations, $\tan R_{on} = R_{on}$ and $\tan R_{2n} = R_{2n} (9-4R_{2n}^2)/(9-R_{2n}^2)$. If $\frac{a}{\delta} << 1$, then Equation (V.14) reduces to a Lorentzian line and is given by

$$P = \frac{\chi_0 \omega_0 \omega T_1 H_1^2 (\frac{4}{3} \pi a^3)}{4} \cdot \frac{1}{1 + T_1^2 (\omega - \omega_0)^2}$$
 (V.15)

The lineshape expressed by Equation (V.14) is not highly asymmetric as is the Dysonian line and the A/B ratio is given by the limit $1 \le \frac{A}{B} \le 2.7$.

2. Results and discussion

a. Trapped electrons in sodides: "F-center alkalides"

As we have seen before (in the discussion of the chemical shift results obtained for different sample preparations of the compound Cs⁺(18C6)₂.Cs⁻) different degrees of electron trapping may affect the chemical shift of both the Cs⁺ cation and the Cs⁻ anion.

EPR spectroscopy proved to be a good way to probe electron trapping in alkalide salts and the interaction of these electrons with their surroundings.

In general, the results obtained with sodide salts show a variety of EPR lines which may vary from a single EPR line of non-interacting electrons to EPR lines characteristic of strongly interacting electrons. However, all the EPR powder patterns described here for some polycrystalline samples of sodides fall under the category of multisite EPR signals.

The compound, Na⁺C222.Na⁻ shows a very weak EPR signal that consists of a single narrow EPR line with a g-value of 2.0024. The narrow EPR line of Na⁺C222.Na⁻ is superimposed on a second, broader line. However, the saturation behavior of both EPR lines are different and practically only one single narrow line is observed at low microwave power (less than 1 μ W). At relatively higher microwave power (≥2 μW) two overlapping lines are observed. Figure 39 shows the EPR spectra of a polycrystalline sample of Na⁺C222.Na⁻ at different microwave power levels. g-value of the narrow line is very close to that of the free electron, indicating weak interaction of the trapped electron with the Na⁺C222 cation. The linewidth of the narrow line, ΔH_{pp} , is about 3.5 G at 123 K. Increasing the temperature causes a decrease in the intensity of the narrow line and makes the spectra very noisy which

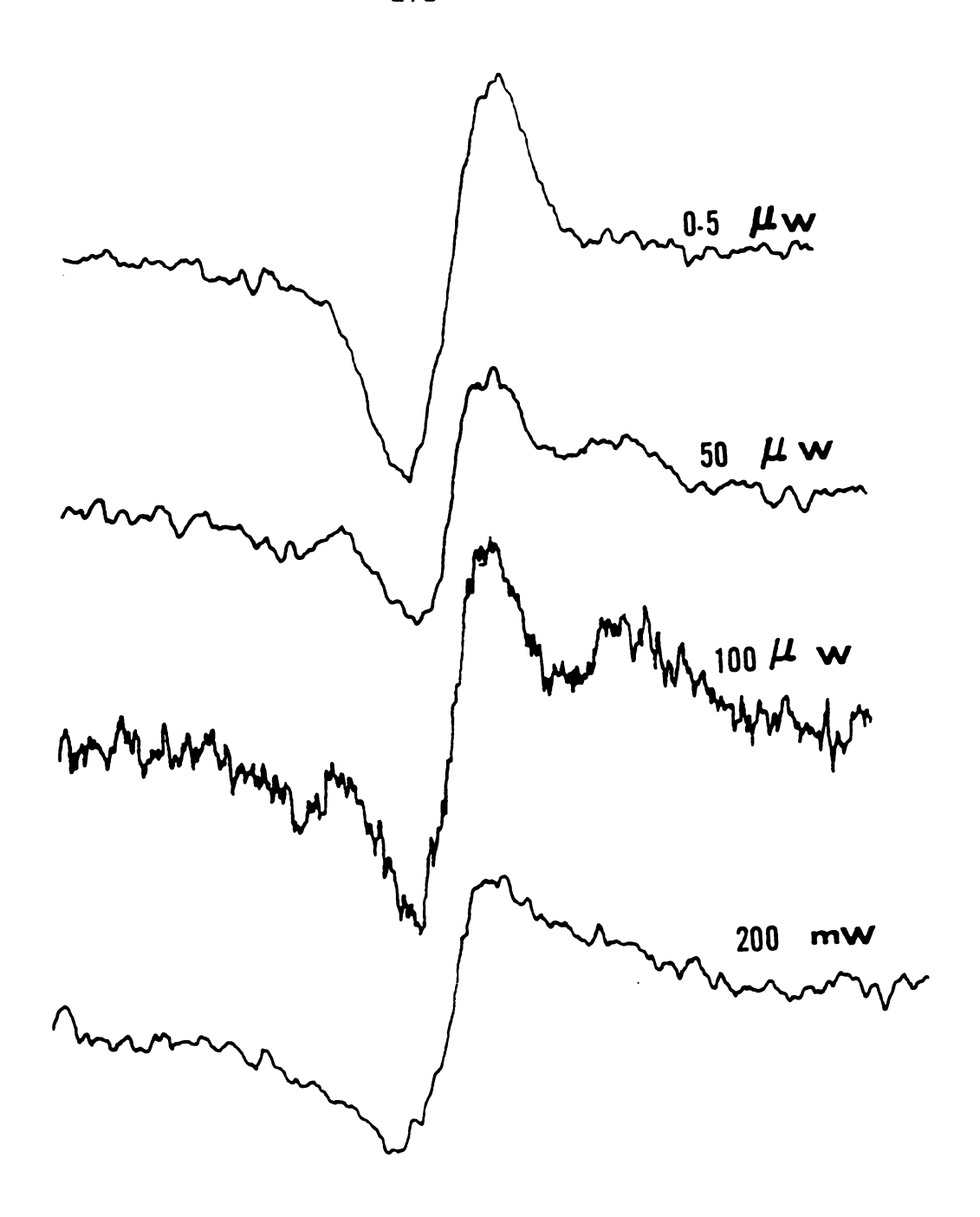


Figure 39: EPR spectra of polycrystalline sample of Na⁺C222.Na at different microwave power levels.

does not permit an accurate measurement of the linewidth as a function of temperature.

The two compounds Li⁺C211.Na⁻ and Rb⁺C222.Na⁻ show similar results to those obtained for Na⁺C222.Na⁻, except that the spectra were more noisy indicating less electron doping in these systems.

The crystalline compound Cs (18C6) 2. Na also shows similar results to those of Na⁺C222.Na⁻ but the EPR signal was rather strong and the spectrum, as shown in Figure 40, indicates that at least three types of electron sites are present in the system. The spectrum consists of a single narrow EPR line of g-value and linewidth of 2.0024 \pm 0.0001 and 0.7 \pm 0.1 G respectively. Both the q-value and the linewidth are remarkably temperature independent over the temperature range of 127 to 311 K. In addition to the central line there are two broader lines which are superimposed on the central line. The behaviors of these three EPR lines at different microwave power levels and temperatures are different. At low microwave power ($\leq 0.6 \mu w$) only a single symmetrical line is observed with no structure. Increasing the microwave power above 200 mw leads to a decrease in the intensity of the central line and the appearance of the other two broader lines. Figure 41 shows the saturation behavior of the central-narrow line of Cs (18C6)2.Na. The temperature has a parallel effect to the microwave power. At low temperatures (~126 K) the spectrum consists of

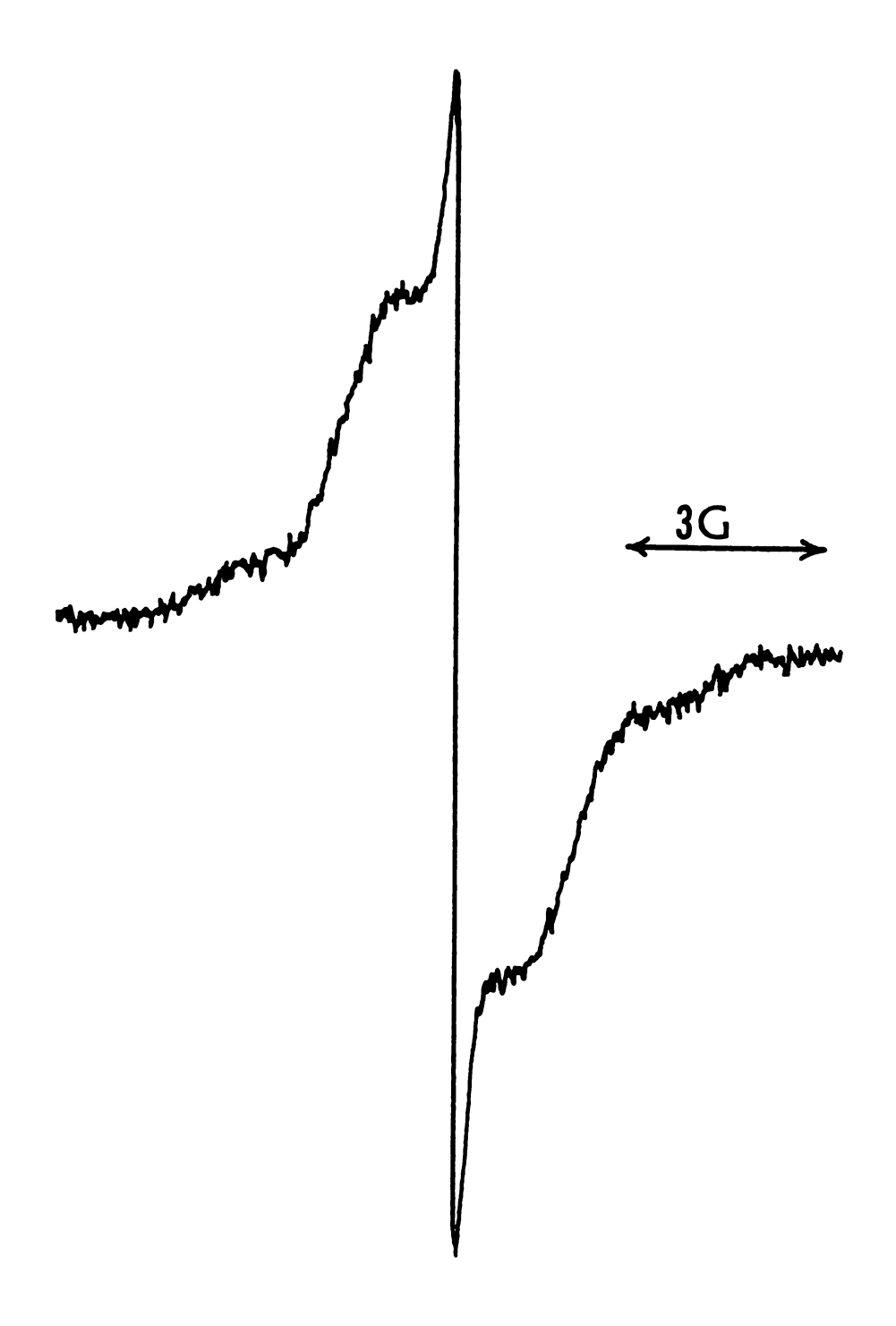
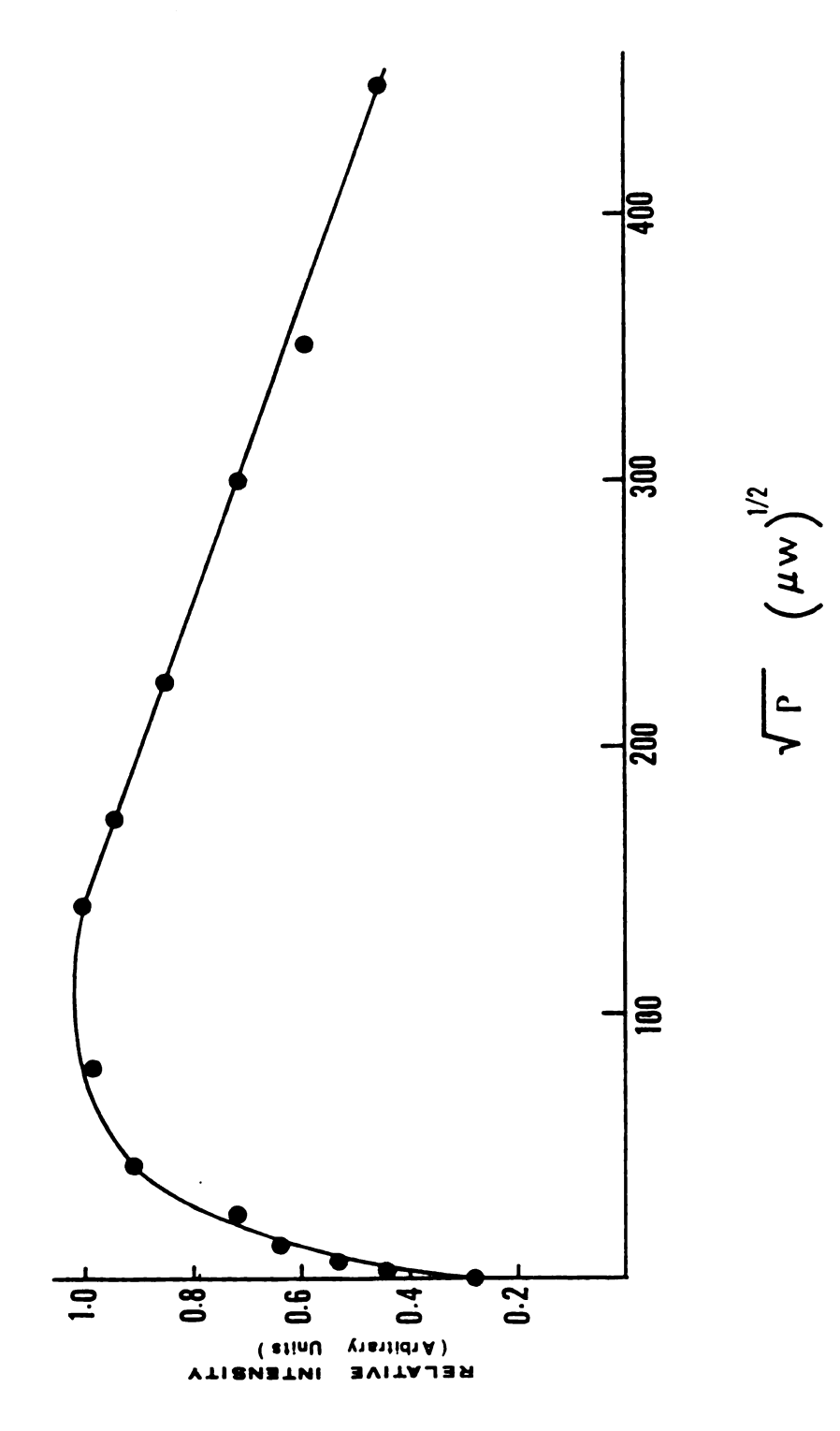


Figure 40: EPR spectrum of polycrystalline sample of Cs⁺(18C6)₂.Na⁻.



Variation of the relative intensity of the central line of the EPR spectrum of Cs⁺(18C6)₂.Na⁻ with the square root of the microwave power level. Figure 41:

the central line and very weak structure on both sides of the line. Increasing the temperature gives a decrease in the relative intensity of the central line and a more resolved structure appears. Figure 42 shows the EPR spectra of a polycrystalline sample of Cs⁺(18C6)₂.Na⁻ at different temperatures.

The crystalline sodide, Rb 18C6.Na shows a rather interesting powder EPR spectrum as shown in Figure 43. The spectrum consists of a central line, six hyperfine lines that correspond to a strong coupling to ⁸⁵Rb and four hyperfine lines that correspond to a coupling to 87 Rb. The central line has a g-value of 2.0023 ± 0.0001 and a linewidth, ΔH_{DD} , of 4.63 ± 0.01 G. Both the g-value and the linewidth are temperature independent over the temperature range of 2.9 K to 248 K. The constant value of the linewidth of the central line over the whole temperature range and the saturation behavior of this line (Figure 44) indicates the absence of any inhomogeneous broadening so that this line represents essentially a single site of electron trapping in Rb⁺18C6.Na⁻. Some of the ten hyperfine lines overlap but the dependence of the linewidth on $\mathbf{m}_{\mathbf{I}}$ is clear. The separation between adjacent hyperfine lines of a given rubidium isotope increases with increasing magnetic field; i.e. the separation is less at low field that that at high field.

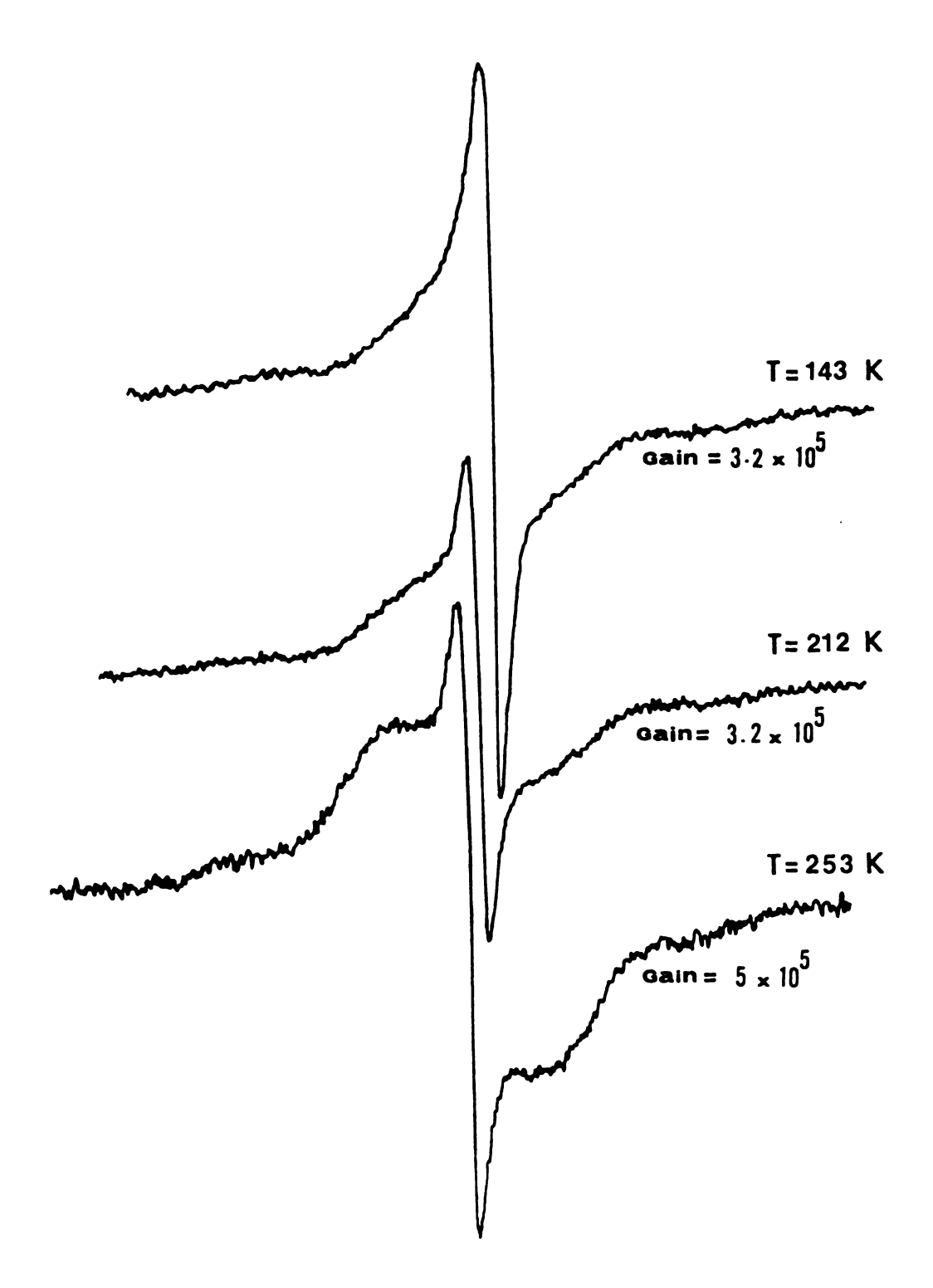
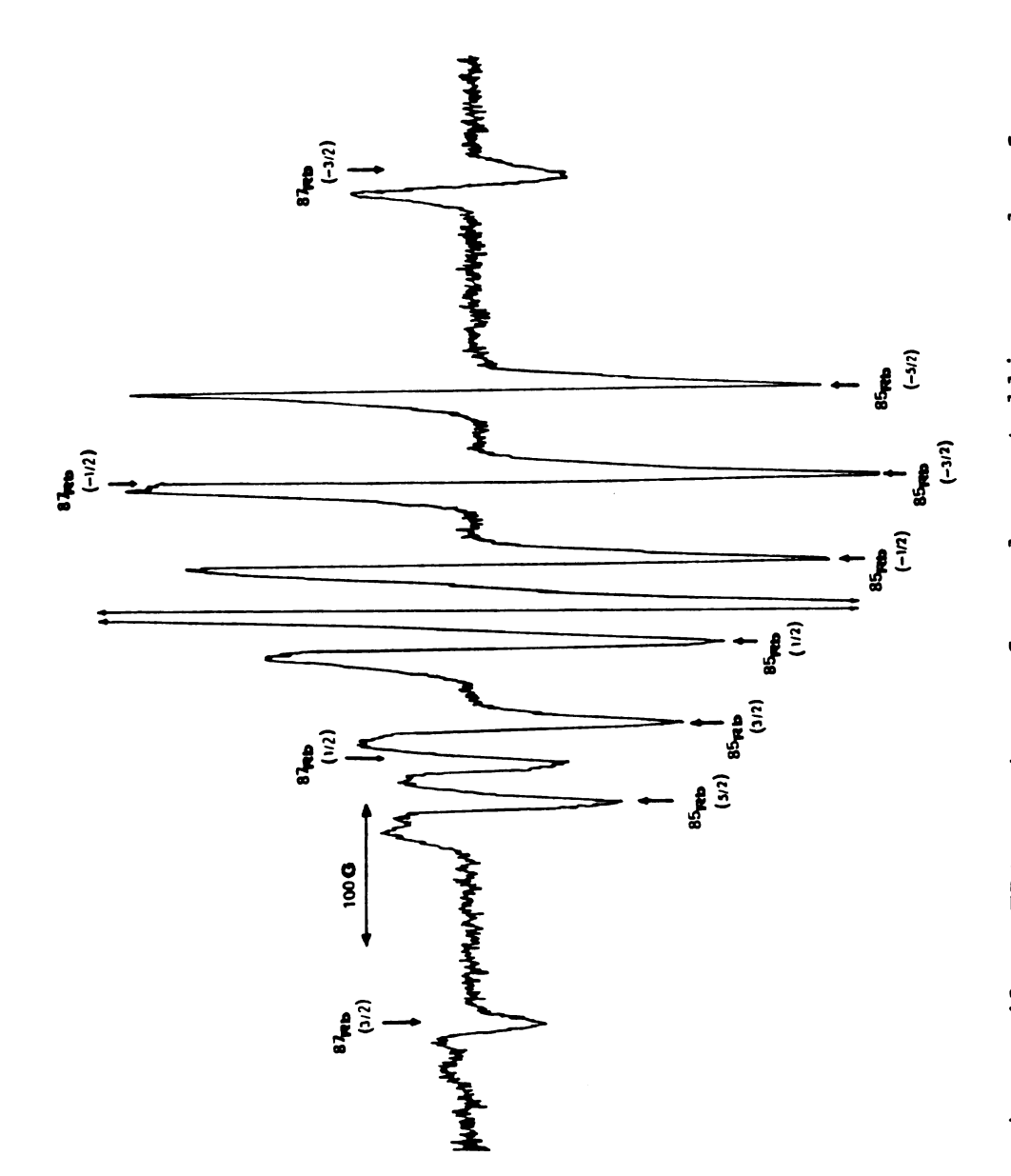
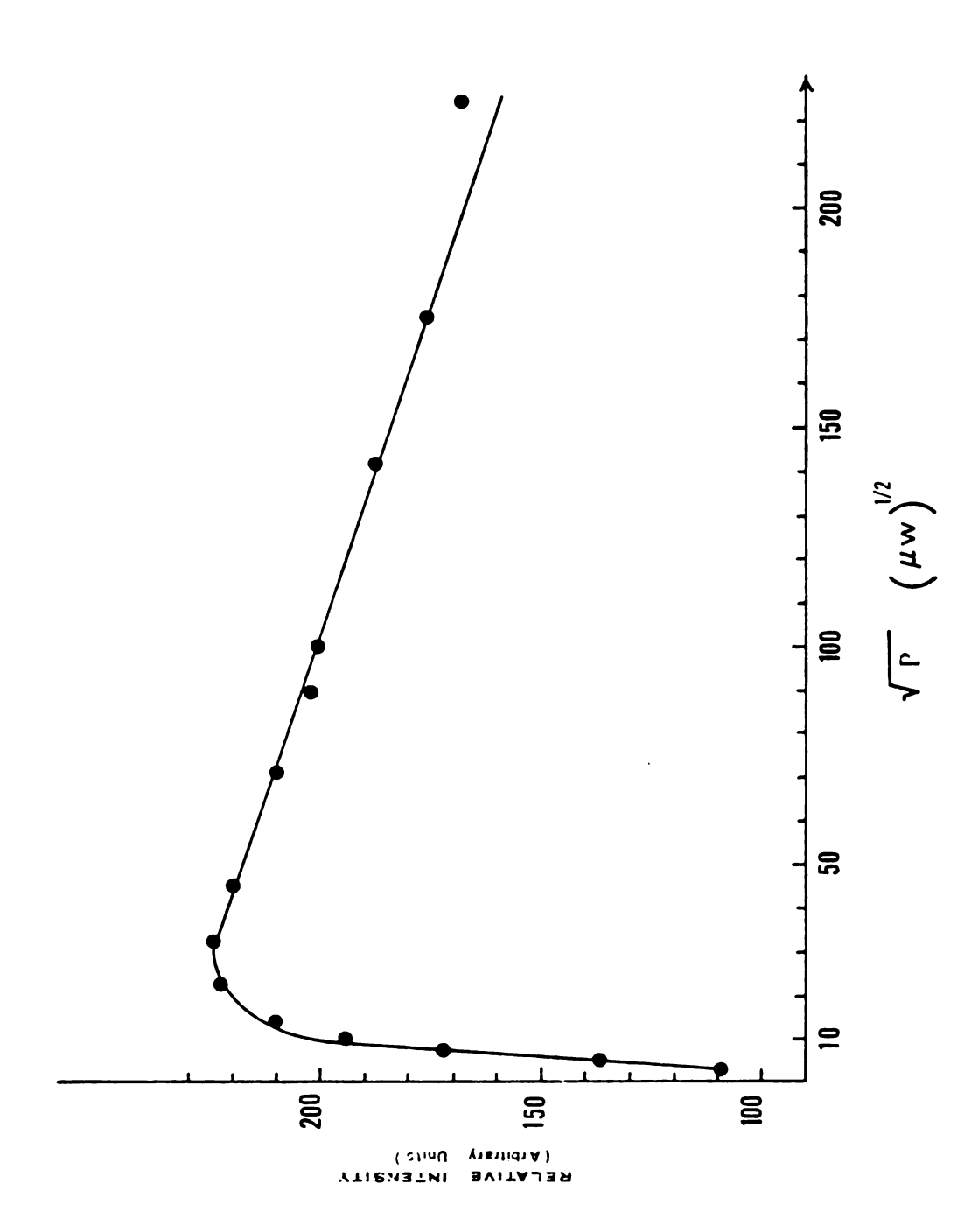


Figure 42: EPR spectra of a polycrystalline sample of Cs⁺(18C6)₂.Na⁻ at different temperatures.



EPR spectrum of a polycrystalline sample of Rb+18C6.Na at 2.8 K. Figure 43:



Variation of the relative intensity of the central line of the EPR spectrum of Rb 18C6.Na with the microwave power level. Figure 44:

The extraction of the EPR parameters from this spectrum is very difficult because of the overlap of the hyperfine lines of the two rubidium isotopes and the further splitting observed for the hyperfine lines at low field. However, if we use isotropic g-values and hyperfine interactions and compare the resonance fields of some of the hyperfine lines with those obtained by complete Breit-Rabi analysis using Equation (V.10) at a given g and $A_{\rm iso}$, some of the EPR parameters may be obtained. Table IX summarizes the observed and calculated resonance fields of some hyperfine lines (labeled by their $m_{\rm T}$) of $^{85}{\rm Rb}$ and $^{87}{\rm Rb}$. The observed g-value, $g_{\rm hf}$,

Table IX: Resonance Field of Some Hyperfine Line

observed calculated	g _{hf} 1.9974 1.9980	85 _A iso 58.8 60.0	$\frac{85_{\text{Rb}}(-\frac{5}{2})}{3553.7}$ 3559.8	$\frac{85_{Rb}(-\frac{3}{2})}{3489.9}$ 3495.2	$\frac{85_{\text{Rb}}(-\frac{1}{2})}{3431.7}$ 3431.8
observed calculated	g _{hf} 1.9974 1.9980	87 _A iso 199.6 200.0	$\frac{87 \text{Rb} \left(-\frac{3}{2}\right)}{3711.1}$ 3706.4	$\frac{87 \text{Rb} \left(-\frac{1}{2}\right)}{3489.9}$ 3486.0	$\frac{87_{\text{Rb}}(\frac{1}{2})}{3083.1}$ 3083.1

is calculated from the spectrum at the field corresponding to the center of the hyperfine pattern, while the observed A_{iso} values for both isotopes are calculated from the average value of the estimated separations between two adjacent hyperfine lines of each isotope. As shown from Table IX, the agreement between the observed and calculated

resonance fields of the hyperfine lines is not very good. This indicates that a Breit-Rabi analysis is not sufficient to explain the Rb⁺18C6.Na⁻ spectrum and that anisotropy in both g and A should be considered. However, the ratio between the observed ⁸⁷A_{iso} and ⁸⁵A_{iso} values is 3.40 which is in agreement with the expected ratio of 3.38, based upon the isotropic hyperfine splitting constants of the neutral atoms of each isotope [121].

The electron density $|\psi(0)|^2$ at the rubidium nucleus which gives rise to the hyperfine splitting can be calculated by using Equation (V.4). This calculation yields a value of 2.5767 × 10²⁴ electrons·cm⁻³. Comparison of this value with the $|\psi(0)|^2$ value obtained for the neutral rubidium atom in the gas phase, 15.8225×10^{24} electrons·cm⁻³ [133], gives 16.3% atomic character at the rubidium nucleus in the compound Rb 18C6.Na. This value suggests that electron trapping occurs at a site that allows substantial interaction with the Rb + cation, perhaps near a defect Rb 18C6 cation. On the other hand, the single narrow line at q = 2.0023 indicates substantial electron localization in a site at which the electrons are very weakly interacting with the surroundings, perhaps at anionic site vacancies. One sample of Rb + 18C6.Na did not show the EPR hyperfine pattern but rather an EPR spectrum that was similar to that of Cs⁺(18C6)₂.Na⁻ which was discussed before.

In summary, electron trapping (or doping) in alkalide salts is unavoidable because of the nature of preparation of these compounds from amine and ether solutions in the presence of the complexing agent. These solutions are rich in the solvated electron which can be trapped during the crystallization process. In general, electron trapping in cryptated sodide salts is less extensive than in 18-crown-6 sodides. This may be related to differences in the structure as well as the cation-complexant size in these compounds.

One might consider two kinds of electron trapping that can occur in the alkalide salts. These are trapping at anionic vacancies (F-centers) and trapping at interstitial sites near a defect cation or missing crown ether. The first kind may be responsible for the narrow EPR lines obtained for all the sodides at g = 2.0023 as well as the broader lines superimposed on the narrow line. The difference between the narrow and broad lines obtained in most of the sodides may then be due to trapping at anionic vacancies which provide different broadening mechanisms. The second kind of electron trapping is responsible for the hyperfine pattern obtained for the Rb 18C6.Na and may be referred to as a Frenkel impurity state [133].

b. Electrons in electrides:

Three crystalline electrides were studied by EPR spectroscopy. These are Rb⁺18C6.e⁻, Cs⁺C222.e⁻ and Cs⁺(18C6)₂.e⁻. The first two electrides are essentially diamagnetic (singlet-ground state) while the third is paramagnetic (doublet-ground state). Accordingly, the EPR spectra of these compounds are classified according to the multiplicity of the ground state of the compound.

i: EPR of singlet-ground state electrides:

Since the two crystalline electrides, Rb + 18C6.e and Cs⁺C222.e⁻ are diamagnetic (see Section B2), their EPR spectra result from single electron trapping or anion defects (since in this case the anion is the trapped electron pair). Figure 45 shows the EPR spectrum of a polycrystalline sample of Rb 18C6.e. The spectrum consists of a single Lorentzian line as indicated from the saturation behavior of the line (Figure 46). The EPR line has a q-value of 2.0017 ± 0.0001 and a linewidth of 4.7 \pm 0.3 G. Both the g-value and the linewidth are temperature independent over the temperature range of 110 to 243 K. The $\frac{A}{B}$ ratio is also temperature independent over the same temperature range with a value of 1.1 ± 0.1 indicating high symmetry of the EPR line. However, the intensity of the EPR decreases with increasing temperature. A plot of the relative intensity of the EPR line (arbitrary units) versus $\frac{1}{T}$ is linear, indicating Curie-behavior of the unpaired spin in this system. However, the small

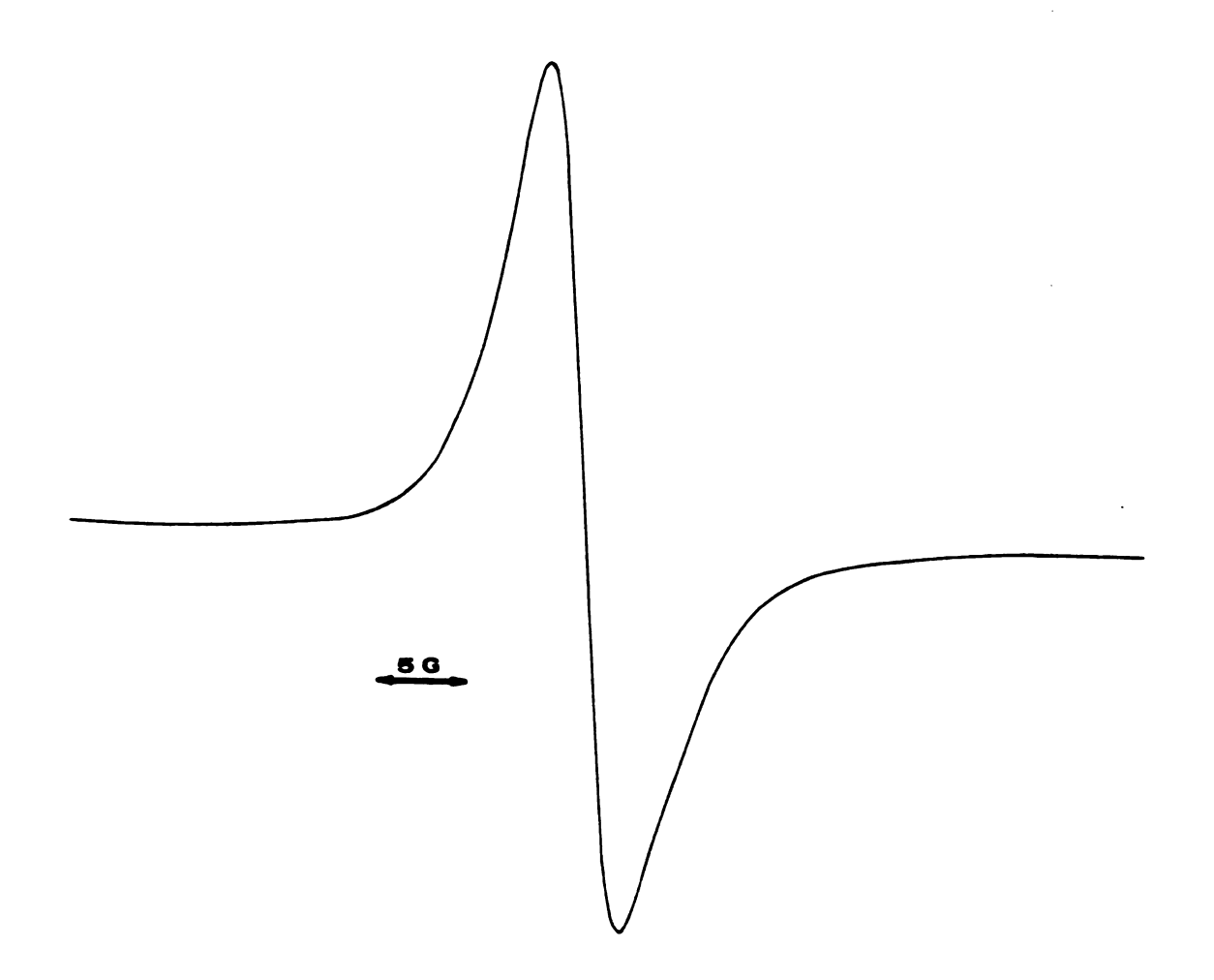
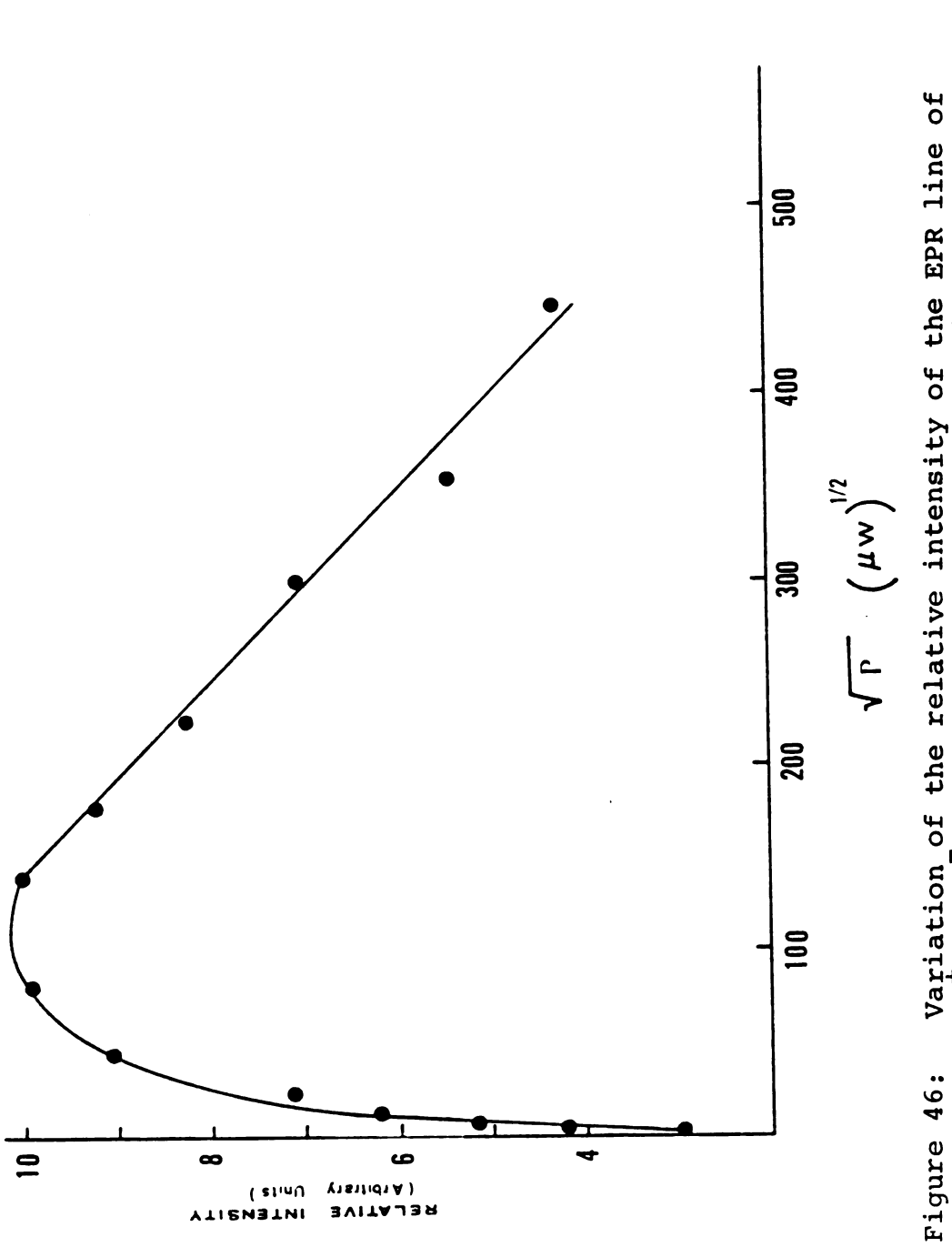


Figure 45: EPR spectrum of a polycrystalline sample of Rb⁺18C6.e⁻ at 123 K.



Variation of the relative intensity of the EPR line of Rb⁺18C6.e with the square root of the microwave power level.

difference between the observed g-value and that of the free electron suggests that the electrons are only weakly interacting with their surroundings.

The compound Cs⁺C222.e⁻ shows an EPR powder pattern that corresponds to an axially symmetric system as shown in Figure 47. The EPR signal is very weak and could only be detected at liquid helium temperatures (2.8-20 K). Above 20 K the signal-to-noise ratio was very poor and no signal could be detected. The value of g_1 is 2.0020 and that of g_{\parallel} is 1.9771, both of which are less than that of the free electron. This suggests that there is some interaction between the electron and Cs⁺C222, probably present as the "exclusive complex cation". Although, it appears from the spectrum that only one site of the trapped electron exists since only a single line is observed, the saturation behavior of the sample shows a behavior characteristic of an inhomogenously broadened line as shown in Figure 48. This indicates that there is a narrow distribution of trapping sites for electrons in this compound.

ii: EPR of doublet-ground state electride:

The electride, $Cs^+(18C6)_2.e^-$, shows a conduction electron spin resonance (CESR) spectrum similar to that observed for a spherical metal particle whose radius, a, is comparable to the skin depth, δ . Figure 49 shows the EPR spectrum of a polycrystalline sample of $Cs^+(18C6)_2.e^-$. The EPR signal is very intense so that the signal could be detected at very low microwave powers (\simeq 200 nW). The

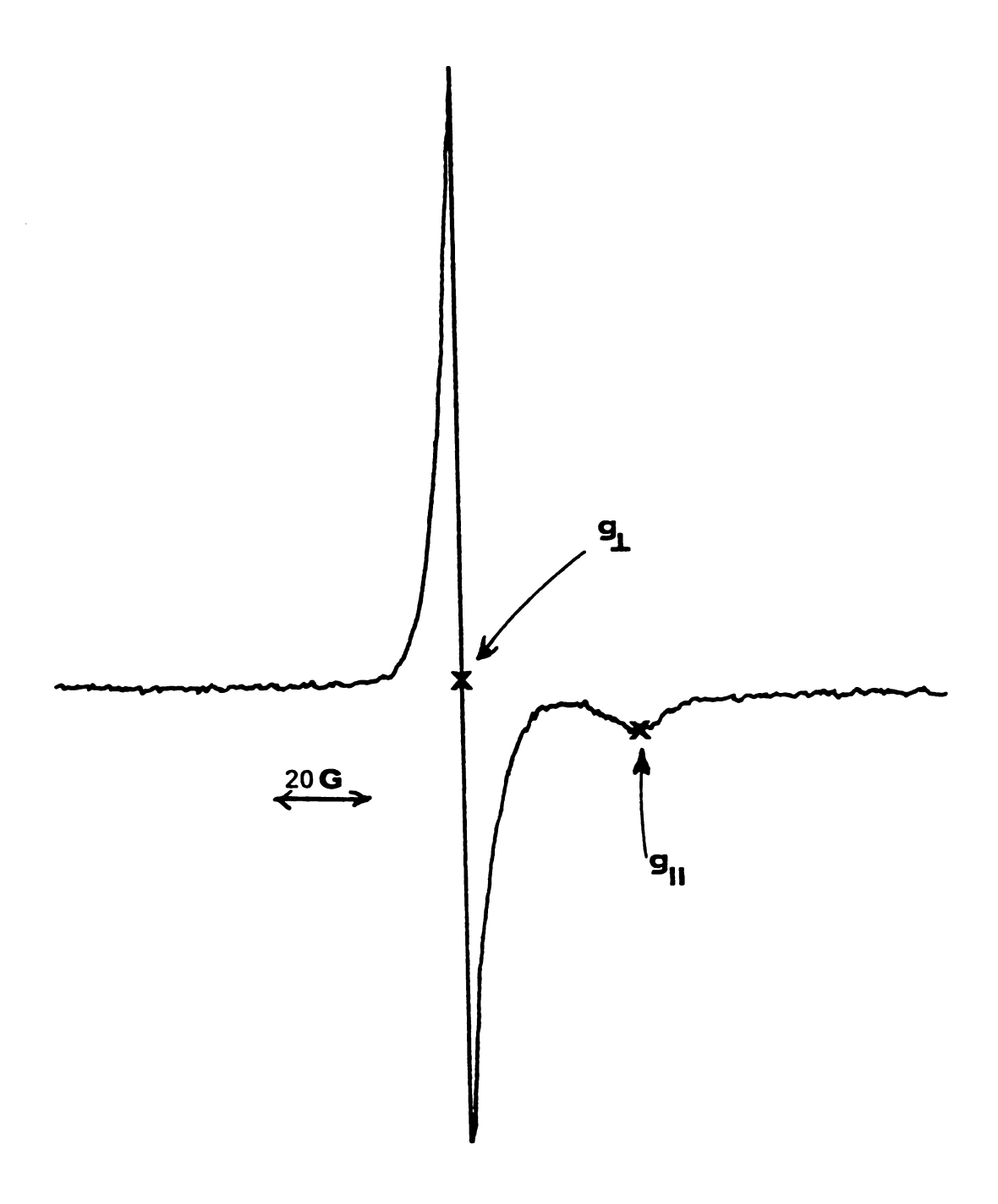


Figure 47: EPR spectrum of a polycrystalline sample of Cs⁺C222.e⁻ at 2.8 K.

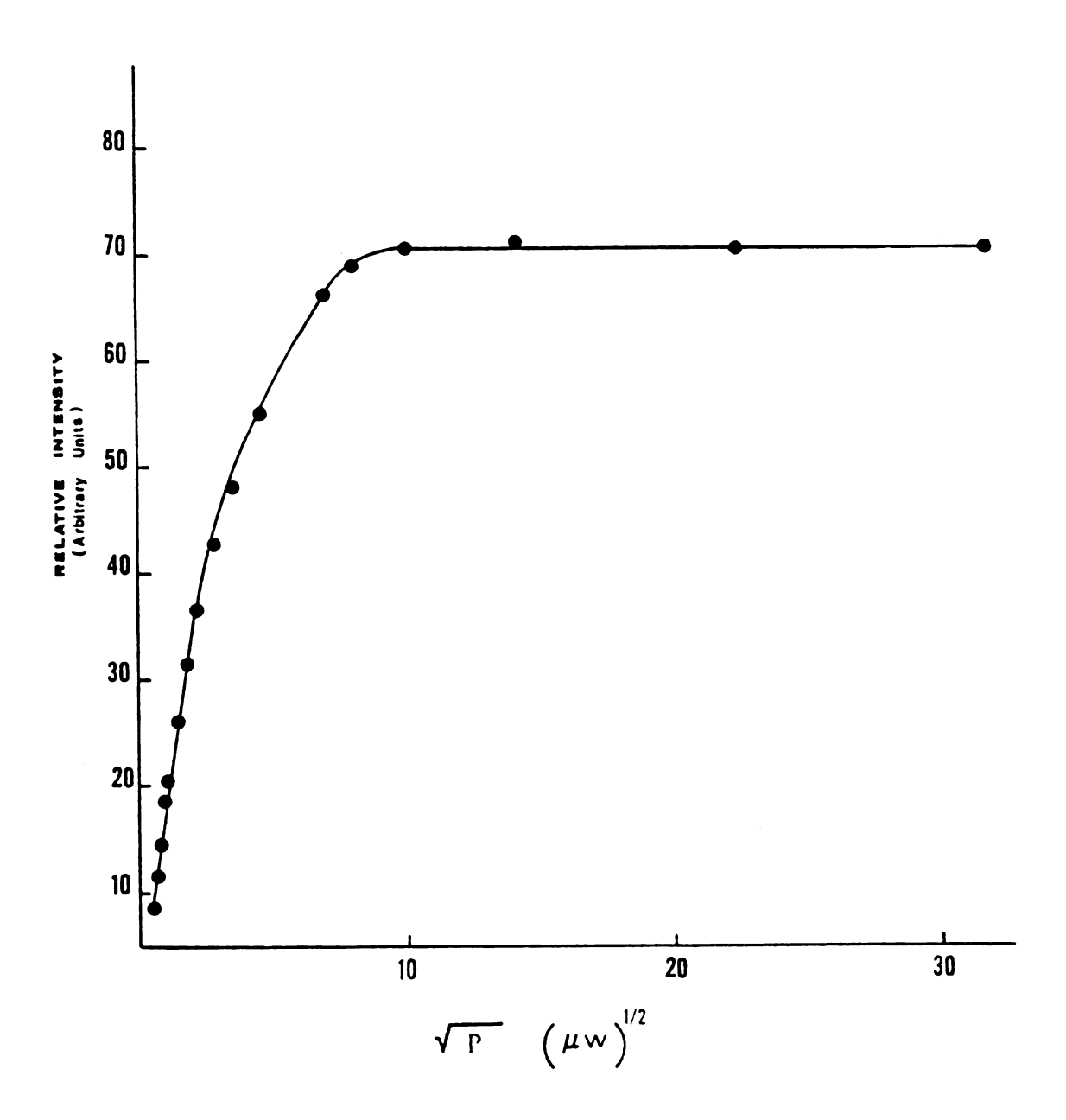


Figure 48: Variation of the relative intensity of the EPR line of Cs⁺C222.e⁻ with the square root of the microwave power level.

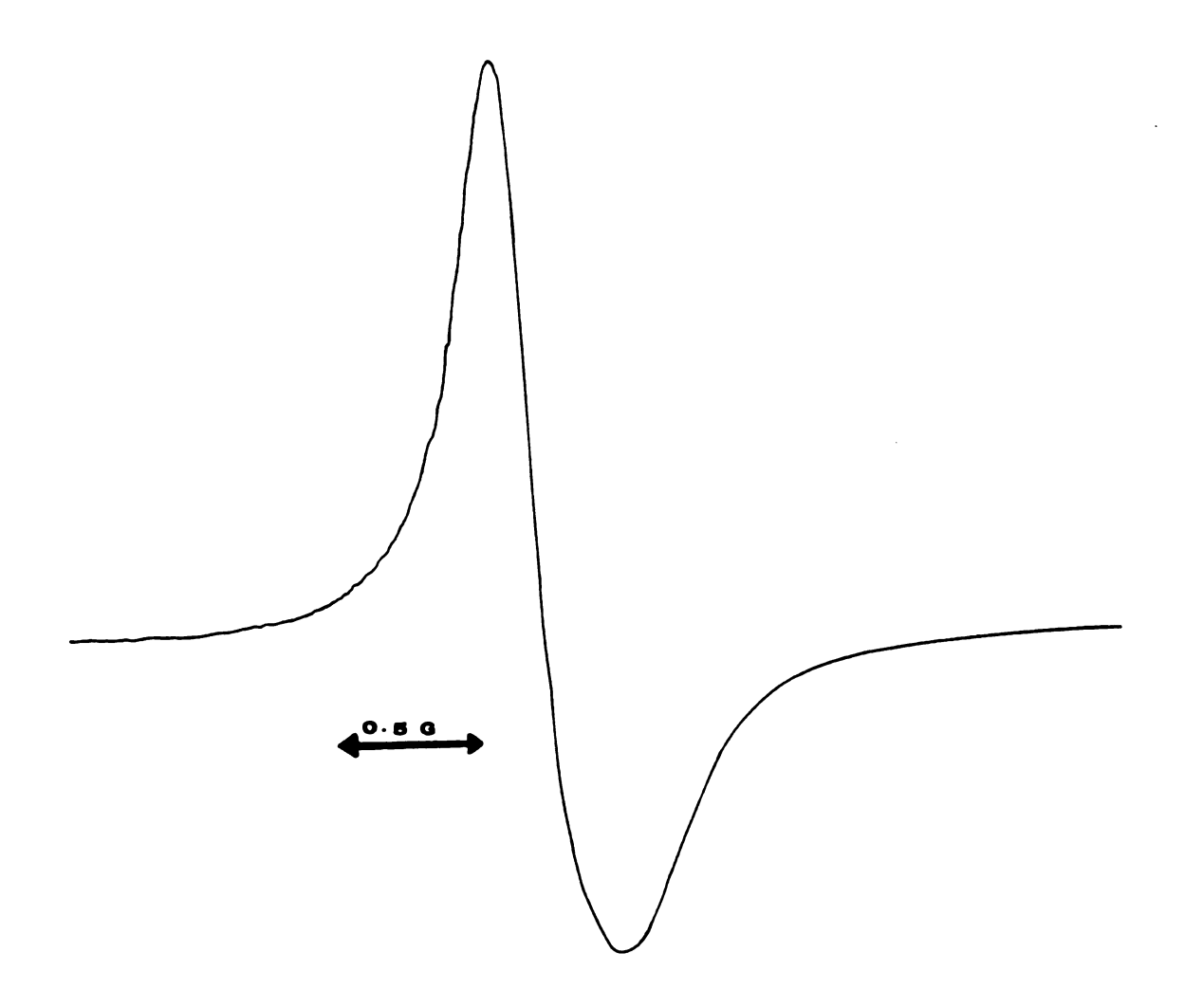
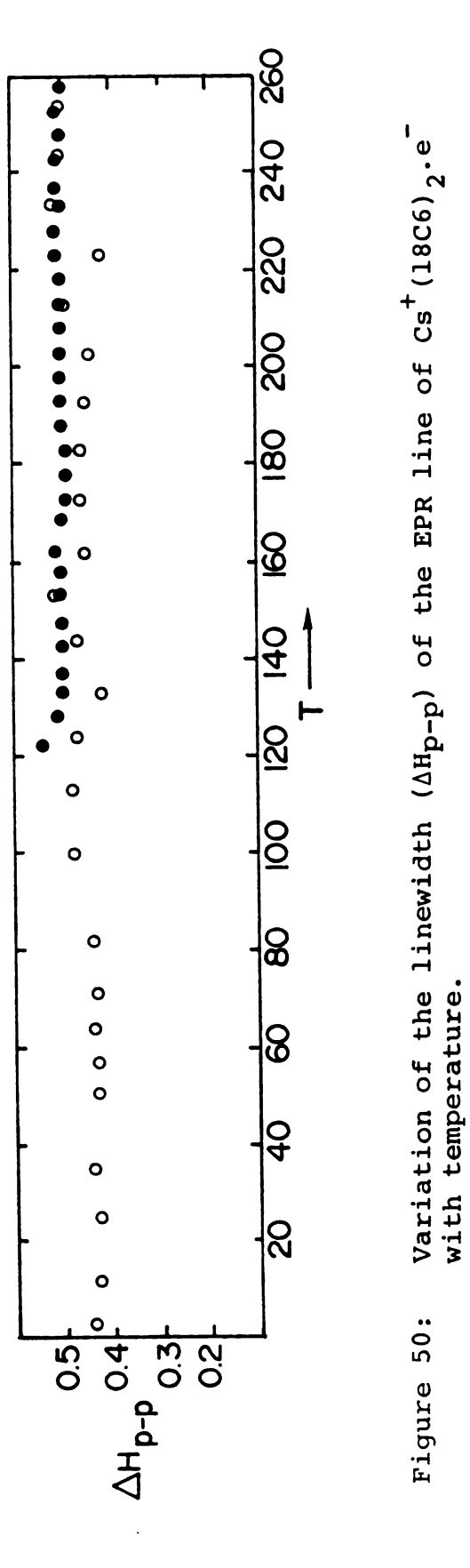
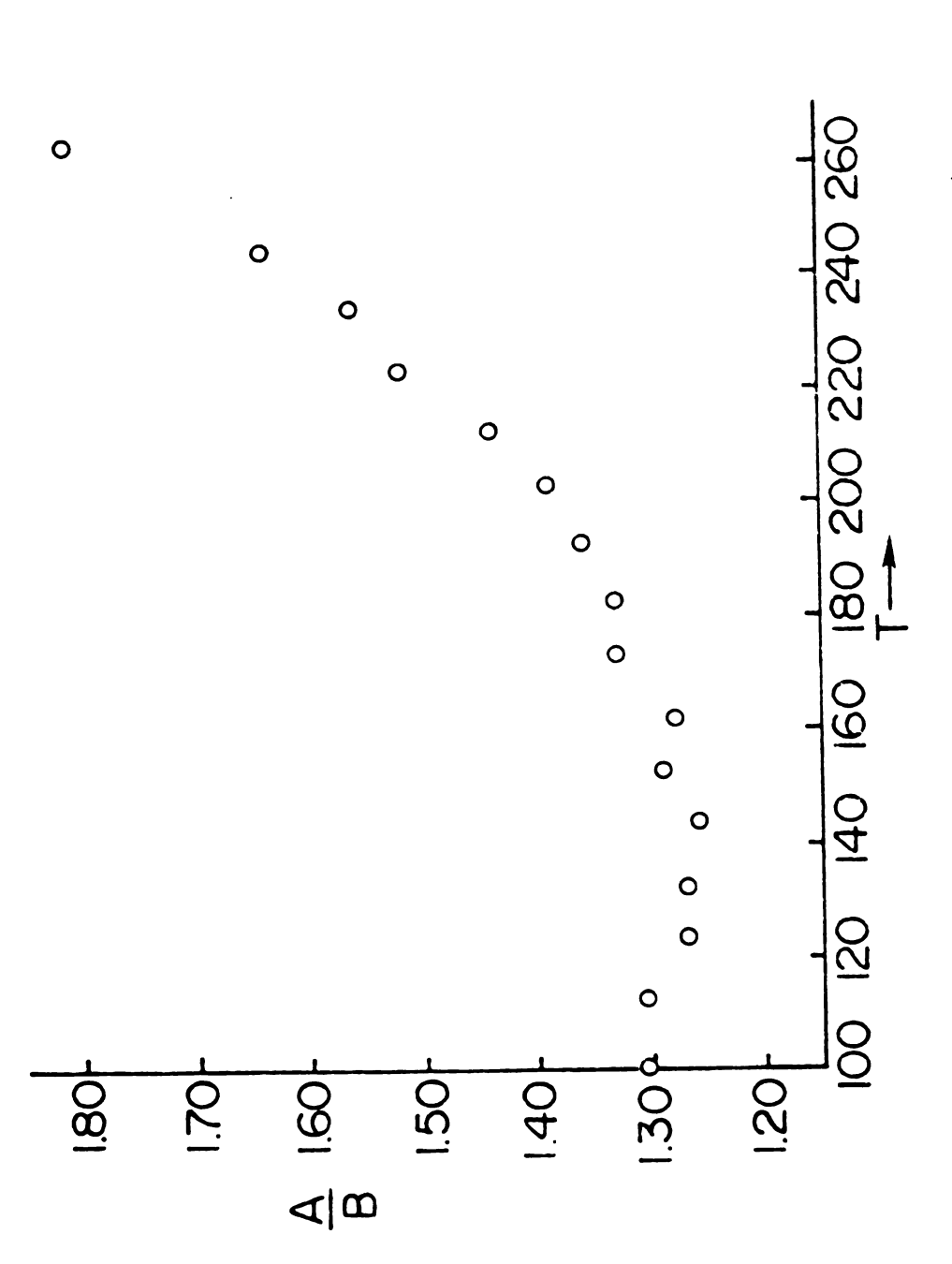


Figure 49: EPR spectrum of a polycrystalline sample of Cs⁺(18C6)₂.e at 174 K (sample in 2 mm tube).

spectrum consists of a single-asymmetric line with $1<\frac{A}{D}<2$. The temperature dependence of the linewidth ΔH_{DD} , of the EPR line is shown in Figure 50. The linewidth is remarkably independent of temperature over the range 2.9 to 254 K and has a value of 0.45 ± 0.05 G. g-value (corresponding to the field at which the first derivative crosses zero) is 2.0023, also independent of temperature. The $\frac{A}{R}$ ratio increases with increasing temperature, showing a greater asymmetry at higher temperatures. However, it was noticed that at a given temperature the $\frac{A}{B}$ ratio increased as the radius of the sample tube decreased. This indicates that the lineshape of the EPR line of Cs (18C6) 2.e may depend on the microwave resistivity of the sample, which decreases in the smaller EPR tube because the sample is more tightly packed. Figure 51 shows the variation of the $\frac{A}{R}$ ratio with temperature for a sample in a 3 mm tube.

The relative magnitude of the A.C. microwave resistivity as a function of temperature was estimated from the data shown in Figure 51 by using the graph of $\frac{a}{\delta}$ versus $\frac{A}{B}$ (shown in Figure 52) given by Glaunsinger and Sienko [144]. The value of the particle radius, a, was assumed to be independent of temperature. The resulting relative resistivities, $\rho/\rho_{ref.}$, are plotted versus temperature in Figure 53. The dashed line shows the D.C. resistivity over the same temperature range (203-260 K). The resistivity at T = 203 was taken as





Variation of A/B ratio of the EPR line of $\mathrm{Cs}^+(18\mathrm{C6})_2$.e with temperature (sample in 3 mm tube). Figure 51:

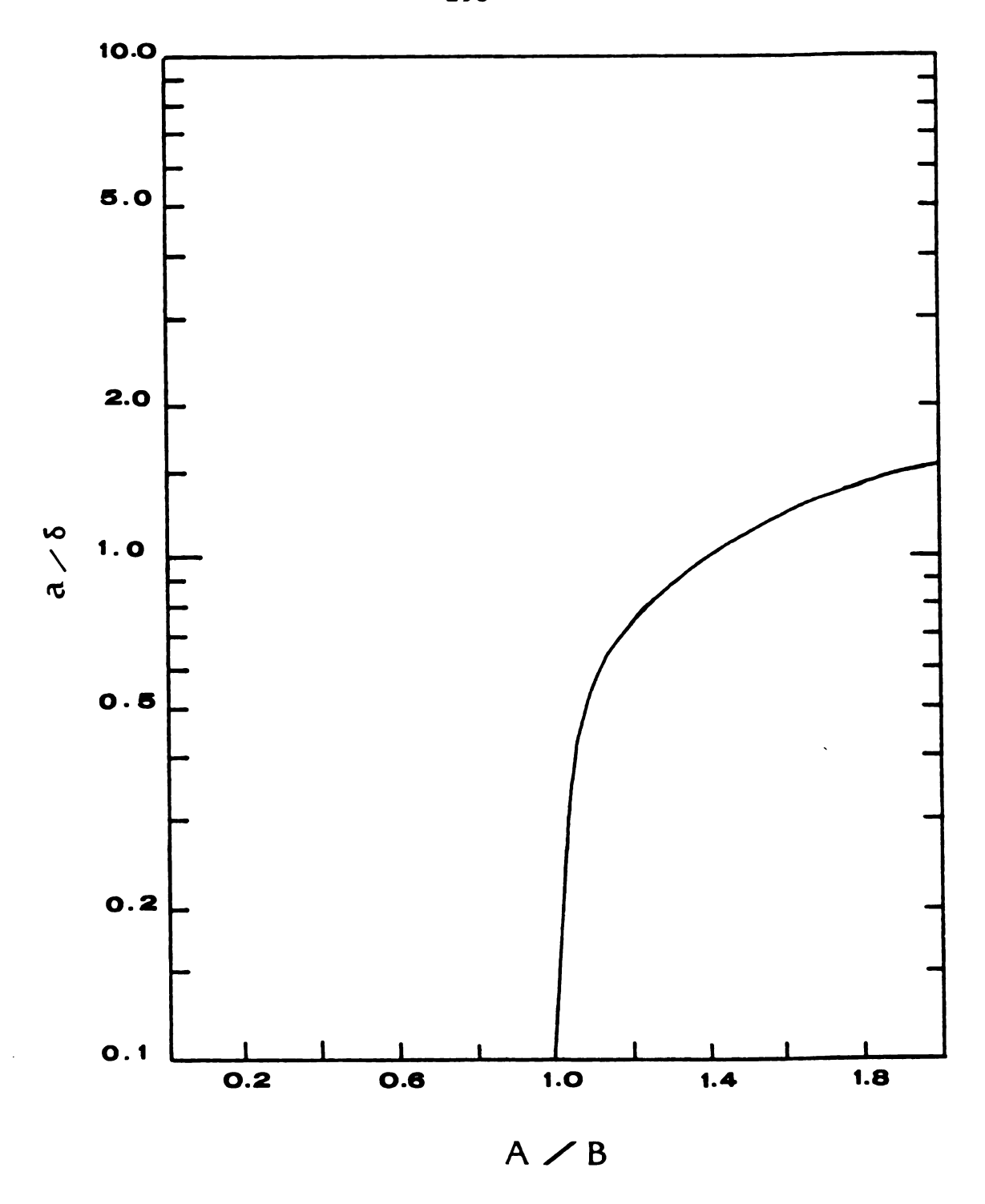


Figure 52: a/δ vs. A/B for spherical metal particles.

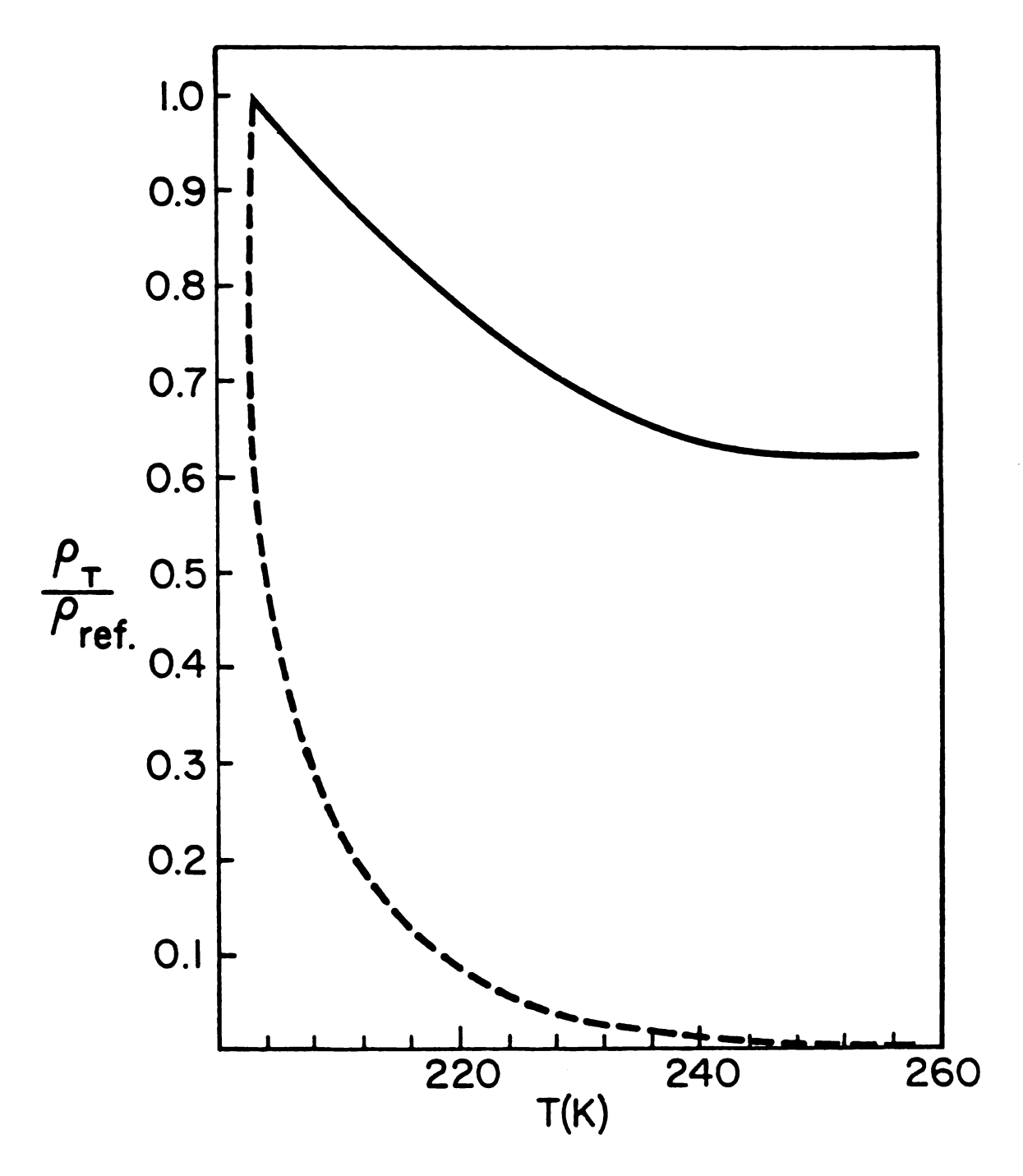


Figure 53: Plot of the relative A.C. resistivity (solid line) at x-band frequency, microwave frequency and D.C. restitivity (dashed line) vs. temperature.

the reference value. The plot of $\ln\rho/\rho_{\rm ref}$ versus 1/T is shown in Figure 54. It is linear and yields an apparent band-gap of only 0.1 eV compared with 0.9 eV from D.C. conductivity. It would be interesting to make corresponding measurements with single crystals in order to determine whether this difference in band-gaps arises from intergrain resistance and/or anisotropy of the electrical conductivity or whether it is an intrinsic frequency dependence of the specific impedance of the compound.

It would also be of great interest to obtain the diffusion time, T_D , as a function of temperature by fitting the spectra to the theoretical expression given by Webb [143], Equation (V.14), and also to obtain the relaxation times (T_1,T_2) of the electrons in this system. The extremely narrow, temperature independent EPR line obtained for this system suggests that the electrons exchange their spins very rapidly even at liquid helium temperatures. Since in the case of "exchange narrowing" T_1 is equal to T_2 , it can be calculated from the relation

$$T_1 = 1.15/\gamma_e \Delta H_{pp} \qquad (V.16)$$

in which γ_e is the magnetogyric ratio of the electron. The calculated value of the relaxation time is 1.45×10^{-7} sec which is only an order of magnitude larger than the relaxation time obtained for spherical lithium particles [144].

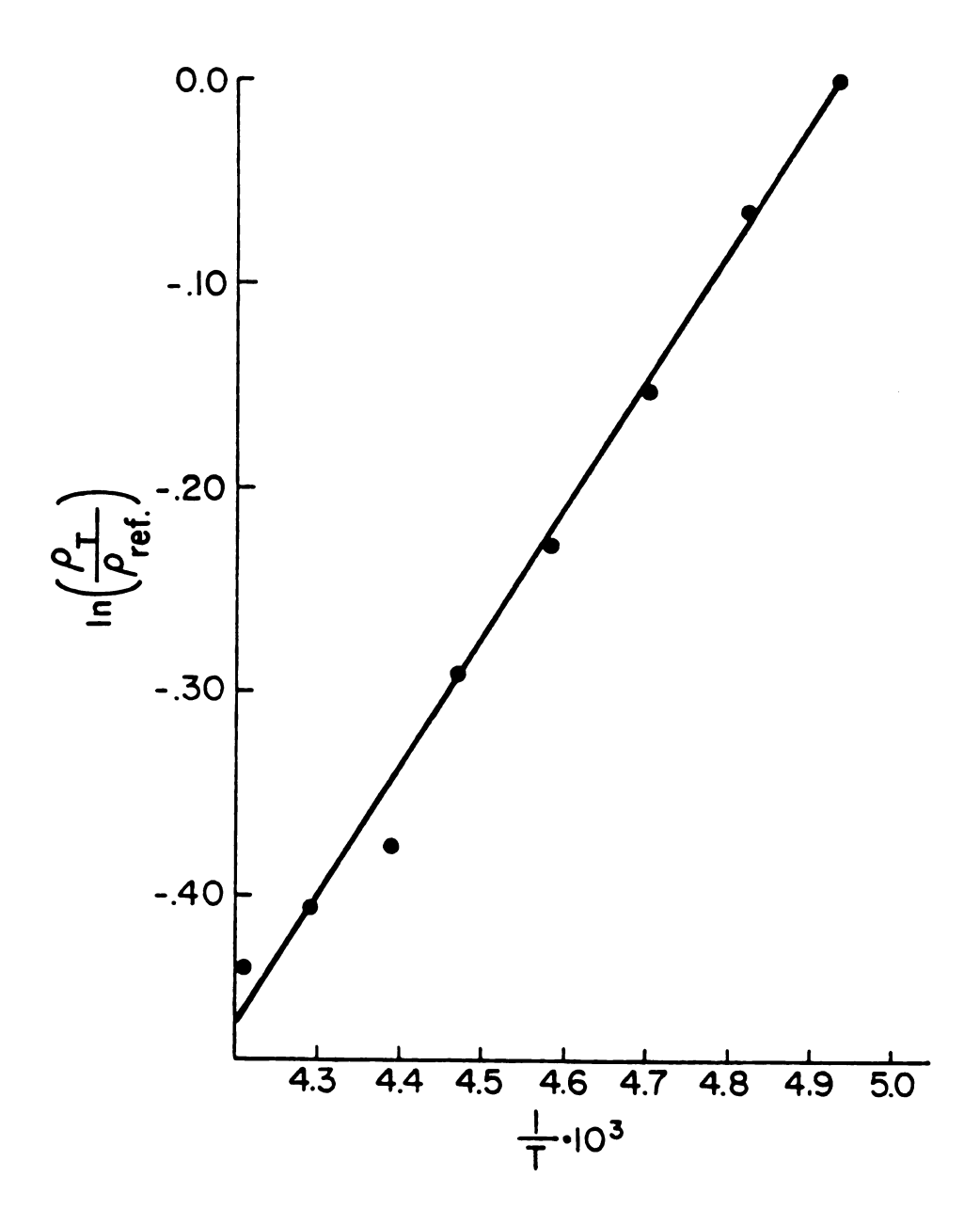


Figure 54: A plot of log relative microwave resistivity with 1/T.

The temperature independent-free electron g-value obtained for the compound Cs⁺(18C6)₂.e⁻ is surprising because most systems which show CESR yield a negative q-shift. This was discussed before in Chapter IV-Section C-2-b and the argument was used to explain the absence of an apparent q-shift in the presence of high symmetry. Another possibility that may be discussed here is a small electron density at the cesium nucleus and hence a very small atomic character as the reason for the absence of a g-shift. The electron density at the cesium nucleus can be calculated by using Equation (IV.22). replacing $\frac{\Delta H}{H}$ by the 140 ppm obtained for the shift in the resonance position of the $^{133}\mathrm{Cs-NMR}$ line of the Cs^+ in Cs⁺(18C6)₂.e⁻, the calculated electron density at the cesium nucleus is 2.39 × 10²¹ electrons·cm⁻³. The value of the electron density at the cesium nucleus of the free cesium atom is $2.65 \times 10^{+25}$. This yields ≈ 0.01 % atomic character at the cesium nucleus in the compound Cs (18C6) 2.e . If we compare the g-value of the compound Cs⁺(18C6)₂.e⁻ with that of the free cesium atom, 2.00258 [139], then a negative g-shift of 2.8×10^{-4} is obtained. This shift is very small compared to the 104.5×10^{-4} obtained for frozen solution of cesium in HMPA [41] (80% atomic character). Accordingly, the small atomic character and hence small electron density may be the reason for the absence of g-shift (relative to the free electron value) in Cs⁺(18C6)₂.e⁻.

B. Magnetic Susceptibility

1. Introduction

The most natural way to classify the magnetic properties of a material is by its response to an applied magnetic field. This response is characterized by the susceptibility χ , through the relation [145]

$$M = \chi H_{O}$$
 (V.17)

where M is the magnetization, or magnetic moment per unit volume, and H_O is the applied field. In general, χ is a function of both H_O and the temperature, T. If the material is magnetically isotropic, M and H_O are parallel and χ is a scalar; for anisotropic materials, χ is a tensor.

The magnetic moment of a free atom arises from three principle causes [146], the spin with which electrons are endowed, their orbital angular momentum about the nucleus, and the change in the orbital moment induced by an applied magnetic field. The first two effects give paramagnetic contributions to the magnetization, and the third gives a diamagnetic contribution. Accordingly, diamagnetism arises from field-induced electron circulation of electrons, which generate a field opposed to the applied magnetic field. Thus, all molecules have contributions from diamagnetic effects. The diamagnetic susceptibility

of an atom, χ_A , is proportional to the number of electrons, and the sum of the squared values of the average orbital radius of the ith electron, $\overline{r_i}$ [121]:

$$\chi_{A} = \frac{Ne^{2}}{6mc^{2}} \sum_{i}^{n} r_{i}^{2}$$

$$= -2.83 \times 10^{10} \sum_{i}^{n} r_{i}^{2}$$
(V.18)

Large atoms with more electrons have greater diamagnetic susceptibilities than small atoms with fewer electrons. The molar diamagnetic susceptibility, $\chi_{\rm d}$, for a molecule can be obtained by summing the diamagnetic contributions from all of the atoms, $\chi_{\rm A}$, and from all of the bonds in the functional groups, $\chi_{\rm B}$:

$$\chi_{d} = \sum_{i} \chi_{A_{i}} + \sum_{j} \chi_{B_{j}} \qquad (V.19)$$

Values for χ_A and χ_B are referred to as Pascal's constants. In general, diamagnetic materials have small negative temperature-independent molar susceptibilities with magnitudes of the order of 10^{-5} .

Paramagnetism occurs only in materials in which individual atoms or molecules have permanent magnetic moments. The molar susceptibility is positive and temperature-dependent; it is of the order of 10⁻² at room temperature and varies approximately as 1/T. For a system with isolated non-interacting spins, the molar

electronic susceptibility may be described by the Curie Law [145]:

$$\chi_{M}^{e} = \frac{N(P\beta)^{2}}{3k_{B}T} = \frac{C}{T}$$
 (V.20)

where N is Avogadro's number, β is the Bohr magneton, k_{B} is the Boltzmann constant, C is the Curie constant and P is the effective number of Bohr magnetons

$$P \equiv g[J(J+1)]^{\frac{1}{2}}$$
 (V.21)

in which J is the total angular momentum quantum number. For a system with a "quenched" orbital angular momentum, P becomes equal to g[S(S+1)] where S is the spin quantum number and the Curie-constant becomes 0.37604 cm K mole for a mole of free spins. This kind of magnetic behavior can be explained as a consequence of two opposing effects [146]: first, the tendency of the applied field to orient the moments in the direction of the field, and second, the tendency of thermal agitation to preserve a random orientation of magnetic moments.

For systems in which the electrons are weakly interacting so that there is no direct coupling between the spins, the internal interaction in the material tends to align the spins. This interaction is electrostatic. and is related to the overlap of charge distribution [147]. Such interaction was first postulated by Weiss and it was

shown later by Heisenberg that it can be described as a result of quantum mechanical exchange interactions [147]. The exchange energy of two electrons can be written as $-2J_{12}(S_1 \cdot S_2)$, where J is the exchange integral and is positive for a ferromagnetic system and negative for an antiferromagnetic system. The electronic susceptibility at sufficiently high temperatures $(T >> |\Theta|)$ can be expressed by Curie-Weiss Law

$$\chi_{M}^{e} = \frac{C}{T - \Theta} \tag{V.22}$$

where Θ is the Weiss-constant and is a characteristic of the material. For ferromagnetic behavior Θ is positive and usually, but not always, negative for antiferromagnetic behavior.

Paramagnetism in metals results in a small, positive temperature-independent susceptibility. Pauli [146] explained this phenomenon by the application of the Fermi-Dirac distribution. In this case, only a fraction T/T_F (where T_F is the Fermi temperature) of the total number of the electrons contribute to the susceptibility. The net magnetic susceptibility for conduction electrons after making correction for diamagnetism is given by

$$\chi_{M}^{e} = \frac{N\beta^{2}}{k_{B}T_{F}} \tag{V.23}$$

2. Results and discussion

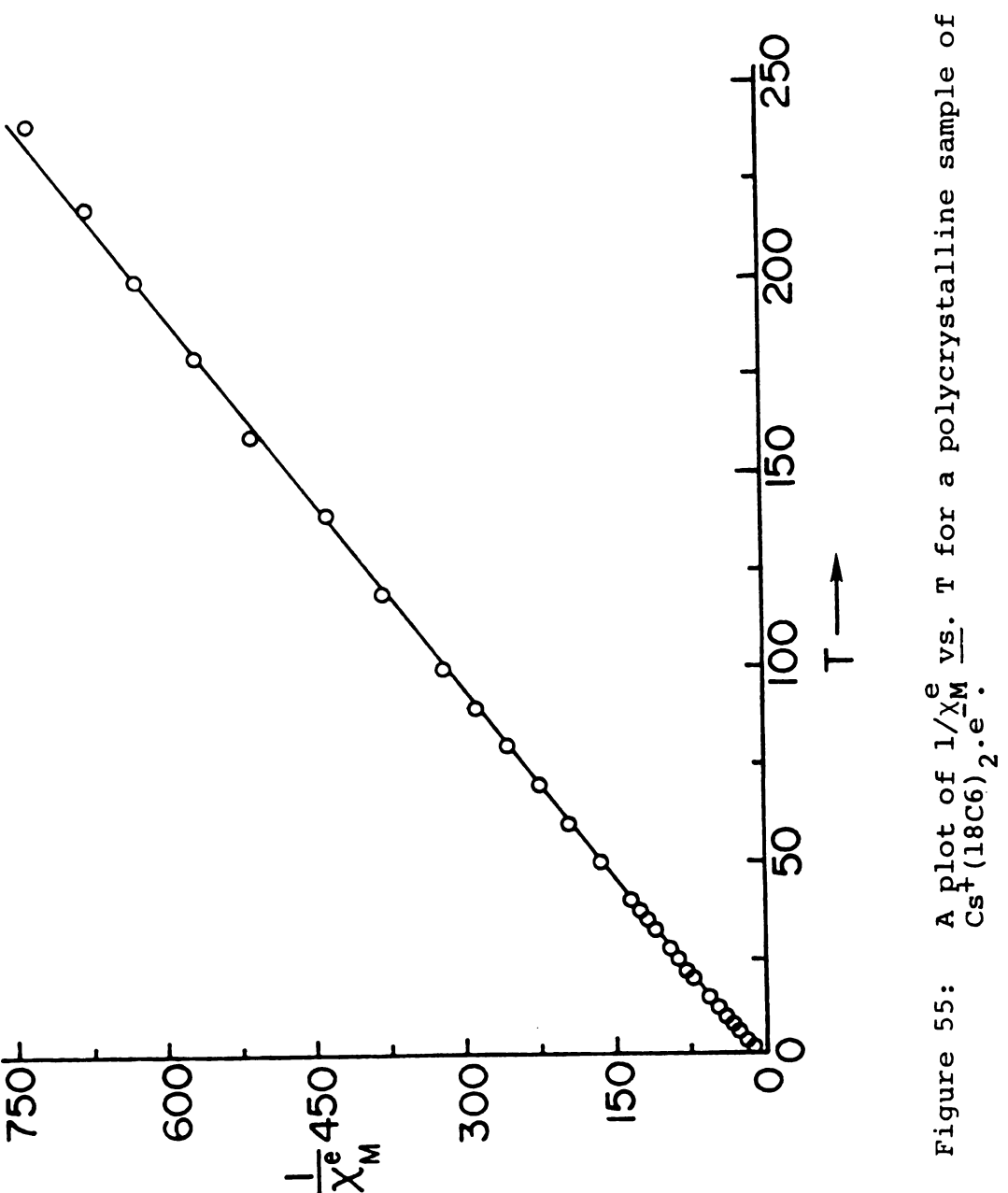
. .

a. The electride, Cs⁺(18C6)₂.e⁻:

Magnetic susceptibility measurements were carried out on a polycrystalline sample of $\operatorname{Cs}^+(18C6)_2$.e in the temperature range of 1.7 K to 250 K. Figure 55 shows a plot of the reciprocal of the molar electronic susceptibility, χ_{M}^{e} versus temperature. The electronic susceptibility is the measured susceptibility of the fresh sample minus that of the decomposed sample [see Equation (II.3)]. The relationship is very nearly linear and shows temperature dependent paramagnetism. The data shown in Figure 55 were fit by the equation

$$\chi_{M}^{e} = \frac{f_{1}^{C}}{T - \Theta} \tag{V.24}$$

where f_1 is the fraction of the electrons contributing to the susceptibilty and is given by $f_1 = n/N_{\rm av}$, where n is the number of unpaired electrons in one mole of the compound. The data nearly fit the Curie-Weiss Law Equation (V.24) with $f_1 = 0.736 \pm 0.009$ and $\theta = -1.44 \pm 0.05$. However, deviations from this equation are systematic. An excellent fit to the total molar susceptibility (susceptibility minus that of the container) can be obtained by adding a simple Curie-Law term and diamagnetic term to give



$$\chi_{\mathbf{M}} = \frac{\mathbf{f}_{1}^{C}}{\mathbf{T} - \Theta} + \frac{\mathbf{f}_{2}^{C}}{\mathbf{T}} + \mathbf{B} \tag{V.25}$$

The new fitting parameters and their standard deviations are $f_1 = 0.595 \pm 0.005$, $\theta = -4.5 \pm 0.2$, $f_2 = 0.262 \pm 0.006$ and $B = -(310 \pm 40) \times 10^{-6}$. The value of B is the same as the (temperature-independent) molar susceptibility of the decomposed sample, indicating that there is no diamagnetic electronic contribution to the molar susceptibility. The sum $f_1 + f_2$ is 86% of the value expected for a mole of unpaired spins, suggesting that the sample probably contained some decomposition product. Alternatively, the Curie-Weiss Law might not be applicable over the entire temperature range. The small and negative value of θ suggests that the electrons are very weakly interacting and the sample exhibits antiferromagnetic behavior.

b. The ceside, Cs (18C6) 2.Cs :

Dheeb Issa [104] prepared the crystalline compound of stoichiometry Cs18C6 by using method 2 and carrying out magnetic susceptibility measurements on polycrystalline samples of this compound. In the present work the magnetic susceptibility measurement of the compound Cs⁺(18C6)₂.Cs⁻, prepared by method 2, was repeated and compared with that obtained for the same compound prepared by method 3 (see Chapter III). The molar electronic susceptibility data were fit by the equation

$$\chi_{M}^{e} = \frac{fC}{T - \Theta} + B \tag{V.26}$$

The fitting parameters of the Curie-Weiss Law [Equation (V.26)] of three independently prepared samples precipitated from 2-aminopropane-diethylether mixtures (method 2) and another sample precipitated from dimethylether-trimethylamine mixtures (method 3) are summarized in Table X. The results of the first three samples of the compound Cs⁺(18C6)₂.Cs⁻ confirmed the presence of trapped electrons which interact only weakly with one another since small-negative 0 values are obtained for these three samples. As expected for electron trapping at anion vacancies during crystallization, the value of f varies somewhat from one preparation to another. contrast, sample 4 showed that 17% of the electrons are unpaired. The results obtained here are consistent with the ¹³³Cs-NMR results obtained for sample 4, which confirmed the presence of mixtures of Cs + (18C6) 2Cs and $\mathrm{Cs}^+(18\mathrm{C6})_2.\mathrm{e}^-$ rather than crystals of $\mathrm{Cs}^+(18\mathrm{C6})_2\mathrm{Cs}^-$ with all electrons trapped at anion vacancies.

The diamagnetic contribution to the electronic susceptibility of $\mathrm{Cs}^+(18\mathrm{C6})_2.\mathrm{Cs}^-(\mathrm{B})$ is interesting. Since this is obtained from the difference between the susceptibilities of fresh sample and that of the decomposed sample, it is difficult to determine accurately, particularly if any of the sample is lost during decomposition.

Table X: Parameters of the Curie-Weiss Equation for χ_m^e of Cs⁺(18C6)₂.Cs⁻

Sample	Method of Preparation	10 ² f	Θ,Κ	10 ⁶ B
1 ^a	2	1.4 ± 0.1°	-2.0 1	-46 ± 4
2 ^a	2	2.01 ± 0.02	-1.1 0.1	-36 ± 1
3 ^b	2	2.13 ± 0.02	-1.2 0.1	-73 ± 2
4 ^b	3	17.0 ± 0.6	-1.5 0.2	-40 ± 5

^aData were taken by Dr. Ramanurthi Janakiraman.

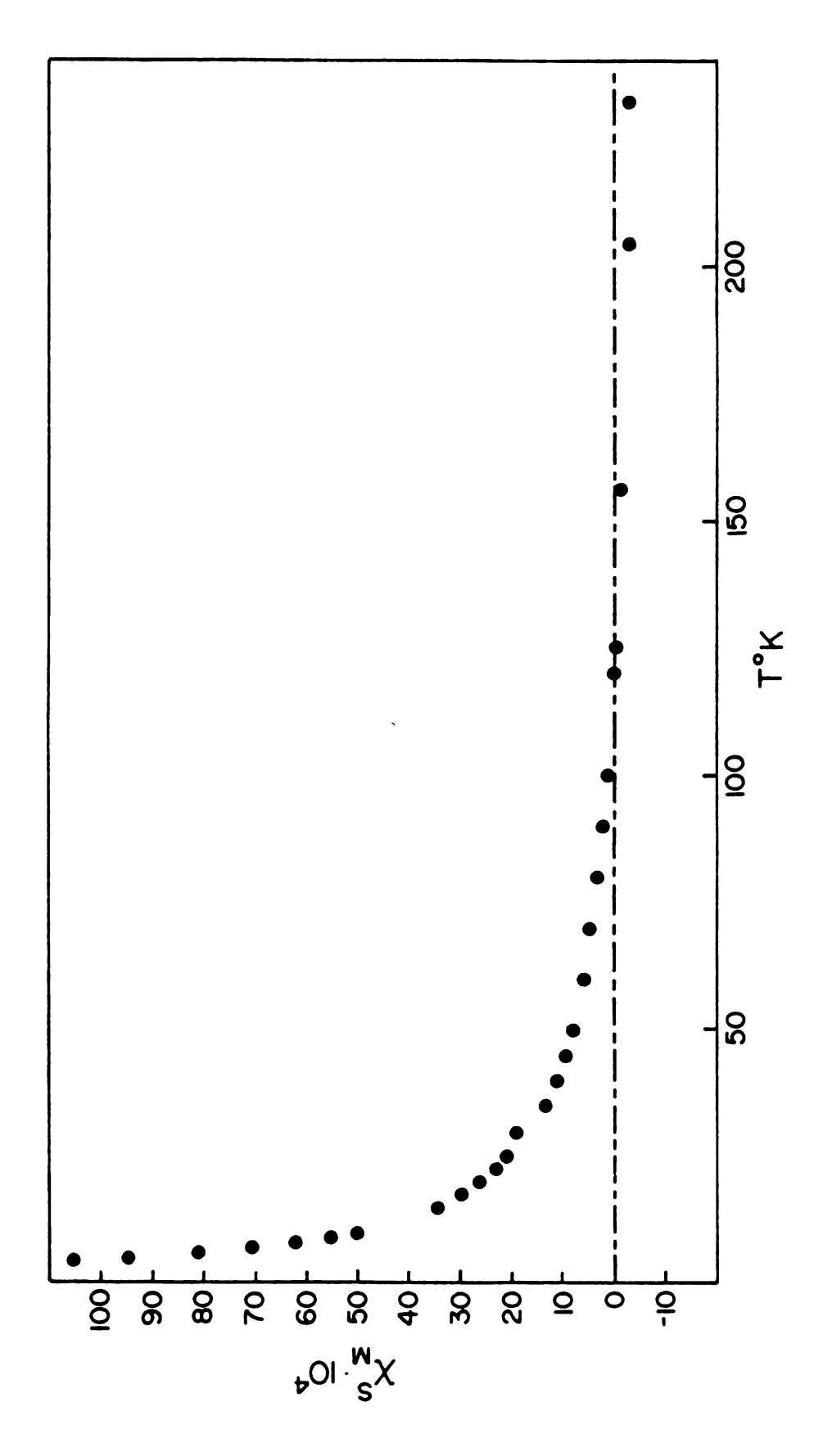
The values obtained, ranging from -36×10^{-6} to -73×10^{-6} per mole, presumably represent the diamagnetism of the 6s electron pair of Cs⁻. For all four samples the value of 0 ranges from -1 to -2 K. This small, negative value shows that antiferromagnetic interactions of the trapped electrons (if any) are very weak. Figure 56 shows the electronic molar susceptibility of Cs⁺(18C6)₂.Cs⁻, prepared by method 3, as a function of temperature.

c. The di-electrides

The prefix, di-, used here to describe the electride does not necessarily imply dimer electrides, rather it describes the ground state of the electride as a diamagnetic state. Two crystalline electrides fulfill this criterion.

bThis work.

^cStandard deviation estimates from the fit of each data set independently.



A plot of XM VS. T for a polycrystalline sample of Cs (18C6) 2.Cs (method 3). Figure 56:

These are Rb 18C6.e and Cs C222.e. Figure 57 shows the variation of the molar electronic susceptibility of a polycrystalline sample of Rb 18C6.e as a function of temperature. In the temperature range of 1.7 K to 120 K the electronic susceptibility shows a temperature dependent paramagnetism. Above 120 K the susceptibility is negative and nearly temperature independent. shown in Figure 57 were fit by Equation (V.26). fitting parameters of the Curie-Weiss equation for $Rb^{+}18C6.e^{-}$ are: $f_1 = (0.85 \pm 0.01) \times 10^{-2}$, $\Theta = +0.15 \pm 0.05$ and B = $(-18.7 \pm 0.7) \times 10^{-6}$. Only 0.85% of the expected number of the unpaired spins are present which indicates that a substantial temperature-independent spin pairing is present in this system. The results indicate that the compound Rb 18C6.e is essentially diamagnetic with some electron doping as an impurity.

The crystalline compound Cs⁺C222.e⁻ shows a negative molar susceptibility in the temperature range 1.7 to 225 K. However, the molar susceptibility becomes more negative upon increasing the temperature. This temperature-dependent diamagnetism can be explained as follows: the molar susceptibility of the compound Cs⁺C222.e⁻ is the sum of a very small positive paramagnetic contribution which is temperature-dependent and a large contribution from the negative temperature-independent diamagnetism. The net magnetization results in a temperature dependent negative susceptibility. Figure 58 shows the variation of

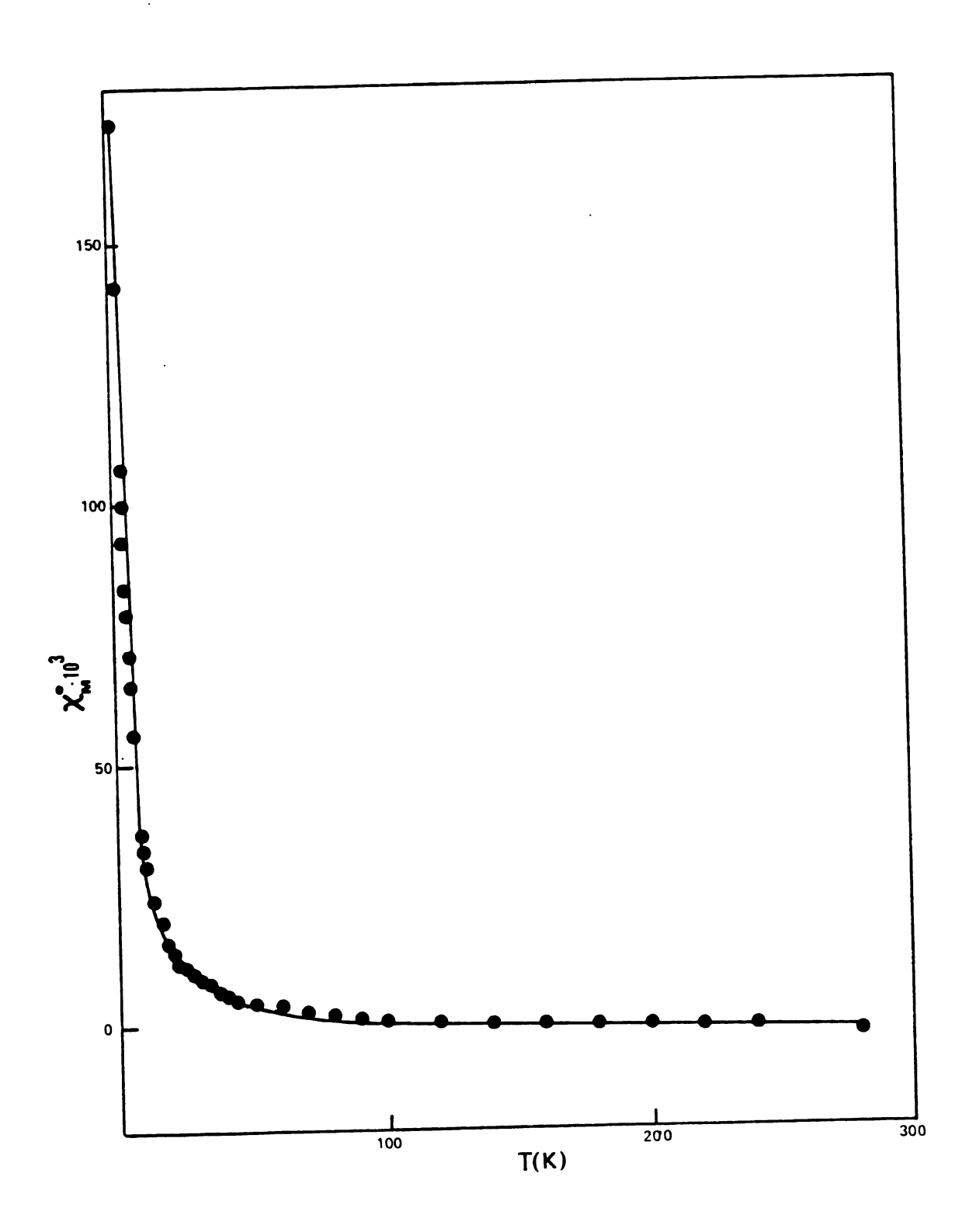


Figure 27: A plot of $\chi_{\underline{M}}^{\underline{e}}$ vs. T for a polycrystalline sample of Rb18C6.e .

 χ_{M}^{S} of a polycrystalline sample of Cs⁺C222.e⁻ as a function of temperature. However, because of the violent thermal decomposition of the sample at room temperature no data could be obtained for the decomposed sample so that the electronic susceptibility could not be calculated. Also, no accurate measurements of the mass of the sample could be obtained because of the loss of part of the sample during the thermal decomposition. Accordingly no fitting of the data could be done.

It is of interest to know why a system such as $Cs^+(18C6)_2.e^-$ is paramagnetic while systems such as $Cs^+C222.e^-$ and $Rb^+18C6.e^-$ are diamagnetic. Spin-pairing processes are of course common for electrons in alkali metal-ammonia solutions [1] as indicated from static and microwave (EPR) susceptibility measurements [1]. Electrides prepared by solvent evaporation [96-98] often show substantial spin-pairing as indicated from magnetic susceptibility measurements. The reason for such spin pairing in these systems is not clear but Cyrot [148] and others pointed out that when electron correlations are taken into account, the singlet ground state is favored over the paramagnetic state.

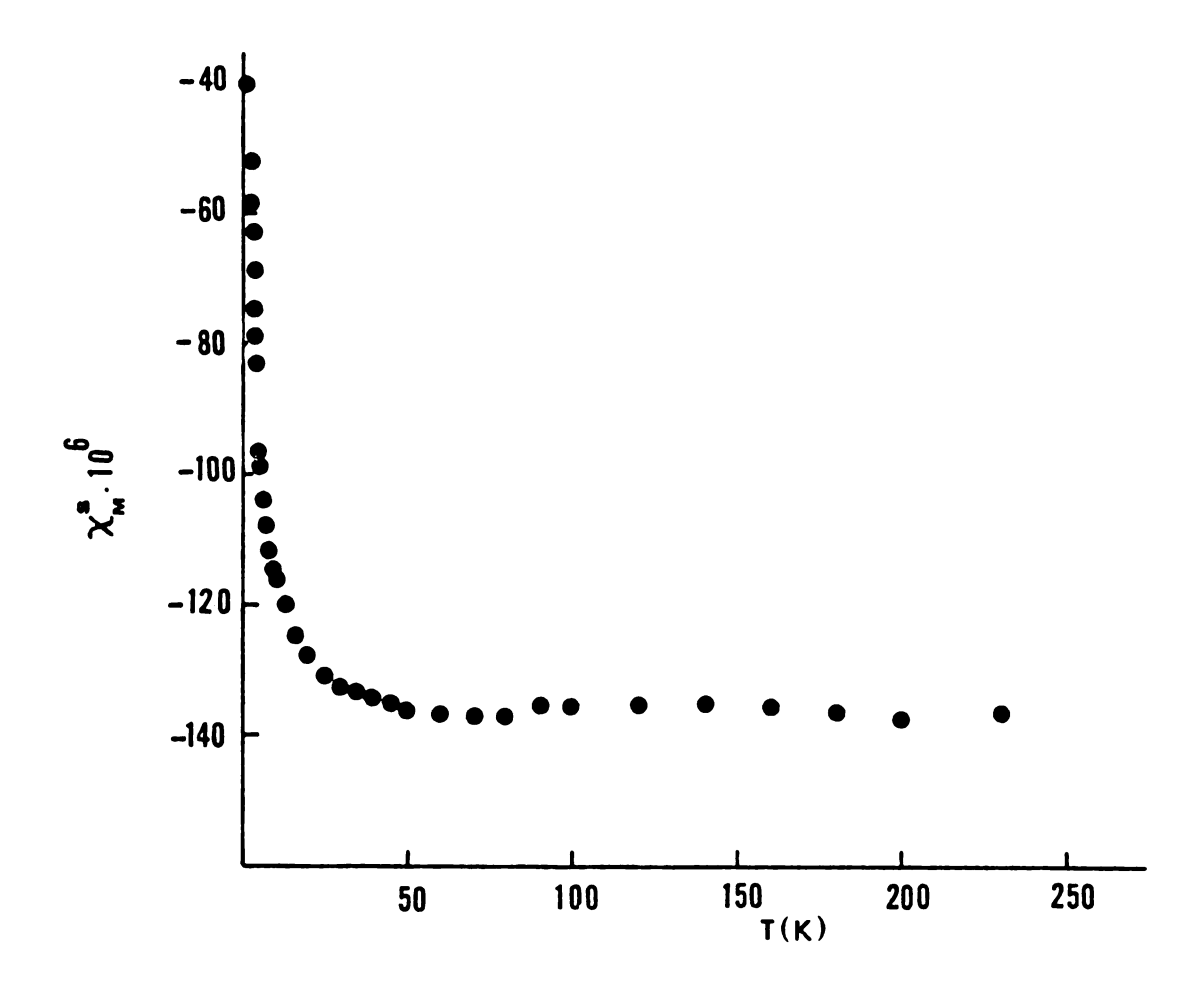


Figure 58: A plot of $\chi_{M}^{S} \underline{vs}$. T for a polycrystalline sample of $Cs^{+}\overline{C2}22.e^{-}$.

CHAPTER VI

CONCLUSIONS AND SUGGESTIONS FOR FUTURE WORK

A. Conclusions

Crystalline electride and alkalide salts can be prepared as stable compounds in vacuo at low temperatures. The alkalide salts have greater stability than the electrides. Solutions of the alkali metal and complexant in the solvent dimethylether were shown to have much greater stability than those in ammonia and methylamine and therefore provide more stable and clean crystals. The stabilization of the solution by adding lithium metal to methylamine solutions of alkali metal and complexant is a general phenomenon and all the crystals prepared were essentially free of lithium.

The new alkalides, Rb⁺18C6.Na⁻ and Rb⁺18C6.Rb⁻ are stable at room temperature for days. Analyses and properties of these compounds confirmed the proposed formulae.

The first crystalline electride, Cs⁺(18C6)₂.e⁻, was synthesized, and its optical, electrical and magnetic properties fulfill all the requirements for the elusive

electride, with the trapped electron present as a genuine localized anion.

Two other crystalline electrides, Rb18C6 and CsC222, were synthesized and their properties were investigated. There is no direct evidence for the molecular formula of the compound Rb18C6, but indirect evidence from syntheses and NMR studies suggests that this compound is the electride, Rb⁺18C6.e⁻. The analysis proves that the compound CsC222 is the electride, Cs⁺C222.e⁻, which forms either as a mixture of two crystals or as single mixed crystals.

Either the packing of the Cs⁺C222 complex cation does not allow enough room for other alkali metal anions, or the compound Cs⁺C222.e⁻ is thermodynamically favored over the alkalides Cs⁺C222.N⁻, where N⁻ is the alkali metal anion, since the compounds Cs⁺C222.Na⁻ and Cs⁺C222.Cs⁻ could not be prepared.

The "pure" ceside compound, Cs⁺(18C6)₂.Cs⁻, can be prepared only in the presence of dissolved lithium metal (method 2); otherwise, a mixture of ceside and electride crystals forms.

The complexation of rubidium and cesium cations by 18-crown-6 in electride and alkalide crystals is different than in crystals formed from simple rubidium and cesium salts with 18-crown-6. In the latter case, both 1:1 and 1:2 complexes between the alkali metal cation and the crown ether could be formed. In alkalide and electride

salts only the 1:1 complex forms with rubidium while only the 1:2 "sandwich" complex forms with cesium.

Analyses and optical spectra cannot be used as definitive tools to identify the species present. Analysis gives only the compound stoichiometry, while the optical spectra are complicated by the sensitivity of the excited state to the environment, and by decomplexation in solution, dissociation of alkali metal anions and solid state reactions in the film.

The magic angle sample spinning (MASS) NMR technique provides a way to identify the species present in alkalides and electrides. The conclusions drawn from NMR studies can be summarized as follows:

- —The heteronuclear alkalide compounds that contain sodium are sodides and no complexation between the sodium cation and 18-crown-6 in the crystalline alkalides occurs.
- —The sodium anion (Na) exists in solution and in the solid state as a stable, long-lived genuine, spherically-symmetric anion. Its ground state is largely unperturbed by the environment and its chemical shift can be used as a diagnostic tool for its identification.
- —In sodide salts, the ²³Na-NMR signal of Na is broadened by magnetic dipole interaction with the protons of the complexant. The Na C222 signal is mainly broadened by quadrupolar interactions whose effects can be minimized by working at high magnetic fields.

- —The two crystalline compounds CsNa(18C6)₂ and Cs18C6 are Cs⁺(18C6)₂.Na⁻ and Cs⁺(18C6)₂.Cs⁻ and not Cs⁺18C6.Na⁻ and Cs⁺18C6.e⁻ as previously believed.
- —The central line of ¹³³Cs-NMR signals in cesium-containing salts is mainly broadened by magnetic dipolar and chemical shift interactions.
- —The chemical shift of the Cs⁺ cation in the electride, Cs⁺(18C6)₂.e⁻, is shifted 140 ppm (at ~-20°C) from the expected resonance position because of the presence of a small contact (Fermi) density at the cesium nucleus (~0.01% of the free atom density). This is also in accord with the paramagnetism of the sample.
- ⁸⁷Rb-NMR is not a good way to identify the rubidium cations in alkalides and electrides because of the large quadrupolar interactions, but it may (or may not) be used to identify the rubidium anion.
- —The ground states of alkali metal anions other than Na have some contribution to their wavefunctions from orbitals other than the outer s orbital.
- —The two crystalline electrides, Rb⁺18C6.e⁻ and Cs⁺C222.e⁻, are essentially diamagnetic while the electride, Cs⁺(18C6)₂.e⁻ is paramagnetic with the electrons showing only a very weak antiferromagnetic interaction.
- —The EPR lineshape of the electride, Cs⁺(18C6)₂.e⁻ depends on the microwave conductivity of the sample. It shows Dysonian asymmetry that increases with increasing

temperature, indicative of activated conductivity. The electrons in this system exchange their spins very rapidly, so the EPR signal is exchange narrowed with the result that a very small, temperature independent linewidth was observed.

Electron trapping (or doping) can occur in alkalides to different extents, which affects the chemical shift of the alkali metal cation and anion as well as the powder EPR pattern. Two kinds of electron trapping can occur in sodide salts. Electron trapping at anionic vacancies (F-centers) produces an EPR spectrum that consists of superimposed lines at the free electron g-value, which indicates trapping at different non-interacting sites with different broadening mechanisms. Electron trapping near a cation defect sometimes produces a hyperfine interaction that indicates a rather large atomic character for the affected alkali metal cation.

B. Suggestions for Future Work.

(1) After the success in preparing the first crystalline electride, Cs⁺(18C6)₂.e⁻, further investigation of its properties such as quantitative chemical shift studies as a function of temperature, quantitative single crystal EPR and single crystal D.C. and A.C. conductivity studies should be made. Systematic procedures for growing high-quality single crystals for

BIBLIOGRAPHY

X-ray structure determination are absolutely essential in order to better understand the properties of electrides.

- (2) The data already obtained for X-ray structure determination of the compound CsNal8C6 should be reevaluated in terms of the more likely molecular formula, Cs⁺(18C6)₂.Na⁻.
- (3) X-ray powder diffraction and differential scanning techniques should be used as analytical tools to investigate the electride and alkalide salts.
- (4) Synthesis of crystalline electrides and alkalides with other macrocyclic polyethers such as 12-crown-4, 15-crown-5, 21-crown-7, "Lariat" ethers and cryptands 211 and 221 should be explored in order to establish trends in the properties of these compounds.
- (5) A systematic procedure should be established to find a way to control electron doping in alkalides, $M^{+}L_{n}.N_{v}^{-}.e_{1-v}^{-}$.
- (6) The crystalline electrides, Cs⁺(18C6)₂.e⁻, Rb⁺18C6.e⁻ and Cs⁺C222.e⁻ might be good candidates for quantum mechanical ab initio calculations in order to understand electron-electron correlations in these systems.

BIBLIOGRAPHY

- 1. J.C. Thompson, "Electrons in Liquid Ammonia", Oxford University Press, Oxford, 1976.
- 2. C.A. Seely, Chem. News 23, 169 (1871).
- 3. G. LePoutre and M.J. Sienko (eds.), "Metal-Ammonia Solutions, Colloque Weyl 1", W.A. Benjamin (New York) 1964.
- 4. J.J. Lagowski and M.J. Sienko (eds.), "Metal-Ammonia Solutions", Butterworth (London) 1970.
- 5. J. Jortner and N.R. Kestner (eds.), "Electrons in Fluids", Springer-Verlag (New York) 1973.
- 6. J. Phys. Chem. 79(26), (1975).
- 7. J. Phys. Chem. 84(10), (1980).
- 8. J. Phys. Chem., Colloque Weyl issue, 1984, in press.
- 9. T.R. Tuttle, Jr. and S. Golden, J. Chem. Soc. Faraday Trans 2 77, 889 (1981).
- J.W. Fletcher and W.A. Seddon, J. Phys. Chem. 84 (10), 3055 (1980).
- 11. E. Beckman and K.S. Pitzer, J. Phys. Chem. <u>65</u>, 1527 (1961).
- 12. D.E. O'Reilly, J. Chem. Phys. 41, 3736 (1964).
- 13. D.E. O'Reilly, J. Chem. Phys. 41, 3729 (1964).
- 14. W.D. Knight in "Solid State Physics", Vol. 2, F. Seitz and D. Turnball (eds.) Academic Press (New York) 1956.
- 15. H.M. McConnell and C.H. Holm, J. Chem. Phys. 26, 1517 (1957).
- 16. J.V. Acrivos and K.S. Pitzer, J. Phys. Chem. <u>66</u> 1693 (1962).

- 17. T.R. Hughes, Jr., J. Chem. Phys. 38, 202 (1963).
- 18. R. Catterall, Phil. Mag. 22, 779 (1970).
- 19. A. Depriester, J. Fackeure and J.P. LeLieur, J. Phys. Chem. 85, 272 (1981).
- 20. S. Freed and N. Sugerman, J. Chem. Phys. <u>11</u>, 354 (1943).
- 21. J.P. LeLieur and R. Rigny, J. Chem. Phys. <u>59</u>, 1142 (1973).
- 22. J.P. LeLieur and R. Rigny, J. Chem. Phys. <u>59</u>, 1148 (1973).
- 23. A Demortier, M. DeBacker and G. LePoutre, J. Chim. Phys., 380 (1972).
- 24. R.L. Harris and J.J. Lagouski, J. Phys. Chem. <u>85</u>, 896 (1981).
- 25. C.A. Hutchison, Jr. and R.C. Paster, Rev. Mod. Phys. 25, 285 (1953).
- 26. D.E. O'Reilly, J. Chem. Phys. 35, 1856 (1961).
- 27. V.L. Pollak, J. Chem. Phys. 34, 864 (1961).
- 28. R.J. Peck and W.S. Glaunsinger, J. Phys. Chem. 84(10), 1176 (1980).
- 29. R.R. Dewald and J.L. Dye, J. Phys. Chem. <u>68</u>, 121 (1964).
- 30. J.L. Dye, in "Progress in Inorganic Chemistry", Vol. 32, Stephen J. Lippard (ed.), John Wiley and Sons Inc., (New York), in press.
- 31. D.M. Holter, P.P. Edwards, W. McFarlane and B. Wood, J. Am. Chem. Soc. <u>105</u>, 2104 (1983).
- 32. Y. Nakamura, T. Toma and M. Shimoji, Phys. Lett A60, 373 (1977).
- 33. C.J. Page, G.M. Millhauser, P.P. Edwards, J.M. Freed and M.J. Sienko, J. Phys. Chem., in press.
- 34. J.L. Dye and L.R. Dalton, J. Phys. Chem. <u>71</u>, 184 (1967).
- 35. J.L. Dye, Pure Appl, Chem. <u>49</u>, 3 (1977).

- 36. D.C. Johnson, C. Page, D.M. Holten, B. Wood, W. McFarlane and P.P. Edwards, to be submitted.
- 37. R. Catterall, J. Slater and M.C. Symons, J. Chem. Phys. 52, 1003 (1970).
- 38. R. Catterall, L.P. Stodulski and M.C. Symons, J. Chem. Soc. (A), 437 (1968).
- 39. H. Normat, Angew. Chem. Int. Edit. Engl. 7, 1046 (1967).
- 40. P.P. Edwards, S.C. Grey and D.M. Holton, J.C.S. Chem. Comm., 1185 (1981).
- 41. R. Catterall and P.P. Edwards, J. Phys. Chem. <u>79</u>, 3010 (1975).
- 42. N. Mammano, "Metal-Ammonia Solutions", J.J. Lagowski and M.J. Sienko (eds.), Butterworth (London) 1970, p. 367.
- 43. R.F. Marzke and W.S. Glaunsinger, J. Phys. Chem. 79, 2976 (1975).
- 44. W.S. Glaunsinger, T.R. White, R.B. Von Dreele, D.A. Gorden, R.F. Marzke, A.L. Bowman and J.L. Yarnell, Nature (London) 271, 414 (1978).
- 45. R.B. Von Dreele, W.S. Glaunsinger, A.L. Bowman and J.L. Yarnell, J. Phys. Chem. 79, 2992 (1975).
- 46. R.B. Von Dreele, W.S. Glaunsinger, P. Chieux and P. Damay, J. Phys. Chem. 84, 1172 (1980).
- 47. F.Y. Robb and W.S. Glaunsinger, J. Mag. Res. <u>46</u>, 98 (1982).
- 48. M.J. Mobley and W.S. Glaunsinger, Solid State Commun. 40, 357 (1981).
- 49. N. Mammano and M.J. Sienko, J. Am. Chem. Soc. <u>90</u>, 6322 (1968).
- 50. A.M. Stacy and M.J. Sienko, Inorg. Chem. <u>21</u>, 2294 (1982).
- 51. A.M. Stacy, D.C. Johnson and M.J. Sienko, J. Chem. Phys. <u>76</u>, 4248 (1982).
- 52. V.M. Dukel'skii, E.Ya. Zandberg and N.I. Ionov, Akad. Nauk SSSR 62, 232 (1948).

- 53. S. Golden, G. Guttman and T.R. Tuttle, Jr., J. Am. Chem. Soc. 85, 135 (1965).
- 54. J.M. Ceraso and J.L. Dye, J. Chem. Phys. <u>61</u>, 1585 (1974).
- 55. J.L. Dye, C.W. Andrew and J.M. Ceraso, J. Phys. Chem. 79, 3076 (1975).
- 56. P.P. Edwards, S.C. Gray, D.M. Holten, D.C. Johnson, M.J. Sienko, W. McFarlane and B. Wood, J. Phys. Chem. 87, 4362 (1983). See also, C.A. Young, R.R. Dewald, J. Chem. Soc. Chem. Commun., 188 (1977).
- 57. J.L. Dye, J.M. Ceraso, M.T. Lok, B.L. Barnett and F.J. Tehan, J. Am. Chem. Soc. 96, 608 (1974).
- 58. F.J. Tehan, B.L. Barnett and J.L. Dye, J. Am. Chem. So. <u>96</u>, 7203 (1974).
- 59. W. Bell Flower, "Physics of Color Centers", Academic Press (New York) 1968.
- 60. J.J. Markham, "F-Centers in Alkali Halides", Academic Press (New York) 1966.
- 61. H.F. Ivey, Phys. Rev. 72, 341 (1947).
- 62. W.C. Holten and H. Blum, Phys. Rev. 175, 89 (1962).
- 63. W.T. Doyle, Phys. Rev. 126, 1421 (1962).
- 64. L. Kevan and B.C. Webser (eds.), "Electron-Solvent and Anion-Solvent Interactions", Elsevier, (Amsterdam) 1976.
- 65. J.E. Hart and W.J. Boag, J. Am. Chem. Soc. <u>84</u>, 4090 (1962).
- 66. J. Jortner, S.A. Rice and E.G. Wilson, "Metal-Ammonia Solutions, Colloque Weyl 1", G. LePoutre and M.J. Sienko (eds.), W.A. Benjamin (New York) 1964.
- 67. L. Kevan, J. Phys. Chem. <u>84</u>, 1232 (1980).
- 68. L. Kevan, J. Phys. Chem. 82, 1144 (1978).
- 69. L. Kevan, Adv. Radiat. Chem. 4, 181 (1974).
- 70. H. Hase, R.Q.H. Ngo and L. Kevan, J. Chem. Phys. 62, 985 (1975).

- 71. D.P. Lin and L. Kevan, Chem. Phys. Lett. <u>40</u>, 517 (1976).
- 72. L. Kevan, J. Phys. Chem. 85, 1628 (1981).
- 73. N. Narayama and L. Kevan, J. Am. Chem. Soc. <u>103</u>, 1622 (1981).
- 74. C.J. Pedersen, J. Am. Chem. Soc. <u>89</u>, 7017 (1967); <u>90</u>, 3299 (1968).
- 75. B. Dietrich, J.M. Lehn and J.P. Sauvage, Tetrahedron Lett., 2885, 2889 (1969).
- 76. B. Metz, D. Moras and R. Weiss, J. Chem. Soc. Perkin II, 423 (1976).
- 77. C.J. Pedersen and H.K. Frensdorff, Andew. Chem. Int. Ed. Engl. 2, 16 (1972).
- 78. J.J. Christensen, D.J. Eatough and R.M. Izatt, Chem. Rev. 74, 351 (1974).
- 79. R.M. Izatt, R.E. Terry, B.L. Haymore, L.D. Hansen, N.K. Dally, A.G. Avonded and J.J. Christensen, J. Am. Chem. Soc. 98, 7620 (1976).
- 80. J.D. Lamb, R.M. Izatt, C.S. Swain and J.J. Christensen, J. Am. Chem. Soc. <u>102</u>, 475 (1980).
- 81. N.S. Poonea and A.V. Bajaj, Chem. Rev. <u>79</u>, 389 (1979).
- 82. R.D. Moras and R. Weiss, Acta Cryst. <u>B29</u>, 383, 388, 396, 400 (1973).
- 83. P. Seiler, M. Dobler and J.D. Dunitz, Acta Cryst. B30, 2744 (1974).
- 84. M. Dobler and R.P. Phizackerley, Acta Cryst. <u>B30</u>, 2746 (1974).
- 85. M. Dobler and R.P. Phizackerley, Acta Cryst. <u>B30</u>, 2748 (1974).
- 86. J.D. Dunitz, M. Dobler, P. Seiler and R.P. Phizaker-ley, Acta Cryst. B30, 2733 (1974).
- 87. M. Dobler, J.D. Dunitz and P. Seiler, Acta Cryst. B30, 2741 (1974).
- 88. D.M. Dishong, C.J. Diamond, M.I. Cinoman and G.W. Gokel, J. Am. Chem. Soc. 105, 587 (1983).

- 89. Y. Nakatsuji, T. Nakamura, M. Okahara, D.M. Dishong and G.W. Gokel, J. Org. Chem. 48, 1238 (1983).
- 90. R.A. Schultz, D.M. Dishong and G.W. Gokel, J. Am. Chem. Soc. 104, 625 (1982).
- 91. D.M. Goli, D.M. Dishong, C.J. Diamond and G.W. Gokel, Tetrahedron Lett. 23, 5243 (1982).
- 92. J.L. Dye, C.W. Andrew and S.E. Mathews, J. Phys. Chem. 79, 3065 (1975).
- 93. F.J. Tehan, B.L. Barnett and J.L. Dye, J. Am. Chem. Soc. 96, 7203 (1974).
- 94. B. Van Eck, L.D. Le, D. Issa and J.L. Dye, J. Inorg. Chem. 21, 1966 (1982).
- 95. J.L. Dye, M.R. Yemen and M.G. DaGue, J. Chem. Phys. 68, 1665 (1978).
- 96. J.S. Landers, Ph.D. Dissertation, Michigan State University, 1981.
- 97. M.G. DaGue, Ph.D. Dissertation, Michigan State University, 1979.
- 98. D. Issa, Ph.D. Dissertation, Michigan State University, 1982.
- J.S. Landers, J.L. Dye, A. Stacy and M.J. Sienko,
 J. Phys. Chem. 85, 1096 (1981).
- 100. B. Van Eck, Ph.D. Dissertation, Michigan State University, 1983.
- 101. M.L. Tinkham, M.S. Thesis, Michigan State University, 1982.
- 102. M.R. Yemen, Ph.D. Dissertation, Michigan State University, 1983.
- 103. M.D. Meadows, K.A. Smith, R.A. Kinsey, T.M. Rothgeb, R.P. Skarjune and E. Oldfield, Proc. Nat'l. Acad. Sci. USA 79, 1351 (1982).
- 104. D. Issa and J.L. Dye, J. Am. Chem. Soc. 104, 3781 (1982).
- 105. Z. Li, unpublished results, this laboratory.

- 106. O. Fussà, unpublished results, this laboratory.
- 107. E. Kanffmann, J.L. Dye, J. Lehn and A.I. Popov, J. Am. Chem. Soc. 102, 2274 (1980).
- 108. N.W. Ashcroft and N.D. Mermiu, "Solid State Physics", D.G. Crane (ed.), Saunders College, (Philadelphia) 1976.
- 109. P.D. Townsend and J.C. Kelly, "Colour Centers and Imperfections in Insulators and Semiconductors", Crane Russak and Co. (New York) 1973.
- 110. E.R. Andrew, Arch. Sci. (Geneva) 12, 103 (1959).
- 111. E.R. Andrew, A. Bradbury and R.G. Eades, Nature 183, 1802 (1959).
- 112. I.J. Lowe, Phys. Rev. Lett 2, 285 (1959).
- 113. J.A. Pople, W.G. Schneider and J.H. Bernstein, "High-Resolution Nuclear Magnetic Resonance", McGraw-Hill (New York) 1959.
- 114. Abragam, "The Principles of Nuclear Magnetism", Oxford University Press (London) 1961.
- 115. E.R. Andrew, Prog. Nucl. Magn. Reson. Spectrosc. 8, 1 (1971).
- 116. E.R. Andrew, Int. Rev. Phys. Chem. 1, 195 (1981).
- 117. M.H. Cohen and F. Reif, Solid State Physics 5, 321 (1957).
- 118. M.D. Meadows, K.A. Smith, R.A. Kinsey, T.M. Rothgeb, R.P. Skarjune and E. Oldfield, Proc. Nat'l. Acad. Sci. USA 79, 1351 (1982).
- 119. A.C. Cunningham and S.M. Day, Phys. Rev. <u>152</u>, 287 (1966).
- 120. E. Oldfield, S. Schramm, M.D. Meadows, K.A. Smith, R.A. Kimsey and J. Ackerman, J. Am. Chem. Soc. 104, 919 (1982).
- 121. R.S. Drago, "Physical Methods in Chemistry", W.B. Saunders Co. (Philadelphia) 1977.
- 122. J.L. Dye, M.G. DaGrue, M.R. Yemen, J.S. Landers,
 H.L. Lewis, J. Phys. Chem. 84, 1096 (1980).
- 123. N. Tientega, unpublished observation, this laboratory.

- 124. A. Beckmann, K.D. Böklen and D. Elke, Z. Phys. 270, 173 (1974).
- 125. G. Malli and S. Fraga, Theor. Chim. Acta 5, 275 (1966).
- 126. M.T. Lok, F.J. Tehan and J.L. Dye, J. Phys. Chem. <u>76</u>, 2975 (1972).
- 127. S. Ganapathy, S. Schramm and E. Oldfield, J. Chem. Phys. 77, 4360 (1982).
- 128. E. Mei, A.I. Popov and J.L. Dye, J. Phys. Chem. <u>81</u>, 1677 (1977).
- 129. S. Khazaell, A.I. Popov and J.L. Dye, J. Phys. Chem. 86, 4238 (1982).
- 130. E.R. Andrew, W.S. Hinshaw and R.S. Tiffen, J. Mag. Res. 15, 191 (1974).
- 131. A. Garroway, D. Vanderhart and W. Earl, Phil. Trans. Roy. Soc. Lond. A299, 609 (1981).
- 132. M. Stoll and T. Majors, Phys. Rev. B24, 2859 (1981).
- 133. R. Catterall and P. Edwards, Advances in Molecular Relaxation and Interaction Processes 13, 123 (1978).
- 134. S. Dawes, unpublished observations, this laboratory.
- 135. C.P. Slichter, "Principles of Magnetic Resonance", Springer-Verlag (New York) 1978.
- 136. M. Tinkham, unpublished observations, this laboratory.
- 137. G. Pake, "Paramagnetic Resonance", W.A. Benjamin, Inc. (New York) 1962.
- 138. G. Breit and I. Rabi, Phys. Rev. 38, 2082 (1931).
- 139. J.E. Wertz and J.R. Bolton, "Electron Spin Resonance: Elementary Theory and Practical Applications", McGraw-Hill (New York) 1972.
- 140. T.W. Griswold, A.F. Kip and C.H. Kittel, Phys. Rev. 88, 951 (1952).
- 141. F.J. Dyson, Phys. Rev. 98, 349 (1955).
- 142. G. Feher and A.F. Kip, Phys. Rev. 98, 337 (1955).

- 143. R.H. Webb, Phys. Rev. 158, 225 (1967).
- 144. W.S. Glaunsinger and M.J. Sienko, J. Chem. Phys. 62, 1883 (1975).
- 145. J. Smart, "Effective Field Theories of Magnetism", W.B. Saunders Co. (Philadelphia) 1966.
- 146. C. Kittle, "Introduction to Solid State Physics", 5th ed., John Wiley & Sons, Inc. (New York) 1976.
- 147. A.H. Morrish, "The Physical Principles of Magnetism", John Wiley & Sons, Inc. (New York) 1965.
- 148. M. Cyrot, J. de Physique (Paris) 33, 125 (1972).

